Modelling, Design and Analysis of a Water Jetpack Powered by an Autonomous Underwater Vehicle (AUV) System

Justin Edwin Naidoo

Supervisor: Professor Freddie L. Inambao

Submitted in fulfillment of the academic requirements for the degree of Master of Science in Mechanical Engineering, College of Agriculture, Engineering and Science, University of KwaZulu-Natal

February, 2017

DECLARATION – PLAGIARISM

I, Justin Edwin Naidoo, declare that:

1. The research reported in this dissertation, except where otherwise indicated, is my original research.
2. This dissertation has not been submitted for any degree or examination at any other university.
3. This dissertation does not contain other persons' data, pictures, graphs or other information, unless specifically acknowledged as being sourced from other persons.
4. This dissertation does not contain other persons' writing, unless specifically acknowledged as being sourced from other researchers. Where other written sources have been quoted, then:
   a. Their words have been re-written but the general information attributed to them has been referenced
   b. Where their exact words have been used, then their writing has been placed in italics and inside quotation marks, and referenced.
5. This dissertation does not contain text, graphics or tables copied and pasted from the internet, unless specifically acknowledged, and the source being detailed in the dissertation and in the References section.

Signed _____ Date _____

Justin Edwin Naidoo

As the candidate's supervisor, I agree/do not agree to the submission of this dissertation.

Signed _____ Date _____

Professor Freddie L. Inambao

ACKNOWLEDGEMENTS

ABSTRACT

This dissertation describes the development and analysis of a water jetpack powered by an AUV system. The UKZN water jetpack has been in development since 2015 and has demonstrated the ability and potential for high performance flight characteristics from tests conducted during the first phase of its development. The objective of the current research is to develop a series of static and dynamic models such as to optimize the performance, efficiency and functionality of the water jetpack along with the development of an AUV concept to serve as a duel controlled power unit to the water jetpack. In particular, this dissertation details the development of an initial proposed water jetpack and AUV system computational model concept, together with static and dynamic modelling, mechanical and control system model development, as well as technical analysis of the water jetpack and AUV system for futuristic development and implementation.

A water jetpack propulsion system utilizes a feed hose which links the water jetpack to a separately tethered power unit, generally referred to as a personal water craft (PWC), which requires either secondary pilot control or tension-type tethering in the feed hose to enable the power unit to track the global positioning system (GPS) coordinates and match the dynamic state of the water jetpack. An AUV is an air independent propulsion (AIP) craft with the ability of GPS tracking, multi-degree of freedom control and simultaneously functioning as a PWC for the water jetpack system.

Research and analysis into the development of water jetpack's, AUV's, fluid dynamics, mechatronics and hydrogen AIP is presented in the study. From the research conducted, it is deduced that the aerodynamic stability and performance of a water jetpack is strongly dependent on the precise control of the mass flow rate, thrust vectoring, tracking and propulsion efficiency of the system. A series of non-transient models were developed and programmed as an optimization code on MATLAB to verify the geometric flow area range and performance of the water jetpack propulsion system under peak steady state conditions.

Development of the combined system control system consisted of modelling the open-loop first and second-order one-, two- and three-dimensional dynamic equations of the water jetpack and AUV on MATLAB Simulink. The open-loop system responses show there is a high degree of aerodynamic instability in the system due to a large overshoot and settling time. Proportional-integral-derivative (PID) controllers were implemented in each open-loop model to form closed-loop feedback control models of the water jetpack and AUV system such that a pilot can attain steady state aerodynamic stability and the AUV can track the GPS coordinates and dynamic state of the water jetpack. The system was modelled and simulated to reach a peak flight altitude of 10 m at which the system attains steady state control. The absolute peak condition for the water jetpack and AUV combined system is flight altitude of 10 m and flight velocity of 15 m/s. The development of the optimization code of the water jetpack propulsion system allowed for determining the system parameters used in the open and closed Simulink models. The development of the control system model and simulations conducted yielded a fully automated water jetpack and AUV system with optimized flight and aerodynamic performance.

A computational model of the system was developed using SolidWorks and optimized as a function of mass, numerical and statistical performance. Thereafter, a series of detailed Computational Fluid Dynamics (CFD) and Finite Element Analyses (FEA) were performed to verify fluid flow optimization and structural integrity of the water jetpack propulsion system and AUV hull model under peak conditions that the system would be subjected to. The outcome of this study is the initial idea and theoretical analysis for a water jetpack and AUV system arising from fundamental theory, system modelling, system architecture, detailed analysis and an initial computational model for future development of the system.

TABLE OF CONTENTS

LIST OF FIGURES

LIST OF TABLES

LIST OF APPENDICES

NOMENCLATURE

a	Acceleration [m/s^2]
A_i	Internal or starting area [m^2]
A_1	Area at point 1 [m^2]
A_2	Area at point 2 [m^2]
A_A	AUV frontal area [m^2]
Aj	Final or end area [m^2]
A_h	Average frontal area of a human [m^2]
A_{AL}	AUV cross-flow area [m^2]
$c(t)$	Second-order unit-step response
C_{Dh}	Coefficient of drag
C_{DA}	Drag coefficient – Frontal
C_{DAL}	Drag coefficient – Cross flow
$C_{D,x}$	Local drag coefficient
dE_{CV}/dt	Rate of change of energy across control volume boundary [J/s]
$\dfrac{dH}{dt}$	Rate of change in angular momentum [kg.rad/s]
dm	Mass of a differential element [kg]
$\dfrac{dm}{dt}$	Mass flow rate [kg/s]
dM/dt	Rate of change of momentum [kg.m/s^2]
dm_{CV}/dt	Rate of change of mass within the boundaries of a control volume [kg/s]
$\dfrac{dr}{dt}$	Instantaneous rate of change of position vector [m/s]
dU	Volume of a differential element [m^3]
$\dfrac{dv}{dt}$	Time rate of change of velocity along the body lateral axis [m/s^2]
$\dfrac{du}{dt}$	Time rate of change of velocity along the body longitudinal axis [m/s^2]
$\dfrac{dv_x}{dt}$	Time rate of change of velocity along the x-direction [m/s^2]

$\dfrac{dv_{xz}}{dt}$	Time rate of change of velocity in the x-z direction [m/s^2]
$\dfrac{d\vec{v}_{xyz}}{dt}$	Acceleration vector in the x-y-z direction [m/s^2]
$\dfrac{dv_z}{dt}$	Time rate of change of velocity in z-direction [m/s^2]
$\dfrac{d\vec{v}_{xyz}}{dt}$	Acceleration vector in the x-y-z direction [m/s^2]
$\dfrac{d\vec{v}_x}{dt}$	Acceleration vector in the x-direction [m/s^2]
$\dfrac{d\vec{v}_y}{dt}$	Acceleration vector in the y-direction [m/s^2]
$\dfrac{d\vec{v}_z}{dt}$	Acceleration vector in the z-direction [m/s^2]
$\dfrac{dv_{xz}}{dt}$	Acceleration in the x-z direction [m/s^2]
$\dfrac{dv_x}{dt}$	Acceleration in the x-direction [m/s^2]
$\dfrac{dv_y}{dt}$	Acceleration in the y-direction [m/s^2]
$\dfrac{dv_z}{dt}$	Acceleration in the z-direction [m/s^2]
$\dot{E}_{in}$	Energy transfer rate into control volume [J/s]
$\dot{E}_{out}$	Energy transfer rate out of control volume [J/s]
E_{ss}	Steady state error
F_B	Buoyant force [N]
$\vec{F}_B$	Buoyant force vector [N]
F_{net}	Net Force [N]
$\vec{F}_{net}$	Net force vector [N]
$\vec{F}_x$	Force vector in the x-direction [N]
$\vec{F}_y$	Force vector in the y-direction [N]
$\vec{F}_z$	Force vector in the z-direction [N]
$\vec{F}_T$	Thrust force vector [N]
F_T	Thrust force generated [N]

$F_T(t)$	Time-varying thrust force [N]
$\vec{F}_D$	Drag force vector [N]
F_{net}	Net force [N]
F_{net_x}	Net force in x-direction [N]
F_{net_x}	Net force in y-direction [N]
F_{net_z}	Net force in z-direction [N]
F_{prop}	Propeller thrust force [N]
F_{rudder}	Rudder sway force [N]
F_{xyz}	Force in the x-z direction [N]
F_{xy}	Force in the x-y direction [N]
F_x	Force in the x-direction [N]
F_y	Force in the y-direction [N]
F_z	Force in the z-direction [N]
g	Gravitation acceleration [m/s^2]
$G(s)$	Controller transfer function
h	Depth, distance or height [m]
h_{loss}	Total pressure head loss [m]
h_{fl}	Head loss due to friction [m]
h_{pump}	Pressure head delivered from pump [m]
H	Angular momentum [kg.rad/s]
H_o	Initial angular momentum [kg.rad/s]
k_B	Loss factor across a bends
k_N	Loss factor across a nozzle
K_P	Proportional gain
K_I	Integral gain
K_D	Derivative gain
l_{BM}	Perpendicular distance between the center of mass and buoyancy [m]
L	Characteristic length [m]
m	Mass [kg]

m_{AUV}	Mass of AUV [kg]
m_{dry}	Dry mass of the jetpack system [kg]
$m_{jetpack}$	Mass of jetpack [kg]
m_{pilot}	Mass of pilot [kg]
$m_{flooded}$	Jetpack flooded mass [kg]
$\dot{m}$	Mass flow rate [kg/s]
$\dot{m}_{in}$	Mass flow rate into control volume [kg/s]
$\dot{m}_{out}$	Mass flow rate out of control volume [kg/s]
M	Momentum [N.s]
M_p	Peak overshoot [%]
$\vec{n}$	normal vector
P_1	Static pressure at state point 1 [Pa]
P_2	Static pressure at state point 2 [Pa]
P_{abs}	Absolute pressure [Pa]
P_{gage}	Gage pressure [Pa]
$P_{g,1}$	Gage pressure at upper surface [Pa]
$P_{g,2}$	Gage pressure at lower surface [Pa]
P_{vac}	Vacuum pressure [Pa]
Q	Flow rate [m³/s]
r	Position vector [m]
Re	Reynolds number
t_d	Delay time [s]
t_s	Settling time [s]
t_r	Rise time [s]
v	Velocity [m/s]
$\vec{v}$	Velocity vector [m/s]
$\vec{v}_r$	Relative velocity vector [m/s]
v_i	Initial Velocity [m/s]
v_f	Final velocity [m/s]

v_x	Velocity in the x-direction [m/s]
v_{x0}	Initial surge velocity [m/s]
$v_x(t)$	Time-varying surge velocity [m/s]
$\vec{v}_x$	Velocity vector in the x-direction [m/s]
v_{xy}	Velocity in the x-y direction [m/s]
$v_{xy}(t)$	Time-varying velocity in the x-y direction [m/s]
v_{xz}	Velocity in the x-z direction [m/s]
v_y	Velocity in the y-direction [m/s]
$v_y(t)$	Time-varying sway velocity [m/s]
v_{y0}	Initial sway velocity [m/s]
v_z	Velocity in the z-direction [m/s]
v_{z0}	Initial heave velocity [m/s]
Vol_{AUV}	Volume of AUV [m³]
V_B	Volume of body [m³]
W	Weight [N]
$\vec{W}$	Weight vector [N]
$\dot{W}_{pump}$	Power delivered by pump [W]
$\dot{W}_T$	Power generated by thrust force [W]
X	Displacement in the x-direction [m]
X_0	Initial displacement in the x-direction [m]
$X(t)$	Time-varying displacement in the x-direction [m]
$XY(t)$	Time-varying displacement in the x-y direction [m]
XY_0	Initial displacement in the x-y direction [m]
Y	Displacement in the y-direction [m]
Y_0	Initial displacement in the y-direction [m]
$Y(t)$	Time-varying displacement in the y-direction [m/s]
Z	Displacement in the z-direction [m]
Z_1	Vertical elevation at state point 1 [m]
Z_2	Vertical elevation at state point 2 / Flight altitude [m]

Z_{20}	Desired flight altitude [m]

Greek Symbols

(x, y, z)	Linear coordinate system components
(ϕ, θ, ψ)	Angular coordinate system components
α_{BM}	Angle between the center of mass and buoyancy [rad]
δ_d	Vertical deviation angle [rad]
δ_r	Horizontal deviation angle [rad]
κ	Correction factor for the mass of water in the jetpack propulsion system
ρ	Density [kg/m³]
ρ_{air}	Density of air [kg/m³]
ρ_s	Density of air [kg/m³]
μ	Dynamic viscosity [N.s/m²]
ξ	Damping factor
v	Kinematic viscosity [m2/s]
ω_n	Natural frequency [rad/s]

Subscripts

net	Total or resultant
sys	System
CV	Control volume
T	Thrust
AUV	Autonomous underwater vehicle
jetpack	Water jetpack
dry	Dry mass

Abbreviations

AUV	Autonomous underwater vehicle
AIP	Air independent propulsion

CFD	Computational fluid dynamics
CV	Control volume
CS	Control surface
CM	Center of mass
FEA	Finite element analysis
GPS	Global positioning system
UKZN	University of KwaZulu-Natal
PWC	Personal water craft
PID	Proportional-integral-derivative

CHAPTER 1 : INTRODUCTION

1.1   Background of Water Jetpack Technology

A water jetpack is a recreational device used by humans for leisure and sport purposes. The invention of a water jetpack was first conceptualized and produced in 2009 (Jetlev-Flyer, 2016). This device works by receiving a high flow rate of water from a separate power unit which is tethered to the jetpack and located on the surface of water as illustrated in Figure 1.1. Water is pumped from the power unit to the jetpack via a feed hose, thereafter the flow exits the jetpack through two converging nozzles (Pacella, 2009). The change in momentum of the flow induces a thrust force which propels the pilot and jetpack system in an upward direction (Vonk and Bohacek, 2013). In most standard water jetpack systems, the mass flow rate of water in the system is controlled manually by the pilot via a throttle cable system.

Figure 1.1: Water Jetpack System and Power Unit
Source: Jetlev-Flyer, 2016

Referring to Figure 1.1, the configuration of this system allows a greater payload (pilot and jetpack system) to be carried as compared to a self-powered jetpack since the bulk of the mass in the combined system (the power unit) is located on the surface of the water. In most commercial jetpacks, such as the Jetlev-Flyer (2016) and Zapata Racing (2015), a high-powered jet ski serves as the power unit. The power unit provides a high flowrate of water to the jetpack with the use of an axial flow propeller; the flow of water is passed through a feed hose and reversed and passes through two converging nozzles which generates an upward thrust force (Vonk and Bohacek, 2013).

The drawbacks of current water jetpack systems are described below:
- **High cost:** Water powered jet packs are the latest and most popular advancement in water sports, however pricing of water powered jetpacks are high and exceed the affordability of an average individual (Jetlev-Flyer, 2016).

- **Power source:** Conventional jetpacks use a jet ski as the power unit which is located on the surface of the water (Naidoo, Ramrup, Gerken and Govender, 2015a). The primary source of power for this entire system is petrol fuel. This form of fuel is exhaustible and ever increasing as oil becomes more scarce. Jet skis consist of an engine which could be either two stroke or four stroke depending on the model, and this engine is coupled to an axial flow impeller which generates hydro power by pumping water at a high flow rate of water. One major drawback of designing a water jetpack is that jet ski manufacturers do not provide any data of the performance characteristics for their crafts and this leads to error and unpredictable pumping performance through the entire system.

- **Emissions:** Personal watercrafts have significant impact on the environment due to fuel combustion and the leakage of unburned fuel and oil from the engines into the water which leak at an approximate rate millions of gallons per year. Scientists estimate that 20% to 25% of the fuel used in these watercrafts leak into the sea and harm the wildlife. Organisms at sea absorb the harmful chemicals and become extremely sensitive to light (an occurrence celled photo toxicity) and thereafter the daylight sun kills the organisms. Further effects are the result of collapse of the food chain which leads to extinction of certain species (Kupperman, Ryan and Turi, 1999).

- **Noise:** Personal watercraft engines produce relatively high pitch and frequency noise which is observed by listeners close to shore. Noise may disturb communication of a pilot and an observer which is undesirable.

- **Boating accidents:** In the United States, personal watercrafts and jet skis contribute to 36% of boating accidents (Kupperman et al., 1999). This is due to the high speed and difficulty of control of these devices. Jetpacks are prone to accidents as the power unit is dragged along the surface of water without a system for controlling its path. A collision may result in injury to humans and severe damage to the power unit.

- **Dynamic stability and control:** The jetpacks currently available require many hours of practice and often pilots require advanced training to enable them to use these devices comfortably. The stability of a water jetpack is dependent of numerous factors such as the thrust vectors, flow rate control, the center of mass of the jetpack and pilot and restrictions in the supply hose. Although manufacturers such as Jetlev-Flyer (2016) and Jetpack America (2016) claim that water jetpacks are inherently stable, experimental data shows that most pilots require at least 10 to15 hours of training to acquire basic stability (Naidoo et al., 2015b).

1.2   Scope of Study

The intention of this work is to research and develop a system in which the above-mentioned factors describing some of the drawbacks of water jetpacks could be avoided with the use of an underwater vehicle system, as well as to extend the application for the future. A brief description of the research conducted in this study to enhance the use of water jetpacks and design and to simulate a system and its implications is given below:

- **Stability and buoyancy:** Stability and buoyancy research for a power unit consists of aerodynamic factors such as wind, drag, lift, and pressure along with fluid propulsion to enable the power unit to function as an autonomous underwater vehicle (AUV) which does not depend on air to provide mechanical power required for the system.

- **Noise reduction:** Noise reducing systems are researched and considered. This research is based on automotive industry research in reducing noise from vehicles and other personal water craft. The use of fuel cells can reduce noise pollution and disturbances caused by petrol engine systems.
- **Dynamic stability and control:** The major issue with current jetpack designs is that they lack dynamic stability during use for most pilots. The design of two water jet nozzle thrusters allows for pitch, roll and yaw control. However, due to the design of these nozzles, the pilot can move only forward and backward and cannot control motion in two planes. The commercial jetpacks consist of complex couplings that allow motion of the nozzle (Jetlev-Flyer, 2016). Naidoo et al. (2015b) designed a water jetpack at UKZN composed of two trim tab flow deflectors which was a cheaper alternative to a coupling, however, results have shown that the issue of back spraying and pressure loss severely affects the dynamic stability of such a system. Research in the fields of jet propulsion, aerodynamics, and mechatronic control can provide the background of work needed to design a control system of sufficient stability for water jetpacks.
- **Fuel supply:** Fuel supply of the system could be replaced by a hydrogen fuel cell with air independent propulsion (AIP). Research in this field would provide a brief description of using hydrogen as a fuel source instead of petrol. This would reduce emissions caused by internal combustions engines.

1.3   Aim and Objectives

The aim of this study was to research, model, simulate and develop an initial proposed computational model of a water jetpack powered by an AUV. This was achieved by detailing the steady state and transient equations that model the water jetpack and AUV separately and thereafter developing an optimization code and Simulink model of the system on MATLAB, which was followed by a proposed computational model of the system which consists of a water jetpack tethered to an AUV which acts as a self-tracking and autonomous power unit.

The objectives of this study were the following:
1. Research current water jetpack systems along with the fundamental aspects of fluid dynamics.
2. Research the elementary aspects of modelling, simulation and control of mechanical systems.
3. Briefly outline the fundamental theory of hydrogen fuel cells and AIP systems.
4. Develop a series of steady state and transient equations for the water jetpack to model motion in one, two and three dimensions.
5. Develop a series of steady state and transient equations for the AUV to model motion in one, two and three dimensions.
6. Model and simulate the water jetpack and AUV under transient conditions using MATLAB Simulink.
7. Develop a Simulink model that describes how a water jetpack and AUV system could be controlled to achieve pilot defined flight specifications.
8. Develop an initial proposed computational model for the system.
9. Perform CFD analysis and FEA simulations on the essential components of the proposed model of the system.

1.4   Dissertation Outline

Chapter 2 of this dissertation is devoted to the literature review of water jetpacks, AUVs, and the fundamental aspects of fluid dynamics, control system modelling, and hydrogen AIP. The literature review investigates the development of the water jetpack together with a survey of commercial AUVs. The fluid dynamics, control system modelling, and hydrogen AIP sections contained in this chapter detail the theoretical background required for the succeeding chapters in this dissertation.

Chapter 3 is dedicated to the development of a system of steady state and transient equations that model the motion and state of the water jetpack for various flight conditions. The derivation of these equations is based on the theoretical background detailed in Chapter 2. Newton's Second Law, the conservation of mass, momentum, and energy along with the Bernoulli equation form the basis for these models. The water jetpack is modelled in one, two and three dimensions.

Chapter 4 of this dissertation is dedicated to the development of the system of steady state and transient equations to model the motion of an AUV in one, two and three dimensions. The approach taken in the development of the models contained in this chapter consists of the development of one-dimensional steady state motion, followed by two- and three-dimensional steady state and transient motion modelling.

Chapter 5 discusses the development and results obtained from an optimization code on MATLAB. The optimization code is based on the steady state peak conditions of the water jetpack. This performance code was used to generate distribution graphs that illustrate various characteristics of the system with variable combinations of feed hose and jet-exit diameter. A set of primary and secondary conditions was used in a methodological manner to determine the optimal selection of the geometric flow parameters in the water jetpack propulsion system.

Chapter 6 of this work details the MATLAB Simulink modelling and simulation of the water jetpack, AUV and combined system mode. The Simulink models are based on the transient Newtonian force balance equations described in Chapters 3 and 4. The water jetpack and AUV were first modelled and simulated on MATLAB Simulink independently and closed-loop systems were formed for each case, including the development of one-, two- and three-dimensional Simulink models. The transient responses of the system were analyzed and PID controllers were implemented to attain desired responses of flight. The last part of this chapter describes the development of a combined system model. The combined system model is a fully automated system that utilizes PID controllers to allow a pilot to attain specified flight conditions and controls the various parameters in the system to attain this.

Chapter 7 describes the initial development of a computational model of the water jetpack and AUV system. This includes a description of the flight specifications and performance of the system under steady state and peak transient conditions as observed from the MATLAB Simulink simulations contained in Chapter 6. An initial proposed

computational model of the water jetpack wye system and AUV hull is described and illustrated, this is followed CFD analysis and FEA of the system under peak conditions.

Chapter 8 forms the discussion of all the work contained in each chapter of this dissertation and is where the main results and findings of this study are detailed. The analysis and interpretation of the results of this study is described such that future development of the water jetpack and AUV system can be based on these findings.

Chapter 9 presents the conclusions of the study and future development recommendations arising therefrom.

1.5   Research Hypothesis

The outcome of this study is the initial idea and theoretical analysis for a water jetpack and AUV system developed by means of presenting the fundamental theory, system modelling, system architecture, detailed analysis and computational model concept for future development of the system.

CHAPTER 2 : LITERATURE REVIEW

2.1   Survey of Jet Propulsion and Jetpack Development

Jet propulsion dates to the 1st century AD where an engine was built by Hero of Alexandria. The engine he designed was called an aerophile and worked in a similar manner to that of a steam turbine where a jet of steam is used to spin a wheel to generate mechanical work. This system designed by Hero was an illustration of the scientific principle formulated by Sir Isaac Newton in 1687 known as Newton's Third Law of motion (Greatrix, 2012). This law states that for every action, there is an equal and opposite reaction (Vonk and Bohacek, 2013). In the engine developed by Hero, the jet of steam formed the action, and the spinning of the wheel formed the reaction, hence these engines are now termed reaction engines (Anderson, 2001).

The development of hydro-propelled flight systems is an aspect of jet propulsion and aerodynamics. Jet propulsion flight systems were first developed in the late 1930s at the time when the jet engine was invented (Humble, Henry and Larson, 1995). Jet refers to turbo engines and solid or liquid based rocket fuel. In general, a jet produces a thrust force that acts in a specific linear direction. The term vectoring refers to the act of steering the thrust force generated by a jet (Greatrix, 2012). A simple example of thrust vectoring is an aircraft that uses flaps and ailerons to control the airflow around the aircraft which results in a change in direction of the aircraft (Stratospheric Industries, 2015). Jet propulsion was initially used for flight systems and thereafter applied for use in high-speed boats and other recreational crafts whereby the intake of water is from the front end of the boat or craft and the water exits at the rear end of the boat or craft via a nozzle (Jetpack America, 2016).

Bell Aerosystems began the development of the first ever jetpack for the United States (US) Army in the mid 1950's and called this development the *Bell Rocket Belt* as shown in Figure 2.1. Wendell Moore worked on the rocket while working as an engineer at Bell Aerosystems. This jetpack was first demonstrated to the US Army in the year 1961, however it failed to impress the army and the development was terminated due to the high fuel consumption to flight time ratio which was five gallons of hydrogen peroxide for a flight time of 21 seconds (Beushausen, 1993).

Figure 2.1: Bell Aerosystems Rocket Belt
Source: Beushausen, 1993

During tests conducted, one of the major problems encountered was attaining steady and stable flight, which was resolved with the use of a control system. The arrangement that optimizes the stability of the jetpack during flight was found to be one in which the nozzle thrust vectors are located above the center of gravity of the pilot and jetpack, as illustrated in Figure 2.1. The development of the Bell Rocket Belt was continued in the year 1990 and has been successful in recent years. Although the Bell Rocket became successful, the use of it by the US Army was limited due to the rocket's limited fuel storage capacity. The US Army thereafter focused on the development of missile systems (Beushausen, 1993).

In 1965, a young Chinese Canadian named Raymond Li watched the actor Sean Connery starring as James Bond in the film *Thunderball* making a daring escape by gliding through the air with the use of a jetpack (Jetpack America, 2016). Li felt compelled to develop his own jetpack, however he was disappointed when he visited local libraries in search for books to detail the design of such a craft (Industries, 2015). Li revisited his idea in the year 2000 when he was living in Toronto. He began to conduct extensive research to develop a new type of jetpack, in which water would be used as a propellant instead of hydrogen or nitrogen. He worked on his ideas then in 2003 felt he had a well-developed concept. He received funding from the National Research Council of Canada and used the grant to further develop his prototype. With the use of this grant, Li developed a working prototype which used a SeaDoo engine from a small boat unit. Instead of pumping and expelling water through a rear end nozzle to generate thrust as in a traditional power boat, the SeaDoo boat unit was used to pump water up a 30-foot hose to the water jetpack located on the pilot. The motion of the jetpack was controlled by up and down arm movements for forward and backward motion pf the system and body shift movements as left or right for sideway motion of the system (Jetpack America, 2016). In 2005, he moved to Fort Lauderdale to work with watercraft experts where he continued to work on his prototype. This marked the year that Li's prototype attained stable and controlled flight. By the year 2008 the prototype was further developed and performed at a much more successful rate during flight tests than any of the previous prototypes, which attracted many investors to invest in this innovation (Morell, 2013).

Li then released a YouTube promo video called "Ever Dreamt of Flying? Stop Dreaming" in February 2009, as illustrated in Figure 2.2.
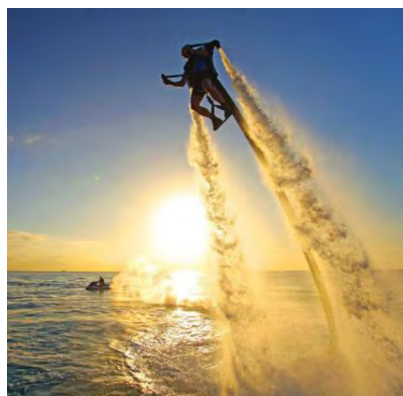
Figure 2.2: Jetlev-Flyer promo video release
Source: Jetlev-Flyer, 2016

This video demonstrated how his latest prototype worked and was used to market the product. Li had opened his own company named Jetlev Sports Inc. and had licenced MS Watersports Gmbh of Germany to manufacture the first Jetlev model. The water jetpack developed by Li was then called the Jetlev-Flyer. The first commercial model of the Jetlev-Flyer worked with a jet ski of 155 HP engines and was marketed at 99 000 Euros (Jetlev-Flyer, 2016).

In June 2009, Stratospheric Industries (2015) loved the idea of the Jetlev as seen in the YouTube video released earlier that year, however they the lack of funds to spend 130 000 USD on a prototype. The designers at Stratospheric Industries then embarked on developing their own prototype. Figure 2.3 shows the structural layout sketch of the first water jetpack design by Stratospheric Industries.
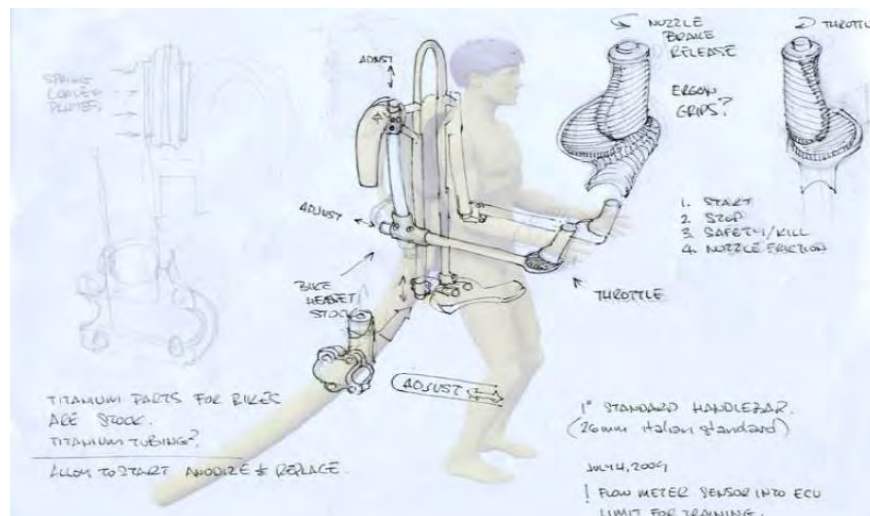
Figure 2.3: Stratospheric Jetpack First Design – Structural Layout
Source: Stratospheric Industries, 2015

Stratospheric's first jetpack design shown in Figure 2.3 differs from the Jetlev-Flyer. Stratospheric Industries the idea of keeping the control arms at a lower position so that the pilot could steer the jetpack with less effort. The first design by Stratospheric Industries also consisted of a light weight frame which was made from tubes of stainless steel (Stratospheric Industries, 2015).

By May 2010, Jetlev announced their product rollout plan for the release of their first model (Jetlev R200) by March 2011 in markets of South Africa, North America, South America and Asia-Pacific at a price of 99 500 USD. The Jetlev-Flyer JF-220, as shown in Figure 2.4, consists of stainless steel 316 marine grade propulsion system pipes, complete carbon fiber backrest, 5-point racing harness, adjustable arms and seat and the jetpack is powered by a 220 HP, 3 cylinder, 4 stroke supercharged power unit with a dry weight of 325 kg and 60 litres fuel capacity. The fuel type used in this power unit is 91-95 octane. The hull of the power unit is made from high grade composites and fiber glass. The power unit is linked to the water jetpack by a 10-m hose made from tightly woven rubber coated textile with aluminium flanges and a protective nylon sleeve (Jetlev-Flyer, 2016).

Figure 2.4: Jetlev-Flyer JF-220
Source: Jetlev-Flyer, 2016

After numerous revisions and test flight crashes, the Jetlev-Flyer was commercially available to the public in 2011. At that time, a business person named John Morris had placed orders for several units to use as rental in California. In this year, a division of the Jetlev group called Jetpack America was established and had business locations in Newport Beach, California and Hawaii (Jetpack America, 2016).

In the year of 2011, a French engineer and water craft rider named Franky Zapata who was the owner of Zapata Racing (2015), had been performing many tests of hydro-propelled machines. His innovation allows for underfoot propulsion and hand stabilization. Zapata had introduced and released a promo video of his innovation on YouTube in December 2011. He received a grant from the French Institute National de la Propriete Industrielle to patent his invention. He then launched the Flyboard in early 2012. The Flyboard without the power unit is shown below in Figure 2.5 (a) and the flight test of the Flyboard is illustrated in Figure 2.5 (b). In the water-propelled configuration, water from the feed hose is forced under high pressure to a pair of jet nozzles which is located under the boots of the Flyboard.

(a)   (b)

Figure 2.5: (a) Zapata Flyboard, (b) Zapata Flyboard Flight Test
Source: Zapata Racing, 2015

The Flyboard works similarly to the Jetlev-Flyer by having a 30-foot hose connected to a power unit or PWC and the Flyboard, but differs since the Flyboard is a foot mounted device that a pilot stands upon as opposed to a traditional jetpack that is attached to the back of a pilot (Zapata Racing, 2015).

The Flyboard was designed to provide sufficient thrust to propel a pilot up to 15 m in the air and is inherently buoyant for safety. The thrust generated by the Flyboard is controlled by the throttle on the PWC which is controlled either by a secondary pilot or by an Electronic Management Kit which is sold separately from the main system (Zapata Racing, 2015).

In September 2012, Stratospheric Industries (2015) performed test flights on their jetpack development called *X-Jetpack NX*. The design of the X-jetpack NX differs slightly from the Jetlev-Flyer and was released for commercial use in 2013. Stratospheric Industries then began working on another type of hydro-propelled device called the Jetblade which was ordered for production in Dubai by August 2014. Figure 2.6 shows the X-Jetpack NX and Jetblade along with the feed hose and propulsion system connections:

Figure 2.6: X-Jetpack NX and Jetblades
Source: Stratospheric Industries, 2015

The X-Jetpack NX consists of propulsion pipes made from stainless steel 316 which is designed for salt water use. The aim of this development by Stratospheric Industries was to design a highly ergonomically friendly water jetpack by including many comfort features in the design. The Jetblade works in the same manner as the Flyboard developed by Zapata Racing and a video of the Jetblade device was released by Stratospheric Industries in September 2014 (Stratospheric Industries, 2015).

In 2014, the three main companies (Jetlev, Stratospheric Industries and Zapata Racing) were in tight competition to gain the highest market share globally. Jetlev released their latest innovative jetpack model called the *JF-120 Shark* which offered a competitive price and excellent flight performance. Jetlev also released their luxury line jetpack model called the JF-300 which was made completely out of carbon fiber which was targeted for customers that desired luxury, quality and the best performance for hydro-propelled flight (Jetlev-Flyer, 2016). Zapata Racing entered a new dimension of hydro-propelled technology with the development and release of the *Zapata Plastic Flyboard* (Figure 2.7 (a)) and Zapata Plastic Jetpack (Figure 2.7 (b)) in May 2015.

<center>(a)</center><center>(b)</center>

Figure 2.7: (a) Zapata Plastic Flyboard, (b) Zapata Plastic Jetpack
Source: Zapata Racing, 2015

Zapata Racing (2015) claims that the innovation used in these devices were made using an advanced software which is like the software used in the design of Formula 1 vehicles. The plastic jetpack allows pilots to fly in a seated position which reduces the demand on balance and dexterity required by the pilot during flight. The development of using plastic in a hydro-propelled device is very attractive since it reduces the mass of the system while delivering the same flight performance as the regular model.

Zapata Racing (2015) announced the development of their latest innovation for 2016. This device is called the *Flyboard Air* and the flight test is illustrated in Figure 2.8 (a) and (b) below respectively.

<center>(a)</center><center>(b)</center>
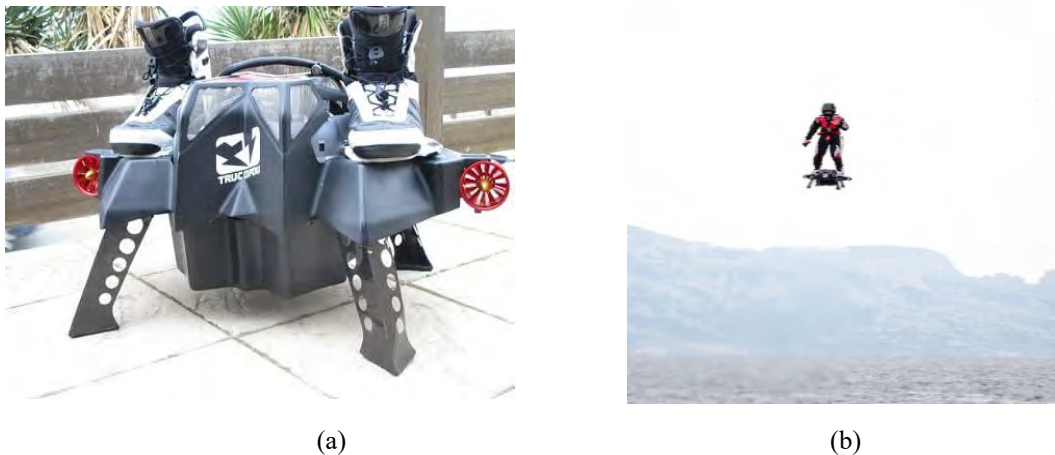
Figure 2.8: (a) Flyboard Air, (b) Flyboard Air flight test
Source: Zapata Racing, 2015

Zapata racing has released a video of the Flyboard Air on their website and YouTube and claims that this independent propulsion unit represents four years of work aside from their line of hydro-propelled devices as mentioned previously. The Flyboard Air is currently in its prototype stage. Numerous flight tests were conducted by Zapata Racing (as illustrated in Figure 2.8 (b)) and results have shown that the Flyboard Air is capable of autonomous flight up to an altitude of 10 000 feet with a flight time of 10 minutes and can attain a maximum steady state flight speed of 150 km/h (Zapata Racing, 2015).

<center>35</center>

2.2   Survey of Autonomous Underwater Vehicles (AUVs)

Autonomous Underwater Vehicles were first developed in the 1960s for use in the US Navy for performing autonomous search and rescue operations in deep sea (Wernli, 2001). Government institutions, universities and other technology industries gained interest in AUVs and started with further investigation, development and experimentation after a decade (in the 1970s) since the development of first AUV in the US Navy. In the 1980s there was significant development in AUVs by the oil and gas industry. The development of AUVs in the 1980's was much greater than the 1960s and 1970s as AUV's were able to travel into far reaches of the sea and reach depths greater than the maximum depth that a professional commercial diver can reach. Oil and gas companies invested in the development of AUVs and used them for development of off shore oil fields located in deep sea (Williams, 2004).

There was a greater interest in academic research of AUVs by universities, the US Navy and technology industries in the 1990s. Bluefin Robotics is a corporation that is a world leading organization in the development of AUVs. Bluefin Robotics was established in 1989 from the Massachusetts Institute of Technology in the US. (Gonzalez, 2004). The Naval Postgraduate School of California is a well-established institute that has been involved with and made significant contributions into research and development of AUVs. This institute researches innovative ideas on AUV modelling, navigation, fault detection, control and automation, optimization and efficiency as well as computer simulation software implementation (Gonzalez, 2004). The Advanced Research Projects Agency (ARPA) AUV shown in Figure 2.9 was built in 1994 by contracted laboratories for specified naval missions, open-ocean minefield operations, tactical oceanography and to explore AUV design for future development (Brutzman, 1994).

Figure 2.9: ARPA AUV
Source: Brutzman, 1994

The ARPA AUV hull was designed from titanium which can withstand pressure up to a depth of 305 m in sea. The net mass of the AUV in air is 680 kg. The main source of power for this AUV is a set high-density silver zinc batteries which allows the AUV to travel at a speed of 2.57 m/s to 5.14 m/s for a duration of 24 hours (Brutzman, 1994).

In 1995, the US and Canadian Defense Establishments developed the Thesus AUV (Figure 2.10) to carry out the operation of laying fiber-optic cables under the arctic ice pack.

Figure 2.10: Thesus AUV
Source: Geridonmez, 2007

Thesus was designed to be 10.7 m in length and 1.27 m in diameter, with a dry mass of 8600 kg with 220 km of on-board cable, and a nominal speed of 4 knots. In 1996, a 190 km fiber-optic cable was laid under a 2.5 m ice pack (Geridonmez, 2007).

REMUS is an AUV that was developed by the Woods Hole Oceanographic Institute and was manufactured by Hydroid Corporation. REMUS (Figure 2.11) was developed for coastal environment operation, research and AUV experimentation at various sea depths (Gonzalez, 2004).

Figure 2.11: REMUS AUV
Source: Gonzalez, 2004

The length of this AUV is 1.6 m and its mass is 37 kg (Gonzalez, 2004). REMUS is propelled by a propeller and steered by fins. During the Iraqi Freedom operation in 2003, REMUS was used by the US Navy to detect mines located in the Persian Gulf harbor of Um Qasr Navy (Geridonmez, 2007).

With the success of research and development of AUVs in the 1990s by various organizations and research institutions around the world, AUVs were finally commercialized in the year 2000 (von Alt, 2003). Since the start of the 20th century, AUV development has occurred at a much more rapid rate and there are a vast range of applications for this craft (Griffiths & Edwards, 2003). Some of the applications for AUVs are search and rescue (Ballard, 1987), scientific research (Lygouras, Lalakos and Tsalides, 1998), sea floor mapping (Tivey, Johnson, Bradley and Yoerger, 1998), infrastructure development in harbors (Willcox, Vaganay, Grieve and Rish, 2004), military and navy missions (Wernli, 2001).

At present, AUVs have proven to be successful and effective in performing complex missions. The advancement in AUV performance is largely due to the development of AUV control system implementation. Since AUVs operate autonomously, they are required to implement an onboard navigation and control system with may consist of a GPS for motion feedback and motors for control of the output motion of the AUV. Leonard, Bennett, Smith and Feder (1998) describe several methods of navigation used in AUVs, the two most common of these being dead-reckoning and inertial navigation system. In dead-reckoning navigation systems, the position of the AUV is computed by integrating the velocity measured. In inertial navigation systems, the position of the AUV is computed by a double integration of the acceleration measured. Two other well-known navigation methods are known as geophysical and acoustic navigation (Lee, Jun, Kim, Lee, Aoki and Hyakudome, 2007). These methods work effectively for determining an AUV's position, however, from tests conducted by Leonard et al. (1998) on AUV navigation systems it was discovered that the position and navigation control of an AUV is greatly improved with the use of a GPS.

AUVs are most commonly propelled by thrusters or propellers for motion in the forward or horizontal direction whereby the thrust is generated in the line of motion (Valavanis, Gracanin, Matijasevic, Kolluru and Demetriou, 1997). Steering control is performed using rudders that are controlled by servo or stepper motors. Motion in the vertical direction is attained with the use of fins, variable buoyancy systems or thrusters that generate thrust in the vertical direction. Both fins and rudders change the path of an AUV in the vertical or horizontal direction by controlling and deflecting the flow of water around the hull of the AUV such that a desired path is attained (Blidberg, 2001).

2.3   Water Jetpack and AUV System Functionality

A water jetpack is designed to carry itself along with its occupant across large volumes of water in locations such as a pool, dam, river or the sea. This system can transport the occupant (pilot) either above, below or on the surface of the water (Little, McKenzie and McKay, 2015). The complete system (as illustrated in Figure 2.12) is composed of the jetpack, pilot, feed hose and a power unit (in this case an AUV) which contains a pump.
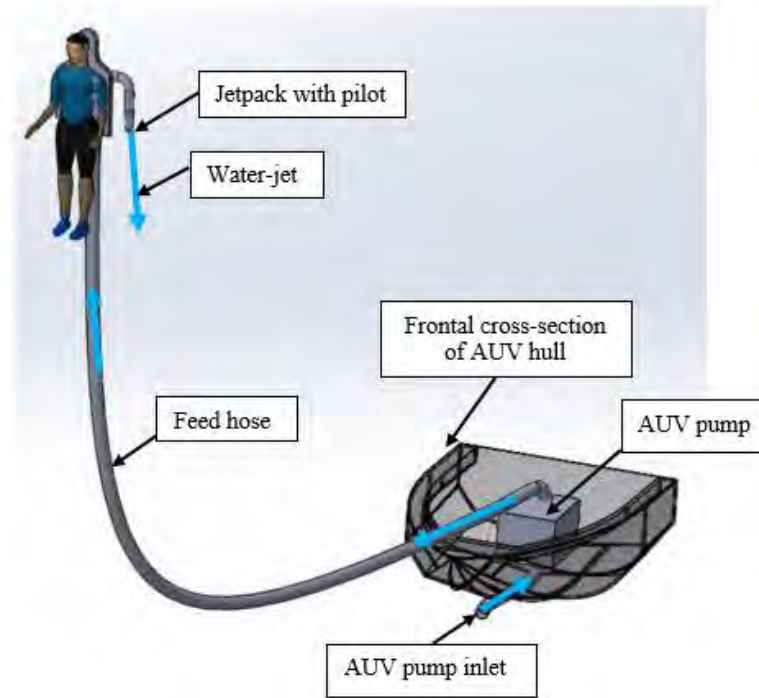
Figure 2.12: Water jetpack and AUV system schematic
Source: Little et al., 2015

The blue arrows in Figure 2.12 indicate the direction of water. The AUV contains a pump whereby water enters the system through the AUV pump inlet, thereafter an impeller within the pump increases the total pressure of the incoming flow and supplies the jetpack with an increased steady volumetric flow rate of water via a feed hose (Little et al., 2015). The flow of water that enters the water jetpack is then split into two 180-degree bends before entering two convergent nozzles (Naidoo et al., 2015a). The convergent nozzles in the jetpack increase the velocity of the flow by an area-proportional factor to attain a thrust force which propels the jetpack, pilot and feed hose in the direction that the nozzles of the jetpack face (Jetlev-Flyer, 2015).

The following terminology relating to the water jetpack and AUV system configuration will be used throughout this dissertation:

- Jetpack system: Refers to the combination of the jetpack, pilot and feed hose.
- Jetpack propulsion system: Refers to all the fluid components of the system that are used to propel the jetpack system. These include: the inlet of the AUV pump, AUV pump, feed hose, and jetpack piping system (referred as the wye system).
- AUV propulsion system: Refers to the AUV and its own propulsion system that allows it to be propelled underwater. This includes the AUV thruster or propeller, fins and rudders.

An AUV is composed of several essential components located internally and externally of its hull as shown in Figure 2.13. The external components include the hull, fin, rudder, nose cone, thruster or propeller, and a GPS antenna. The internal components include the electronic components, control boards and interfaces, sensors such as a rate gyroscope

and Doppler Velocity Log, batteries and power sources and motors that control the external propulsion components of the AUV (Chowdbury and Singh, 2011).
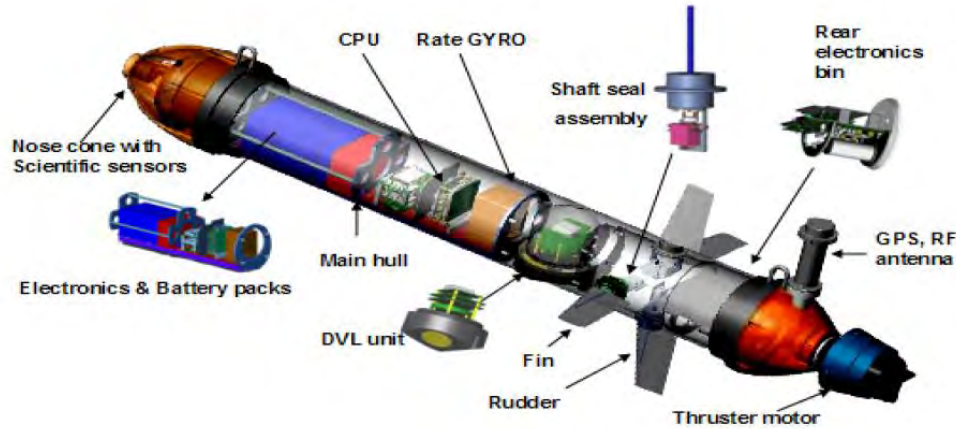
Figure 2.13: AUV hull and essential internal components
Source: Chowdbury and Singh, 2011

The main hull of an AUV is designed to be light weight and accommodate the internal components. The hull is also responsible for ensuring that the buoyant force experienced by the AUV is within an acceptable range for stability and performance (Blidberg, 2001). The nose cone is designed with an aerodynamic profile such that the flow of water around the hull of the AUV follows a streamlined profile (Fox, Pritchard and McDonald, 2010). The nose cone also contains navigation sensors which form part of the main control system. The rudders are motor controlled hinged flow deflecting structures positioned vertically towards the rear end of the AUV and control the yaw motion or left-right steering. The fins are also motor controlled hinged flow deflecting structures that control the pitch or up-down motion of the AUV. The thruster or propeller located at the extreme rear of the AUV is responsible for providing forward thrust for the AUV (Barr and Etter, 1975). The orientation of an AUV may change due to the dynamic state of the craft and thus there is often an internal water-resistant hull located within the main hull. Essentially, this configuration renders the electronic and power supply devices in a separate compartment which reduces the risk of component damage (Griffiths and Edwards, 2003).

2.4   Fundamentals of Jet Propulsion and Fluid Dynamics Theory

The functionality of water jetpacks and AUVs together with the basic derivation and details of the governing equations are presented in this chapter. This chapter covers the essential physical quantities, laws, and conservation principles that is mathematically manipulated to model a water jetpack and an AUV system which is detailed in Chapter 3 of this dissertation. Such a system requires several laws of fluid dynamics to accurately model its fluid and aerodynamic performance characteristics. This includes the following: Newton's Second Law, conservation of momentum, conservation of mass and the continuity equation, conservation of energy and Bernoulli's equation, and the drag force equation.

2.4.1 Newton's Second Law and the Thrust Equation

Newton's Second Law of motion defines the resultant force vector for a system of mass m experiencing an acceleration vector a. This is given by the expression:

$$F_{net} = ma \tag{2.1}$$

where F_{net} is the net force. This equation is the universally defined version of Newton's Second Law, it implies that the vector sum of all the forces acting on a system within the bounds of a control volume of interest, is directly proportional to both the mass and acceleration vector at the center of mass of the system enclosed by the control volume. The net or resultant force can also be defined as the rate of change of momentum (Etter, Krishnamoorthy and Sherer, 1980), M, and is given by:

$$F_{net} = dM/dt \tag{2.2}$$

Momentum is defined as the product of mass and velocity (Vonk and Bohacek, 2013) therefore the net force is given as:

$$F_{net} = d(mv)/dt \tag{2.3}$$

where mv is the momentum of the system. In some cases, the mass, density and velocity in the system may change (Fox et al., 2010). A more general expression for Newton's Second Law is given as:

$$F_{net} = \frac{d}{dt}\int (\rho v)\, dU \tag{2.4}$$

where $\rho v\, dv$ is the momentum of a differential element of volume dU. The mass of the differential element dm is given by:

$$dm = \rho\, dU \tag{2.5}$$

Equation 2.4 is used for systems in which the mass is for solids or fluids. The limitations of this form of Newton's Second Law is that it can be applied for simple systems in which control volumes are not used for the analysis. In the case of a force analysis for a control volume, the principle of conservation of momentum is used. The conservation of momentum states that the sum of all external forces acting on a control volume is equal to the sum of the time rate of change of linear momentum of the system within the boundary of the control volume and the net flow of linear momentum out of the control surface by mass flow of the system (Fox et al., 2010). The conservation of momentum, known as the momentum equation is given by:

$$\sum F_{net} = \frac{d}{dt}\left(\int (\rho v)dU\right)_{CV} + \left(\int \rho v(\vec{v}_r \cdot \vec{n}) \cdot dA\right)_{CS} \tag{2.6}$$

where $\sum F_{net}$ is the net force acting on the control volume, $\vec{v}_r$ is the fluid velocity relative to the control surface, $\vec{n}$ is the normal vector from the control surface, v is the fluid velocity, and $\rho(\vec{v}_r \cdot \vec{n}) \cdot dA$ represents the net mass flow rate for an infinitesimal area dA located on the control volume.

2.4.2   Water Jet Thrust

Thrust is the force that is generated when fluid accelerates from a duct into a median such as air or water. The thrust on a system is generated by reaction of the accelerating fluid exiting the duct and the fluid particles in the median it enters. This reaction force is explained by Newton's Third Law of motion which states that for every action, there exists an equal and opposite reaction (Vonk and Bohacek, 2013). In the case of fluid flow, thrust force is generated when fluid flows through a duct that varies in cross-sectional area. In the case of rockets, the thrust force generated during the take-off stage must be equal to or greater than the net mass of the rocket (Greatrix, 2012). This implies that the force generated by water leaving the duct can lift the entire system above a specific reference point.

Before discussing the theory of water jet thrust, it is essential to understand the mathematical equations relating to volumetric and mass flow rate. In all fluid flow analysis, a flow rate exists when the flow has kinetic energy (Miller, 1996). Flow rate may be defined as the volume of fluid that flows past a given cross-sectional area per second (Naidoo et al., 2015a). The equation for volumetric flow rate Q is given by:

$$Q = v\, A_i \tag{2.7}$$

where v is the fluid velocity and A_i is the internal area of the pipe. Mass flow rate may be defined as the mass of fluid that flows past a point in a system per unit time (Sabersky, Acosta, Hauptmann and Gates, 1999). Mathematically, mass flow rate is determined by finding the first derivative of mass with respect to time. The notation used for mass flow rate is given by $\dot{m}$ or $\frac{dm}{dt}$. Mass flow rate can be obtained by multiplying the flow rate of a fluid by the density of the fluid (Fox et al., 2011). The equation for mass flow rate for a fluid flowing through some cross-sectional area A at velocity of V is given by:

$$\dot{m} = \rho Q \tag{2.8}$$

According to Newton's Second Law, force is equal to the rate of change of momentum as described previously. In general, the differential form of thrust force is given by:

$$F_T = \left| \frac{d}{dt}(mv) \right|_i^f \tag{2.9}$$

where F_T represents the thrust force generated, mv represrnts the momentum of the system, i represents the initial or lower limit and f represents the final or upper limit at which the derivative for momentum is evaluated. Equation 2.9 can be simplified using the product rule for differential calculus:

$$F_T = \left|\left(v\frac{dm}{dt}\right) + \left(m\frac{dv}{dt}\right)\right|_i^f \tag{2.10}$$

By using the rules of calculus, the two terms in Equation 2.10 may be separated as follow:

$$F_T = \left|\left(v\frac{dm}{dt}\right)\right|_i^f + \left|\left(m\frac{dv}{dt}\right)\right|_i^f \tag{2.11}$$

This is the general equation for thrust force using Newton's Second Law of motion. This equation models the thrust force generated by a second-order system (Dorf and Bishop, 2001). Equation 2.11 may be expanded using the continuity equation for replacing $\frac{dm}{dt}$ and replacing $\frac{dv}{dt}$ by the second derivative of fluid displacement as follows:

$$F_T = \left|(\rho A v \cdot v)\right|_i^f + \left|\left(m\frac{dv}{dt}\right)\right|_i^f \tag{2.12}$$

Replacing v by $\frac{dx}{dt}$ and $\frac{dv}{dt}$ by $\frac{d}{dt}\left(\frac{dx}{dt}\right)$ and simplifying the result, Equation 2.12 may be expressed as:

$$F_T = \rho A \left|\left(\frac{dx}{dt}\right)^2\right|_i^f + m\left|\frac{d^2x}{dt^2}\right|_i^f \tag{2.13}$$

This equation is a second-order differential equation which requires a mathematical solution for solving an ordinary differential equation (Bennett, 1993). Most fluid flow problems are complex; however, linearization of the thrust equation is sufficient for analyzing most problems (Cengal and Cimbala, 2010). Assuming steady state fluid flow analysis in which the power supply remains constant, implying that mass flow rate remains fixed, then, by continuity:

$$\frac{dm}{dt} = \rho A \frac{dx}{dt} = \text{Constant} \tag{2.14}$$

Differentiating Equation 2.14 with respect to time results in Equation 2.15:

$$\rho A \frac{d^2x}{dt^2} = 0 \tag{2.15}$$

This implies that for steady state fluid flow analysis in which mass flow rate is constant, the acceleration of the fluid flow is zero. Thus, the thrust equation becomes:

$$F_T = \rho A \left|\left(\frac{dx}{dt}\right)^2\right|_i^f \tag{2.16}$$

Back substitution of Equation 2.16 into Equation 2.14 and evaluating the equation from initial to final fluid flow velocity across the system yields:

$$F_T = \left(\frac{dm}{dt}v_f - \frac{dm}{dt}v_i\right) \tag{2.17}$$

Since the assumption for steady state fluid flow analysis is that mass flow rate remains constant, one may factor out $\frac{dm}{dt}$ from Equation 2.17 give the following equation for thrust force (Hall, 2016):

$$F_T = \frac{dm}{dt}(v_f - v_i) \qquad (2.18)$$

The above equation is valid for steady state fluid flow (constant mass flow rate throughout the system of interest) and can be defined by stating that the thrust force generated (rate of change of momentum) by steady state fluid flow is equal to the product of mass flow rate and the change of velocity of the fluid across the system containing the fluid flow (White, 2007). It can be noted that the relationship between thrust force and velocity is exponential to the order of 2. Now consider a system which experiences thrust force from its propulsion system, the power generated from thrust force is given by:

$$\frac{dW_T}{dt} = \dot{W}_T = F_T\,|\vec{v}| \qquad (2.19)$$

where $\dot{W}_T$ represents the power generated by thrust force, F_T represents the thrust force and $|\vec{v}|$ is the absolute value of the velocity of the system being propelled by the thrust force. Substituting Equation 2.18 into Equation 2.19 gives the following equation for power generated by thrust force for a system:

$$\dot{W}_T = \frac{dm}{dt}\,|\vec{v}|\,(v_f - v_i) \qquad (2.20)$$

2.4.3   Control Volume System Analysis

The term system is used to define a subset containing matter or space which is of interest for analysis. A boundary is a fixed or movable surface that separates a system from its surrounding region of matter or space. In general, two types of systems exist: closed system and open system. A closed system is one in which energy transfer may occur across the system boundary, however the net mass of matter within the boundary of the system remains constant. An open system is one in which both mass and energy transfer may occur across the boundary of the system. An alternate term for an open system is a *control volume.* A control volume is used to aid problem solving in various engineering problems. The method of using a control volume is by selecting a region within a device such as turbine or nozzle in which mass flow and energy transfer occurs across the boundary of the system. The use of control volumes may be generalized for any type of mass and energy flow analysis. By considering the laws of classical and quantum physics, this mathematically implies that an arbitrary region in space of finite dimensions may be selected as a control volume for a particular analysis (Belvins, 1989). Figure 2.14 shows an example of a control volume chosen for analysis of fluid flow through convergent nozzle:
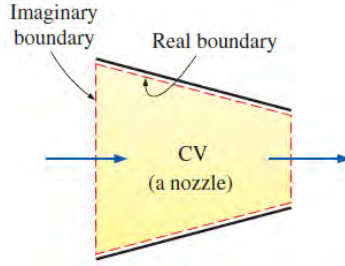
Figure 2.14: Control Volume within a convergent nozzle
Source: Cengal and Cimbala, 2010

Figure 2.14 shows a control volume (bounded by the red-dashed lines) selected for a region of flow within a convergent nozzle. The blue arrows denote the fluid flow directions. Two types of boundaries are used for this analysis: real and imaginary boundary. As illustrated in Figure 2.14, a real boundary is a physical boundary which acts similarly to a closed system type of boundary such that mass flow across a real boundary is not possible. An imaginary boundary permits mass flow and is not physically present in the system (Cengal and Cimbala, 2010).

2.4.4   Conservation Laws

2.4.4.1   Conservation of mass

Consider the control volume of an arbitrary system shown below in Figure 2.15. The control volume is represented by a cube with dimensions x_1, y_1 and z_1. To derive the conservation of mass in differential form, it is required that the control volume is imagined to be shrunk to an infinitesimal size as shown by the small cube having dimensions dx, dy and dz.
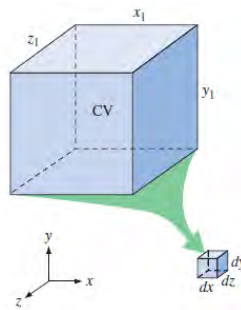
Figure 2.15: Control volume of an arbitrary system
Source: Cengal and Cimbala, 2010

The conservation of mass for a control volume can be expressed in differential form as:

$$\int \frac{\partial \rho}{\partial t} \, dV \bigg|_{CV} + \int \rho(\vec{v}_r \cdot \vec{n}) \, dA \bigg|_{CS} = 0 \qquad (2.21)$$

where $\frac{\partial \rho}{\partial t}$ represents the rate of change of density of the control volume, dV represents the volume of the infinitesimal control volume, $\vec{v}_r$ is velocity relative to the control surface, $\vec{n}$ is the normal vector from the control surface, v is the

fluid velocity, and $\rho(\vec{v}_r \cdot \vec{n}) \cdot dA$ represents the net mass flow rate for an infinitesimal area dA located on the control volume. In the case of a fixed control volume, $\vec{v}_r$ is equal to the fluid velocity. Equation 2.21 is valid for control volume analysis in which the control volume of the system is either in a fixed or dynamic state. In the case when there is an inlet and outlet in the system, the net mass flow rate expression can be defined as:

$$\int \rho(\vec{v}_r \cdot \vec{n}) \, dA \bigg|_{CS} = -\sum_{in} \frac{dm}{dt} + \sum_{out} \frac{dm}{dt} \bigg|_{CV} \tag{2.22}$$

where $\sum_{in} \frac{dm}{dt}$ and $\sum_{out} \frac{dm}{dt}$ represents the net mass flow in and out of the control volume respectively. Substituting Equation 2.22 into Equation 2.21 results in the following:

$$\int \frac{\partial \rho}{\partial t} \, dV \bigg|_{CV} = \sum_{in} \frac{dm}{dt} - \sum_{out} \frac{dm}{dt} \bigg|_{CV} \tag{2.23}$$

This expression represents the conservation of mass. This implies that the rate of change of mass within the control volume is equal to the change of mass flow rate that occurs in the control volume. In another form, it states that the net mass of a closed system, m_{sys}, during some process is constant. That is, the rate of change of the mass of the system, dm_{sys}/dt, within the bounds of a control volume with respect to time is zero (Cengal and Cimbala, 2010). An alternate expression to Equation 2.23 is given by:

$$\dot{m}_{in} - \dot{m}_{out} = dm_{CV}/dt \tag{2.24}$$

where $\dot{m}_{in}$ and $\dot{m}_{out}$ are the total mass flow rates in and out of the control volume bounding the system of reference respectively, and dm_{CV}/dt is the rate of change of mass within the boundaries of the control volume. The conservation of mass equation is better known as the continuity equation (Cengal and Cimbala, 2010). Using the divergence theorem (also known as Gauss's theorem) and applying it to Equation 2.23, the general differential equation for the conservation of mass is given by:

$$\frac{\partial \rho}{\partial t} + \vec{\nabla} \cdot (\rho \cdot \vec{v}) = 0 \tag{2.25}$$

where $\frac{\partial \rho}{\partial t}$ is the rate of change of density, $\vec{\nabla}$ is the grad differential vector, $\vec{v}$ is the velocity vector. Equation 2.25 is valid for both compressible and incompressible flow situations. The grad differential vector is given by:

$$\vec{\nabla} = \left[\frac{\partial}{\partial x} + \frac{\partial}{\partial y} + \frac{\partial}{\partial z} \right] \tag{2.26}$$

where $\frac{\partial}{\partial x}, \frac{\partial}{\partial y}, \frac{\partial}{\partial z}$ represent the partial derivatives in the x-, y- and z-directions respectively. Substituting Equation 2.26 into Equation 2.25 yields the expression for the conservation of mass in Cartesian coordinates:

$$\frac{\partial \rho}{\partial t} + \left[\frac{\partial}{\partial x} + \frac{\partial}{\partial y} + \frac{\partial}{\partial z} \right] \cdot (\rho \cdot \vec{v}) = 0 \tag{2.27}$$

46

The velocity vector in three dimensions can be given by:

$$\vec{v} = \begin{bmatrix} v_x \\ v_y \\ v_z \end{bmatrix} \tag{2.28}$$

where v_x, v_x and v_x represent the fluid velocity vectors in the x-, y- and z-directions respectively. If the density of the fluid remains constant in all three dimensions within the control volume, then the conservation of mass in Cartesian coordinates is given by:

$$\frac{\partial \rho}{\partial t} + \rho \left(\frac{\partial v_x}{\partial x} + \frac{\partial v_y}{\partial y} + \frac{\partial v_z}{\partial z} \right) = 0 \tag{2.29}$$

An alternate form of the conservation of mass is found by expanding Equation 2.27 using the dot product for vector calculus results in:

$$\frac{\partial \rho}{\partial t} + \vec{\nabla} \cdot (\rho \cdot \vec{v}) = \frac{\partial \rho}{\partial t} + \vec{v} \cdot \vec{\nabla}\rho + \rho \vec{\nabla} \cdot \vec{v} \tag{2.30}$$

The term $\frac{\partial \rho}{\partial t} + \vec{v} \cdot \vec{\nabla}\rho$ is called the material derivative of ρ. Dividing Equation 2.30 by ρ yields the expression for the compressible continuity equation in an alternate form:

$$\frac{1}{\rho} \frac{d\rho}{dt} + \vec{\nabla} \cdot \vec{v} = 0 \tag{2.31}$$

Equation 2.31 implies that the density of a fluid particle changes per the change in the divergence of the velocity vector represented by $\vec{\nabla} \cdot \vec{v}$. The divergence of the velocity vector term represents a streamline function which shows the velocity vector along each point of the flow path that a fluid particle follows. Contrary, in the case where changes in fluid density are relatively small that it may be negligible and the magnitude of the divergence of the velocity vector is greater, then the flow may be assumed incompressible. The condition for incompressible flow is expressed by the following relationship:

$$\frac{1}{\rho} \frac{d\rho}{dt} = 0 \tag{2.32}$$

With regards to fluid flow within a duct between two points of reference, state points 1 and 2, the continuity equation may be expressed as:

$$\rho_1 A_1 v_1 = \rho_2 A_2 v_2 \tag{2.33}$$

where ρ_1, A_1, v_1 are the fluid density, duct area and fluid velocity respectively at state point 1, similarly, ρ_2, A_2, v_2 are the fluid density, duct area and fluid velocity respectively at state point 2.

2.4.4.2   Law of Conservation of Energy

The conservation of energy is represented by the Bernoulli equation. The conservation of energy for a closed or open system implies that the total energy transfer to and from a system is equal to the summation of energy content within and the energy transfer across the boundary of the control volume boundary of the system (Cengal and Cimbala, 2010). The conservation of energy is expressed as:

$$\dot{E}_{in} - \dot{E}_{out} = dE_{CV}/dt \qquad (2.34)$$

where $\dot{E}_{in}$ and $\dot{E}_{out}$ are the energy transfer rates in and out of the control volume respectively, and dE_{CV}/dt is the rate of change of energy within the boundary of the control volume of a system.

2.4.5   Fluid Flow Fundamentals

2.4.5.1   Pressure

Pressure is a fluid property that causes forces applied by fluids at rest or in motion as a rigid body. This property is defined as normal force exerted by a fluid per unit area. There are two types of pressure that is commonly referred to, that is absolute pressure and gage pressure. Absolute pressure is the pressure measured relative to a vacuum or absolute zero pressure, and gage pressure is the difference between absolute pressure and local atmospheric pressure. Gage pressure may be either positive or negative in magnitude (Cengal and Cimbala, 2010). The relationship between absolute, gage and atmospheric pressure is given by:

$$P_{gage} = P_{abs} - P_{atm} \qquad (2.35)$$

In the case of negative gage pressure ($P_{abs} < P_{atm}$), the term vacuum pressure is used to indicate the difference between absolute and atmospheric pressure, this is given by:

$$P_{vac} = P_{atm} - P_{abs} \qquad (2.36)$$

2.4.5.2   Reynolds Number

The Reynolds number is a dimensionless number that quantifies the relative influence that viscous and inertia forces have on flow characteristics (Fox et al., 2011). The Reynolds number Re is defined as the ratio of these forces (viscous to inertial) as given below:

$$Re = \frac{\rho \, v \, L}{\mu} \qquad (2.37)$$

In general fluid flow analysis, the density of the fluid, ρ, as well the viscosity of the fluid, μ, are assumed to remain constant (Fox et al., 2011). In this case, the Reynolds number depends only on fluid velocity, v, and the characteristic

length, L. In some cases, the dynamic or kinematic viscosity of a fluid is known. This is defined as the ratio of fluid viscosity and density. The relationship defining kinematic viscosity is shown below:

$$\nu = \mu/\rho \tag{2.38}$$

When kinematic viscosity is more readily available than density and viscosity, one may use the kinematic viscosity for determining the Reynolds number. The Reynolds number can be defined in an alternate form as:

$$Re = uL/\nu \tag{2.39}$$

The Reynolds number is an indicator of the state of fluid flow being either laminar, turbulent or in-between (transitional). One may determine the fluid flow state as laminar, turbulent or transitional by numerically evaluating the Reynolds number. See Appendix A1 for further information on fluid flow state with respect to the Reynolds number.

2.4.5.3   The Bernoulli Equation

The Bernoulli equation is a degenerate form of the conservation of energy and energy equation. This equation gives an approximate relationship between velocity, elevation and pressure (Cengal and Cimbala, 2010). The Bernoulli equation is valid for analysis of fluid flow systems that involve regions of steady state and incompressible flow in which the effects of friction and viscous are negligible; these regions are referred to as inviscid regions of flow. An inviscid region of flow is a region in which the viscous and frictional forces of the flow are not zero, but rather negligible or small in comparison to the other forces acting on the fluid particles. These are regions outside the boundary layers and wakes (Fox et al., 2011). Control volumes are used in which energy transfer occurs by fluid mass flow. The Bernoulli equation may be expressed in various forms, however in most fluid systems it is common to express this equation in terms of pressure and head representations. The Bernoulli equation for the analysis of steady state, inviscid and incompressible fluid flow along a streamline between state points 1 and 2 is expressed as:

$$P_1/\rho g + v_1^2/2g + Z_1 = P_2/\rho g + v_2^2/2g + Z_2 \tag{2.40}$$

In the Bernoulli equation above, $P_1/\rho g$ and $P_2/\rho g$ are called the pressure heads at state point 1 and 2 respectively, $v_1^2/2g$ and $v_2^2/2g$ are called the dynamic heads at state point 1 and 2 respectively, and Z_1 and Z_2 are the vertical elevations at state point 1 and 2 respectively. The units of all terms in the equation given above are in meters. It must be noted that Z_1 and Z_2 are always evaluated above the same reference level. In some cases, where state point 1 is used as a reference point for use of the Bernoulli equation, Z_1 can be assumed to be zero and Z_2 will be the vertical elevation measured from state point 1 to state point 2 (Fox et al., 2011). Bernoulli's equation for fluid flow analysis may also be represented in units of specific energy, J/s. This is achieved by multiplying the equation above by the gravitational acceleration constant, g. In general, Bernoulli's equation states that the sum of the flow, kinetic and potential energies (per unit mass) of some fluid particle in motion under steady state flow conditions along a

streamline is constant, assuming there is no loss of energy from the flow due to friction (Cengal and Cimbala, 2010). A generalized form of the Bernoulli equation in terms of specific energy is given by:

$$P/\rho + v^2/2 + Zg = \text{Constant} \tag{2.41}$$

where, P/ρ is the specific flow energy, $v^2/2$ is the specific kinetic energy, and Zg is the specific potential energy. The Bernoulli equation in terms of specific energy, between state points 1 and 2 along a streamline, is expressed as:

$$P_1/\rho + v_1^2/2 + Z_1 g = P_2/\rho + v_2^2/2 + Z_2 \text{g} \tag{2.42}$$

Bernoulli's equation may also be represented in terms of pressure. This is achieved by multiplying the Bernoulli equation (in specific energy form) by the fluid density, ρ. In general form as stated previously, the Bernoulli equation is expressed as:

$$P + \rho\, v^2/2 + \rho Z g = \text{Constant} \tag{2.43}$$

Each term of this equation is in units of pressure (Pascal). P is the static pressure, $\rho\, v^2/2$ is the dynamic pressure, and $\rho Z g$ is the hydrostatic pressure. The constant, which is the sum of static, dynamic and hydrostatic pressure is called total pressure. The sum of static and dynamic pressure is called stagnation pressure, which represents the pressure at a point where the fluid flow is brought to rest in an isentropic manner (ideally), this can be expressed as:

$$P_{stag} = P + \rho\, v^2/2 \tag{2.44}$$

2.4.5.3.1   Bernoulli equation for pumping systems

The Bernoulli equation given by Equation 2.42 previously is valid for a system in which all energy losses in the system are negligible and there are no external energy devices that add or extract energy from the system. Most real life fluid flow situations involve the use pumps and turbines which add and extract energy from the flow respectively. Furthermore, the effects of losses are present in all fluid flow scenarios involving internal and external flow. Consider a simple pumping system shown in Figure 2.16 in which fluid is transported from the reservoir at state point 1, along the path denoted by the blue arrows, up to the reservoir at state point 2.
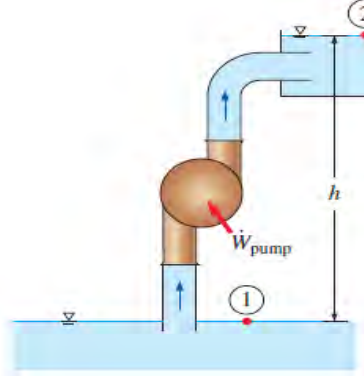
Figure 2.16: Simple pumping system with frictional losses and gravitational effects
Source: Cengal and Cimbala, 2010

It can be observed that state point 2 is located at a vertical height h above state point 1. To achieve transportation of fluid from state point 1 to 2, a pump located between these state points is used to provide the power, $\dot{W}_{pump}$, needed to transport fluid from 1 to 2 as well as overcome the effects of gravity and pressure losses along the flow path. The Bernoulli equation for the system in Figure 2.16 is given by:

$$P_1/\rho g + v_1^2/2g + Z_1 + h_{pump} = P_2/\rho g + v_2^2/2g + Z_2 + h_{loss} \qquad (2.45)$$

where $P_1/\rho g$ and $P_2/\rho g$ are called the pressure heads at state point 1 and 2 respectively, $v_1^2/2g$ and $v_2^2/2g$ are called the dynamic heads at state point 1 and 2 respectively, Z_1 and Z_2 are the vertical elevations at state point 1 and 2 respectively, h_{pump} is the pressure head delivered from the pump, and h_{loss} is the total pressure head loss present in the system between state points 1 and 2. In this system, h is the absolute value of the vertical displacement between state point 1 and 2 which can be represented by Equation 2.46:

$$h = |Z_2 - Z_1| \qquad (2.46)$$

2.4.5.4 Pressure Loss in Fluid Flow Systems

Losses in fluid flow can be characterized as major and minor losses. Major losses consist of the pressure losses caused by frictional effects. Minor losses are caused by changes in pipe geometry which result in expansion of diffusion of fluid flow. Minor losses result in non-linear velocity profiles (Howe, 2006). Assuming there are n sections of pipe with variation in geometry and friction, and m components contributing to minor losses in the system, the equation for total loss of pressure head can be expressed as:

$$\sum h_{loss} = \sum_{0}^{n} h_{fL_i} + \sum_{0}^{m} h_{KL_j} \qquad (2.47)$$

51

where: h_{loss} is total head loss, $\sum_0^n h_{fL_i}$ is the sum of n pipe sections causing friction or major losses, and $\sum_0^m h_{KL_j}$ is the sum of m components causing minor losses in the system. Note that I and j are limited by n and m respectively, which is expressed by the following set of inequalities:

$$0 \ll i \ll n$$

$$0 \ll j \ll m$$

2.4.5.5   Major Losses

Imperfections along the interior surface of pipes result in the development of turbulent boundary layers along the walls of the pipes' inner surfaces. The effects of friction in pipe inner walls can be modelled and understood by use of classical Newtonian physics, Newton's Second Law of motion. The term friction head is a common name used to represent the head loss due to friction in a fluid flow system. The relationship between friction head and flow rate is exponential as shown in Figure 2.17.
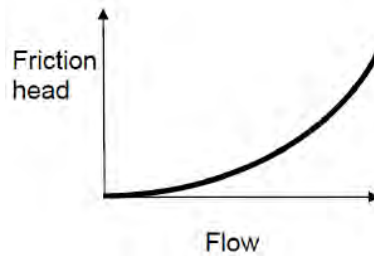
Figure 2.17: Relationship between friction head and flow rate
Source: Howe, 2006

The relationship between friction head and flow rate shown in Figure 2.17 can be mathematically expressed as follows:

$$h_{fL} \propto Q^2$$

If the pipe has constant cross-sectional area, then friction head is proportional to the square of fluid flow velocity:

$$h_{fL} \propto v^2$$

Several other parameters influence the effects of friction for internal fluid flow such as: length of pipe between state points, pipe geometry, gravity, internal pipe surface finish and roughness, Reynolds number, fluid density and fluid viscosity. These relationships can be mathematically expressed as:

$$h_{fL} \propto L$$

$$h_{fL} \propto 1/d$$

$$h_{fL} \propto 1/g$$

$$h_{fL} \propto \epsilon$$

$$h_{fL} \propto \rho$$

$$h_{fL} \propto \mu$$

The relationships given above can be expressed in the form of an equation for friction head, known as the Darcy-Weisbach equation:

$$h_{fL} = \frac{fLv^2}{2dg} \tag{2.48}$$

where f is the Darcy friction factor, L is the total length of pipe between the two state points of interest, v is the fluid flow velocity, d is the internal pipe diameter and g is the gravitational acceleration constant. As previously stated, head loss due to friction in a pipe depends on pipe roughness and the Reynolds number which do not appear in Equation 2.48 (Kiijarvi, 2005). However, the Darcy friction factor is a dimensionless number that accounts for the effects of pipe roughness, Reynolds number, pipe diameter and length of pipe. Several cases for calculating the Darcy friction factor are given in Appendix A.

2.4.5.6 Minor Losses

Minor losses result from components such as fittings, valves, bends, elbows, tees, inlets, outlets, expansions and contractions. When smooth and steady fluid flow encounters such components, flow separation occurs in which non-linearity becomes present in the velocity profile of the flow. Minor losses depend on the loss factor of a component in the system and the square of the maximum fluid velocity in the component. Manufacturers of these components typically specify the loss factors on their data sheets (Fox et al., 2011). In general, a component that causes greater degree of separation and mixing of flow would have a greater loss factor. The equation for minor loss, in the form of pressure head, is given by:

$$h_{KL} = K_L(v^2/2g) \tag{2.49}$$

The total head loss in a piping system can be mathematically expressed by substituting Equation 2.48 and 2.49 into Equation 2.47 which results in the following equation:

$$\sum h_{loss} = \sum_i f_i \frac{L_i v_i^2}{2d_i g} + \sum_j K_{L_j}(v_j^2/2g) \tag{2.50}$$

where i represents each pipe section with constant internal pipe diameter and j represents each component that causes minor loss in the system. In the case of the pipe diameter being constant throughout the system, equation (26) can be expressed as:

$$\sum h_{loss} = \left(f\frac{L}{d} + \sum K_L\right)\left(v_j{}^2/2g\right) \qquad (2.51)$$

2.4.6 External and Aerodynamic Drag Force

When fluid flow occurs over the boundary of a mass, there are aerodynamic forces that are induced on the surface of the mass. These aerodynamic forces are referred to as: lift and drag force. In any environment, which has an atmosphere containing fluid (liquid or gas) of non-zero density (such as air), these forces would be present. Each element of fluid that interacts with the surface of a mass, does so in a two-dimensional manner. The force that each fluid element exerts on a mass can be modelled using Newton's Second Law of motion. In the case of a force analysis on a control volume, the momentum equation can be used. A detailed understanding of the physical phenomena of life and drag force is fundamentally important to engineers and scientists when designing or modelling systems such as an automobile, submarine, aircraft, jets, ships, buildings and megastructures (Cengal and Cimbala, 2010). Drag force is defined as the force that a flowing stream of fluid particles exert on a mass in the direction of the flow stream. Drag is experienced around the body of a rocket after take-off from the earth surface. This is caused by the high-velocity interaction of air particles on the body of the rocket. Drag is also experienced when one drives an automobile along a freeway, leading to increased power requirements from the engine of the automobile to achieve a set magnitude of speed as compared the power requirements from the engine to achieve the same speed in the presence of zero-drag or air resistance (Hoerner, 1966).

There are two types of forces contributing to drag force when fluid flows over a mass of solid particle: pressure and shear stress forces. The drag caused by pressure and shear stress are called pressure drag and skin friction drag respectively. The drag force on a differential element, considering pressure and shear stress forces, is given by:

$$dF_D = -P\,dA\,\cos\theta + \tau_w\,dA\,\sin\theta \qquad (2.52)$$

where P represrnts pressure, τ_w represents shear stress, θ is the angle between the normal vector on the surface of the mass and the flow velocity vector, dA is the area of a differential element located on the surface of the mass. Equation 2.52 represents the drag force experienced by a single differential element, to determine the total drag on the surface of the mass, dF_D must be integrated with respect to area:

$$\sum F_D = \int_{Ai}^{Aj} dF_D \qquad (2.53)$$

where $\sum F_D$ represents the total drag force on the mass, Ai represents the starting area on the surface of the mass, Aj represents the end area on the surface of the mass and dF_D represents the differential drag force on each differential element on the surface of the mass. By substituting the expression for dF_D given in Equation 2.52 into 2.53:

$$\sum F_D = \int_{Ai}^{Aj} \{-P\cos\theta + \tau_w\,\sin\theta\}\,dA \qquad (2.54)$$

These equations predict the total drag force experienced by a mass interacting with a stream of fluid flow. Drag force depends on the density of the fluid, fluid velocity, frontal area of the mass, geometry and orientation of the mass. A dimensionless coefficient, known as the drag coefficient, is used to consider some the effects of shape, size and orientation of mass. The equation defining drag coefficient is given by:

$$C_D = \frac{F_D}{\frac{1}{2} \rho v^2 A} \tag{2.55}$$

where C_D is the drag coefficient, F_D is the drag force, ρ is the fluid density, v is the fluid velocity and A is the frontal area of the mass. The term $\frac{1}{2} \rho v^2$ is referred to as the dynamic pressure. Equation 2.55 shows that drag coefficient is a primary function of the shape and size of the mass, in some cases the drag coefficient may depend on the value of the Reynolds number and surface roughness of the mass. For masses with complex geometry, the drag coefficient at each surface, known as the local drag coefficient, may vary. In this case, the average drag coefficient is used for numerical drag force analysis (Cengal and Cimbala, 2010). The average drag coefficient is given by:

$$C_D = \frac{1}{L} \int_0^L C_{D,x} \, dx \tag{2.56}$$

where: C_D is the average drag coefficient, L is the length of the surface of the mass (known as the characteristic length), $C_{D,x}$ is the local drag coefficient on the surface of the mass of length x, and dx is the length of a differential element on the surface of the mass.

2.4.7 Buoyancy and Stability

2.4.7.1 Buoyancy

Buoyancy is a phenomenon that occurs when an object is submersed in a fluid, such that the fluid exerts an upward force, known as the *buoyant force*, on the object. The buoyant force increases linearly with depth of fluid above the object being submerged. This is due to an increase in the gage pressure at the point where the surfaces of the submerged object are located. Consider a uniformly shaped object of thickness δ, upper surface area, lower surface area, submerged in a fluid, then the gage pressure at the upper and lower surface of the object is given by Equation 2.57 and 2.58 respectively:

$$P_{g,1} = \rho g h \tag{2.57}$$

$$P_{g,2} = \rho g (h + \delta) \tag{2.58}$$

The hydrostatic force exerted on the surface object with area A submerged in a fluid at a point where the gage pressure is above zero, is given by:

$$F_{HYD} = P_{gauge} \, A \qquad (2.59)$$

The buoyant force is determined by the finding the difference of the forces experienced on the upper and lower surface of a submerged body, this is given by:

$$F_B = P_{g,2}A_2 - P_{g,1}A_1 \qquad (2.60)$$

$$F_B = \rho g(h + \delta)A_2 - \rho g h A_1 \qquad (2.61)$$

In the case of a uniformly orientated body with uniform cross-sectional area along its entire thickness, such that the upper and lower surface areas are equal, then the buoyant force can be expressed as:

$$F_B = \rho g \delta A \qquad (2.62)$$

where A is the cross-sectional area of the object submerged. The term δA represents the volume of the body, V_B. The buoyant force equation reduces to:

$$F_B = \rho g V_B \qquad (2.63)$$

where $\rho g V_B$ represents the buoyant force experienced by a body of volume V_B. If the fluid is incompressible, then when a body is submerged in fluid, there would be a volume of fluid being displaced which must be equal to the volume occupied by the body being submerged. In general, the buoyant force acting at the center of mass of a submerged body is equal to the weight of fluid displaced by the object (Gonzalez, 2004). This is referred to as Archimedes' principle, developed by the Greek mathematician and scientist, Archimedes (287-212 BC) (Cengal and Cimbala, 2010). Archimedes' principle can be applied to determine if a body submerged in fluid will float or sink. A body that is partially submerged in fluid will float if the buoyant force acting on the surface of the object is equal to the weight of the object. If the weight of the object is greater than the buoyant force exerted on the surface of the object, the object will sink (Gonzalez, 2004). Figure 2.18 illustrates a case in which the buoyant force is greater than the weight of a submerged object.
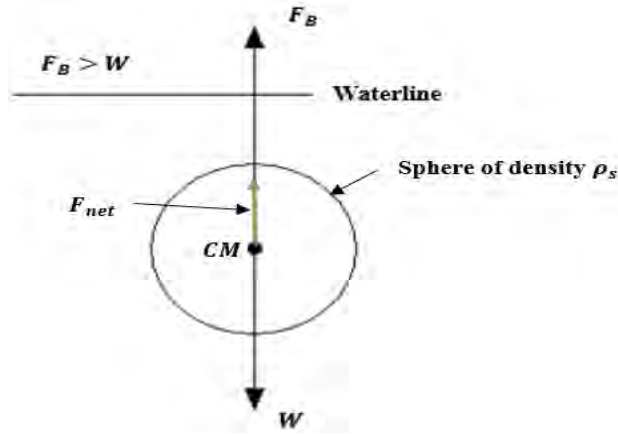
Figure 2.18: Buoyant force greater than weight of submerged object
Source: Gonzalez, 2004

In Figure 2.18 the upward directed arrow labelled by F_B represents the buoyant force acting at the center of mass of the sphere labelled by CM, the downward directed arrow labelled by W, represents the weight of the sphere. The net force, denoted by F_{net}, experienced by the sphere is shown by the green arrow, this is given by the vector sum of the forces acting on the sphere:

$$\vec{F}_{net} = \vec{F}_B + \vec{W} \tag{2.64}$$

By taking forces directed upwards as positive, the magnitude of the net force is given by:

$$F_{net} = F_B - W \tag{2.65}$$

Substituting Equation 2.62 into 2.65:

$$F_{net} = \rho g V_B - mg \tag{2.66}$$

Mass can be expressed as the product of the density of the sphere, ρ_s, and its volume V_B:

$$F_{net} = \rho g V_B - \rho_s V_B g \tag{2.67}$$

Noting that the expression $V_B g$ is common in Equation 2.68, the resulting equation for the net force on the sphere is given by:

$$F_{net} = V_B \, g(\rho - \rho_s) \tag{2.68}$$

In Equation 2.68, if the volume of the submerged object remains fixed, then the term $V_B \, g$ can be treated as a constant, thus the net force is dependent on the difference between the fluid density and the submerged object's density, mathematically expressed as:

$$F_{net} \propto (\rho - \rho_s)$$

Three cases are possible: positive net force, zero net force or negative net force.

Case 1. Positive net force:

$$F_{net} > 0$$

$$\rho - \rho_s > 0$$

$$\therefore \rho_s < \rho$$

This implies that if the density of the object is less than the density of the fluid that it is submerged in, then the object would experience positive net force, directed upwards, and would float on the surface of the fluid.

Case 2. Zero net force:

$$F_{net} = 0$$

$$\rho - \rho_s = 0$$

$$\therefore \rho_s = \rho$$

This implies that if the density of the object is equal to the density of the fluid that it is submerged in, then the object would experience zero net force and would remain neutrally buoyant in the fluid that is submerged in. This assumes that there are no other external forces acting on the object, as this may vary the state of buoyancy of the object.

Case 3. Negative net force:

$$F_{net} < 0$$

$$\rho - \rho_s < 0$$

$$\therefore \rho_s > \rho$$

This implies that if the density of the object is greater than the density of the fluid that it is submerged in, then the object would experience negative net force, directed downwards, and would sink in the fluid that it is submerged in.

2.4.7.2   Stability of Immersed and Submerged Objects

The stability of immersed and submerged objects is a fundamental aspect for the design of water-type crafts such as ships, boats, submarines, jet skis and oil rigs (Cengal and Cimbala, 2010). The variables that affect an immersed or submerged object's stability are: the object's center of mass (CM), and the object's center of buoyancy (CB) (Gonzalez, 2004). The CM is defined as the position in which the weight vector of an object acts. The CB is defined as the centroid position of the volumetric displacement of the object (Brutzman, 1994). When an object is submerged in a fluid, the object's weight acts at the CM and the buoyant force acts at the CB. The condition for stability is that the net moment acting on an object is zero. This differs from the condition for equilibrium which requires both the net force and net moment acting on an object to both equal zero. A submerged or immersed object remains stable when the buoyant force equals to the weight of the object and both these forces act in the same vertical line of action (Fox

et al., 2011), as illustrated in Figure 2.19 (a). In the case when the CM and CB are not located on the same vertical axis, instability would be present. This is illustrated in Figure 2.19 (b).
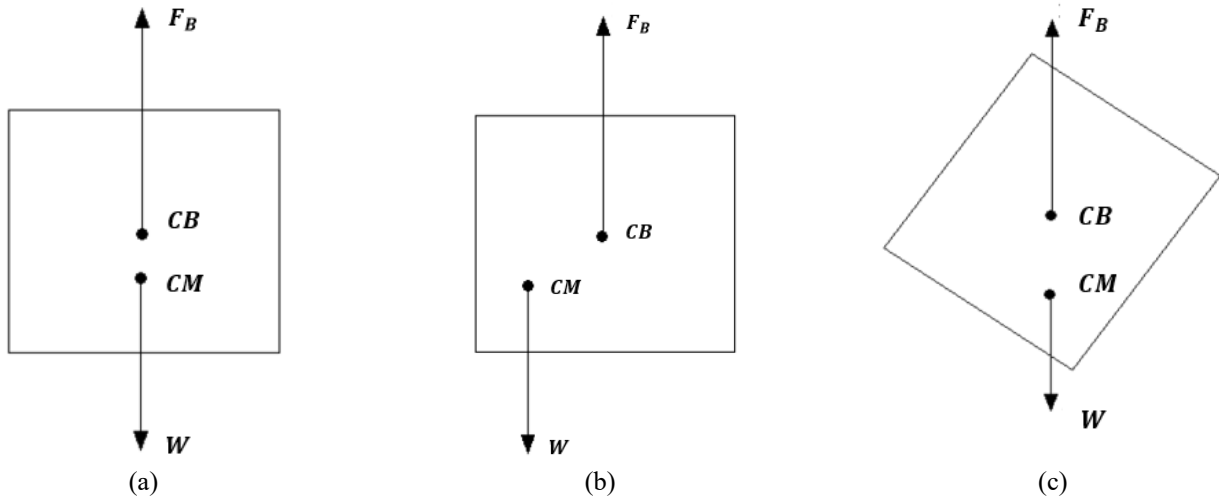
Figure 2.19: Stability of immersed and submerged objects: (a) CM and CB located on same vertical axis, (b) CM and CB located on separate vertical axis, and (c) Heavy bottom configuration
Source: Gonzalez, 2004

In Figure 2.19 (a) the CM and CB are located on the same vertical axis of the object. This would result in zero moment and thus the object remains stable when immersed or floating in a fluid. When the CM and CB are located at the same position, the object would be susceptible to perturbations. From Figure 2.19 (b), it can be noted that when the CM and CB are not located on the same vertical axis, the horizontal distance between *CM* and *CB* is non-zero. Ideally, the CM and CB of the object would be located with a vertical distance apart such that the CM located below the CB. This results in the orientation of the object as shown below in Figure 2.19 (c), such that the object attains dynamic stability with a bottom-heavy configuration where the objects tendency to pitch, roll and yaw movements approach zero when the static and dynamic buoyant force acting along the objects surface cancel each other (Gonzalez, 2004). In Figure 2.19 (c) the object's CM and CB are positioned on the same vertical axis. This orientation is attained when the CM and CB are not aligned and a non-zero horizontal distance exists between *CM* and *CB*. The object would experience a righting moment, M_R. The righting moment would cause the object to rotate about its centroid until it reaches an orientation where *CM* and *CB* are aligned. The righting moment, in general form is given by:

$$M_R = \frac{1}{2} d_{BM} (F_B + W) \qquad (2.69)$$

where M_R represents the righting moment, F_B represents the buoyant force, d_{BM} represents the horizontal distance from the CM to the CB, and W represents the weight of the object. Figure 2.20 illustrates the righting moment caused by an initial unstable state of an object submerged or immersed in a fluid.
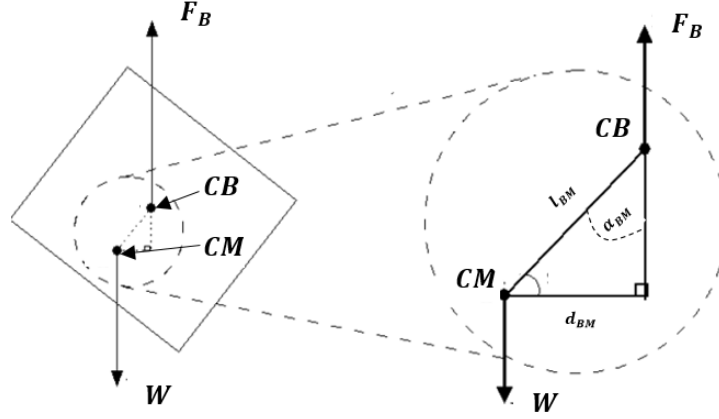
Figure 2.20: Righting moment caused by an initially unstable state of a submerged object
Source: Gonzalez, 2004

Figure 2.20 shows an initially unstable object caused by roll and pitch perturbations (left) in which the horizontal distance between the CM and buoyancy is non-zero, the perpendicular distance between the CM and buoyancy, l_{BM}, can be found by using the horizontal distance, d_{BM} and the angle between the CM and buoyancy, α_{BM}. Equation 2.70 models the righting moment with respect to the horizontal distance between the CM and buoyancy. Using the vector triangle (right of Figure (2.20)), the righting moment equation can be expressed in terms of α_{BM} and l_{BM}:

$$M_R = \frac{1}{2}\, l_{BM}\, (F_B + W) \sin \alpha_{BM} \qquad (2.70)$$

Equation 2.70 shows that in the case where the perpendicular distance between the CM and buoyancy, and the buoyant force and weight all remain constant, then the righting moment varies sinusoidal with respect to the angle between the CM and buoyancy. Equation 2.70 may be re-expressed by substituting the equation for buoyant force and weight as shown in Equation 2.66 previously, which results in the following expression:

$$M_R = \frac{1}{2}\, l_{BM}\, (\rho g V_B + \rho_s V_B g) \sin \alpha_{BM} \qquad (2.71)$$

Factorizing out gV_B as a common factor yields:

$$M_R = \frac{1}{2}\, l_{BM}\, g V_B (\rho + \rho_s) \sin \alpha_{BM} \qquad (2.72)$$

Equation 2.72 for the righting moment is valid for the case of static objects that have no external forces acting on it. In real life situations that involve an object or water craft with propulsion devices such as propeller, then the object or water craft would experience drag force as detailed previously in this chapter. This would require a dynamic analysis and righting moment equation would have to include an expression that approximates the moment caused by the average drag force on the surface of the object or water craft, at a point known as the center of drag (CD). Depending on the complexity of the surface of the object or water craft, the CD can be determined analytically for simple shaped objects or computationally in the case of complex shaped surfaces of an object or water craft. However, the general principle for stability of an immersed or submerged object would still apply for a dynamic analysis such that stability

would be attained when the center of mass, buoyancy and drag are vertically aligned. The righting moment for a dynamic analysis can be expressed as:

$$M_R = \frac{1}{2} l_{BM} (F_B + W) \sin \alpha_{BM} + \frac{1}{2} l_{DM} (F_D + W) \sin \alpha_{DM} \qquad (2.73)$$

where l_{DM} represents the perpendicular distance from the CM and drag, F_D represents the drag force, α_{DM} represents the angle between the CM and drag. Substituting the expression for average drag force across the surface of an object as given previously, considering the expression for the drag coefficient which is also dependent on the orientation of the object, and substituting it into Equation 2.73 yields the general expression for the righting moment equation for an arbitrarily shaped object or water craft:

$$M_R = \frac{1}{2} l_{BM} \, g V_B (\rho + \rho_s) \sin \alpha_{BM} + \frac{1}{2} l_{DM} \left(\left(\frac{1}{L} \int_0^L C_{D,x} \, dx \right) \frac{1}{2} \rho v^2 A + V_B \, \rho_s \right) \sin \alpha_{DM} \quad (2.74)$$

where $\frac{1}{L}\int_0^L C_{D,x} \, dx$ represents the average drag coefficient in integral form, L is the characteristic surface length of the object, $C_{D,x}$ is the local drag coefficient on the surface of the object of length x, dx is the length of a differential element on the surface of the object, $\left(\frac{1}{L}\int_0^L C_{D,x} \, dx \right) \frac{1}{2} \rho v^2 A$ represents the total drag force, and $V_B \, \rho_s$ represents the weight of the object. The remaining symbols represent the physical quantities as previously stated in the previous equations for drag force and the righting moment equation.

2.5   Dynamic Control System Modelling

The theory of control engineering is based on linear system analysis and feedback theory. Control engineering generates the concepts of communication and network theory. The applications of control theory are vast and can be applied in mechanical, civil, chemical, electrical, environmental, and aerospace engineering. A control system is the interconnection of the components that make up the configuration of a system such that a desired system response is achieved. The systematic approach to designing a control system is illustrated in Figure 2.21. There are seven key steps in this process. This approach is applicable to both open-loop and closed-loop feedback control systems.

```
┌─────────────────────────────────────┐
│     1. Establish control goals      │
└─────────────────────────────────────┘
                  │
                  ▼
┌─────────────────────────────────────┐
│   2. Identify the variables to control │
└─────────────────────────────────────┘
                  │
                  ▼
┌─────────────────────────────────────┐
│    3. Write the specifications for the │
│              variables              │
└─────────────────────────────────────┘
                  │
                  ▼
┌─────────────────────────────────────┐
│  4. Establish the system configuration │
│       and identify the actuators    │
└─────────────────────────────────────┘
                  │
                  ▼
┌─────────────────────────────────────┐
│   5. Obtain a model of the process, the │
│        actuator, and the sensor     │
└─────────────────────────────────────┘
                  │
                  ▼
┌─────────────────────────────────────┐
│  6. Describe a controller and select key │
│      parameters to be adjusted      │
└─────────────────────────────────────┘
                  │
                  ▼
┌─────────────────────────────────────┐
│     7. Optimize the parameters and  │
│        analyze the performance      │
└─────────────────────────────────────┘
```
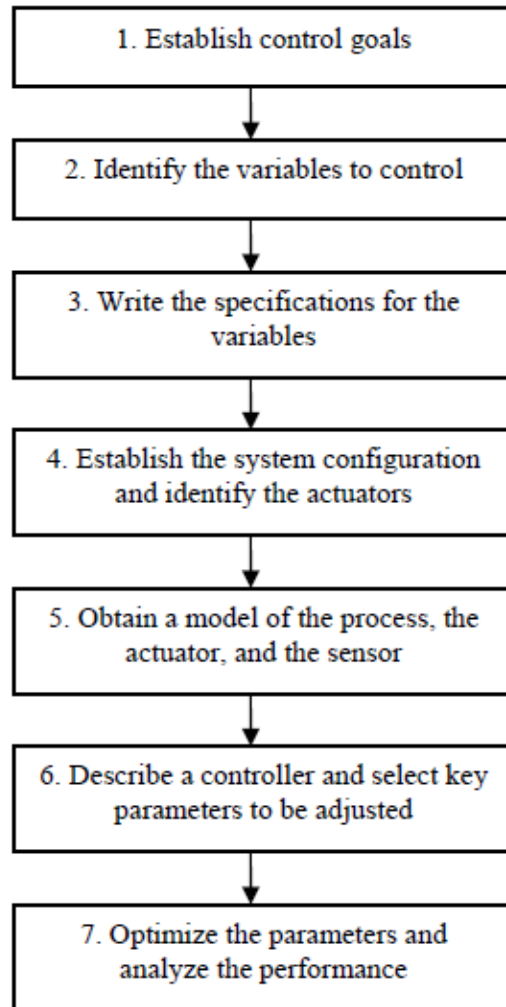
Figure 2.21: Control system design process
Source: Dorf and Bishop, 2001

The first step is to establish the goals of the system. The goals are referred to as *reference signals* of the system. Step 2 is to identify the variables to control, these are the variables that can be changed and are controllable. The controlled variables may be inputs or arbitrary parameters involved in the dynamics of the system. Step 3 involves stating the specifications of the system variables. Step 4 involves establishing a system configuration and identifying the actuators and sensors in the system. Step 5 involves obtaining a dynamic model of system's process, actuator and feedback sensor. Step 6 involves describing a controller and selecting the key parameters to be adjusted. Step 7 involves optimization of the parameters and observation or analysis of the performance of the system with respect to the desired goals set in step 1 (Dorf and Bishop, 2001).

2.5.1　Open-loop Control Systems (OLCS)

An open-loop control consists of an input, an actuating device, a process and an output. In an open-loop system, there is no feedback of the output signal response for comparison with the reference input. Each distinct input results in a corresponding output and therefore the accuracy of the system depends on the accuracy of modelling and calibrating of the system (Bennett, 1993). A block diagram representation of an open-loop control system is shown in Figure 2.22.
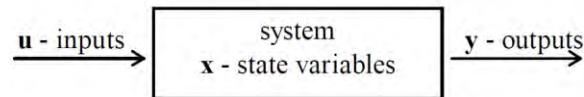
Figure 2.22: Open-loop control system
Source: Dorf and Bishop, 2001

An example of an open-loop system is a washing machine. A washing machine performs three tasks: soaking, washing and rinsing. The process by which these tasks are performed are programmed and performed as a function of time. There is no feedback of the effectiveness and efficiency of the entire process. Open-loop systems are used when the relationship between the input and output of the system are well defined and there are no external factors affecting the performance of the system. The factors affecting the performance of a system are known as *disturbances*. There are two types of disturbances: *input disturbances* and *output disturbances*. Closed-loop feedback control is used to overcome the effects of disturbances (Bennett, 1993). Closed-loop feedback control systems differ from open-loop feedback control systems by measuring the output and comparing the output with a reference signal, which is done using feedback and a controller (Ogata, 2013). Closed-loop feedback control is detailed in Section 2.5.2 to follow.

2.5.2　Closed-Loop Feedback Control Systems (CLFCS)

A closed-loop feedback control system is a system in which the relationship between the output and reference state is maintained by measuring the difference between the reference and output as a form of control of the system. The aim of a feedback control system is to ensure that the output tracks the reference value, this process is termed *tracking*. Other purposes of feedback are to stabilize unstable processes, reduce the effects of external factors that affect the input or output, known as *disturbances*, and lastly to reduce the effect of plant variation (Bennett, 1993). Closed-loop feedback control systems measure the real output of a process and compare this measurement with the desired response, and thereafter send feedback to the systems controller. The measurement of the output of the process occurring in the system is called the feedback signal. The difference between the desired response and the actual output response is the called the *error signal*. The purpose of a controller is to minimize the error signal such that the desired response approximately equals the actual output response of the system over a short period (Ogata, 2013). The controller may be in the form of a manual or digital controller which is discussed in Section 2.5.2.1 and 2.5.2.2 to follow.

2.5.2.1 Manual Control – Closed-Loop Feedback Control Systems

Figure 2.23 shows an example of a car speed closed-loop feedback control system. This is an example of a manually controlled system since the controller is the driver of the car instead of a computer or robot. The process is the car and engine system whereby chemical energy (in the form of fuel) is converted to mechanical energy after a combustion process that occurs in the engine. This results in motion of the car. The input in the system is the angular displacement of the foot pedal (accelerator) and the output is the speed of the car (Packard 2005). This closed-loop feedback control system can be represented by a block diagram as illustrated in Figure 2.23.
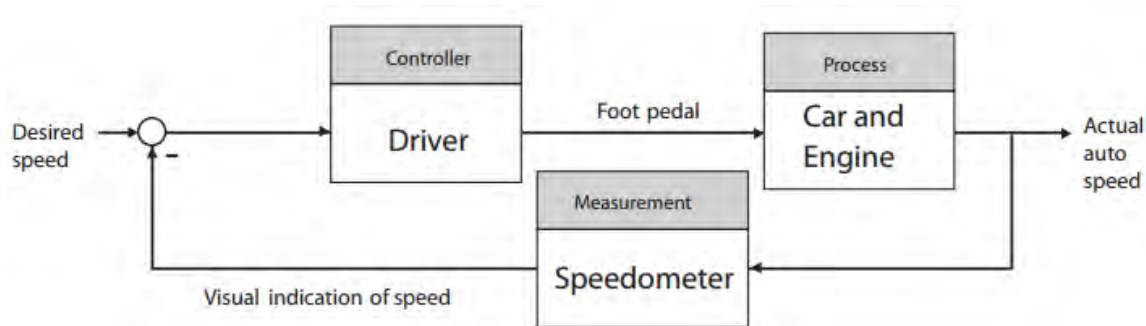
Figure 2.23: Manual closed-loop feedback control system for car speed control
Source: Packard, 2005

The desired speed is referred to as a *reference signal.* The is the controller and has control over the input (angular displacement of foot pedal). The process is the engine and car which converts the input into the output which is the actual speed of the car. A speedometer measures the speed of the car and this signal displays to the driver or controller where the actual speed of the car is compared to the desired speed. The controller then adjusts such as increasing or decreasing the angular displacement of the foot pedal to either increase or decrease the actual speed of the car (Packard, 2005).

2.5.2.2 Digital Speed Control System

The speed control system in an automobile may be digitalized using a computer type controller as illustrated by the digital speed control system in Figure 2.24. In a digitally controlled closed-loop feedback control system, the controller is in the form of a computer or programmed board.
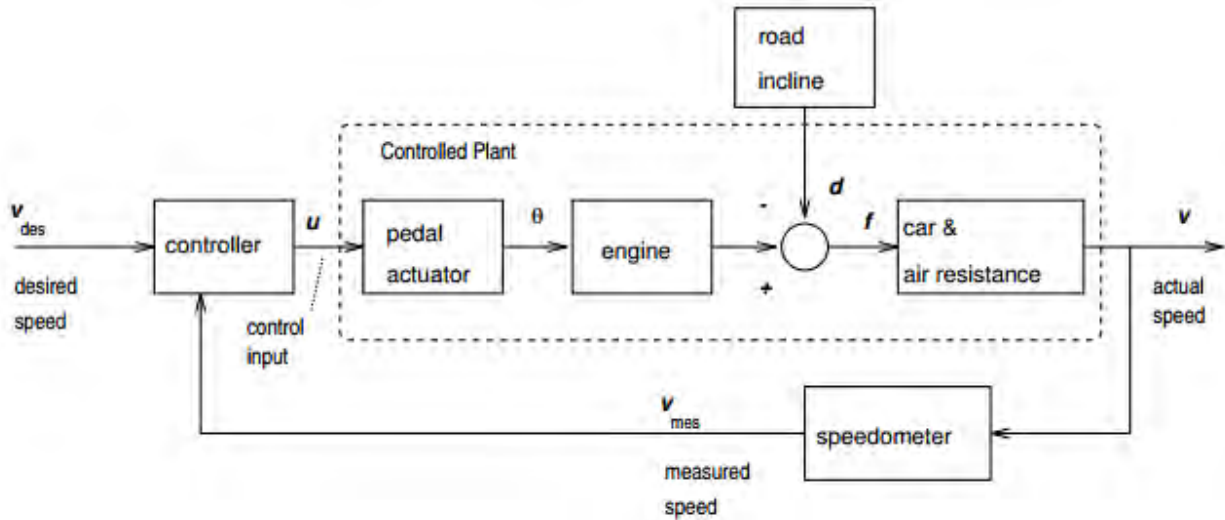
Figure 2.24: Digital closed-loop feedback control system for car speed control
Source: Packard, 2005

In Figure 2.24, the desired speed is set by the driver as a digital input, the controller is in the form of a control board which sends digital signals to the pedal actuator which controls the angular displacement of the accelerator which controls the power output and overall speed of the vehicle. Disturbances such as road inclination may affect the actual speed of the vehicle (Ogata, 2013). Car and air resistance also affect the output speed of the vehicle, which is depending on the aerodynamic drag coefficient and speed of the vehicle, this is represented by a filter block in Figure 2.24. The actual speed of the vehicle is measured by a speedometer and is sent to the controller to change the control input until the actual vehicle speed matches the desired speed as set by the driver. Another example of such a system is an aircraft's autopilot system as illustrated in a block diagram form shown in Figure 2.25.
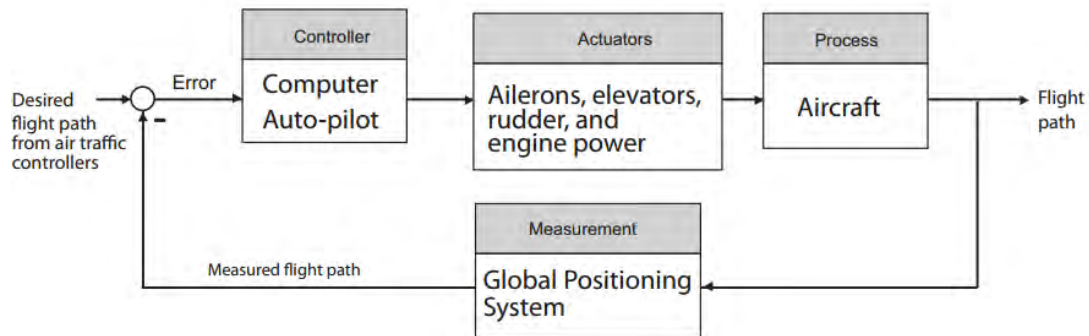
Figure 2.25: Aircraft autopilot closed-loop feedback control system
Source: Packard, 2005

In the case of an auto-pilot flight path control system shown in Figure 2.25, the reference signal is the desired flight path from the air traffic controllers. The controller is the computer auto-pilot which controls the actuators such as the ailerons, elevators, rudder and engine power (Ogata, 2013). The process or plant is the aircraft's aerodynamic performance such as surge, sway, heave motion as well as pitch, roll and yaw moments. The output is the flight path of the aircraft resulting from the aircraft's aerodynamic process. Measurement of the aircrafts flight path is performed

65

by a sensor such as an on-board GPS and the actual flight path of the aircraft is compared to the desired path from the air traffic controllers. The auto-pilot computer system then adjusts the actuators. For example, if the desired path of the aircraft is to reach an arbitrary position (x_2, y_2, z_2) from its current position (x_2, y_1, z_1) in a time of t minutes or hours, then the controller would send signals to the actuators to change the position of the rudder and adjust the power output of the engine such that the aircraft reaches the desired coordinate position in the desired time interval (Packard, 2005).

2.5.3   Proportional-Integral-Derivative (PID) Controllers

A proportional-integral-derivative controller (PID) is a three-term controller that is simple but efficient for the control of most real-world control problems. PID controllers where invented in 1910. PID controllers are the most widely used controllers in industry with more than 90% of industrial controllers based in PID algorithms. PID controllers work by finding the error between a desired response and the actual response of a system, and thereafter controller will minimize the error by adjusting the processes (Ogata, 2013). The transfer function $G(s)$ of a PID controller is given by:

$$G(s) = K_P + \frac{K_I}{s} + K_D s \tag{2.73}$$

where K_P is the proportional gain, K_I is the derivative gain and K_D is the derivative gain. The proportional gain K_P provides overall control action which is proportional to the error signal through the all-pass gain factor. The integral term K_I reduces the steady state error in the system via low-frequency compensation by an integrator. The derivative term K_D improves transient/time response of the system via high-frequency compensation by a differentiator (Kiam; Gregory and Yun, 2005).

2.5.4   Second-Order Transient Response

The transient response of a second-order system is dependent on the dynamic characteristics of the system such as damping factor ξ and natural frequency ω_n (Ogata, 2013). A set of second-order unit-step response curves of *c(t)* against $\omega_n t$ for various damping factor values ranging from 0 to 2 are shown in Figure 2.26 (a) and a second-order transient step response curve is shown in Figure 2.26 (b).
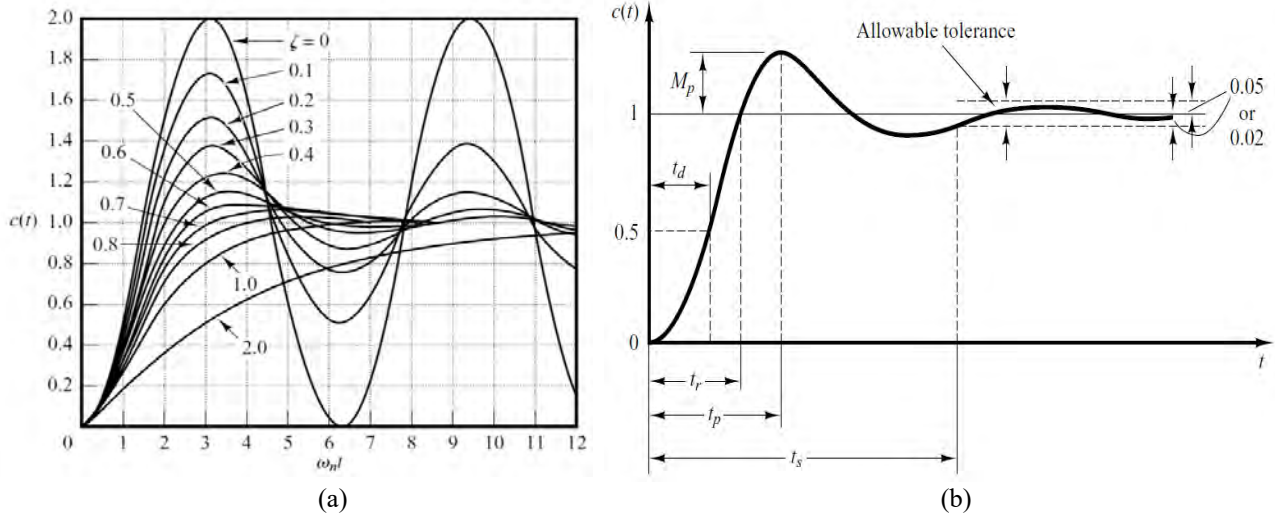
Figure 2.26: Second-order transient response: (a) Series of second-order step response curves, (b) Second-order transient step response curve
Source: Ogata, 2013

Referring to Figure 2.26 (a), it is observed that as the damping factor decreases, the peak amplitude and of the response increases. In Figure 2.26 (b), M_p is the overshoot, $c(t)$ is the system output response as a function of time, t_d is the delay time, t_s is the settling time which represents the time taken for the system to reach its steady state point, t_p is the time to first peak and t_r is the rise time (Ogata, 2013). The equation defining overshoot, is given as:

$$M_p = e^{\frac{-\pi\xi}{\sqrt{1-\xi^2}}} \tag{2.74}$$

A high overshoot is undesirable in most systems, this factor can be controlled using a robust controller (Ogata, 2013). The settling time t_s, is given as:

$$t_s = \frac{4}{\xi\omega_n} \tag{2.75}$$

2.6   Hydrogen Fuel Cells and Air Independent Propulsion

2.6.1   Principle of a Fuel Cell

Fuel cells run on hydrogen which may be derived from hydrocarbons, natural gas or water hydrogen may be extracted through electrolysis which may be powered by renewable energy sources such as solar, wind or electricity from burning fuel. The first demonstration of a fuel cell was shown by a scientist named William Grove in 1839, using an experiment along the lines of that shown in Figure 27. The structure of a fuel cell is basic and consists of two electrodes, anode and cathode and a layer of electrolyte between the anode and cathode. The layer of electrolyte allows the flow of ions to occur. In Figure 2.27 (a) below, water is being electrolyzed into hydrogen and oxygen by passing an electric current through it, this is called the separation phase. In Figure 2.27 (b), the power supply has been replaced

with an ammeter, and a small current is flowing, this is called the recombining phase. The electrolysis is reversed such that the hydrogen and oxygen recombine such that electric current is generated (Karlström, 2007).

(a)   (b)
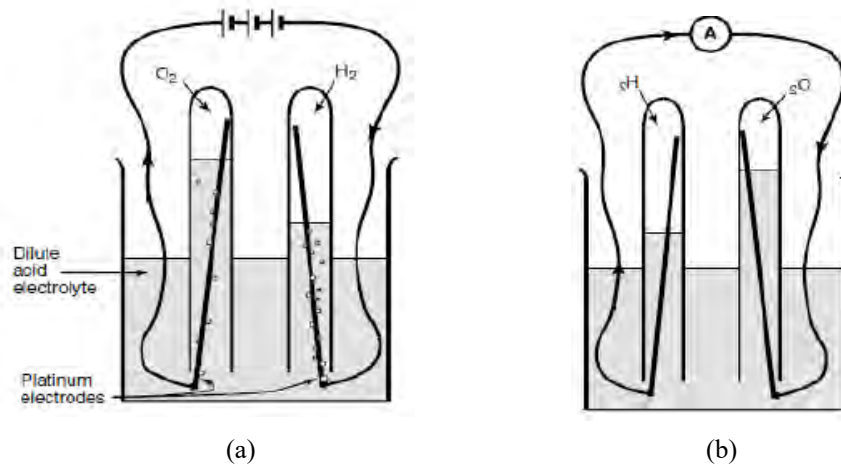
Figure 2.27: The electrolysis of water: (a) Separation phase, (b) Recombining stage

Source: Karlström, 2007

2.6.2   Advantages and Disadvantages of Fuel cells

The main advantages of fuel cell systems are that fuel cells have: low emissions of greenhouse gases, higher efficiency than conventional internal combustion engines, simplicity by having fewer moving components, good reliability and long lasting system, silent source of power. The disadvantages of a fuel cell are: limited lifetime, high cost, hydrogen must be produced for operation of the cell (Emanuelsson and Persson, 2007).

2.6.3   Efficiency, Power and Lifetime

The efficiency of a fuel cell depends on the quantity and type of components used. Typical energy efficiency of a fuel stack can reach up to 80%. The efficiency from chemical to kinetic energy in an average car engine ranges from 30% to 40% compared to that of a typical internal combustion engine which has efficiencies in the range of 12% to 22% (Karlström, 2007). The power consumed by the load effects the lifetime of a fuel cell such that a smooth power consumption without peaks is desired as this increases the life of a fuel cell. This means that lifespan of a fuel cell is higher when there are minimum fluctuations of power consumption by a given load (Emanuelsson and Persson, 2007).

2.6.4   Hydrogen Air Independent Propulsion

Air Independent Propulsion (AIP) is a type of system in which a fuel and its oxidizer are reacted within a device that generates electrical energy and can occur in air or underwater. When used for underwater applications, AIP may improve an underwater craft's (such as an AUV) submerged capability since the propulsion system may operate underwater. The difference between traditional batteries and AIP systems is that batteries contain a finite amount of

energy which is dependent on the amount of reactant contained internally in the battery, however, AIP systems are limited by the number of reactants that are carried. When comparing an AIP and battery system of same size and capacity, the difference is that AIP systems may be refueled at a quicker rate than the rate at which the battery would recharge (Karlström, 2007).

The input of an AIP system is chemical energy from the reactants and the output of an AIP system is electrical energy that is generated, thus the efficiency of an AIP system is the ratio of the AIP system output to input. An increase in the AIP system efficiency results in an increase in attainable depth of an AUV containing an AIP system. Furthermore, increasing the AIP system efficiency would reduce the cost of the fuel and oxide in the system as well as improve the AUV performance. The performance of the system is dependent on the power density, higher power density results in greater performance of the system. Fuel cells are suitable for AIP propulsion in an underwater vehicle. Figure 2.28 illustrates the use of a fuel cell for AIP propulsion in an underwater vehicle. The system illustrated shows how power is delivered to the propeller of the underwater vehicle (Mart and Margeridis, 1995).
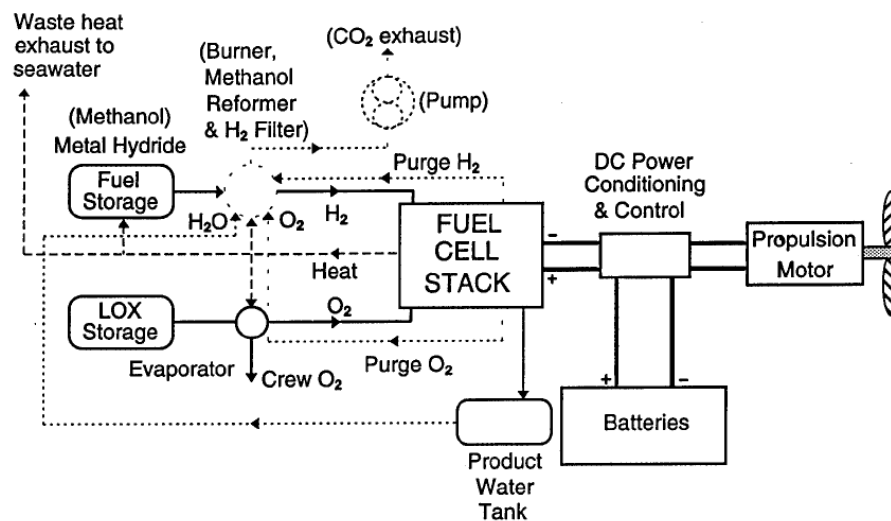
Figure 2.28 Fuel cell system for AIP propulsion of an underwater vehicle
Source: Mart and Margeridis, 1995

The waste heat flow of the exhaust is either sent to the sea water or recirculated into the system such that heat exchangers are used to perform heat transfer to essential subsystems. The fuel source (hydrogen) is generally stored in metal hydrides. Oxygen is obtained through an evaporation process of liquid oxygen (LOX) which enters the fuel cell stack. The essential subsystems required for operation of the fuel are shown by the dotted line boundaries. Heat is supplied for the endothermic reaction of burning fuel and hydrogen gas. Carbon dioxide is an exhaust gas which is disposed to seawater by a pump. The fuel cell stack utilizes the hydrogen and oxygen gas to generate electrical power. The electrical power is passed to a direct current (DC) motor with a controller, which then passes electrical current to the propulsion motor and batteries. The propulsion motor converts electrical energy to mechanical energy which results in rotation of the propeller (Mart and Margeridis, 1995).

CHAPTER 3 : MODELLING OF A WATER JETPACK AND AUV SYSTEM

3.1   Scope and Aim

In this chapter, a series of static and dynamic models of the water jetpack and its propulsion system are presented. The aim of this chapter is to develop a system of equations to model the steady state and transient motion of a water jetpack and AUV system which is used to generate an optimization model code for the water jetpack propulsion system in Chapter 5, develop a MATLAB Simulink model in Chapter 6, and develop a computational model of the system in Chapter 7. Several laws of fluid dynamics are required to accurately model the fluid and aerodynamic performance of a water jetpack. This includes Newton's Second Law, conservation of momentum, conservation of mass and the continuity equation, conservation of energy and Bernoulli's equation, and the drag force equation. The basic derivation and details of the governing equations contained in this chapter are presented in the fluid dynamics literature of Chapter 2. To model the water jetpack and its propulsion system, it is required to select several state points of interest whereby the laws of fluid dynamics at each state point may be used. It must be noted that the wye system located on the jetpack is by-passed in this analysis as this system requires greater detail to model its fluid propulsion characteristics which depend largely on geometry of this system (Naidoo et al., 2015a). A computational model and simulation of the wye system is presented in Chapter 7.

3.2   Water Jetpack Propulsion System State Points

Figure 3.1 shows the three state points used in this model: 1) AUV inlet (state point 0), feed hose (state point 1) and jet-exit (state point 2). These state points are essential and sufficient to model the propulsion characteristics and performance of the jetpack system for various states of motion. Figure 3.1 shows the three state points (state points 0, 1 and 2) along with the corresponding fluid velocity, area and vertical height at each state point. State point 0 is the region where water enters the AUV's inlet section to the water jetpack propulsion system pump. The total pressure at state point 0 depends on the dynamic state and depth of the AUV. State point 1 may be assigned to the flow characteristics on any point along the full length of the feed hose, which is located between the exit of the water jetpack propulsion system pump and the inlet of the water jetpack wye system. State point 2 is the exit of water jetpack nozzle, this point will be referred to as the 'jet-exit' throughout this dissertation. Since the pressure at the jet-exit point is equal to atmospheric pressure, the total pressure at the jet-exit is dependent on the velocity of the water at the exit of the nozzle. The greater the velocity at the jet-exit, the greater the total pressure, causing an increase in the thrust force generated by the water jetpack propulsion system (Etter et al., 1980).
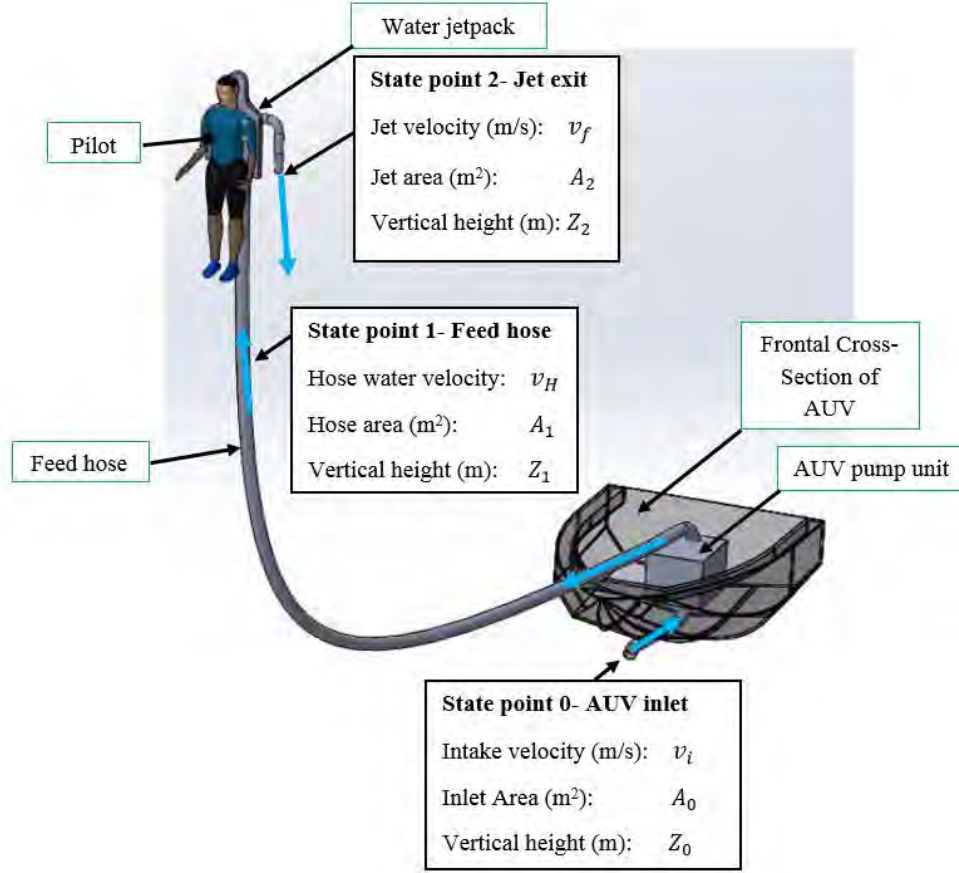
Figure 3.1: Water jetpack propulsion system state points
Source: Little et al., 2015

3.3   Model Development and Newton's Second Law

The water jetpack propulsion system along with static and dynamic modelling of the entire jetpack propulsion system is highly dependent on the physical state of the system. The physical state refers to the position, velocity and acceleration of the water jetpack, pilot and feed hose which together form the jetpack propulsion system. It is fundamental to apply Newton's Second Law of motion to any type of mathematical model when describing the state of water flow in the propulsion system or to understand the motion of the system. A detailed description of Newton's Second Law along with the thrust equation is presented in Section 2.3 of Chapter 2 in this dissertation and the resulting form of this law is applied in the modelling presented in this chapter. Newton's Second Law in vector form for a system is given by:

$$\vec{F}_{net} = m\vec{a} \tag{3.1}$$

where $\vec{F}_{net}$ is the net force vector on the system, m is the total mass of the system and $\vec{a}$ is the acceleration vector of the system. Equation 3.1 is applied and used as the baseline equation of force balance for all mathematical models developed in this chapter. The notation of Equation 3.1 is varied for each type of model and depends on direction

since the net force and acceleration term in Equation 3.1 are vectors. For all vectors, upward direction is taken as positive throughout this dissertation.

3.4   Accumulative Mass Model

The mass term in Newton's Second Law is usually constant for most dynamic systems. However, since the jetpack propulsion system is modelled from state point 0 to state point 2, the mass of the jetpack system (pilot, jetpack and feed hose) varies with respect to vertical height of the jetpack and pilot. This is due to the linear increase of volume of water contained in the feed hose being lifted along with the jetpack and pilot. This changes the dynamics of the system as the added mass from water being lifted must be modelled into the force balance equation. In the case of rocket propulsion, the mass of the system decreases with height since the fuel is burned and thus the total mass changes. The water jetpack works in a similar, opposing manner. Assume there are N masses of different mass contributing to the total weight of the jetpack system. Then the net force on the system can be expressed as:

$$\sum F_{net} = \sum_{k=1}^{N} m_k \frac{dv}{dt} \qquad (3.2)$$

where m_k is the mass of some sub-system k, and dv/dt is the rate of change of velocity with respect to time. The sub-script k varies incrementally from 1 to N. N is the total number of sub-systems that contribute to the mass of the jetpack system. In general, the mass model represents the mass of the system that is above the surface of the water. These masses are: dry mass of the jetpack and hose, mass of the pilot, and the mass of the water contained in the system above reference water level. Setting N as 3, the total mass of the system can be expressed as:

$$\sum_{k=1}^{3} m_k = m_{jetpack} + m_{pilot} + m_{water} \qquad (3.3)$$

where m_{water} is the mass of water being lifted, $m_{jetpack}$ is the mass of the jetpack and m_{pilot} is the mass of the pilot. The fixed masses in Equation 3.3 are the mass of the jetpack and pilot. The mass of water in the system varies with respect to vertical height such that:

$$m_{water} = \rho A_1 Z_2 \qquad (3.4)$$

where m_{water} is the mass of water is in the system, ρ is the density of water, A_1 is the area of the feed hose and Z_2 is the vertical height above the level of the water surface. Equation 3.4 models the mass of water in the feed hose. However, the mass of water in the wye system located on the jetpack is not accounted for in this model. One method of accounting for this mass is by adding the mass of water in the wye to the mass of the jetpack itself, the resulting mass is called the *jetpack flooded mass,* denoted by $m_{flooded}$. The flooded mass of the jetpack depends on the exact geometry of the wye system to determine the volume and mass of water in the wye system. This is unknown at this stage of the model development and therefore a method of approximating the mass ratio of water in the feed hose and wye system is employed. This alternate approach is employed by modifying Equation 3.4 with a correction factor κ.

The correction factor accounts for the mass of water contained in the miscellaneous components of the jetpack propulsion system. In general, a correction factor between 1.05 and 1.2 yields sufficient accuracy. As the vertical height increases κ tends closer to 1.05 as mass of the miscellaneous sub-systems becomes negligible when compared to the mass of water in the hose and κ tends closer to 1.2 as vertical height decreases, this is when the mass of water in the miscellaneous sub-systems become significant (Little et al., 2015). Modifying Equation 3.4 with the use of this correction factor gives:

$$m_{water} = \kappa \, \rho \, A_1 \, Z_2 \tag{3.5}$$

where m_{water} is the mass of water in the system, κ is a general correction factor, ρ is the density of water, A_1 is the area of the hose feeding water into the jetpack, and Z_2 is the height above the level of the water surface. For the analysis contained in this dissertation, κ is assumed as 1.1 as this accounts for both high and low altitude flight modelling of the system. Substituting Equation 3.5 into Equation 3.3 gives the equation for the mass accumulative model as:

$$\sum_{k=1}^{3} m_k = m_{jetpack} + m_{pilot} + \kappa \, \rho \, A_1 \, Z_2 \tag{3.6}$$

Since the mass of the jetpack and pilot remain fixed, one may replace $m_{jetpack} + m_{pilot}$ by a new mass variable denoted by m_{dry} which represents the total mass of the system being lifted excluding the mass of water in the system. Therefore, the summation of mass in the system given in Equation 3.6 can be expressed as:

$$\sum m = m_{dry} + \kappa \, \rho \, A_1 \, Z_2 \tag{3.7}$$

It can be deduced from Equation 3.7 that the total mass of the system increases when the feed hose diameter is high and when vertical height/flight altitude increases. In mathematical terms, the total mass of the system is proportional to the square of feed hose diameter and linearly proportional to flight altitude. A graphic representation of the mass accumulation model obtained from analysis of the UKZN Water Jetpack designed by Naidoo et al. (2015a) is illustrated in Figure 3.2 showing the mass of water being lifted by a jetpack propulsion system which contained a feed hose diameter of 100 mm, pilot mass of 70 kg and a jetpack mass of 15 kg giving a dry mass of 85 kg.
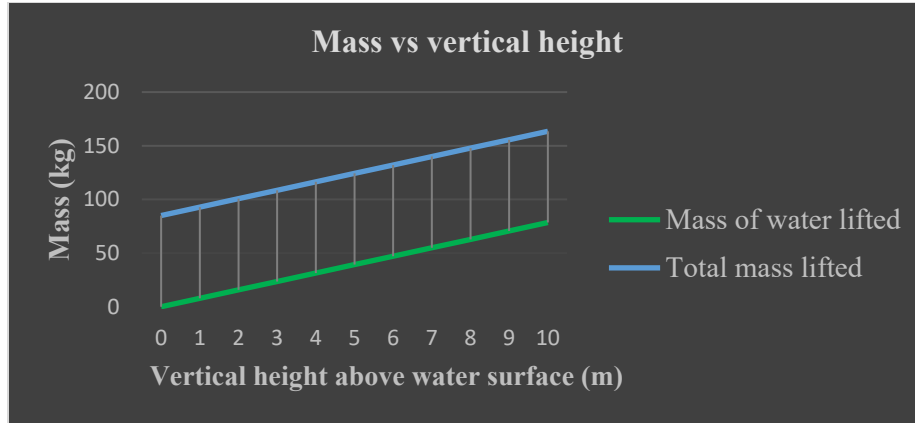
Figure 3.2: Mass of water and total mass lifted
Source: Naidoo et al., 2015a

Referring to Figure 3.2, the vertical axis represents mass, the horizontal axis represents the vertical height above the water surface/flight altitude, the green line shows the increase in mass of water contained in the feed hose, and the blue line shows the total increase of mass in the system. At the take-off phase, the vertical height above the water surface is zero, hence the total mass of the system is equal to the dry mass. As vertical height above the water surface increases, the mass of water in the feed hose being lifted increases linearly as described by Equation 3.7. According to Newton's Second Law, increasing vertical height would also require an increase in thrust force generated by the jetpack propulsion system. Referring to the blue line representing total mass in Figure 3.2, at a vertical height of 10 m above the water surface, the mass of water being lifted reaches approximately 78 kg. In an ideal situation, this would require almost double the amount of thrust force required to sustain a steady state flight by hovering at a fixed position of 10 m above the water surface. This observation clearly proves the significance of using the accumulative mass model as described by Equation 3.6.

3.5   Water Jetpack Coordinate System

In this study, the entire water jetpack system along with the pilot and feed hose is modelled for flight in the x, y and z-directions respectively. This requires the selection of an appropriate three-dimensional coordinate system for both the pilot and jetpack system (referred to as the body-fixed coordinate system) and an earth fixed or global coordinate system, such a system is illustrated in Figure 3.3.

Body fixed coordinate system

Heave velocity (m/s): v_z
Yaw angular rate (rad/s): v_ψ
Force in z-direction (N): F_z
Yaw moment (N.m): M_ψ

Earth fixed /global coordinate system

Height (m): z
Yaw angle (rad): ψ

Y-position (m): y
Pitch angle (rad): ψ

z

θz

θy

r

θx

X-position (m): x
Roll angle (rad): ϕ

Sway velocity (m/s): v_y
Pitch angular rate (rad/s): v_θ
Force in y-direction (N): F_y
Pitch moment (N.m): M_θ

Surge velocity (m/s): v_x
Roll angular rate (rad/s): v_ϕ
Force in x-direction (N): F_x
Roll moment (N.m): M_ϕ

Figure 3.3: Water jetpack coordinate system

The purpose of using both the body-fixed coordinate system and the earth fixed coordinate system is to develop the static and dynamic models of jetpack system relative to the earth fixed coordinate system. The earth fixed or global coordinate system is shown on the right in Figure 3.3 and defines the x-, y- and z-directions and their angular components denoted by ϕ, θ and ψ respectively. Angular positions about the x-, y- and z-directions are termed as roll, pitch and yaw angle respectively. The body-fixed coordinate system shown on the left in Figure 3.3 defines the velocity, angular rate, force and moment experienced by the water jetpack system in the x-, y- and z-directions. The velocity in the x-, y- and z-directions are termed surge, sway and heave velocity respectively. The angular rate in the x-, y- and z-directions are termed as roll, pitch and yaw angular rate respectively. The moment in the x-, y- and z-directions are termed roll, pitch and yaw moment respectively.

3.6   Water Jetpack One-Dimensional Modelling

In this section, one-dimensional steady state and transient models are developed for the water jetpack system for motion in the z-direction. The analysis contained in this section detail the force, velocity, acceleration and thrust force experienced by the water jetpack system along with the pressure rise and power requirements from the propulsion system pump located in the AUV. The steady state models developed in Section 3.6.1 are used as part of the propulsion system optimization process modelling in Chapter 5. Throughout this section, the water jetpack system is modelled to

travel linearly in the z-direction without the effects of drag force. However, the effects of drag force on the water jetpack system is considered in the models developed in Section 3.7 and Section 3.8.

3.6.1   Steady State Static Hovering

In this model, the jetpack system will be modelled for steady state static hovering at a fixed position in air such that its flight altitude remains constant. Newton's Second Law in the z-direction may be expressed as:

$$\sum F_z = \sum m \frac{dv_z}{dt} \tag{3.8}$$

where $\sum F_z$ is the net force in the z-direction, $\sum m$ is the total mass of the jetpack system, and $\frac{dv_z}{dt}$ is the rate of change in velocity of the jetpack system in the z-direction. In the z-direction, two forces act on the jetpack and human: 1) thrust and 2) weight, therefore the force balance in the z-direction is given by:

$$\sum F_z = F_T - \sum W \tag{3.9}$$

where F_T is the thrust force produced by the water jet and $\sum W$ is the total weight of the jetpack system. Equating Equation 3.8 with Equation 3.9 gives the following result:

$$\sum m \frac{dv_z}{dt} = \dot{m}(v_f - v_z) - \sum m\, g \tag{3.10}$$

where $\dot{m}$ is the mass flow rate of water through the system, v_f is the water jet-exit velocity and g is the gravitational acceleration constant. For the condition of steady state static hovering, the jetpack will be assumed to hover stationary in the air, thus the acceleration term $\frac{dv_z}{dt}$ and the velocity term v_z, are both equal to zero. For these conditions, Equation 3.10 reduces to the following:

$$0 = \dot{m}(v_f - 0) - \sum m\, g \tag{3.11}$$

Since this model is based on static hovering conditions, the mass flowrate or water in the propulsion system can be assumed to be in the steady state transition, and thus assumed to remain constant. Using the continuity equation defined in Section 2.3 of Chapter 2, the mass flow rate may be expressed in terms of the jet-area and jet velocity such that:

$$\dot{m} = \rho A_2 v_f \tag{3.12}$$

where ρ is the density of water and A_2 is the jet-exit area. The differential notation for mass flow rate is dm/dt. This notation was used when deriving an expression for the rate of change of a differential mass element from first principles using the conservation of mass as detailed in Section 2.3 of Chapter 2. Making the jet-exit velocity v_f the subject of Equation 3.12:

$$v_f = \frac{\dot{m}}{\rho A_2} \tag{3.13}$$

Substituting Equation 3.13 into Equation 3.11 and manipulating the result to obtain an expression for the mass flow rate during steady state static hovering gives:

$$\dot{m} = \sqrt{\rho A_2 g \sum m}$$ (3.14)

where the expression $\sqrt{\rho A_2 g \sum m}$ represents the minimum required mass flow rate through the propulsion system to attain steady state static hovering. By manipulating Equation 3.14, the total mass carried at this steady state static hovering condition for a fixed mass flow rate is given by:

$$\sum m = \frac{\dot{m}^2}{\rho A_2 g}$$ (3.15)

Substituting the mass accumulative model equation into Equation 3.14 gives an expression relating mass flow rate and static hover height:

$$\dot{m} = \sqrt{\rho A_2 g \left(m_{dry} + \kappa \rho A_1 Z_2 \right)}$$ (3.16)

Equation 3.12 models the relationship between mass flow rate and flight altitude. Contrary to this, by manipulating Equation 3.16, the model for flight altitude as a function of mass flow rate is given by:

$$Z_2 = \frac{\dot{m}^2 - \rho g A_2 m_{dry}}{\kappa \rho^2 g A_1 A_2}$$ (3.17)

Substituting the continuity expression in Equation 3.12 into Equation 3.16 and manipulating the result to obtain the jet-exit velocity results in the following:

$$v_f = \sqrt{\frac{\left(m_{dry} + \kappa \rho A_1 Z_2 \right) g}{\rho A_2}}$$ (3.18)

Equation 3.18 models the jet-exit velocity as a function of dry mass, feed hose and jet-exit area, and flight altitude. By applying the continuity equation given in Section 2.3 of Chapter 2, the velocity of water in the feed hose is given by:

$$v_H = \frac{A_2}{A_1} v_f$$ (3.19)

Substituting Equation 3.19 into Equation 3.18 gives:

$$v_H = \frac{A_2}{A_1} \sqrt{\frac{\left(m_{dry} + \kappa \rho A_1 Z_2 \right) g}{\rho A_2}}$$ (3.20)

Equations 3.8 to 3.20 model the performance of the jetpack propulsion system from state point 1 to state point 2. The next step required to model the system between state point 0 to state point 2 uses the Bernoulli equation across these

state points to determine the total power required and total pressure rise across the AUV pump. Bernoulli's equation is detailed in Section 2.3 of Chapter 2; applying the Bernoulli equation between state point 0 and 2 results in Equation 3.21:

$$P_0/\rho g + v_i^2/2g + Z_0 + h_{pump} = P_2/\rho g + v_f^2/2g + Z_2 + h_{loss} \qquad (3.21)$$

To simplify the model and account for ideal flow characteristics, Equation 3.21 is altered by the following assumptions:

1. The internal surfaces of all the propulsion system elements are hydraulically smooth, hence a friction factor for the feed hose can be selected using the Moody diagram (Moody, 1944) or one of the empirical methods presented in Appendix A.
2. The pressure at state point 0 and state point 2 are both equal to atmospheric pressure such that: $P_0 = P_2 = P_{atm}$. This allows cancellation of the static pressure terms in Equation 3.21.
3. Since this model is developed for the case of the entire jetpack and AUV under static condition, the intake velocity is zero ($v_i^2 = 0$).
4. The reference height is taken at state point 0, thus $Z_0 = 0$.

By applying the assumptions mentioned above to Equation 3.21, the expression for the pressure head required by the pump of the AUV is obtained and given by:

$$h_{pump} = v_f^2/2g + Z_2 + h_{loss} \qquad (3.22)$$

Substituting the expression for the pressure head loss in Section 2.3, into Equation 3.22 yields:

$$h_{pump} = v_f^2/2g + Z_2 + \sum_i f_i \frac{L_i v_i^2}{2d_i g} + \sum_j K_{Lj}\left(v_j^2/2g\right) \qquad (3.23)$$

where i represents each pipe section of the jetpack propulsion system that has a constant internal pipe diameter and j represents each component of the water jetpack propulsion system that contributes to a minor loss in the jetpack propulsion system. In Equation 3.23, the major loss term is related to the losses that occur due to friction in the feed hose and therefore i would represent the conditions at state point 1. The minor losses, as detailed in Chapter 2, are due to the bends and flow area reduction leading to flow acceleration and flow area expansion which leads to flow diffusion (Fox et al., 2011). Therefore, j cannot represent the conditions at a single and isolated state point in the system; it represents a summation of the minor losses at each state point with its distinct variable flow area conditions. Therefore, Equation 3.23 may be simplified to:

$$h_{pump} = v_f^2/2g + Z_2 + f \frac{L v_H^2}{2d_1 g} + \sum_j K_{Lj}\left(v_j^2/2g\right) \qquad (3.24)$$

The minor loss term, $\sum_j K_{Lj}\left(v_j^2/2g\right)$, is the only term that is unknown at this stage as it depends on the flow area within the wye system of the water jetpack. Referring to Fox et al. (2010) and the work by Naidoo et al. (2015b), the

total pressure loss due to minor losses in the system is proportional to the dynamic head term by a factor of approximately 0.2. Thus, to simplify Equation 3.24, it will be assumed that the total pressure head loss due to minor losses in the system equate to approximately 20% of the dynamic head term, $v_f^2/2g$, such that:

$$\sum_j K_{L_j}\left(v_j{}^2/2g\right) \cong 0.2\, v_f^2/2g \tag{3.25}$$

Substituting Equation 3.25 into Equation 3.24 gives the following:

$$h_{pump} = 1.2 v_f^2/2g + Z_2 + f\frac{L v_H{}^2}{2 d_1 g} \tag{3.26}$$

The assumption of using an approximate value of 20% assumes that the major loss is primarily due to the loss that occurs through the wye system of the jetpack at the region where the incoming flow from the feed hose is divided equally and turned by an angle of 180 degrees before exiting the nozzles of the jetpack. The loss factor, K_L, for a standard flanged 180-degree bend is 0.2 (Fox et al., 2011), thus the loss in the wye can be approximated as 20% of the dynamic head term in Equation 3.24. However, it must be noted that this assumption is only valid for the case of a rounded 180-degree bend with smooth internal surfaces. Furthermore, the actual fluid velocity in the wye system is always less than the jet velocity exiting the nozzles since the jet-area is less than the area of the pipes in the wye system, which implies that using the jet velocity to approximate the minor losses in the wye system is a slightly over-estimated velocity value for Equation 3.25 since the minor loss is proportional to the square of this velocity term. However, the effects of over-estimating the velocity term in Equation 3.26 balances out with other minor contributors in the wye system. These are due to the design of the wye system which is composed of two 180-degree bends and a flow coupling located between the wye and the feed hose. (Naidoo et al., 2015a). The actual loss in the wye system will be determined in Chapter 6 where the wye system is accurately modelled based on geometry design and CFD simulation is conducted. Substituting the jet and feed hose velocity expressions given by Equation 3.18 and 3.20 respectively into Equation 3.26 gives an expression for the pressure head rise across the pump in terms of the constant parameters in the system:

$$h_{pump} = \frac{1.2}{2g}\left(\frac{(m_{dry} + \kappa\,\rho\,A_1\,Z_2)g}{\rho A_2}\right) + Z_2 + \left(f\frac{L}{2 d_1 g}\right)\left(\frac{A_2}{A_1}\right)^2\left(\frac{(m_{dry} + \kappa\,\rho\,A_1\,Z_2)g}{\rho A_2}\right) \tag{3.27}$$

By mathematically manipulating Equation 3.27, it may be shown that a simplified expression for the pressure head required by the AUV pump is given by:

$$h_{pump} = \left(\frac{2.4\,A_1^{\frac{5}{2}} + fL\sqrt{\pi}A_2{}^2}{4\rho A_1^{\frac{5}{2}} A_2}\right)(m_{dry} + \kappa\,\rho\,A_1\,Z_2) + Z_2 \tag{3.28}$$

The pressure rise across the AUV pump is given by:

$$P_{pump} = \rho g h_{pump} \tag{3.29}$$

where P_{pump} is the pressure rise across the AUV pump. Substituting Equation 3.28 into Equation 3.29 gives the following expression for the pressure rise across the AUV pump as a function of the constant parameters in the system:

$$P_{pump} = \rho g \left[\left(\frac{2.4\, A_1^{\frac{5}{2}} + fL\sqrt{\pi}A_2{}^2}{4\rho A_1^{\frac{5}{2}}A_2} \right) \left(m_{dry} + \kappa\, \rho\, A_1\, Z_2 \right) + Z_2 \right] \tag{3.30}$$

Equation 3.30 may be simplified by multiplying ρg into the expression contained within the square brackets, this gives the following:

$$P_{pump} = \left(\frac{2.4\, A_1^{\frac{5}{2}} + fL\sqrt{\pi}A_2{}^2}{4 A_1^{\frac{5}{2}}A_2} \right) \left(m_{dry}g + \kappa\, \rho g\, A_1\, Z_2 \right) + \rho g Z_2 \tag{3.31}$$

The power required by the pump is given by:

$$\dot{W} = Q P_{pump} \tag{3.32}$$

where Q is the volumetric flow rate through the system. Referring to Cengal and Cimbala (2010), the relationship between mass, volume and density of a fluid is given by:

$$\rho = \frac{m}{V} \tag{3.33}$$

where m is mass and V is volume. By making volume be the subject of Equation 3.31 and differentiating both sides with respect to time, it can be shown that the expression for volumetric flow rate is given by:

$$Q = \frac{dV}{dt} = \frac{1}{\rho}\left(\frac{dm}{dt}\right) \tag{3.34}$$

where dV/dt denotes an alternate expression for volumetric flow rate. Note that $dm/dt = \dot{m}$. Substituting Equation 3.34 into Equation 3.32 gives the following:

$$\dot{W} = \left(\frac{\dot{m}}{\rho}\right) P_{pump} \tag{3.35}$$

Substituting Equation 3.29 into Equation 3.35 and simplifying the resulting expression gives the following expression for the power required by the AUV pump:

$$\dot{W} = \dot{m} g h_{pump} \tag{3.36}$$

Substituting the expressions for mass flow rate given by Equation 3.16 and the expression for pressure head given by Equation 3.27, both into Equation 3.36 results in the following:

$$\dot{W} = \left(\sqrt{\rho A_2 g \left(m_{dry} + \kappa\, \rho\, A_1\, Z_2 \right)} \right) g \left[\left(\frac{2.4\, A_1^{\frac{5}{2}} + fL\sqrt{\pi}A_2{}^2}{4\rho A_1^{\frac{5}{2}}A_2} \right) \left(m_{dry} + \kappa\, \rho\, A_1\, Z_2 \right) + Z_2 \right] \tag{3.37}$$

By mathematically manipulating Equation 3.37, it can be shown that Equation 3.38 is obtained, which models the power required by the AUV as a function of the constant parameters in the system:

$$\dot{W} = \left(\frac{2.4\,A_1^{\frac{5}{2}} + fL\sqrt{\pi}A_2^{2}}{4\rho^{\frac{1}{2}}A_1^{\frac{3}{2}}A_2} \right) g^{\frac{3}{2}} \left(m_{dry} + \kappa\,\rho\,A_1\,Z_2 \right)^{\frac{3}{2}} + \rho^{\frac{1}{2}}g^{\frac{3}{2}}A_2^{\frac{1}{2}}Z_2 \left(m_{dry} + \kappa\,\rho\,A_1\,Z_2 \right)^{\frac{1}{2}} \quad (3.38)$$

3.6.2   Z-Direction First-Order Transient Modelling

The mathematical models described in Section 3.6.1 are applicable for steady state static hovering which is a non-transient condition. In this section, the water jetpack system is modelled as a first-order transient system. This condition implies that the velocity term in the force balance equation of the jetpack system (Newton's Second Law) is a time-varying quantity in the system. However, since this is a first-order analysis, the acceleration of the system is equal to zero. Applying this condition to the force balance equation for the jetpack system in the z-direction given as Equation 3.10 previously results in the following:

$$\dot{m}\left(v_f - v_z(t)\right) - \sum m\,g = 0 \quad (3.39)$$

where $v_z(t)$ is the time-varying heave velocity. Now by substitution of the accumulative mass model given as Equation 3.6 into Equation 3.39:

$$\dot{m}\left(v_f - v_z(t)\right) - \left(m_{dry} + \kappa\,\rho\,A_1\,Z_2(t) \right) g = 0 \quad (3.40)$$

where $Z_2(t)$ is the time-varying flight altitude. The time-varying heave velocity may be expressed as the first-order derivative of the flight altitude such that:

$$v_z(t) = \frac{dZ_2}{dt} \quad (3.41)$$

where dZ_2/dt is the rate of change of flight altitude with respect to time. Substituting Equation 3.41 into Equation 3.40 and simplifying the resulting expression leads to the following first-order linear differential equation:

$$\dot{m}v_f - \dot{m}\left(\frac{dZ_2}{dt}\right) - m_{dry}\kappa\,\rho\,A_1 g Z_2(t) = 0 \quad (3.42)$$

Since the only time-varying parameters are heave velocity and flight altitude, applying the rules of integral calculus described in Stewart (2011) results in another differential equation. Equation 3.42 may be solved by various means of using linearization techniques described by Ogata (2013), or using classical Newtonian integral calculus described by Stewart (2011) and Hirsch, Smale and Devaney (2012). However, a solution to Equation 3.42 can be obtained for a simple case where the initial flight altitude is zero. This is done using the following equations of motion (Young et al., 2010):

$$v_z(t) = v_z + \left(\frac{dv_z}{dt}\right) t \quad (3.43)$$

81

$$Z_2(t) = Z_0 + \left(\frac{dZ_2}{dt}\right)t + \frac{1}{2}\left(\frac{d^2Z_2}{dt^2}\right)t^2 \qquad (3.44)$$

where Z_0 is the initial flight altitude. Since acceleration and the initial flight altitude are equal to zero for this analysis, Equation 3.43 and Equation 3.44 simplifies to Equation 3.45 and Equation 3.46 respectively:

$$v_z(t) = v_z \qquad (3.45)$$

$$Z_2(t) = \left(\frac{dZ_2}{dt}\right)t = v_z\,t \qquad (3.46)$$

where v_z is the steady state heave velocity that remains constant. By substituting Equation 3.45 and Equation 3.46 into Equation 3.42, it can be shown that the steady state heave is given by:

$$v_z = \frac{\dot{m}^2 - \rho A_2 m_{dry} g}{\rho A_2(\dot{m} + \kappa \rho A_1\,g\,t)} \qquad (3.47)$$

Equation 3.47 models the steady state velocity attained at a defined time interval when the mass flow rate in the jetpack propulsion system is constant. By substituting Equation 3.47 into Equation 3.46, the flight altitude as a function of time is given by:

$$Z_2(t) = \frac{\dot{m}^2 t - \rho A_2 m_{dry} g t}{\rho A_2(\dot{m} + \kappa \rho A_1\,g\,t)} \qquad (3.48)$$

Equation 3.48 is a transient model of flight altitude that is valid only for steady state flight at a constant heave velocity. Equation 3.47 and Equation 3.48 may be mathematically manipulated to compute any variable depending on the flight conditions present, alternatively it may also be used to optimize and determine the magnitude of a controlled variable, such that the desired flight condition is attained. For instance, it is possible to determine the mass flow rate required to reach a defined flight altitude or a certain steady state heave velocity in a desired time interval by making mass flow rate the subject of Equation 3.47 or Equation 3.48. This would require solving a quadratic equation since both the steady state heave velocity and flight altitude are dependent on the square of mass flow rate in Equation 3.47 and Equation 3.48. It is also possible to determine the conditions for the jetpack system to take-off from a reference position. By differentiating Equation 3.47 with respect to time, the acceleration is given by:

$$\frac{dv_z}{dt} = \frac{d}{dt}\left[\frac{\dot{m}^2 - \rho A_2 m_{dry} g}{\rho A_2(\dot{m} + \kappa \rho A_1\,g\,t)}\right] \qquad (3.49)$$

Since it is known that the acceleration is zero, equating Equation 3.49 to zero and solving for mass flow rate results in the following:

$$\dot{m} = \sqrt{\rho A_2 g m_{dry}} \qquad (3.50)$$

Equation 3.50 gives a similar result to Equation 3.16 which was derived previously, however it is noted that in Equation 3.50, mass flow rate is independent of flight altitude which differentiates Equation 3.16 and Equation 3.50.

This implies that Equation 3.50 describes the minimum mass flow rate required for take-off conditions where thrust-to-weight ratio of the jetpack system reaches 1. This observation validates the use of Equation 3.47 for first-order transient analysis of the system.

The pressure head rise across the AUV pump may be expressed as a function of time for the conditions relating to Equation 3.48 by substituting Equation 3.13, Equation 3.19 and Equation 3.48 into Equation 3.26 which results in the following:

$$h_{pump}(t) = \frac{0.6}{g}\left(\frac{\dot{m}}{\rho A_2}\right)^2 + \frac{\dot{m}^2 t - \rho A_2 m_{dry} g t}{\rho A_2 (\dot{m} + \kappa \rho A_1 \ g \ t)} + f\frac{L}{2 d_1 g}\left(\frac{\dot{m}}{\rho A_1}\right)^2 \tag{3.51}$$

By substituting Equation 3.51 into Equation 3.29, the pressure rise across the AUV pump is given by:

$$P_{pump}(t) = \frac{0.6}{\rho}\left(\frac{\dot{m}}{A_2}\right)^2 + \frac{\dot{m}^2 g t - \rho A_2 m_{dry} g^2 t}{A_2 (\dot{m} + \kappa \rho A_1 \ g \ t)} + f\frac{L}{2 d_1 \rho}\left(\frac{\dot{m}}{A_1}\right)^2 \tag{3.52}$$

By substituting Equation 3.51 into Equation 3.36, the power required by the AUV pump is given by:

$$\dot{W}(t) = 0.6\dot{m}\left(\frac{\dot{m}}{\rho A_2}\right)^2 + \frac{\dot{m}^3 g t - \dot{m}\rho A_2 m_{dry} g^2 t}{\rho A_2 (\dot{m} + \kappa \rho A_1 \ g \ t)} + f\frac{\dot{m}L}{2 d_1}\left(\frac{\dot{m}}{\rho A_1}\right)^2 \tag{3.53}$$

3.6.3   Z-Direction Second-Order Transient Modelling

In this section, the water jetpack system will be modelled as a second-order transient system. This implies that the acceleration term in the force balance equation of the jetpack system (Newton's Second Law) is a time-varying quantity in the system. Applying this condition to the force balance equation for the jetpack system in the z-direction given by Equation 3.10 results in the following:

$$\sum m\frac{dv_z}{dt} = \dot{m}(v_f - v_z) - \sum m\,g \tag{3.54}$$

Now by substitution of the accumulative mass model given as Equation 3.6 into Equation 3.39:

$$\left(m_{dry} + \kappa \rho A_1 Z_2(t)\right)\frac{dv_z}{dt} = \dot{m}(v_f - v_z(t)) - \left(m_{dry} + \kappa \rho A_1 Z_2(t)\right)g \tag{3.55}$$

The acceleration in the z-direction may be expressed as a second-order derivative of the flight altitude with respect to time:

$$\frac{dv_z}{dt} = \frac{d^2 Z_2}{dt^2} \tag{3.56}$$

Substituting Equation 3.41 and 3.56 into Equation 3.55 gives the following second-order non-linear differential equation as:

$$m_{dry}\frac{d^2Z_2}{dt^2} + \kappa\,\rho\,A_1\,Z_2(t)\frac{d^2Z_2}{dt^2} = \dot{m}v_f - \dot{m}\frac{dZ_2}{dt} - m_{dry}g + \kappa\,\rho\,A_1 g\,Z_2(t) \qquad (3.57)$$

Equation 3.57 is considered as a second-order non-linear differential equation since it consists of terms of flight altitude multiplied by its second-order derivative and therefore Equation 3.57 cannot be solved by simple analytical means. Charkrit (2013) describes a mathematical approach of using the Laplace decomposition algorithm to solve both first and second differential equations. The mathematical theory related to solving complex differential equations are beyond the scope of this study. However, Ogata (2013) describes the use of a computational package called Simulink in MATLAB to simulate transient system models, which is the approach detailed in Chapter 6 of this dissertation.

3.7   Water Jetpack Modelling in Two-Dimensions

In this section, the water jetpack system is modelled by considering motion in two dimensions: x- and z-directions. Motion in the y-direction is not considered in this analysis. The motion of the jetpack system in the x-direction is attained using the water jetpack nozzles which are controlled by the user and/or a control system such that the jetpack system experiences a thrust force in the x- and z-direction. A free-body diagram is necessary for this analysis and is shown in Figure 3.4. This is used to aid in the development of the models for the water jetpack system.
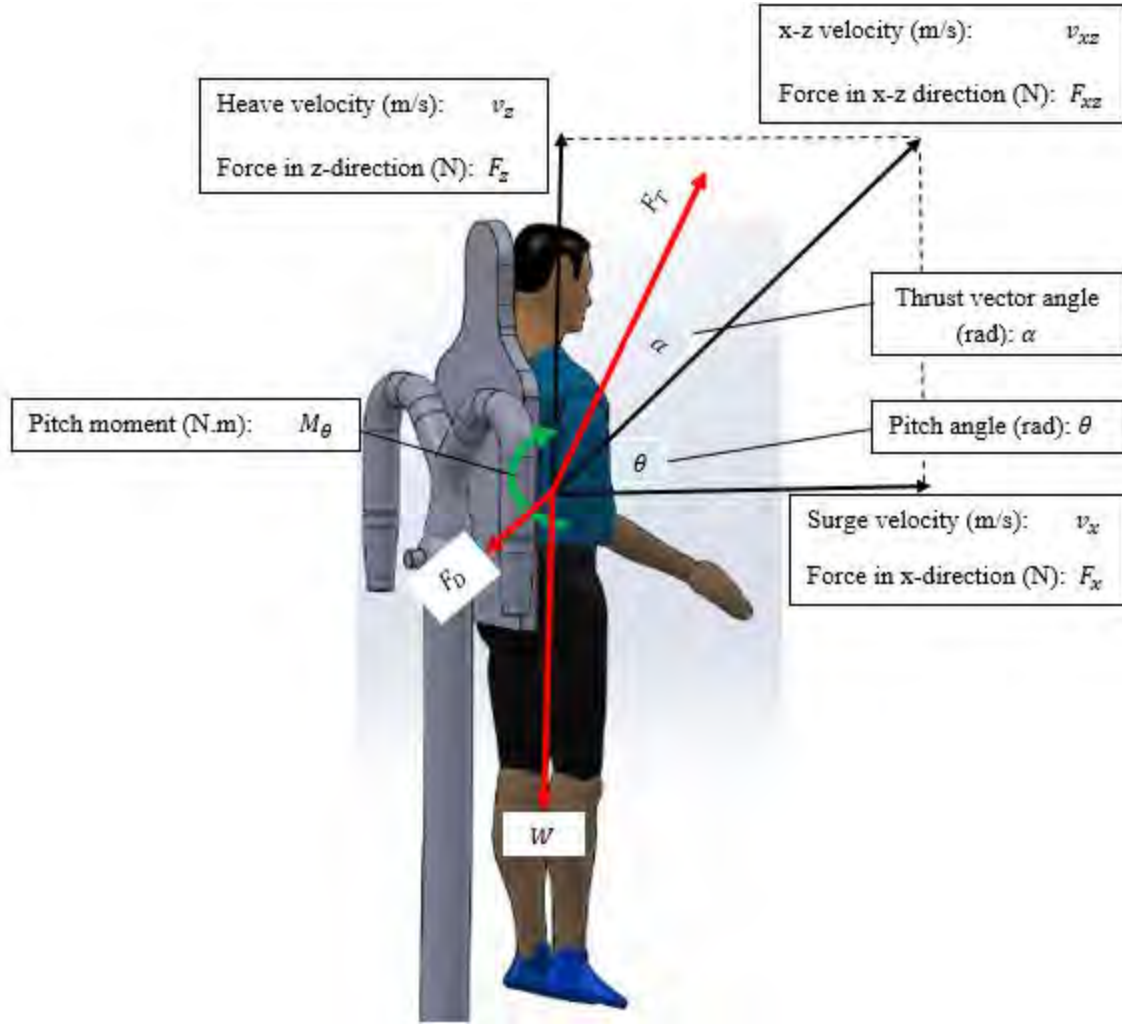
Figure 3.4: Water jetpack free-body diagram

In Figure 3.4, the three forces acting on the water jetpack system are shown by the red arrows: 1) thrust force (F_T), 2) weight (W) and 3) drag force (F_D). The thrust force vector is shown by the up-right facing red arrow, the drag force is shown by the down-left facing red arrow and the weight vector is shown by the downward facing red arrow. The pitch angle is the angle of the jetpack system relative to the fixed earth coordinate system as illustrated in Figure 3.3 previously. The pitch moment is shown by the circular green arrow, this is the moment experienced by the water jetpack system about the fixed earth y-axis. The thrust vector angle shown is the angle that the nozzles are directed from the neutral position (zero degrees).

3.7.1   Force Analysis and Newton's Second Law

Newton's Second Law in the x-z direction in vector form may be expressed as:

$$\sum \vec{F}_{xz} = \sum m\, \vec{a}_{xz} \tag{3.58}$$

where $\sum \vec{F}_{xz}$ is the net force vector and $\vec{a}_{xz}$ is the acceleration vector of the water jetpack system in the in the x-z direction. The force vector may be expressed as a vector sum of its individual components such that:

$$\vec{F}_{xz} = \vec{F}_x + \vec{F}_z \tag{3.59}$$

where $\vec{F}_x$ is the force vector in the x-direction and $\vec{F}_z$ is the force vector in the z-direction. The magnitude of the force in the x-z direction is given by:

$$F_{xz} = \sqrt{F_x{}^2 + F_z{}^2} \tag{3.60}$$

where F_{xz} is the force in the x-z direction, F_x is the force in the x-direction and F_z is the force in the z-direction. The acceleration vector may be expressed as:

$$\vec{a}_{xz} = \frac{d\vec{v}_{xz}}{dt} = \frac{d\vec{v}_x}{dt} + \frac{d\vec{v}_z}{dt} \tag{3.61}$$

where $\vec{a}_{xz}$ and $d\vec{v}_{xz}/dt$ is the acceleration vector in the x-z direction, $d\vec{v}_x/dt$ is the acceleration vector in the x-direction and $d\vec{v}_z/dt$ is the acceleration vector in the z-direction. The magnitude of the acceleration in the x-z direction is given by:

$$a_{xz} = \frac{dv_{xz}}{dt} = \sqrt{\left(\frac{dv_x}{dt}\right)^2 + \left(\frac{dv_z}{dt}\right)^2} \tag{3.62}$$

where a_{xz} and dv_{xz}/dt is the acceleration in the x-z direction, dv_x/dt is the acceleration in the x-direction and dv_z/dt is the acceleration in the z-direction. Regarding Figure 3.4 and applying Newton's Second Law in Equation 3.58, the force balance in the x-z direction in vector form is given by:

$$\vec{F}_{xz} = \vec{F}_T + \vec{F}_D + \vec{W} \tag{3.63}$$

where $\vec{F}_T$ is the thrust force vector, $\vec{F}_D$ is the drag force vector, and $\vec{W}$ is the weight vector acting on the jetpack system in the x-z direction. The magnitude of the net force in the x-direction and z-direction respectively is given by:

$$F_x = F_T \sin(\theta + \alpha) - F_D \cos\theta \tag{3.64}$$

$$F_z = F_T \cos(\theta + \alpha) - F_D \sin\theta - W \tag{3.65}$$

where θ is the pitch angle, α is the thrust vector angle, F_D is the drag force and W is the weight of the water jetpack system. The pitch angle is non-zero only when the water jetpack system moves in the x-z direction which is encountered during take-off and descent phase conditions. For safety purposes, it is preferable to perform take-off and descent phase conditions at zero pitch angle such that the pilot and jetpack system is at an upright position since inducing a non-zero pitch may result in instability of the water jetpack system (Naidoo et al., 2015b). In the case of zero pitch angle, Equation 3.64 and Equation 3.65 may be expressed as:

$$F_x = F_T \sin\alpha - F_D \tag{3.66}$$

$$F_z = F_T \cos\alpha - W \tag{3.67}$$

It can be noted that the drag force term in Equation 3.67 falls away when the pitch angle is assumed to be zero. This is expected since during any flight, the surge velocity is much greater than the heave velocity, and since drag force is proportional to the square of velocity, the drag force in the z-direction may be assumed to be negligible.

3.7.2   Steady State Analysis at Constant Flight Altitude

In this model, the system maintains steady state motion in the x-direction while staying at constant flight altitude such that $v_z = 0$. In this analysis, the drag force acts only in the x-direction as motion is the z-direction is not considered. Furthermore, the pitch angle is assumed to be zero such that the motion of the water jetpack system is in the x-direction only. The first condition for the heave velocity and net force in the z-direction to be zero is given by:

$$F_T \cos\alpha - W = 0 \tag{3.68}$$

where W may be expressed as $\sum m\, g$, therefore the minimum thrust force required to obey Equation 3.68 is given by:

$$F_T = \frac{\sum m\, g}{\cos\alpha} \tag{3.69}$$

Substituting Equation 3.7 into Equation 3.69:

$$F_T = \frac{\left(m_{dry} + \kappa\, \rho\, A_1\, Z_2\right)g}{\cos\alpha} \tag{3.70}$$

The thrust force equation for two-dimensional motion is given by:

$$F_T = \dot{m}\left(v_f - v_{xz}\right) \tag{3.71}$$

where $\dot{m}$ is mass flow rate, v_f is the water jet exit velocity and v_{xz} is the velocity of the water jetpack system in the x-z direction. The velocity of the water jetpack system in the x-z direction is given by the vector sum of the velocity in x- and z-direction:

$$\vec{v}_{xz} = \vec{v}_x + \vec{v}_z \tag{3.72}$$

where $\vec{v}_{xz}$ is the velocity vector in the x-z direction, $\vec{v}_x$ is the velocity vector in the x-direction and $\vec{v}_z$ is the velocity vector in the z-direction. The magnitude of the velocity in the x-z direction is given by:

$$v_{xz} = \sqrt{v_x{}^2 + v_z{}^2} \tag{3.73}$$

Since the heave velocity is zero in this analysis, the velocity in the x-z direction is equal to the surge velocity such that Equation 3.73 simplifies to Equation 3.74:

$$v_{xz} = \sqrt{v_x{}^2} = \pm v_x \tag{3.74}$$

where $+v_x$ implies that the water jetpack system moves in the positive x-direction and $-v_x$ implies that the water jetpack system moves in the negative x-direction. In this analysis, v_x will be taken as positive. Substituting Equation 3.74 and Equation 3.13 into Equation 3.71:

$$F_T = \dot{m}\left(\frac{\dot{m}}{\rho A_2} - v_x\right) \tag{3.75}$$

By substituting Equation 3.75 into Equation 3.70 and solving for the steady state surge velocity gives the following:

$$v_x = \frac{\dot{m}^2 - \rho A_2 g\left(m_{dry} + \kappa\,\rho\,A_1\,Z_2\right)}{\dot{m}\rho A_2 \cos\alpha} \tag{3.76}$$

Equation 3.76 models the steady state surge velocity attained for a fixed mass flow rate, flight altitude and thrust vector angle (alpha). It is noted that the surge velocity is inversely proportional to the cosine of the thrust vector. Since the maximum angle for thrust vectoring of a water jetpacks is 45 degrees (Jetlev-Flyer, 2015), referring to the cosine function (Stewart, 2011), it is deduced that as the thrust vector angle increases, the cosine of the thrust vector angle decreases. This implies that the surge velocity is directly proportional to the thrust vector angle. The drag force experienced by the water jetpack system in the x-direction is a function of the steady state surge velocity and is given by:

$$F_D = C_{D_h}\frac{1}{2}\,\rho_{air}A_h{v_x}^2 \tag{3.77}$$

where C_{D_h} is the coefficient of drag, ρ_{air} is the density of air and A_h is the average frontal area of a human. Substituting Equation 3.76 into Equation 3.77 gives an expression for the drag force in terms of mass flow rate, flight altitude and thrust vector angle:

$$F_D = C_{D_h}\frac{1}{2}\,\rho_{air}A_h\left(\frac{\dot{m}^2 - \rho A_2 g\left(m_{dry} + \kappa\,\rho\,A_1\,Z_2\right)}{\dot{m}\rho A_2 \cos\alpha}\right)^2 \tag{3.78}$$

The second condition for steady state flight in the x-direction is given by:

$$F_T \sin\alpha - F_D = 0 \tag{3.79}$$

By substituting Equation 3.78 and Equation 3.79, it can be shown that the thrust force is given by:

$$F_T = C_{D_h}\frac{1}{2}\,\rho_{air}A_h\left(\frac{\dot{m}^2 - \rho A_2 g\left(m_{dry} + \kappa\,\rho\,A_1\,Z_2\right)}{\dot{m}\rho A_2 \sin\alpha \cos\alpha}\right)^2 \tag{3.80}$$

Since $2\sin\alpha\cos\alpha = \sin 2\alpha$ (Stewart, 2011), Equation 3.80 may be simplified to Equation 3.81:

$$F_T = C_{D_h}\,\rho_{air}A_h\left(\frac{\dot{m}^2 - \rho A_2 g\left(m_{dry} + \kappa\,\rho\,A_1\,Z_2\right)}{\dot{m}\rho A_2 \sin 2\alpha}\right)^2 \tag{3.81}$$

Equation 3.81 models the thrust force required to maintain steady state flight in the x-direction for a given mass flow rate, flight altitude and thrust vector angle. The equation of motion for this analysis is given by:

$$X(t) = X_0 + v_x t + \frac{1}{2}\left(\frac{dv_x}{dt}\right)t^2 \tag{3.82}$$

where $X(t)$ is the time-varying displacement and X_0 is the initial displacement of the water jetpack system in the x-direction. In this analysis, the initial displacement will be assumed to be zero, and since the acceleration in the x-direction is zero, it can be shown that the displacement as a function of time is given by:

$$X(t) = \frac{\dot{m}^2 t - t\rho A_2 g\left(m_{dry} + \kappa \rho A_1 Z_2\right)}{\dot{m}\rho A_2 \cos \alpha} \tag{3.83}$$

Equation 3.83 represents the time-varying displacement as a function of time, mass flow rate and thrust vector angle. By controlling mass flow rate and the thrust vector angle, it is possible to attain a desired flight altitude and steady state surge velocity. This analysis is detailed in Chapter 6 with the use of a Simulink control system model of the system.

3.7.3   X-Direction First-Order Transient Modelling

The mathematical models described in Section 3.7.2 are applicable for steady state static hovering which is a non-transient condition. In this section, the water jetpack system will be modelled as a first-order transient system with non-zero acceleration in the x-direction. This condition implies that the velocity term in the force balance equation of the jetpack system (Newton's Second Law) is a time-varying quantity in the system. In this analysis, the drag force acts only in the x-direction as motion is the z-direction is not considered. Furthermore, the pitch angle is assumed to be zero such that the motion of the water jetpack system is in the x-direction only. The condition for the heave velocity and net force in the z-direction to be zero is given by:

$$F_T \cos \alpha - W = 0 \tag{3.84}$$

Now by substitution of the accumulative mass model given as Equation 3.6 into Equation 3.84, the thrust force is given by:

$$F_T = \frac{\left(m_{dry} + \kappa \rho A_1 Z_2\right)g}{\cos \alpha} \tag{3.85}$$

Substituting the expression for thrust force in Equation 3.85 and the expression for drag force in the x-direction in Equation 3.77 into the net force in the x-direction given by Equation 3.66, the net force in the x-direction is given by:

$$F_x = \frac{\left(m_{dry} + \kappa \rho A_1 Z_2\right)g}{\cos \alpha}\sin\alpha - C_{Dh}\frac{1}{2}\rho_{air}A_h v_x^2 = \sum m \frac{dv_x}{dt} \tag{3.86}$$

since $\sin\alpha/\cos\alpha = \tan\alpha$ and $\sum m = m_{dry} + \kappa \rho A_1 Z_2$, Equation 3.86 simplifies to:

$$\left(m_{dry} + \kappa \, \rho \, A_1 \, Z_2\right)g \tan\alpha - C_{Dh} \frac{1}{2} \rho_{air} A_h v_x{}^2 = \left(m_{dry} + \kappa \, \rho \, A_1 \, Z_2\right) \frac{dv_x}{dt} \tag{3.87}$$

3.7.3.1   3.7.3.1 Case 1: Negligible Drag Force

In this case, a model of the water jetpack system is developed for a case when the drag force does not severely affect the acceleration and net force of the water jetpack system. For this to be valid, the surge velocity term must be relatively small. By referring to Equation 3.66, it is noted that drag force is proportional to the square of velocity which can be represented mathematically:

$$F_D \propto v_x{}^2$$

For $v_x < 1$, the drag force can be assumed negligible since the square of a number less than 1 decreases in value. For instance, for a surge velocity of 1/4 m/s, the drag force would be computed by multiplying $C_{Dh} \frac{1}{2} \rho_{air} A_h$ by 1/16. However, one must be cautious when making this assumption since drag force is also dependent on the coefficient of drag, density of air and area. Thus, for high values of drag coefficient and area, computing the term $C_{Dh} \frac{1}{2} \rho_{air} A_h$ would give a clear indication of the effects of drag on the system being analyzed. In the case of a water jetpack system, drag may be assumed negligible for surge velocities less than 1 m/s since the average area of a human is 0.55 m^2 and the drag coefficient is 1.16. These values along with the density of air and surge velocity less than 1 m/s result in the drag force being less than 1 N (Hoerner, 1966). If the drag force is neglected, then Equation 3.87 may be expressed as:

$$F_x = \left(m_{dry} + \kappa \, \rho \, A_1 \, Z_2\right)g \tan\alpha = \left(m_{dry} + \kappa \, \rho \, A_1 \, Z_2\right) \frac{dv_x}{dt} \tag{3.88}$$

By cancellation of the accumulative mass term on both sides of Equation 3.88, the acceleration in the x-direction is given by:

$$\frac{dv_x}{dt} = g \tan \alpha \tag{3.89}$$

Equation 3.89 shows that the acceleration in the x-direction is a function of the thrust vector angle. Since $0 \leq \alpha \leq 45$ degrees, the acceleration in the x-direction is in the region of $0 < \frac{dv_x}{dt} < g$. The time-varying surge velocity can be determined by integrating Equation 3.89 with respect to time:

$$v_x(t) = \int \left(\frac{dv_x}{dt}\right) dt = \int (g \tan \alpha) \, dt = v_{x0} + (g \tan \alpha)t \tag{3.90}$$

where $v_x(t)$ is the time-varying surge velocity and v_{x0} is the initial surge velocity. The displacement equation can be determined by double integration of Equation 3.89 with respect to time:

$$X(t) = \iint \left(\frac{dv_x}{dt}\right) dt = \int (v_0 + g \tan \alpha \, t) \, dt = X_0 + v_{x0}t + \frac{1}{2}(g \tan \alpha)t^2 \tag{3.91}$$

where $X(t)$ is the time-varying displacement and X_0 is the initial displacement of the water jetpack system in the x-direction. In the case where the initial surge velocity and displacement in the x-direction are both zero, Equation 3.90 and Equation 3.91 reduce to:

$$v_x(t) = (g \tan \alpha)t \tag{3.92}$$

$$X(t) = \frac{1}{2}(g \tan \alpha)t^2 \tag{3.93}$$

Equation 3.92 and Equation 3.93 model the surge velocity and displacement in the x-direction respectively as a function of the thrust vector angle and time. Substituting Equation 3.92 into the thrust force equation as given in Equation 3.75 gives an expression for the thrust force as a function of mass flow rate, thrust vector angle and time:

$$F_T(t) = \dot{m}\left(\frac{\dot{m}}{\rho A_2} - (g \tan \alpha)t\right) \tag{3.94}$$

where $F_T(t)$ is the time-varying thrust force. It must be noted again that Equation 3.88 to Equation 3.94 is only valid for the case of $v_x \ll 1$ whereby the drag force is negligible. In this case, the models predict that the water jetpack system experiences an acceleration that is dependent on the thrust vector angle.

3.7.3.2   Case 2: Non-Negligible Drag Force

In this case, the drag force term in Equation 3.86 is considered in the analysis of developing a set of equations that model the performance of the water jetpack system under second-order transient conditions in the x-direction while flight altitude remains constant. The surge velocity and acceleration term in Equation 3.86 may be expressed as first and second-order time-varying derivatives of displacement with respect to time:

$$v_x(t) = \frac{dX}{dt} \tag{3.95}$$

$$\frac{dv_x(t)}{dt} = \frac{d^2X}{dt^2} \tag{3.96}$$

Substituting Equation 3.95 and Equation 3.96 into Equation 3.87 and rearranging the resulting expression:

$$\left(m_{dry} + \kappa \rho A_1 Z_2\right)\frac{d^2X}{dt^2} + C_{Dh}\frac{1}{2}\rho_{air}A_h\left(\frac{dX}{dt}\right)^2 - \left(m_{dry} + \kappa \rho A_1 Z_2\right)g \tan\alpha = 0 \tag{3.97}$$

Equation 3.97 is a second-order non-linear differential equation with respect to the displacement in the x-direction (Zraiqat and Al-Hwawcha, 2015), which cannot be solved by simple analytical means since the initial conditions are unknown at this stage. Charkrit (2013) describes a mathematical approach of using the Laplace decomposition algorithm to solve both first and second-order differential equations. However, in the case of a defined constant acceleration in the x-direction, the acceleration may be expressed by altering the equation of motion (Young, Freedman and Ford, 2010) which is given by:

$$\frac{dv_x}{dt} = \frac{d^2X}{dt^2} = \frac{v_x(t) - v_{x0}}{t} \tag{3.98}$$

If the initial surge velocity is zero, substituting Equation 3.98 into Equation 3.97 gives the following second-order time-varying polynomial function for the surge velocity:

$$C_{Dh}\frac{1}{2}\rho_{air}A_h(v_x(t))^2 + (m_{dry} + \kappa\rho A_1 Z_2)\left(\frac{v_x(t)}{t}\right) - (m_{dry} + \kappa\rho A_1 Z_2)g\tan\alpha = 0 \tag{3.99}$$

Equation 3.99 may be solved by using the quadratic formula (Stewart, 2011):

$$v_x(t) = \frac{-b \pm \sqrt{b^2 - 4ac}}{2a} \tag{3.100}$$

where the coefficients of a, b and c are given by Equation 3.101, Equation 3.102 and Equation 3.103 respectively:

$$a = C_{Dh}\frac{1}{2}\rho_{air}A_h \tag{3.101}$$

$$b = \frac{(m_{dry} + \kappa\rho A_1 Z_2)}{t} \tag{3.102}$$

$$c = -g\tan\alpha\left(m_{dry} + \kappa\rho A_1 Z_2\right) \tag{3.103}$$

There are two solutions to Equation 3.100. For $0 < \alpha < 45$ degrees, the water jetpack system moves in the positive x-direction and therefore the surge velocity is positive. Likewise, when $0 > \alpha > -45$ degrees, the water jetpack system moves in the negative x-direction and therefore the surge velocity is negative. These relations can be expressed mathematically as follows:

$$v_x(t) > 0 \leftrightarrow 0 < \alpha < 45$$

$$v_x(t) < 0 \leftrightarrow 0 > \alpha > -45$$

These conditions must be satisfied for Equation 3.100 to be valid for modelling the surge velocity of the water jetpack system. Once the surge velocity is computed, the time-varying displacement in the x-direction may be obtained by integrating Equation 3.100 such that:

$$X(t) = \int v_x(t)\, dt \tag{3.104}$$

The acceleration can be computed by substituting Equation 3.100 into Equation 3.98. The drag force can be computed by substituting Equation 3.100 into Equation 3.77 and the thrust force can be computed by substituting Equation 3.100 into Equation 3.71, which may be used to solve for the mass flow rate required for this type of flight of the water jetpack system.

3.8 Water Jetpack Modelling in Three Dimensions

In this section, the water jetpack system is modelled for motion in three dimensions. Motion in the x-, y- and z-direction is considered in this analysis. The motion of the jetpack system in the x-y direction is attained by a horizontal component of the thrust force generated by the water jetpack nozzles, which are controlled by the user and/or a control system. The water jetpack system experiences a component of the thrust force in the y-direction by inducing a yaw angle. As illustrated previously in Figure 3.3, yaw is the angle about the z axis. In water jetpacks, the yaw angle is controlled by the pilot shifting his/her weight such that the CM of the pilot is located a certain distance from the CM of the jetpack and feed hose combined. When the CM of the pilot changes from the neutral position, this induces a yaw angle in the water jetpack system and the thrust force generated has a component in all three directions. To simplify the analysis contained in this section, the effects of pitch, roll and yaw moments are assumed to be equal to zero, such that the water jetpack system moves linearly in the x-, y- and z-directions respectively without any rotational effects. In the case of the water jetpack system experiencing pitch, roll or moments that cause a net non-zero moment on the water jetpack system and partial instability, the pilot would have to adjust his/her position of the CM or adjust the thrust vector angle until stability is regained and linear or steady state motion is attained. In this analysis, the variables that the pilot has control of are: 1) mass flow rate, 2) thrust vector angle, and 3) yaw angle relative to the earth fixed coordinate system as illustrated in Figure 3.3.

3.8.1 Force Analysis and Newton's Second Law

Newton's Second Law in the x-y-z direction in vector form may be expressed as:

$$\sum \vec{F}_{xyz} = \sum m\,\vec{a}_{xyz} \tag{3.105}$$

where $\sum \vec{F}_{xyz}$ is the net force vector and $\vec{a}_{xyz}$ is the acceleration vector of the water jetpack system in the in the x-y-z direction. The force vector may be expressed as a vector sum of its individual components such that:

$$\vec{F}_{xyz} = \vec{F}_x + \vec{F}_y + \vec{F}_z \tag{3.106}$$

where $\vec{F}_x$ is the force vector in the x-direction, $\vec{F}_y$ is the force vector in the y-direction and $\vec{F}_z$ is the force vector in the z-direction. The magnitude of the force in the x-y-z direction is given by:

$$F_{xyz} = \sqrt{F_x{}^2 + F_y{}^2 + F_z{}^2} \tag{3.107}$$

where F_{xyz} is the force in the x-z direction, F_x is the force in the x-direction and F_z is the force in the z-direction. The acceleration vector may be expressed as:

$$\vec{a}_{xyz} = \frac{d\vec{v}_{xz}}{dt} = \frac{d\vec{v}_x}{dt} + \frac{d\vec{v}_y}{dt} + \frac{d\vec{v}_z}{dt} \tag{3.108}$$

where $\vec{a}_{xyz}$ and $d\vec{v}_{xyz}/dt$ is the acceleration vector in the x-y-z direction, $d\vec{v}_x/dt$ is the acceleration vector in the x-direction, $d\vec{v}_y/dt$ is the acceleration vector in the y-direction and $d\vec{v}_z/dt$ is the acceleration vector in the z-direction. The magnitude of the acceleration in the x-y-z direction is given by:

$$a_{xyz} = \frac{dv_{xyz}}{dt} = \sqrt{\left(\frac{dv_x}{dt}\right)^2 + \left(\frac{dv_y}{dt}\right)^2 + \left(\frac{dv_z}{dt}\right)^2} \qquad (3.109)$$

where a_{xz} and dv_{xz}/dt is the acceleration in the x-z direction, dv_x/dt is the acceleration in the x-direction, dv_y/dt is the acceleration in the y-direction and dv_z/dt is the acceleration in the z-direction. Regarding Figure 3.4 and applying Newton's Second Law in Equation 3.58, the force balance in the x-y-z direction in vector form is given by:

$$\vec{F}_{xyz} = \vec{F}_T + \vec{F}_D + \vec{W} \qquad (3.110)$$

where $\vec{F}_T$ is the thrust force vector, $\vec{F}_D$ is the drag force vector and $\vec{W}$ is the weight vector acting on the jetpack system in the x-y-z direction. In this analysis, the forces in the vertical and horizontal place will be segregated such that a model is obtained for the physical quantities in the x-y direction and z-direction. Thereafter, the physical quantities may for the x- and y-direction can be obtained from the model for the x-y direction. The magnitude of the net force in the z and x-y direction is given by:

$$F_{xy} = F_T \sin(\theta + \alpha) - F_D \cos\theta \qquad (3.111)$$

$$F_z = F_T \cos(\theta + \alpha) - F_D \sin\theta - W \qquad (3.112)$$

where F_{xy} is the force in the x-y direction, θ is the pitch angle, α is the thrust vector angle, F_D is the drag force and W is the weight of the water jetpack system. The pitch angle is non-zero only when the water jetpack system moves in the x-y-z direction which is encountered during take-off and descent phase conditions. In the case of motion at constant flight altitude, the pitch angle is zero, and the drag force acts only in the x-y direction since the heave velocity is zero, thus Equation 3.111 and 3.112 reduces to:

$$F_{xy} = F_T \sin\alpha - F_D \qquad (3.113)$$

$$F_z = F_T \cos\alpha - W \qquad (3.114)$$

Now suppose that the pilot induces yaw angle such that the water jetpack system maintains stability but moves linearly with a component of thrust force acting in the y-direction, the force in the x- and y-direction is given by:

$$F_x = F_{xy} \cos\psi = F_T \sin\alpha \cos\psi - F_D \cos\psi \qquad (3.115)$$

$$F_y = F_{xy} \sin\psi = F_T \sin\alpha \sin\psi - F_D \sin\psi \qquad (3.116)$$

where F_x is the force in the x-direction, F_y is the force in the y-direction, and ψ is the yaw angle. It can be deduced from Equation 3.115 and Equation 3.116 that as the yaw angle increases, sine of the yaw angle increases, consequently the sway velocity, force and acceleration increase in the y-direction. Furthermore, it must be noted that the drag force

term in the above equations is dependent on the velocity in the x-y direction as the drag in the z-direction is negligible as discussed in Section 3.2.5. Therefore, drag force is given by:

$$F_D = C_{Dh} \frac{1}{2} \rho_{air} A_h v_{xy}{}^2 \qquad (3.117)$$

where v_{xy} is the velocity in the x-y direction. In the case where the water jetpack system takes-off at an initially high heave velocity, then the initial take-off phase may be modelled by using the velocity in the x-y-z direction in Equation 3.117. However, modelling of the take-off phase is beyond the scope of this chapter as this phase requires transient simulation analysis which is accurately modelled using MATLAB Simulink in Chapter 6.

3.8.2   Steady State Analysis at Constant Flight Altitude

In this model, the system maintains steady state motion in the x-y direction while remaining at constant flight altitude such that $v_z = 0$. In this analysis, the drag force acts only in the x-y direction as motion in the z-direction is not considered. The first condition for the heave velocity and net force in the z-direction to be zero is given by:

$$F_T \cos \alpha - W = 0 \qquad (3.118)$$

where W may be expressed as $\sum m\, g$, therefore the minimum thrust force required to obey Equation 3.118 is given by:

$$F_T = \frac{\sum m\, g}{\cos \alpha} \qquad (3.119)$$

Substituting Equation 3.7 into Equation 3.119:

$$F_T = \frac{\left(m_{dry} + \kappa\, \rho\, A_1\, Z_2\right)g}{\cos \alpha} \qquad (3.120)$$

The general thrust force equation is given by:

$$F_T = \dot{m}\left(v_f - v_{xyz}\right) \qquad (3.121)$$

where $\dot{m}$ is mass flow rate, v_f is the water jet exit velocity and v_{xyz} is the velocity of the water jetpack system in the x-y-z direction. The velocity of the water jetpack system in the x-y-z direction is given by the vector sum of the velocity in x- and z-direction:

$$\vec{v}_{xz} = \vec{v}_x + \vec{v}_y + \vec{v}_z \qquad (3.122)$$

where $\vec{v}_{xyz}$ is the velocity vector in the x-y-z direction, $\vec{v}_x$ is the velocity vector in the x-direction, $\vec{v}_y$ is the velocity vector in the x-direction and $\vec{v}_z$ is the velocity vector in the z-direction. The magnitude of the velocity in the x-y-z direction is given by:

$$v_{xz} = \sqrt{v_x{}^2 + v_y{}^2 + v_z{}^2} \qquad (3.123)$$

Since the heave velocity is zero in this analysis, the velocity in the x-y-z direction is equal to the velocity in the x-y direction such that Equation 3.123 simplifies to Equation 3.124:

$$v_{xyz} = \sqrt{v_x{}^2 + v_y{}^2} = v_{xy} \qquad (3.124)$$

where v_{xy} is the velocity in the x-y direction. Substituting Equation 3.124 and Equation 3.13 into Equation 3.121:

$$F_T = \dot{m}\left(\frac{\dot{m}}{\rho A_2} - v_{xy}\right) \qquad (3.125)$$

Substituting Equation 3.125 and Equation 3.117 into Equation 3.111, the force in the x-y direction is given by:

$$F_{xy} = \dot{m}\left(\frac{\dot{m}}{\rho A_2} - v_{xy}\right)\sin\alpha - C_{Dh}\frac{1}{2}\rho_{air}A_h v_{xy}{}^2 \qquad (3.126)$$

Since the water jetpack system motion is steady state in the x-y direction, the force in the x-y direction is zero. Equating Equation 3.126 to zero results in the following second-order polynomial:

$$C_{Dh}\frac{1}{2}\rho_{air}A_h v_{xy}{}^2 + v_{xy}\dot{m}\sin\alpha - \frac{\dot{m}^2\sin\alpha}{\rho A_2} = 0 \qquad (3.127)$$

Equation 3.127 may be solved using the quadratic formula (Stewart, 2011):

$$v_{xy} = \frac{-b \pm \sqrt{b^2 - 4ac}}{2a} \qquad (3.128)$$

where the coefficients of a, b and c are given by Equation 3.101, Equation 3.102 and Equation 3.103 respectively:

$$a = C_{Dh}\frac{1}{2}\rho_{air}A_h \qquad (3.129)$$

$$b = \dot{m}\sin\alpha \qquad (3.130)$$

$$c = \frac{\dot{m}^2\sin\alpha}{\rho A_2} \qquad (3.131)$$

There are two solutions to Equation 3.128. When $0 < \alpha < 45$ degrees, the water jetpack system moves in the positive x-y direction and therefore the surge velocity is positive. Likewise, when $0 > \alpha > -45$ degrees, the water jetpack system moves in the negative x-y direction and therefore the velocity in the x-y direction is negative. These relations can be expressed mathematically as follows:

$$v_{xy} > 0 \leftrightarrow 0 < \alpha < 45$$

$$v_{xy} < 0 \leftrightarrow 0 > \alpha > -45$$

These conditions must be satisfied for Equation 3.128 to be valid for modelling the velocity of the water jetpack system in the x-y direction. Equation 3.128 models the velocity in the x-y direction by satisfying the condition for the net force in the x-y direction to be zero to attain steady state motion. It is also noted that this equation is dependent on the thrust vector, mass flow rate and the drag force. After solving for the velocity of the water jetpack system in the x-y direction, the velocity in the x- and y-directions (surge and sway velocity) may be computed as follows:

$$v_x = v_{xy} \cos \psi \tag{3.132}$$

$$v_y = v_{xy} \sin \psi \tag{3.133}$$

Once the surge and sway velocity is computed, the time-varying displacement in the x- and y-direction may be obtained by integrating Equation 3.132 and Equation 133 such that:

$$X(t) = \int v_x \, dt = \int v_{xy} \cos \psi \, dt \tag{3.134}$$

$$Y(t) = \int v_y \, dt = \int v_{xy} \sin \psi \, dt \tag{3.135}$$

where $X(t)$ and $Y(t)$ are the time-varying displacement functions in the x- and y-directions respectively.

3.8.3   X-Y Direction Second-Order Transient Modelling

The mathematical models described in Section 3.8.2 are applicable for steady state motion in the x-y direction which is a first-order transient condition. In this section, the water jetpack system will be modelled as a second-order transient system with a non-zero acceleration in the x-y direction. However, flight altitude will be kept constant such that the heave velocity of the water jetpack system is zero, this is done to simplify the analysis. The condition for the heave velocity and net force in the z-direction to be zero is given by:

$$F_T \cos \alpha - W = 0 \tag{3.136}$$

Now by substitution of the accumulative mass model given as Equation 3.6 into Equation 3.136, the thrust force required to satisfy Equation 3.136 is given by:

$$F_T = \frac{(m_{dry} + \kappa \rho A_1 Z_2)g}{\cos \alpha} \tag{3.137}$$

Substituting the expression for thrust force in Equation 3.137 and the expression for drag force in the x-y direction in Equation 3.117 into Equation 3.113, the net force in the x-y direction is given by:

$$F_{xy} = \frac{(m_{dry} + \kappa \rho A_1 Z_2)g}{\cos \alpha} \sin\alpha - C_{Dh} \frac{1}{2} \rho_{air} A_h v_{xy}{}^2 = \sum m \frac{dv_{xy}}{dt} \tag{3.138}$$

since $\sin\alpha/\cos\alpha = \tan\alpha$ and $\sum m = m_{dry} + \kappa \rho A_1 Z_2$, Equation 3.138 simplifies to:

$$\left(m_{dry} + \kappa \rho A_1 Z_2\right)g \tan\alpha - C_{Dh}\frac{1}{2}\rho_{air}A_h v_{xy}{}^2 = \left(m_{dry} + \kappa \rho A_1 Z_2\right)\frac{dv_{xy}}{dt} \qquad (3.139)$$

3.8.3.1   Case 1: Negligible Drag Force

In this case, a model of the water jetpack system is developed such that the drag force is small and does not severely affect the acceleration and net force of the water jetpack system. For this to be valid, the surge velocity term must be relatively small as discussed previously in Section 3.7.3.1. Equation 3.139 simplifies to:

$$F_{xy} = \left(m_{dry} + \kappa \rho A_1 Z_2\right)g \tan\alpha = \left(m_{dry} + \kappa \rho A_1 Z_2\right)\frac{dv_{xy}}{dt} \qquad (3.140)$$

By cancellation of the accumulative mass term on both sides of Equation 3.140, the acceleration in the x-y direction is given by:

$$\frac{dv_{xy}}{dt} = g \tan\alpha \qquad (3.141)$$

Equation 3.141 shows that the acceleration in the x-direction is a function of the thrust vector angle. Since $-45 \leq \alpha \leq 45$ degrees, the acceleration in the x-y direction is in the region of $-g < \frac{dv_x}{dt} < g$. The acceleration in the x- and y-direction is given by:

$$\frac{dv_x}{dt} = \left(\frac{dv_{xy}}{dt}\right)\cos\psi = g \tan\alpha \cos\psi \qquad (3.142)$$

$$\frac{dv_y}{dt} = \left(\frac{dv_{xy}}{dt}\right)\sin\psi = g \tan\alpha \sin\psi \qquad (3.143)$$

The time-varying velocity in the x-y direction, x-direction and y-direction can be determined by integrating Equation 3.141, Equation 3.142 and Equation 3.143 respectively with respect to time:

$$v_{xy}(t) = \int \left(\frac{dv_{xy}}{dt}\right)dt = \int (g \tan\alpha)\,dt = v_{xy0} + (g \tan\alpha)t \qquad (3.144)$$

$$v_x(t) = \int \left(\frac{dv_x}{dt}\right)dt = \int (g \tan\alpha \cos\psi)\,dt = v_{x0} + (g \tan\alpha \cos\psi)t \qquad (3.145)$$

$$v_y(t) = \int \left(\frac{dv_y}{dt}\right)dt = \int (g \tan\alpha \sin\psi)\,dt = v_{y0} + (g \tan\alpha \sin\psi)t \qquad (3.146)$$

where $v_{xy}(t)$ is the time-varying velocity in the x-y direction, $v_y(t)$ is the time-varying sway velocity, v_{xy0} is the initial velocity in the x-y direction and v_{y0} is the initial sway velocity. The displacement functions in the x-y, x- and y-direction can be determined by double integrating Equation 3.141, Equation 3.142 and Equation 3.143 with respect to time:

$$XY(t) = \iint \left(\frac{dv_{xy}}{dt}\right) dt = \int \left(v_{xy0} + g \tan \alpha\, t\right) dt = XY_0 + v_{x0}t + \frac{1}{2}(g \tan \alpha)t^2 \qquad (3.147)$$

$$X(t) = \iint \left(\frac{dv_x}{dt}\right) dt = \int \left(v_{x0} + g \tan \alpha \cos \psi\, t\right) dt = X_0 + v_{x0}t + \frac{1}{2}(g \tan \alpha \cos \psi)t^2 \qquad (3.148)$$

$$Y(t) = \iint \left(\frac{dv_y}{dt}\right) dt = \int \left(v_{y0} + g \tan \alpha \sin \psi\, t\right) dt = Y_0 + v_{y0}t + \frac{1}{2}(g \tan \alpha \sin \psi)t^2 \qquad (3.149)$$

where $XY(t)$ is the time-varying displacement in the x-y direction, and XY_0 is the initial displacement in the x-y direction, $Y(t)$ is the time-varying displacement in the y-direction and Y_0 is the initial displacement in the y-direction of the water jetpack system. In the case where the initial velocity and displacement in the x-y direction are both zero, Equation 3.144 and Equation 3.147 reduces to:

$$v_{xy}(t) = (g \tan \alpha)t \qquad (3.150)$$

$$XY(t) = \frac{1}{2}(g \tan \alpha)t^2 \qquad (3.151)$$

Equation 3.150 and Equation 3.151 model the velocity and displacement of the water jetpack system in the x-y direction respectively as a function of the thrust vector angle and time. Substituting Equation 3.150 into the thrust force equation as done in Equation 3.94 gives an expression for the thrust force as a function of mass flow rate, thrust vector angle and time:

$$F_T(t) = \dot{m}\left(\frac{\dot{m}}{\rho A_2} - (g \tan \alpha)t\right) \qquad (3.152)$$

where $F_T(t)$ is the time-varying thrust force. It must be noted again that Equation 3.140 to Equation 3.152 are only valid for the case of $v_x \ll 1$ whereby the drag force is negligible. In this case, the models predict that the water jetpack system experiences an acceleration that is dependent on the thrust vector angle. It can be deduced from Equation 3.152 that since there is negligible drag force acting on the system, for fixed mass flow rate and thrust vector angle, as time increases, the thrust force decreases and consequently the flight altitude would decrease according to Equation 3.137. Therefore, to sustain a constant flight altitude, thrust force must increase as time increases. This is achieved by increasing mass flow rate or decreasing the thrust vector angle such that the force in the x-y and z-direction remains zero according to Equation 3.136 and Equation 3.140.

3.8.3.2   Case 2: Non-Negligible Drag Force

In this case, the drag force term in Equation 3.139 is considered in the analysis of developing a set of equations that model the performance of the water jetpack system under second-order transient conditions in the x-y direction while flight altitude remains constant. The x-y velocity and acceleration terms in Equation 3.139 may be expressed as first and second-order time-varying derivatives of displacement with respect to time:

$$v_{xy}(t) = \frac{dXY}{dt} \tag{3.153}$$

$$\frac{dv_{xy}}{dt} = \frac{d^2XY}{dt^2} \tag{3.154}$$

Substituting Equation 3.153 and Equation 3.154 into Equation 3.139 and rearranging the resulting expression:

$$\left(m_{dry} + \kappa \rho A_1 Z_2\right)\frac{d^2XY}{dt^2} + C_{Dh}\frac{1}{2}\rho_{air}A_h\left(\frac{dXY}{dt}\right)^2 - \left(m_{dry} + \kappa \rho A_1 Z_2\right)g \tan\alpha = 0 \tag{3.155}$$

Equation 3.155 is a second-order non-linear differential equation with respect to the displacement in the x-y direction (Zraiqat and Al-Hwawcha, 2015), which cannot be perfectly solved by simple analytical means since the initial conditions are unknown at this stage. In the case of a defined constant acceleration in the x-y direction, the acceleration may be expressed by altering the equation of motion for the x-y direction (Young et al., 2010) which is given by:

$$\frac{dv_{xy}}{dt} = \frac{d^2XY}{dt^2} = \frac{v_{xy}(t) - v_{xy0}}{t} \tag{3.156}$$

Assuming the initial velocity in the x-y direction is zero, substituting Equation 3.156 into Equation 3.139 gives the following second-order time-varying polynomial function for the velocity in the x-y direction:

$$C_{Dh}\frac{1}{2}\rho_{air}A_h\left(v_{xy}(t)\right)^2 + \left(m_{dry} + \kappa \rho A_1 Z_2\right)\left(\frac{v_{xy}(t)}{t}\right) - \left(m_{dry} + \kappa \rho A_1 Z_2\right)g \tan\alpha = 0 \tag{3.157}$$

Equation 3.157 may be solved by using the quadratic formula (Stewart, 2011):

$$v_{xy}(t) = \frac{-b \pm \sqrt{b^2 - 4ac}}{2a} \tag{3.158}$$

where the coefficients of a, b and c are given by Equation 3.159, Equation 3.160 and Equation 3.161 respectively:

$$a = C_{Dh}\frac{1}{2}\rho_{air}A_h \tag{3.159}$$

$$b = \frac{\left(m_{dry} + \kappa \rho A_1 Z_2\right)}{t} \tag{3.160}$$

$$c = -g \tan\alpha \left(m_{dry} + \kappa \rho A_1 Z_2\right) \tag{3.161}$$

There are two solutions to Equation 3.158. However, when $0 < \alpha < 45$ degrees, the water jetpack system moves in the positive x-y direction and therefore the velocity in the x-y direction is positive. Likewise, when $0 > \alpha > -45$ degrees, the water jetpack system moves in the negative x-y direction and therefore the velocity in the x-y direction is negative. These relations can be expressed mathematically as follows:

$$v_{xy}(t) > 0 \leftrightarrow 0 < \alpha < 45$$

$$v_{xy}(t) < 0 \leftrightarrow 0 > \alpha > -45$$

These conditions must be satisfied for Equation 3.158 to be valid for modelling the velocity of the water jetpack system in the x-y direction. The surge and sway velocity may be computed using Equation 3.132 and Equation 3.133 respectively. Once the velocities are computed, the time-varying displacement functions in the x, y and x-y direction may be obtained by integrating Equation 3.132, Equation 3.133 and Equation 3.158 respectively such that:

$$X(t) = \int v_x(t)\, dt \qquad (3.162)$$

$$Y(t) = \int v_y(t)\, dt \qquad (3.163)$$

$$XY(t) = \int v_{xy}(t)\, dt \qquad (3.164)$$

The acceleration can be computed by substituting Equation 3.158 into Equation 3.156. The drag force can be computed by substituting Equation 3.158 into Equation 3.117 and the thrust force can be computed by substituting Equation 3.158 into Equation 3.121 which may be used to solve for the mass flow rate required for this type of flight of the water jetpack system. The equations in this section describe that to sustain constant flight altitude while accelerating in the x-y direction, the thrust force in the z-direction must remain constant while the thrust force in the x-y direction must increase with time. This is achieved by either increasing the mass flow rate while increasing the thrust vector angle or decreasing the mass flow rate while decreasing the thrust vector angle. Either of these actions would result in a zero net force in the z-direction. However, the latter action of decreasing mass flow rate and thrust vector angle leads to a drop in the acceleration of the water jetpack system in the x-y direction. Increasing the yaw angle also increases the velocity in the y-direction without affecting the force balance in the z-direction. This is only valid in the case where the water jetpack system remains in the stable state and the experiences zero moment about the x, y and z axis of the fixed earth coordinate system.

CHAPTER 4 : AUTONOMOUS UNDERWATER VEHICLE MODELLING

Mathematical modelling of AUVs is based upon the theory of water jet propulsion and fluid dynamics as detailed in Chapter 2. Modelling an AUV consists of mathematical modelling of the propeller thrust, external fluid flow theory, and hydrostatic forces. This chapter details the development of a series of static and dynamic differential equations in one, two and three dimensions for a hypothetical AUV system using the fundamental theory of fluid dynamics presented in Chapter 2. The assumption in the analysis contained in this chapter is that the AUV behaves as a rigid body of fixed mass. The primary forces acting on the AUV are gravitational, buoyant, propeller thrust, forces from control surfaces such as fins and rudders, and drag force. The forces that can be controlled are: propeller thrust and control surface forces which control the forward velocity and steering of the AUV.

4.1 AUV Coordinate System

Figure 4.1 shows the coordinate system used for the mathematical models in this chapter. A six-degree of freedom coordinate system is used which contain the variables (x, y, z) to represent linear motion in the respective directions bracketed and (ϕ, θ, ψ) to represent angular or rotational motion in the x-, y- and z-directions respectively.
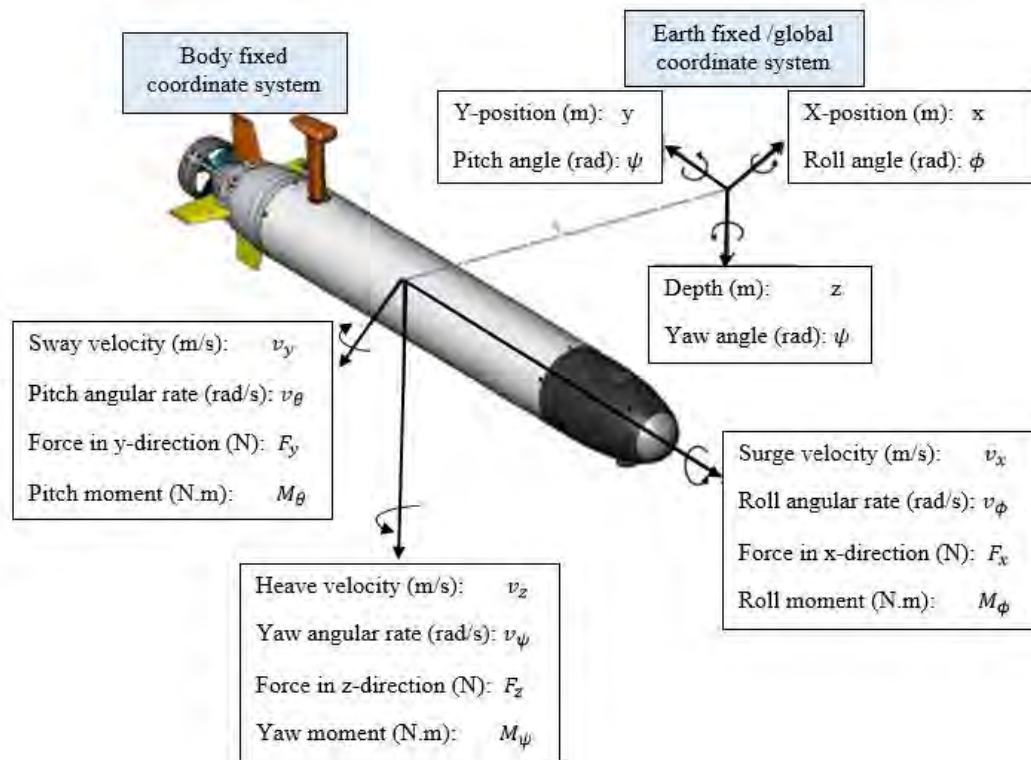

Figure 4.1: Autonomous Underwater Vehicle coordinate system
Source: Leveille, 2007

Figure 4.1 shows an AUV with the body-fixed and earth fixed coordinate system which is identical to the coordinate systems in Figure 3.1 which was used to model the water jetpack system in Chapter 3. Surge, sway and heave are the terms that denote linear motion in the x-, y- and z-directions respectively. Roll, pitch and yaw are the terms denoting angular motion with respect to the x-, y- and z-directions respectively. The linear velocities in the x-, y- and z-directions are denoted b v_x, v_y and v_z respectively. The angular velocities with respect to the x, y and z axis are denoted by v_ϕ, ω_θ and v_ψ respectively. The force and moment for each degree of freedom are denoted by $F_x, F_y, F_z, M_\phi, M_\theta, M_\psi$.

4.2   AUV One-Dimensional Modelling

In this section, one-dimensional steady state and transient models are developed for the AUV system with motion in the x-direction. The analysis contained in this section detail the force, velocity, acceleration and thrust force experienced by the AUV system along with the power requirements from propeller of the AUV. Throughout this section, the AUV system is modelled to travel linearly in the x-direction with the effects of drag force. The fundamental law governing the equations presented in this section is Newton's Second Law of motion as presented by Equation 3.1 in Chapter 3.

4.2.1   Steady State Speed Control

In this model, the AUV system travels in the x-direction at constant surge velocity. In this analysis, the forces in the z-direction (buoyant, fin and weight) are assumed to not affect the steady state velocity of the AUV and that the only force affecting the surge velocity is drag force. By applying these assumptions to the model, Newton's Second Law is given by:

$$\sum F_x = m_{AUV} \frac{dv_x}{dt} \tag{4.1}$$

where $\sum F_x$ is the net force in the x-direction, m_{AUV} is the mass of the AUV, and dv_x/dt is the acceleration of the AUV in the x-direction. In the x-direction, there are two forces that act on the AUV: 1) propeller thrust and 2) drag force, therefore the force balance in the x-direction is given by:

$$\sum F_x = F_{prop} - F_D \tag{4.2}$$

where F_{prop} is the propeller thrust force and F_D is the total drag force acting on the AUV. Equating Equation 4.2 and Equation 4.3 gives the following:

$$m_{AUV} \frac{dv_x}{dt} = F_{prop} - F_D \tag{4.3}$$

The propeller thrust is given by:

$$F_{prop} = \dot{m}_{prop}(v_j - v_x) \tag{4.4}$$

where $\dot{m}_{prop}$ is the mass flow rate through the AUV propeller, v_j is the velocity of the water exiting the propeller, and v_x is the surge velocity of the AUV. The mass flow rate through the propeller and the velocity of water exiting the propeller are related by the conservation of mass and the continuity equation given in Section 2.3 of Chapter 2, this is expressed as:

$$\dot{m}_{prop} = \rho \, A_{prop} \, v_p \tag{4.5}$$

where ρ is the density of water, A_{prop} is the area of the propeller, and v_p is the mean velocity of water through the propeller. The mean velocity through the propeller is given by the average of velocity of water entering and exiting the propeller and is given by:

$$v_p = \frac{1}{2}\left(v_j + v_x \right) \tag{4.6}$$

where v_j is the velocity of water exiting the propeller and v_x is the velocity of water entering the propeller which is equal to the surge velocity of the AUV. Substituting Equation 4.6 into Equation 4.5 gives an expression of mass flow rate in terms of the inlet and exit velocity:

$$\dot{m}_{prop} = \frac{1}{2}\rho \, A_{prop}\left(v_j + v_x \right) \tag{4.7}$$

Substituting Equation 4.7 into Equation 4.4, the propeller thrust is given by:

$$F_{prop} = \frac{1}{2}\rho \, A_{prop}\left(v_j{}^2 - v_x{}^2\right) \tag{4.8}$$

In the case of controlling the thrust force generated by a propeller, it is more useful to express Equation 4.8 in terms of mass flow rate and surge velocity since mass flow rate through a given propeller with fixed geometry is dependent on the rotational speed of the propeller (Brutzman, 1994). By solving for v_j in Equation 4.7 and substituting the resulting expression into Equation 4.8, the propeller thrust in terms of mass flow rate and surge velocity is given by:

$$F_{prop} = \frac{1}{2}\rho \, A_{prop}\left(\left(\frac{2\,\dot{m}_{prop}}{\rho \, A_{prop}} - v_x\right)^2 - v_x{}^2\right) \tag{4.9}$$

Simplifying Equation 4.9 gives the following:

$$F_{prop} = \frac{2\left(\dot{m}_{prop}{}^2 - \rho \, A_{prop}\,\dot{m}_{prop}\,v_x\right)}{\rho \, A_{prop}} \tag{4.10}$$

The mass flow rate through the propeller is related to the rotational speed of the propeller. Consequently, the propeller thrust is related to the rotational speed (Brutzman, 1994). Geridonmez (2007) modelled an AUV and analyzed the steady state performance for an AUV travelling in a straight path. He established that the ratio of propeller thrust is proportional to the square of the ratio of the propeller's rotational speed. This relationship is described as:

$$\frac{F_{prop_1}}{F_{prop_2}} \propto \frac{\dot{m}_{prop_1}}{\dot{m}_{prop_2}} \propto \left(\frac{N_{prop_1}}{N_{prop_2}}\right)^2$$

The above affinity law is valid only for a propeller with fixed area and geometry. In general, propeller manufacturers supply a set of performance curves that illustrate the characteristics of propellers at different speeds and diameters.

The drag force acting on the AUV is given by:

$$F_D = C_{D_A} \frac{1}{2} \rho v_x^2 A_A \tag{4.11}$$

where C_{D_A} is the drag coefficient of the AUV, ρ is the density of water and A_A is the area of the AUV that experiences drag force. Since the acceleration term in Equation 4.3 is zero for steady state analysis, substituting the expressions for propeller thrust force in Equation 4.10 and AUV drag force in Equation 4.11 results in the following:

$$\frac{2\left(\dot{m}_{prop}^2 - \rho A_{prop} \dot{m}_{prop} v_x\right)}{\rho A_{prop}} - C_{D_A} \frac{1}{2} \rho v_x^2 A_A = 0 \tag{4.12}$$

Simplifying Equation 4.12 results in the following second-order polynomial equation:

$$\frac{2\dot{m}_{prop}^2}{\rho A_{prop}} - 2 \dot{m}_{prop} v_x - C_{D_A} \frac{1}{2} \rho v_x^2 A_A = 0 \tag{4.13}$$

Equation 4.13 is a first-order differential equation since the surge velocity is the first derivative of displacement in the x-direction with respect to time. Equation 4.13 may be expressed as:

$$\frac{2\dot{m}_{prop}^2}{\rho A_{prop}} - 2 \dot{m}_{prop} \left(\frac{dX(t)}{dt}\right) - C_{D_A} \frac{1}{2} \rho \left(\frac{dX(t)}{dt}\right)^2 A_A = 0 \tag{4.14}$$

where $X(t)$ is the time-varying displacement in the x-direction. Equation 4.13 and Equation 4.14 can be used to determine the mass flow rate through the propeller for a defined steady state surge velocity. Hence it is possible to determine the propeller speed required to reach a defined steady state surge velocity. A similar approach to solving second-order polynomial functions as done in Section 3.8.3.2 can be used to solve Equation 4.13. Once the mass flow rate through the propeller is determined, the thrust force generated by the propeller can be computed using Equation 4.10. The power generated by the AUV propulsion system is given by:

$$\dot{W} = F_{prop} v_x \tag{4.15}$$

where $\dot{W}$ is the power generated by the AUV propulsion system. The propeller is powered by an electric motor which is linked to the propeller by a shaft and in some cases, a gearbox. If the mechanical efficiency of the gearbox and shaft that couples the electric motor to the propeller is η_{mech}, then the power required by the electric motor is given by:

$$\dot{W}_{motor} = \frac{\dot{W}}{\eta_{mech}} \tag{4.16}$$

where $\dot{W}_{motor}$ is power required by the electric motor and η_{mech} is the mechanical efficiency of the gearbox and shaft coupling the electric motor to the propeller.

4.2.2 X-Direction Second-Order Transient Modelling

The mathematical models relating to Newton's Second Law as described in Section 4.3.1 are applicable for the case of steady state motion in the x-direction. In the case of transient motion in the x-direction, a new set of equations must be derived to describe the performance of the AUV as a second-order system. Newton's Second Law for this case is given by:

$$m_{AUV} \frac{dv_x}{dt} = F_{prop} - F_D \tag{4.17}$$

where dv_x/dt is the non-zero acceleration of the AUV in the x-direction. Substituting Equation 4.10 and Equation 4.11 into Equation 4.17 and simplifying the result gives the following second-order non-linear differential equation:

$$m_{AUV} \frac{dv_x}{dt} - C_{D_A} \frac{1}{2} \rho v_x^2 A_A - 2 \, \dot{m}_{prop} \, v_x - \frac{2 \dot{m}_{prop}^2}{\rho \, A_{prop}} = 0 \tag{4.18}$$

Equation 4.18 may be expressed in terms of displacement as in Equation 4.14:

$$m_{AUV} \left(\frac{d^2 X(t)}{dt^2} \right) - C_{D_A} \frac{1}{2} \rho \left(\frac{dX(t)}{dt} \right)^2 A_A - 2 \, \dot{m}_{prop} \left(\frac{dX(t)}{dt} \right) - \frac{2 \dot{m}_{prop}^2}{\rho \, A_{prop}} = 0 \tag{4.19}$$

Equation 4.19 can be completely solved by using the Laplace decomposition method as detailed by Charkrit (2013). Alternatively, in the case of a constant acceleration and zero initial condition approach as done in Section 3.7.3.2, the equation of motion given by Equation 3.98 is applicable for use in Equation 4.18. This would result in a second-order polynomial which can be solved using Equation 3.100 with a similar approach. Once the surge velocity function of the AUV and mass flow rate through the propeller function is determined, Equation 4.10 and Equation 4.11 is used to compute the propeller thrust and drag force on the AUV respectively. Thereafter, Equation 4.15 and Equation 4.16 can be used to compute the power generated by the AUV propulsion system and the power required by the electric motor.

4.3 AUV Modelling in Two-Dimensions

The steering control of an AUV is performed by a set of rudders. The rudders may be positioned at the rear of the propeller such that the actual propeller thrust is deflected by an angle known as the rudder angle, denoted by δ_{rudder}. In this section, a model is developed for AUV motion in the x- and y-directions. The underlying assumption is that the rudders are ideal thruster controllers such that they control the path of the AUV in the x-y plane. Furthermore, the models developed in this section are based on steady state and transient motion of the AUV in the x- and y-direction after a change in the rudder angle has occurred and the desired path is attained.

4.3.1 Force Analysis and Newton's Second Law

Newton's Second Law in the x-y direction in vector form may be expressed as:

$$\sum \vec{F}_{xy} = m_{AUV}\, \vec{a}_{xy} \tag{4.20}$$

where $\sum \vec{F}_{xy}$ is the net force vector and $\vec{a}_{xy}$ is the acceleration vector of the AUV in the in the x-y direction. The force vector may be expressed as a vector sum of its individual components such that:

$$\vec{F}_{xy} = \vec{F}_x + \vec{F}_y \tag{4.21}$$

where $\vec{F}_x$ is the force vector in the x-direction and $\vec{F}_y$ is the force vector in the y-direction. The magnitude of the force in the x-y direction is given by:

$$F_{xz} = \sqrt{F_x{}^2 + F_y{}^2} \tag{4.22}$$

where F_{xy} is the force in the x-y direction, F_x is the force in the x-direction and F_y is the force in the y-direction. The acceleration vector may be expressed as:

$$\vec{a}_{xy} = \frac{d\vec{v}_{xy}}{dt} = \frac{d\vec{v}_x}{dt} + \frac{d\vec{v}_y}{dt} \tag{4.23}$$

where $\vec{a}_{xy}$ and $d\vec{v}_{xy}/dt$ is the acceleration vector in the x-y direction, $d\vec{v}_x/dt$ is the acceleration vector in the x-direction and $d\vec{v}_y/dt$ is the acceleration vector in the y-direction. The magnitude of the acceleration in the x-y direction is given by:

$$a_{xy} = \frac{dv_{xy}}{dt} = \sqrt{\left(\frac{dv_x}{dt}\right)^2 + \left(\frac{dv_y}{dt}\right)^2} \tag{4.24}$$

where a_{xy} and dv_{xy}/dt is the acceleration in the x-y direction, dv_x/dt is the acceleration in the x-direction and dv_y/dt is the acceleration in the y-direction. The force balance in the x-y direction in vector form is given by:

$$\vec{F}_{xy} = \vec{F}_{prop} + \vec{F}_D \tag{4.25}$$

where $\vec{F}_{prop}$ is the propeller thrust force vector and $\vec{F}_D$ is the drag force vector. The magnitude of the net force in the x-direction and y-direction respectively is given by:

$$\sum F_x = m_{AUV}\frac{dv_x}{dt} = F_{prop}\cos(\delta_{rudder}) - F_{D_x} \tag{4.26}$$

$$\sum F_y = m_{AUV}\frac{dv_y}{dt} = F_{prop}\sin(\delta_{rudder}) - F_{D_y} \tag{4.27}$$

107

where δ_{rudder} is the rudder angle (also referred to as the thrust vector angle) and F_{D_x} is the drag force in the x-direction (called axial drag) and F_{D_x} is the drag force in the y-direction (called cross-flow drag). The drag in the x- and y-direction is given by:

$$F_{D_x} = C_{D_A} \frac{1}{2} \rho v_x{}^2 A_A \qquad (4.28)$$

$$F_{D_y} = C_{D_{AL}} \frac{1}{2} \rho v_y{}^2 A_{AL} \qquad (4.29)$$

where C_{D_A} is the coefficient of drag along the longitudinal section of the AUV, v_y is the sway velocity and A_{AL} is the surface area of the longitudinal section of the AUV. Substituting Equation 4.10, Equation 4.28 and Equation 4.29 into Equation 4.26 and 4.27:

$$\sum F_x = m_{AUV} \frac{dv_x}{dt} = \frac{2\cos(\delta_{rudder}) \left(\dot{m}_{prop}{}^2 - \rho\, A_{prop}\, \dot{m}_{prop}\, v_x \right)}{\rho\, A_{prop}} - C_{D_A} \frac{1}{2} \rho v_x{}^2 A_A \qquad (4.30)$$

$$\sum F_y = m_{AUV} \frac{dv_y}{dt} = \frac{2\sin(\delta_{rudder}) \left(\dot{m}_{prop}{}^2 - \rho\, A_{prop}\, \dot{m}_{prop}\, v_x \right)}{\rho\, A_{prop}} - C_{D_{AL}} \frac{1}{2} \rho v_y{}^2 A_{AL} \qquad (4.31)$$

Equation 4.30 and Equation 4.31 model the net force experienced by the AUV due to a change in the rudder angle. The rudders are modelled to act as thrust vectors. A change in the rudder angle induces a yaw angle and hence a change in path of the AUV as illustrated in Figure 4.2.
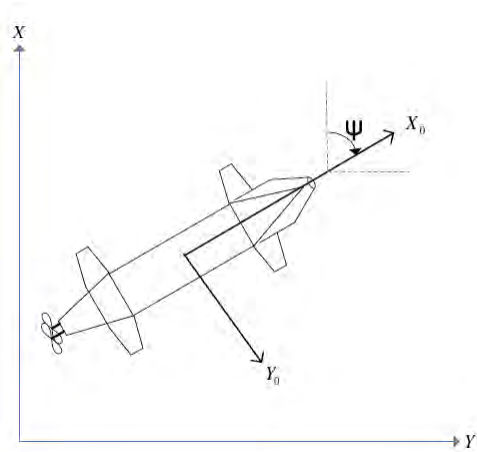
Figure 4.2: Heading of an AUV in the x-y plane
Source: Geridonmez, 2007

As shown in Figure 4.2, the yaw angle ψ is measured relative to the fixed earth coordinate system (X-Y axis). The body-fixed coordinate axis is X_0 and Y_0. The AUV in Figure 4.2 is travelling in the positive X_0 direction which is rotated through an angle ψ from the fixed earth X axis. This rotation of the body-fixed coordinate axis from the earth fixed coordinate axis is brought about by a temporary change in rudder angle which reaches a peak angle and then decays to zero again as the yaw angle of the AUV approaches the reference yaw angle that is desired (Geridonmez,

2007). However, once a desired yaw angle is attained, the rudder angle must decrease to zero such that the sway velocity of the AUV is zero and thereafter the equations in Section 4.3 are used to model the AUV motion in a straight path. Detailed modelling analysis on heading control of an AUV using six-degrees of freedom motion is detailed in Appendix B; further analysis can be obtained from Geridonmez (2007) as well as Mishra and Dinesh (2001) in which a model is developed to describe the yaw rate of the AUV as a function of the geometry of the AUV and added masses. The results by Mishra and Dinesh (2001) show that for a fixed rudder angle and propeller thrust, a circular path is obtained as shown in Figure 4.3.
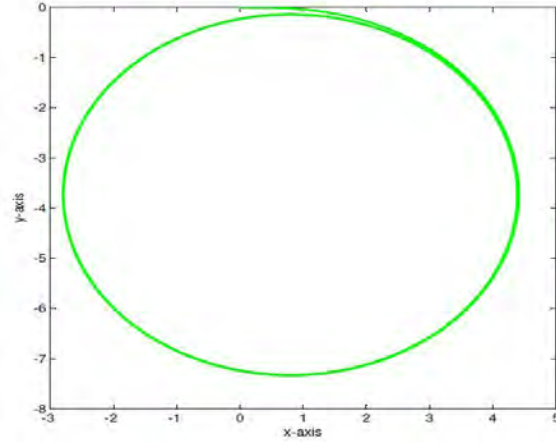

Figure 4.3: Path of an AUV with fixed propeller thrust and rudder angle
Source: Mishra and Dinesh, 2001

The radius of the green circular path shown in Figure 4.3 is dependent on the propeller thrust and rudder angle. Mishra and Dinesh (2001) established a model that shows that as propeller thrust and rudder angle increases, there is a corresponding decrease in the radius of the circular path attained by the AUV. This holds true for fixed ruder angle. In the case of changing the rudder angle to attain a certain reference yaw angle, the rudder angle must decrease to zero once the AUV reaches the desired yaw angle. This action involves complex coupling of the dynamic equation of the AUV along with the characteristics of the hull of the AUV which is beyond the scope of the current study. During the phase of the rudder angle being non-zero, the AUV would experience a force in the y-direction and thus a corresponding sway velocity. Once the AUV reaches the desired yaw angle, the rudder angle must return to zero and the force in the y-direction decays to zero according to Equation 4.31.

4.3.2   Steady State Analysis

In this section, the AUV will be modelled for steady state conditions whereby the acceleration of the AUV is zero in both the x- and y-directions. In this case, Equation 4.30 and Equation 4.31 are reduced to:

$$F_{prop}\cos(\delta_{rudder}) - C_{D_A}\frac{1}{2}\rho v_x{}^2 A_A = 0 \tag{4.32}$$

$$F_{prop}\sin(\delta_{rudder}) - C_{D_{AL}}\frac{1}{2}\rho v_y{}^2 A_{AL} = 0 \tag{4.33}$$

To solve Equation 4.32 and 4.33, it is required to substitute the expression for propeller thrust given by Equation 4.10 into Equation 4.32 first, which results in a second-order polynomial of the surge velocity v_x which can be computed using the quadratic formula (Stewart, 2011). Once the surge velocity is obtained, the propeller thrust can be computed using Equation 4.10. Thereafter the sway velocity can be determined by substituting of F_{prop} into Equation 4.33. In the case of the AUV attaining a desired yaw angle, this action can be achieved by controlling the propeller speed and hence the mass flow rate through the propeller which controls propeller thrust, and simultaneously control the rudder angle such that Equation 4.32 and Equation 4.33 hold and the system attains the desired yaw angle at steady state conditions. The rudder angle required to attain a desired a steady state surge velocity for a given mass flow rate through the propeller may be computed by Equation 4.34:

$$\delta_{rudder} = \cos^{-1}\left[\frac{C_{D_A}\,\rho^2 {v_x}^2\,A_{prop}A_A}{4\left({\dot{m}_{prop}}^2 - \rho\,A_{prop}\,\dot{m}_{prop}\,v_x\right)}\right] \tag{4.34}$$

Once Equation 4.34 is solved, the result may be substituted into Equation 4.33 to compute the sway velocity and drag force in the y-direction. Once the propeller thrust and surge velocity is obtained by following this procedure, the power generated by the AUV propulsion system and the electric motor can be computed thereafter by using Equation 4.15 and Equation 4.16. Once the AUV reaches the desired yaw angle, the rudder angle would have to decay to zero as discussed and the system attains steady state motion in the x-direction, such that the equations in Section 4.3 apply to the model.

4.4   AUV Modelling in Three Dimensions

This section details the steady state and transient modelling of an AUV in the x-, y- and z-directions. In general, an AUV experiences forces in both the horizontal and vertical directions. In Section 4.4, the forces acting on the AUV in the horizontal plane were propeller thrust and drag force. The vertical forces acting on an AUV are weight and the buoyant force. A free-body diagram of an AUV is shown in Figure 4.4. The underlying assumption made in the development of this model is that all the forces acting on the AUV act through the CM and center of gravity of the AUV. This assumption implies that the net pitch, roll and yaw moment acting on the AUV are zero since the forces are assumed to act through the CM and center of gravity of the AUV.
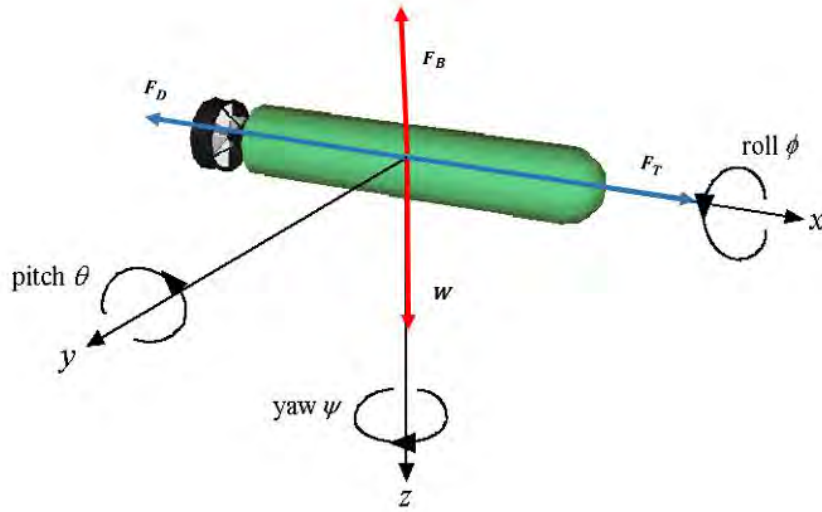
Figure 4.4: Free-body diagram of AUV in three-dimensions
Source: Gonzalez, 2004

By referring to Figure 4.4, the forces in the z-direction are: 1) weight W and 2) buoyant force F_B, these forces are denoted by the red arrows and point in the directions in which these forces act. In the free-body diagram in Figure 4.4, the positive z-direction is chosen as the upward direction. The buoyant force always acts in the positive z-direction and the weight of the AUV acts in the negative z-direction. The forces acting in the x-direction are: 1) propeller thrust F_{prop} and 2) drag force F_D, these forces are denoted by the blue arrows and point in the direction in which these forces act. As discussed in Section 4.3 and Section 4.4, propeller thrust causes a force on the AUV in the positive x-direction and drag acts in the direction that opposes the motion of the AUV (Young et al., 2011). Thus, if the AUV travels in the positive x-y direction at yaw angle ψ, then the drag force acts in the negative x-y direction, at an angle of $-\psi$.

4.4.1   Force Analysis and Newton's Second Law

Newton's Second Law for the water jetpack system which was modelled in three dimensions in Chapter 3 is applicable in this section of modelling the AUV in three dimensions. The vector analysis of these equations is identical to the analysis conducted when modelling the water jetpack system in the x-, y- and z-direction. However, the force balance differs and this requires a new set of differential equations to be analyzed. Newton's Second Law in the x-y-z direction in vector form may be expressed as:

$$\sum \vec{F}_{xyz} = m_{AUV} \, \vec{a}_{xyz} \qquad (4.35)$$

where $\sum \vec{F}_{xyz}$ is the net force vector, m_{AUV} is the mass of the AUV, and $\vec{a}_{xyz}$ is the acceleration vector of the AUV in the in the x-y-z direction. The force vector may be expressed as a vector sum of its individual components such that:

$$\vec{F}_{xyz} = \vec{F}_x + \vec{F}_y + \vec{F}_z \tag{4.36}$$

where $\vec{F}_x$ is the force vector in the x-direction, $\vec{F}_y$ is the force vector in the y-direction and $\vec{F}_z$ is the force vector in the z-direction. The magnitude of the force in the x-y-z direction is given by:

$$F_{xyz} = \sqrt{F_x{}^2 + F_y{}^2 + F_z{}^2} \tag{4.37}$$

where F_{xyz} is the force in the x-z direction, F_x is the force in the x-direction and F_z is the force in the z-direction. The acceleration vector may be expressed as:

$$\vec{a}_{xyz} = \frac{d\vec{v}_{xz}}{dt} = \frac{d\vec{v}_x}{dt} + \frac{d\vec{v}_y}{dt} + \frac{d\vec{v}_z}{dt} \tag{4.38}$$

where $\vec{a}_{xyz}$ and $d\vec{v}_{xyz}/dt$ is the acceleration vector in the x-y-z direction, $d\vec{v}_x/dt$ is the acceleration vector in the x-direction, $d\vec{v}_y/dt$ is the acceleration vector in the y-direction and $d\vec{v}_z/dt$ is the acceleration vector in the z-direction. The magnitude of the acceleration in the x-y-z direction is given by:

$$a_{xyz} = \frac{dv_{xyz}}{dt} = \sqrt{\left(\frac{dv_x}{dt}\right)^2 + \left(\frac{dv_y}{dt}\right)^2 + \left(\frac{dv_z}{dt}\right)^2} \tag{4.39}$$

where a_{xz} and dv_{xz}/dt is the acceleration in the x-z direction, dv_x/dt is the acceleration in the x-direction, dv_y/dt is the acceleration in the y-direction and dv_z/dt is the acceleration in the z-direction. By referring to the forces in the respective directions shown in Figure 4.4 and applying Newton's Second Law into Equation 4.36, the force balance in the x-y-z direction in vector form is given by:

$$\vec{F}_{xyz} = \vec{F}_T + \vec{F}_B + \vec{F}_D + \vec{W} \tag{4.40}$$

where $\vec{F}_T$ is the thrust force vector, $\vec{F}_B$ is the buoyant force vector, $\vec{F}_D$ is the drag force vector and $\vec{W}$ is the weight vector acting on the jetpack system in the x-y-z direction. The net force in the x-, y- and z-direction is given by Equation 4.41, Equation 4.42 and Equation 4.43 respectively:

$$\sum F_x = m_{AUV}\frac{dv_x}{dt} = F_{prop}\cos(\delta_{rudder}) - F_{D_x} \tag{4.41}$$

$$\sum F_y = m_{AUV}\frac{dv_y}{dt} = F_{prop}\sin(\delta_{rudder}) - F_{D_y} \tag{4.42}$$

$$\sum F_z = m_{AUV}\frac{dv_z}{dt} = F_B - W + F_L \tag{4.43}$$

where F_B is the buoyant force, W is the weight of the AUV, F_L is the lift force acting on the AUV (vertically upwards in the positive z-direction). It must be noted that the effects of drag in the z-direction are negligible in this model and hence there is no drag force term in Equation 4.43. The lift force acting on the AUV is due to the angular position and

size of the fins on the AUV as well as the surge velocity of the AUV. The force caused by the fins of the AUV is given by:

$$F_L = C_{L_{fin}} \frac{1}{2} \rho \, A_{fin} \delta_{fin} v_{xy}{}^2 \qquad (4.44)$$

where $C_{L_{fin}}$ is the coefficient of lift for the fins, ρ is the density of water, A_{fin} is the total surface area of the fins, δ_{fin} is the effective fin angle in radians, and v_{xy} is the velocity in the x-y direction. In the design of most AUV's, the fin angle is controlled by servomechanism. However, the fin angle is often limited and the lift force generated by the fins depends on the square linear velocity of the AUV. This implies that the sensitivity of this system to generate lift force increases with linear velocity and thus may lead to increased demand on controller processing and the accuracy of the control system that controls the vertical position of the AUV. The use of fins to control an AUV's depth in water is limited. Early work by Le Page and Holappa (2000) involved research on a two-dimensional thrust vectoring system for an AUV which controlled the depth of an AUV by rotating the entire propeller system by an angle to attain a desired path. Cavallo and Michelini (2004) worked on the design of a three-dimensional thrust vectoring mechanism to implement on an AUV and proposed the SWAN idea as shown in Figure 4.5, this system is based on the early work of Gosselin and Angels (1989).
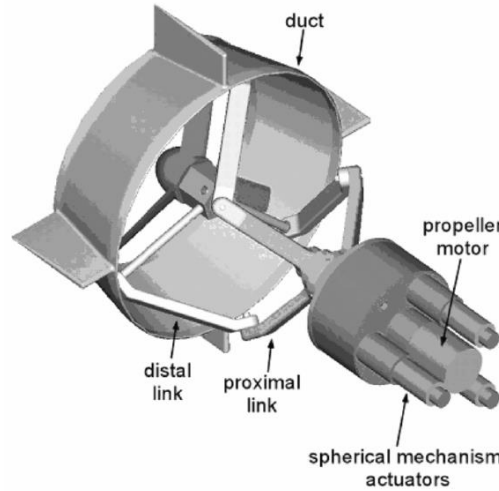

Figure 4.5: Three-dimensional AUV thruster model
Source: Cavallo, Michelini, Filaretov and Ukhimets, 2005

Figure 4.5 shows the thruster model that was proposed by Cavallo et al. (2005) which consist of a duct that is controlled by three distal and proximal links. There is an inner bearing and a joint that connects the propeller to the actuation mechanism. The duct has a set of fixed fins attached to it for stability of the AUV while in motion. The entire system works such that the propeller thrust may be directed in any desired direction which is a combination of vertical and horizontal angular positioning. The two angles that define the orientation of the duct and the propeller thrust are called the deviation angles and are denoted by δ_d and δ_f. The vertical deviation angle is denoted as δ_d and the horizontal

deviation angle is denoted as δ_r. The vertical deviation angle controls the pitch angle and depth of the AUV and the horizontal deviation angle controls the yaw angle and steering of the AUV. Figure 4.6 shows a virtual model of an AUV with the three-dimensional thrust vectoring system.
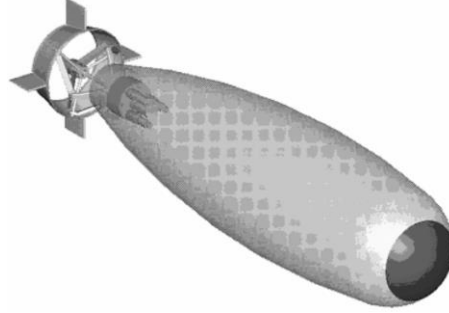

Figure 4.6: Three-Dimensional thrust vectoring system on an AUV model
Source: Cavallo et al., 2005

The three-dimensional thrust vectoring system is positioned at the rear of the AUV and has three-degree of freedom control. The power supply for control of the actuators and propeller rotation is achieved by three electric motors. The propeller thrust generated by this system in the x-, y- and z-direction is given by:

$$F_{prop\ x} = F_{prop}\ \cos(\delta_d)\cos(\delta_r) \tag{4.45}$$

$$F_{prop\ y} = F_{prop}\ \cos(\delta_d)\sin(\delta_r) \tag{4.46}$$

$$F_{prop\ z} = F_{prop}\ \sin(\delta_d) \tag{4.47}$$

where $F_{prop\ x}$ is the propeller thrust in the x-direction, $F_{prop\ y}$ is the propeller thrust in the y-direction, $F_{prop\ z}$ is the propeller thrust in the z-direction, δ_d is the vertical deviation angle and δ_r is the horizontal deviation angle. The propeller thrust in three dimensions is given by:

$$F_{prop} = \frac{2\left(\dot{m}_{prop}^2 - \rho\ A_{prop}\ \dot{m}_{prop}\ v_{xyz}\right)}{\rho\ A_{prop}} \tag{4.48}$$

where v_{xyz} is the absolute velocity of the AUV. Equation 4.48 represents the total propeller thrust generated by the propulsion system of the AUV. The absolute velocity v_{xyz} is computed similarly to the equations for computing the acceleration and force in the x, y and z-direction, the absolute velocity is given by:

$$v_{xyz} = \sqrt{v_x^2 + v_y^2 + v_z^2} \tag{4.49}$$

To determine the steady state and transient equations for an AUV with a three-dimensional thrust vectoring system, a new set of equations must be derived by applying Newton's Second Law to the AUV. By applying Newton's Second Law and using Equation 4.45, Equation 4.46 and Equation 4.47 as the model for the propeller thrust in the x-, y- and z-directions respectively, the net force in the x-, y- and z-direction is given by:

$$\sum F_x = m_{AUV} \frac{dv_x}{dt} = F_{prop}\cos(\delta_d)\cos(\delta_r) - F_{D_x} \qquad (4.48)$$

$$\sum F_y = m_{AUV} \frac{dv_y}{dt} = F_{prop}\cos(\delta_d)\sin(\delta_r) - F_{D_y} \qquad (4.49)$$

$$\sum F_z = m_{AUV} \frac{dv_z}{dt} = F_B - W + F_{prop}\sin(\delta_d) \qquad (4.50)$$

Equation 4.48 and Equation 4.49 are almost identical to the force balance equations given in Section 4.4 except with the inclusion of $\cos(\delta_d)$ in the propeller thrust term. This implies that increasing the vertical deviation angle causes a decrease in the net force experienced by the AUV in the x- and y-direction, consequently there is an increase in the net force experienced by the AUV in the z-direction. However, this depends on the direction and sign of δ_d relative to the pitch angle of the AUV. There are three forces acting on the AUV in the z-direction as given by Equation 4.50. The buoyant force F_B and weight W in Equation 4.50 is given by:

$$F_B = \rho g V_B \qquad (4.51)$$

$$W = m_{AUV}\, g \qquad (4.52)$$

where ρ is the density of water, V_B is the volume of the AUV and g is the gravitational acceleration constant.

4.4.2   Steady State Analysis

In this section, the AUV will be modelled for steady state conditions whereby the acceleration of the AUV is zero in the x-, y- and z-directions are zero. This model includes the steady state model developed in Section 4.4, however, this model is based on the three-dimensional thrust vectoring system as detailed previously. In this case, Equation 4.48, 4.49 and 4.50 are reduced to:

$$\sum F_x = F_{prop}\cos(\delta_d)\cos(\delta_r) - F_{D_x} = 0 \qquad (4.53)$$

$$\sum F_y = F_{prop}\cos(\delta_d)\sin(\delta_r) - F_{D_y} = 0 \qquad (4.54)$$

$$\sum F_z = \rho g V_B - m_{AUV}\, g + F_{prop}\sin(\delta_d) = 0 \qquad (4.55)$$

The above equations can be solved simultaneously by making F_{prop} the common variable. The type of solution obtained from these equations is dependent on the variables that are controlled to achieve a desired output. For instance, if the yaw angle ψ is directly proportional to the horizontal deviation angle δ_r, and that the depth of the AUV is constant for a pre-determined fixed vertical deviation angle δ_d, then the above equations may be solved firstly setting F_{prop} as the subject of each equation such that there are three expressions for the propeller thrust:

$$F_{prop} = \frac{F_{D_x}}{\cos(\delta_d)\cos(\delta_r)} \qquad (4.56)$$

115

$$F_{prop} = \frac{F_{Dy}}{\cos(\delta_d)\sin(\delta_r)} \tag{4.57}$$

$$F_{prop} = \frac{m_{AUV}\, g - \rho g V_B}{\sin(\delta_d)} \tag{4.58}$$

The propeller thrust may be computed directly from Equation 4.58, this would result in determining the propeller thrust required to maintain a certain depth under water for some fixed vertical deviation angle such that the velocity in the z-direction is zero. Once the propeller thrust is obtained, a substitution may be made into Equation 4.56 and Equation 4.57 to determine the surge and sway velocity resulting from a certain value of the horizontal deviation angle or vice versa. The key element in this analysis is to ensure that all three equations that model the force balance in the x-, y- and z-direction are valid and that the desired surge and sway velocity is attained. In the case where the AUV remains stationary, such that $F_{prop} = 0$, the AUV remains neutrally buoyant if the density of the AUV hull is less than or equal to the density of water, that is $\rho_s \leq \rho$, as detailed in the theory of buoyancy and stability section of Chapter 2.

CHAPTER 5 : PROPULSION SYSTEM OPTIMIZATION PROCESS MODELLING

5.1   Scope and Specification

This chapter details the initial development of the water jetpack system model. In particular, this chapter details the development of a MATLAB optimization code for the water jetpack's propulsion system geometric parameters based on one-dimensional (z-direction) steady state static hovering conditions that were developed in Chapter 3, along with a set of performance criteria for the system. The performance and efficiency for the water jetpack system is dependent on the size and design of the entire propulsion system that contains the flow of water, thus it is critical to accurately size each state point of the propulsion system. In this analysis, state point 1 and 2 represent the input and output state points for the water jetpack system respectively. The optimization process employed in this chapter involves an iterative process whereby the optimum combination of the feed hose and water jet exit diameter is determined from analyzing a set of color-bar distribution graphs.

5.2   Code Development and Methodological Approach

The methodological approach used to determine the propulsion system geometric flow parameters that optimize the performance of the system is illustrated by the flow diagram shown in Figure 5.1. The optimization process involved the development of a MATLAB code (see Appendix C) This code models the steady state performance characteristics of the jetpack system as defined in Chapter 3. Under steady state conditions, the system is assumed to remain at rest, hence the velocity and acceleration terms in Newton's Second Law for the jetpack system, are equal to zero. At the start of the code, input data such as the steady state flight altitude, mass of water in system correction factor (kappa), fluid density, dry mass of the system and gravity was defined.

Step 2 involved implementing a double loop structure within the code for varying the feed hose diameter and jet-exit diameter values within a reasonable range within the bounds of the diameter values established in literature from Little et al. (2015) and Naidoo et al. (2015b). The loop involved varying the feed hose diameter (D1) between 80 mm to 150 mm and the jet-exit diameter (D2) between 30 mm to 70 mm such that performance of the jetpack system could be analyzed for each linear combination of D1 and D2 in the form of a color-bar distribution showing the result of the performance variables of interest against variable combinations of D1 and D2.

Step 3 involved running the code, observing the results, and selecting feasible values for D1 and D2 that optimize the performance of the system. The values of D1 and D2 selected was 100 mm and 50 mm respectively as this diameter combination was observed to satisfy all the optimization process conditions as detailed below. The performance variables observed during the simulation where: minimum thrust force required, mass and volumetric flow rate, fluid

feed hose and jet-exit velocity, weight increase of the system with respect to feed hose diameter, total head, head loss due to friction, power generated by the pump, power to overcome friction, Reynolds number, pressure rise across the pump, absolute pressure rise and the Darcy friction factor.
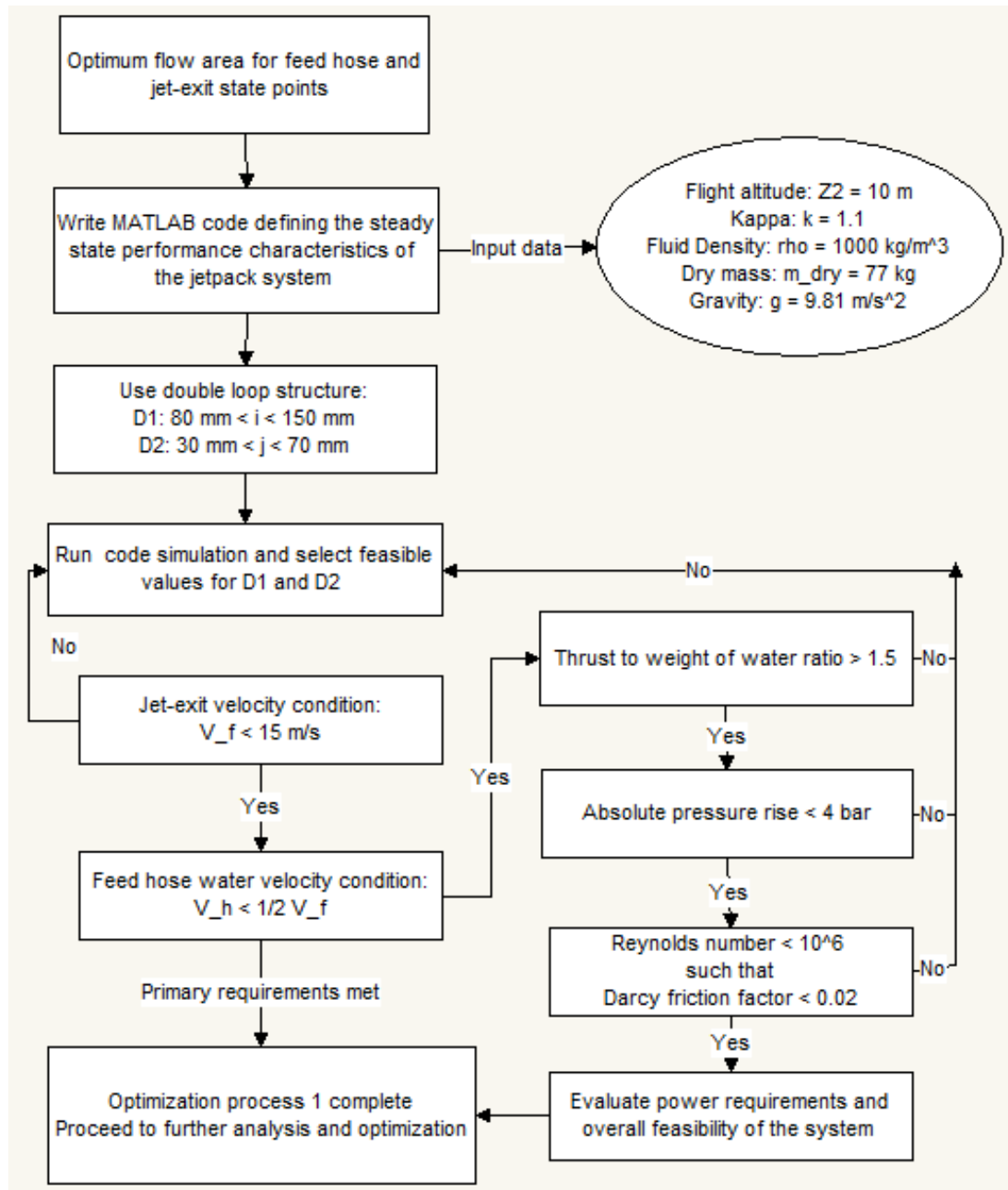

Figure 5.1: Water jetpack propulsion system development optimization process

5.3 Primary and Secondary Conditions

Steps 1 to 3 form the preliminary steps for the optimization process. The steps that follow step 3 form the primary and secondary condition requirements. The primary and secondary requirements are fundamental in the development of an efficient, safe and optimized water jetpack model. The selection of D1 and D2 was based on five performance conditions: 1) jet-exit water velocity condition, 2) feed hose water velocity condition, 3) thrust-to-weight of water condition, 4) absolute pressure rise condition, and 5) Reynolds number condition. The first two of the five conditions (jet-exit water velocity and feed hose water velocity) form the primary conditions and the latter three conditions form the secondary conditions to be met.

5.3.1 Primary Condition 1: Jet-Exit Velocity

The first condition to be met was that the jet-exit water velocity does not exceed 15 m/s (54 km/h). The water jet-exit velocity distribution is shown in Figure 5.2.
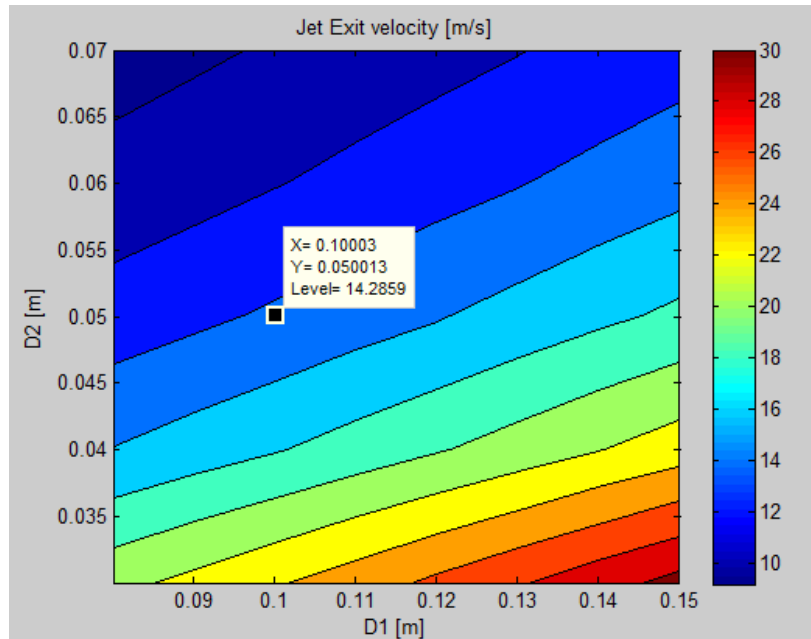

Figure 5.2: Water jet exit velocity distribution for peak steady state conditions

The selected value for D1 and D2 (100 mm and 50 mm respectively) yield a jet-exit velocity of approximately 14.3 m/s, which is below the maximum velocity of 15 m/s that was imposed by the jet-exit velocity condition. This condition was imposed as a measure of safety, such that the water jet velocity is low enough to not cause injury to the arms or legs of the pilot. Water jetpacks depend on high flow rates to generate thrust force; however, high water jet velocity could potentially cause low-level pain or bruise the skin of humans (Jetlev-Flyer, 2016). The design of the 'Pelico Water Jetpack' by Little et al. (2015) was based on the water jet velocity being limited to 20 m/s for peak conditions. In this work, a maximum jet-exit a velocity of 15 m/s was selected for peak steady state conditions at an

altitude of 10 m. It must be noted that although a lower value for the jet-exit velocity is favorable in terms of pilot safety, there is a proportional decrease of the thrust force generated by the water jetpack and thus the efficiency of the jetpack system would decrease and require higher mass flow rate to generate an equivalent magnitude of thrust force. Ideally, a limit should be set for the maximum and minimum jet-exit velocity such that the jetpack generates sufficient thrust force and at the same time the jetpack is safe enough and the water jet would not cause injury to the pilot. One should also note that the jet-exit velocity changes with mass flow rate in the system, and therefore when the system is subjected to transient state conditions, the jet-exit velocity may exceed value imposed by primary condition 1.

5.3.2   Primary Condition 2: Feed Hose Velocity

Primary condition 2 was set such that the feed hose water velocity remains under 7.5 m/s (half the jet-exit velocity). This velocity value was chosen such that the feed hose velocity is minimized and the effects of major head loss due to friction do not significantly decrease the performance of the system. Thus, the water jet-exit velocity to feed hose water velocity ratio is approximately 2. The feed hose water velocity distribution is illustrated in Figure 5.3.
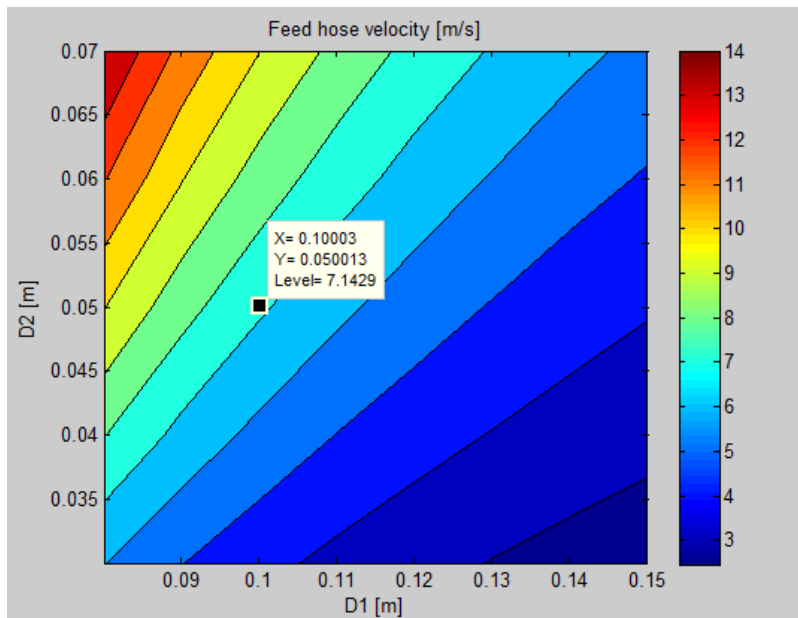

Figure 5.3: Feed hose water velocity distribution

As seen in Figure 5.3, the feed hose velocity remains under 7.5 m/s for the selected D1, D2 combination of 100 mm and 50 mm respectively. The feed hose water velocity at this point in the distribution is approximately 7.14 m/s. This condition along with the water jet-exit velocity condition implies that the two primary condition requirements for the system are met. Thereafter, three secondary conditions were imposed to validate the feasibility of the jetpack system, this is detailed below.

5.3.3   Secondary Condition 1: Thrust-To-Weight Ratio

Secondary condition 1 was that the ratio of thrust generated to the weight of water lifted by the system results in a minimum specified ratio of 1.5. This condition was imposed to ensure efficiency of the jetpack system with respect to the combined weight of the water and pilot. Under steady state conditions, the thrust generated is equal to the net weight of the system (weight of jetpack, pilot and water). The aim was to ensure that the mass of water lifted does not far exceed the mass of the pilot and jetpack, thus improving the load-carrying efficiency of the system. The weight of the system increases incrementally with D1 for a fixed flight altitude, as shown in Figure 5.4.
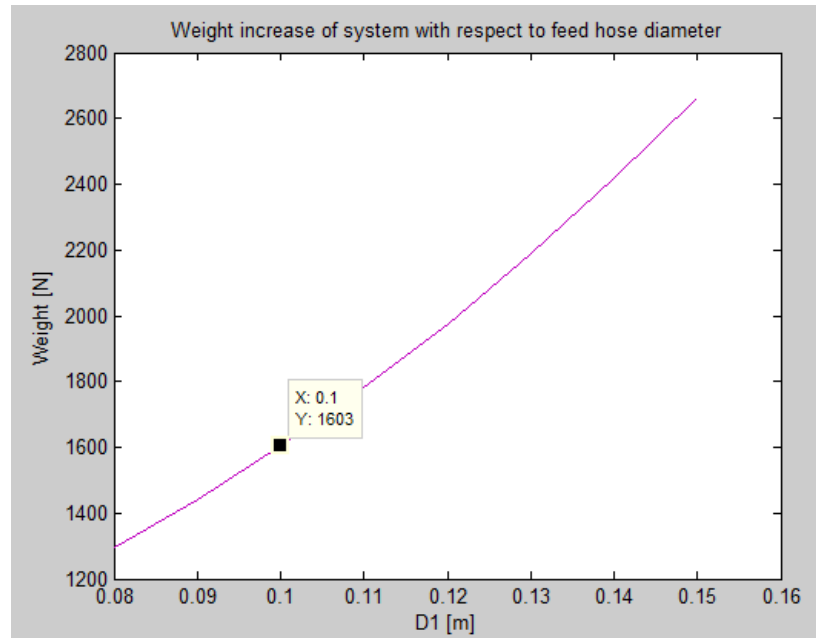

Figure 5.4: Incremental weight increase of water jetpack system

For the chosen feed hose diameter of 100 mm, the net weight of the system is 1603 N. Since the dry mass of the system is 77 kg (weight of 755.37 N), the weight of water lifted is 847.63 N. Therefore, thrust-to-weight of water ratio is approximately 1.9. A ratio lower than 1.9 would imply that there is extra weight of water lifted in the system and that the bulk of the thrust generated is used to lift the water instead of the pilot and jetpack. Following this analysis, a minimum value of 1.5 was selected and imposed in this condition such that the mass of water lifted in the system is minimized. It can be noted from Figure 5.4 that the weight of water in the system could be minimized by decreasing D1. However, this would result in violating primary condition 1 (feed hose water velocity condition) as detailed previously since a smaller value of D1 results in higher feed hose water velocity. Furthermore, commercial water jetpacks such as the Jetlev-Flyer (2016) use feed hoses with diameter of 4 inches (approximately 100 mm), this was used as a guideline for justifying and validating the selection of D1 in this optimization process.

5.3.4   Secondary Condition 2: Absolute Pressure Rise

Secondary condition 2 was that the absolute pressure rise by the AUV pump system remains under 4 bar for steady state conditions at the maximum flight altitude. This condition was imposed as a measure of safety for the propulsion system. The absolute pressure rise in the system is shown in Figure 5.5.
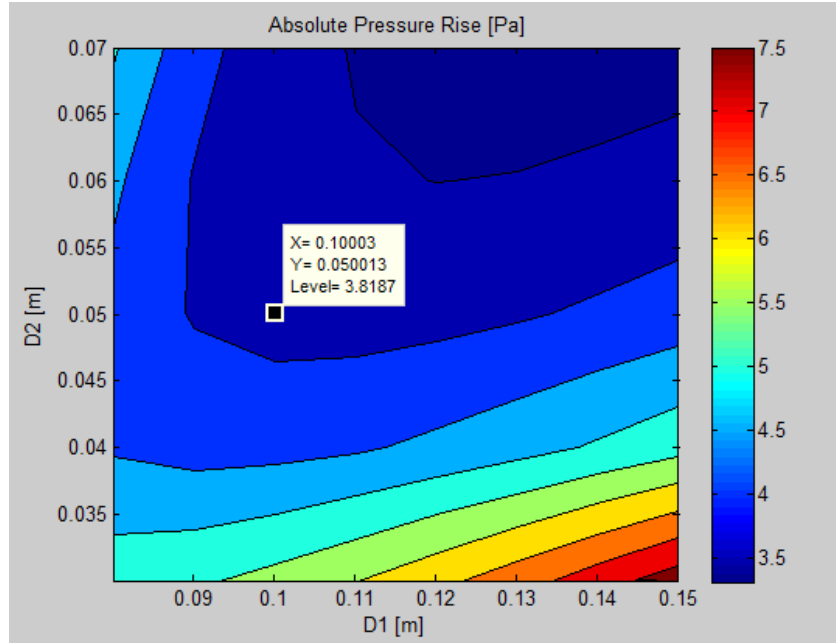

Figure 5.5: Absolute pressure rise in the water jetpack propulsion system

The absolute pressure rise for the chosen value of D1 and D2 is found to be 3.82 bar. It can be observed that the absolute pressure rise in the system is greater as D1 increases while D2 decreases. This observation comes directly from the Bernoulli equation. To attain steady state flight, a certain, fixed mass flow rate and jet velocity is required. The absolute pressure of the water on the outlet side of the pump is a measure of the total energy of the water. This energy is in the form of static and kinetic energy. When the water in the system encounters a reduction in flow area, the static energy is converted into kinetic energy. When the total pressure in the system rises, the components in the propulsion system are under greater stress, therefore increasing the chance of component failure which commonly arises from stress concentration points in the system. The actual strength and stress tolerance of the system is unknown at this stage in this work and therefore a value of 4 bar is based on the maximum total pressure in the system such as the pressures found in Little et al. (2015) and UKZN Water Jetpack designed by Naidoo et al. (2015b). Furthermore, the maximum total pressure in the propulsion system of the Jetlev-Flyer jetpack range is 4.1 bar or 60 psi (Jetlev-Flyer, 2015), this was used as a guideline for the maximum pressure specification for this analysis.

5.3.5 Secondary Condition 3: Reynolds Number

Secondary condition 3 was that the Reynolds number be greater than 60000, such that the Darcy friction factor be less than 0.02. This observation and specification of the Reynolds number was aided with the use of the Moody diagram (see Appendix A). This condition was imposed to minimize the head loss due to friction in the feed hose. Using the selected value of D1 as 100 mm and a roughness value of 0.0025 (drawn tubing), the relative roughness value is 0.000025. Following the line for this relative roughness value, as the Reynolds number increases, there is a decrease in the friction factor. The Reynolds number of 60000 is found to be the value at which the Darcy friction factor is at 0.02. Increasing the Reynolds number from this point results in lower values for the Darcy friction factor. The Reynolds number for the selected value of D1 and D2 is shown in Figure 5.6 below
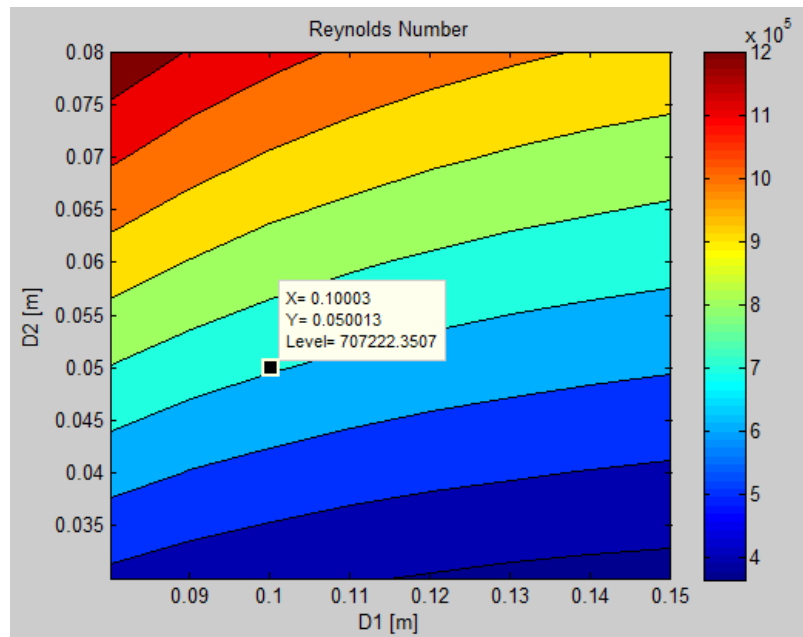

Figure 5.6: Reynolds number distribution

The Reynolds number at the selected point is found to be 707222.35. Referring to the Moody diagram in Appendix A, the resulting Darcy friction factor for the feed hose is approximately 0.0185. The absolute roughness value for flexible smooth piping is 0.07 mm. Thus, the relative roughness e/D for this case is 0.0007 (for the 100 mm feed hose diameter). This result validates the selection of the feed hose and jet-exit diameter.

5.3.6 Power Analysis

The last observation from the MATLAB optimization was the ideal power distribution for steady state conditions. The ideal power required by the pump of the AUV distribution is shown in Figure 5.7.
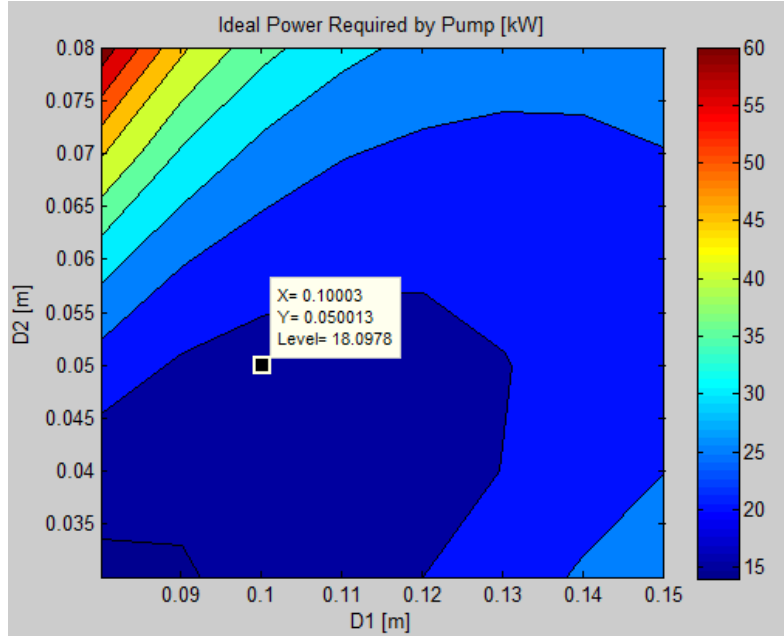
Figure 5.7: Ideal power required by pump distribution

Under the steady state conditions for this analysis, the ideal power required by the pump is found to be 18.1 kW. As shown by Figure 5.7, the power required by the pump increases significantly as D1 decreases and D2 increases, this relation is due to the jetpack generating less thrust at the regions of low D1 and high D2.

It must be noted that the steady state power required is the lowest power that the AUV pump would generate as the water jetpack system accelerates from zero to maximum altitude, and thus the initial power required would be significantly greater than the steady state power required. However, this analysis is detailed in Chapter 6 of this dissertation in which a dynamic/transient analysis of the system is conducted on MATLAB Simulink.

CHAPTER 6 : MODELLING, SIMULATION AND CONTROL ON MATLAB

6.1   Scope and Specifications

Modelling and simulating the water jetack and AUV system under transient state conditions is essential prior to the design and analysis of such a system for a specified flight. This chapter details the step-wise development of a closed-loop feedback control system for the water jetpack and AUV system using MATLAB Simulink. The development of such a system is based on the second-order non-linear and transient mathematical models developed for the water jetpack and AUV system in Chapter 3 and 4 respectively. The utility of a closed-loop feedback control system model for the water jetpack and AUV system is to determine the response obtained for the closed-loop model such that the entire system may be fully automated. The step-wise development of the complete closed-loop feedback control system model contained in this chapter consists of firstly developing an open- and closed-loop Simulink model of the water jetpack for motion in the the z, x-z and x-y-z direction (one, two and three dimensions), and thereafter developing an open- and closed-loop Simulink model of the AUV for motion in the x, x-y and x-y-z direction (1-, 2- and 3-dimensional). This is done such that once a closed-loop feedback control system is developed for the water jetpack and AUV system independently, a combined model is developed by linking the systems.

The development of the combined system Simulink model is depicted in Figure 6.1. Referring to Figure 6.1, the combined system Simulink model development starts with the development of an open- and closed-loop, one-dimensional Simulink model for the water jetpack. Thereafter the model is altered to an open-loop two-dimensional Simulink model in which a second controller is implemented to form a closed-loop system. The model is further altered to form a three-dimensional Simulink model for the water jetpack system. A similar procedeur is conducted for the AUV modelling. The final part of this chapter consists of the development of linking the three-dimensional water jetpack and AUV Simulink models to form the combined system Simulink model. The function of the combined system Simulink model is to enable speed control and tracking between the water jetpack and AUV. This system has a set of pilot defined system inputs which are: 1) desired flight altitude, 2) desired steady state velocity, and 3) yaw angle. The combined system registers the inputs of the pilot and controls several variables of the water jetpack and AUV propulsion system which are: 1) mass flow rate, 2) thrust vectoring, 3) speed saturation, 4) AUV propeller mass flow rate, 5) AUV propeller thrust vectoring, and 6) AUV depth control.

The outcome of this chapter is the development of the Simulink model, control architecture, and controller parameters required to attain autonomous flight of the complete system. This includes observation of the following transient responses: flight alitude and speed control along control of mass flow rate and thrust vectoring. This chapter sets the foundation as the theoretical framework and dynamic analysis required for the development and implementation of a mechatronic system for a water jetpack and AUV system.
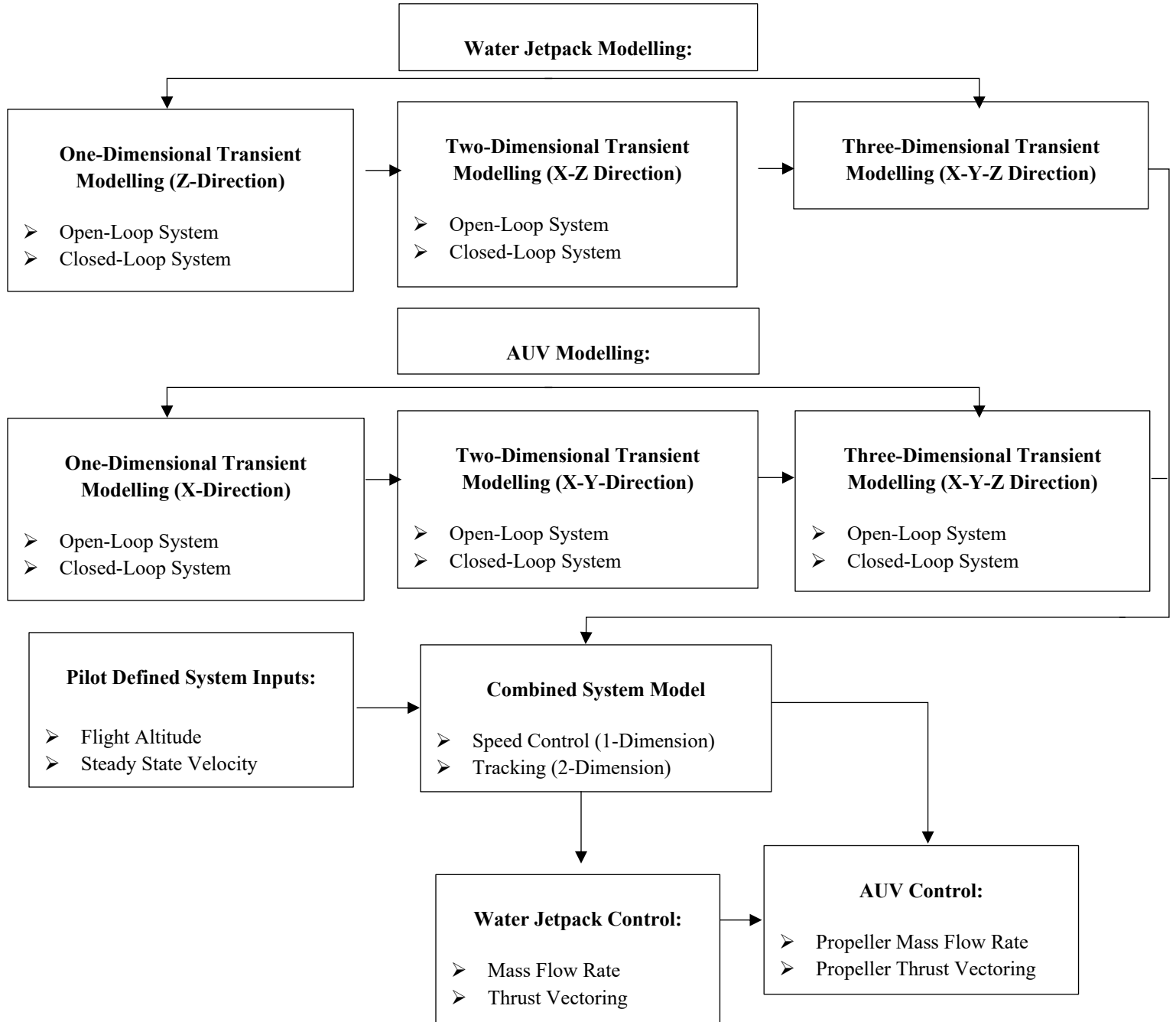
Figure 6.1: Water jetpack and AUV combined Simulink model development process

6.2   Water Jetpack Simulink Modelling

6.2.1   Input Parameters

The MATLAB Simulink models developed in this section are based on the parameters used in the optimization process modelling contained in Chapter 5. Table 6.1 shows the default values selected for the parameters used in the development of the Simulink model of the water jetpack for motion in all three dimensions (z, x-z and x-y-z direction).

Table 6.1: Input parameters for water jetpack Simulink modelling

Parameter	Symbol	Units	Value
Dry mass	m_{dry}	kg	77
Gravitational acceleration	g	m/s^2	9.81
Jet-exit area	A_2	m^2	0.002
Kappa	κ	(Dimensionless)	1.1
Feed hose area	A_1	m^2	0.0079
Density of water	ρ	kg/m^3	1000
Desired flight altitude*1	Z_{20}	m	10
Initial input mass flow rate*	$\dot{m}$	kg/s	56.1
Pitch angle	θ	Degrees/Radians	0
Roll angle	ϕ	Degrees/Radians	0
Yaw angle	ψ	Degrees/Radians	20
Thrust vector angle (alpha)*	α	Degrees/Radians	Variable
Drag coefficient of human	C_{Dh}	(Dimensionless)	1.16
Density of air	ρ_{air}	kg/m^3	1.23
Desired surge velocity*	v_x	m/s	15

The dry mass of the water jetpack system m_{dry} is approximated as 77 kg, this includes the summation of the average mass of the pilot and the maximum mass of the water jetpack unit. The gravitational acceleration constant is taken as 9.81 m/s^2. The results obtained from the optimization process modelling in Chapter 5 show that the optimum combination for development of the water jetpack propulsion system is the selection of using a feed hose and jet-exit diameter of 100 mm and 50 mm respectively. The jet-exit area is computed as the cross-sectional area of the nozzle exit points (state point 2 of Figure 3.1) which is 0.002 m^2. The feed hose area is computed as the cross-sectional of the feed hose which is 0.0079 m^2. The value of kappa is chosen as 1.1 as detailed in Chapter 3. The density of water is taken as 1000 kg/m^3. The jetpack propulsion system was optimized in Chapter 5 to achieve a targeted flight altitude of 10 m, in the simulation of the system in the z-direction, an ideal input mass flow rate of 56.1 kg/s is required to attain steady state conditions at the desired flight altitude.

The mass flow rate varies depending on the dynamic state of the water jetpack system. In the case of one-dimensional transient analysis or steady state and transient motion in two or three dimensions of space, the mass flow rate may

vary depending on the requirements of the system. The motion of the water jetpack system is assumed to be ideal such that the effects of pitch, roll and yaw moments are negligible. The aim of a control system implementation is to keep the moments acting on the system zero to avoid the occurrence of dynamic instability. Furthermore, when simulating motion in two dimensions (x-z direction), the ideal response desired by a pilot is to take-off vertically upwards such that pitch, roll and yaw angle is zero. However, when simulating motion in three dimensions (x-y-z direction), pitch and roll are assumed zero and a fixed yaw angle is used to induce a component of the water jet thrust force in the y-direction, the default value selected for initial simulation use is 20 degrees. The thrust vector angle is the angle at which the water jet that exits the nozzles of the water jetpack is positioned relative to the body-fixed coordinate system. As the thrust vector angle is increased, the surge velocity of the system increases, this is parameter is variable. When the water jetpack system travels in the x-direction, drag force always resists this motion, the average value for the coefficient of drag for a human is 1.16 and the density of air is 1.23 kg/m^3 (Fox et al., 2010). The initial desired surge velocity is 15 m/s for the first simulation of the system in the x-z direction.

6.2.2   Simulink Model 1: Motion in One-Dimension (Open-Loop)

6.2.2.1   Mathematical and Simulink Model

The Simulink model developed in this section is based on Newton's Second Law for the water jetpack system in the z-direction, this is given by Equation 6.1 below. The derivation of Equation 6.1 is detailed in Chapter 3.

$$\sum F_z = \left(m_{dry} + \kappa\,\rho\,A_1\,Z_2\right)\frac{dv_z}{dt} = \dot{m}\left(v_f - v_z\right) - \left(m_{dry} + \kappa\,\rho\,A_1\,Z_2\right)g \qquad (6.1)$$

The utility of Equation 6.1 is to develop a Simulink model in which mass flow rate is an input and flight altitude is the output. For each discrete value of a given mass flow rate input, a certain flight altitude is attained when the system reaches the steady state condition and the heave velocity and acceleration in the z-direction become zero. When the system reaches steady state conditions, Equation 6.2 models the relationship between flight altitude attained as a function of mass flow rate:

$$Z_2 = \frac{\dot{m}^2 - \rho g A_2 m_{dry}}{\kappa\,\rho^2 g\,A_1 A_2} \qquad (6.2)$$

The Simulink model developed to represent the open-loop response of the water jetpack system is shown in Figure 6.2. This Simulink model represents Equation 6.1 as a system. The utility of such a model at this stage is to observe the transient behavior and dynamic response of the system for a defined mass flow rate input.

Figure 6.2: Water jetpack z-direction Simulink model (open-loop sysem)

Referring to Figure 6.2, the parameters defined in Table 6.1 are represented by constant blocks, this includes: mass flow rate, kappa, density of water, feed hose area, dry mass and the gravitational acceleration constant. There are three main function blocks, these represent the equations for thrust force, accumulative mass of the system, and Newton's Second Law. The type of physical quantity computed after each function is labelled and shown next to the signal lines. There is a single gain block that computes the water jet-exit velocity from mass flow rate by the contuinuity equation. There are two integrators in the Simulink model, the first intrator integrates the acceleration in the z-direction to compute heave velocity and the second integrator integrates velocity to compute flight altitude. There are seven scopes in the Simulink model, the function of these scopes is to display the response of the signals in the system. The scopes have no effect on the actual dynamics of the Simulink model. The inputs and outputs of the Simulink model in Figure 6.2 are summarized in Table 6.2.

Table 6.2: Input and output parameters for one-dimensional Simulink modelling

Inputs		Outputs	
Dry mass	m_{dry}	**Flight altitude**	Z_2
Gravitational acceleration	g	**Thrust force**	F_T
Jet-exit area	A_2	**Net force**	F_{net}
Kappa	κ	**Heave velocity**	v_z
Feed hose area	A_1	**Acceleration**	dv_z/dt
Density of water	ρ	**Mass of system**	$\sum m$
Mass flow rate	$\dot{m}$		

129

The inputs for simulating motion of the water jetpack system in the z-direction are: dry mass, gravitational acceleration, jet-exit area, kappa, feed hose area, density of water, and mass flow rate. The values of the input parameters are given in Table 6.1. The outputs are: flight altitude, thrust force, heave velocity, net force, acceleration, and mass of system. The most significant output in this simulation and the simulation in Section 6.2.3 (closed-loop system) is flight altitude. However, the response of all the outputs are illustrated and discussed.

6.2.2.2   Flight Altitude and Heave Velocity Response

The Simulink model in Figure 6.2 was run with a simulation time of 50 seconds. Figure 6.3 (a) shows the flight altitude response and Figure 6.3 (b) shows the heave velocity response. These represent the actual motion of the water jetpack system, it is nessessary to observe these responses in order to understand the motion of the system that results from a set mass flow rate input when there is no form of control or automation used in the design of the system.

(a)   (b)
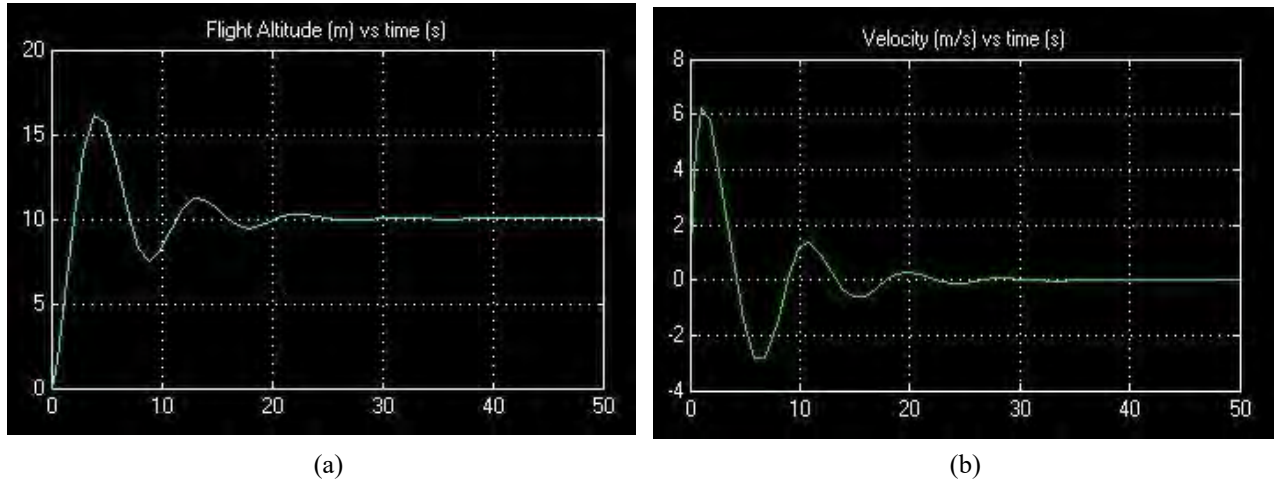
Figure 6.3: (a) Flight altitude, (b) Heave velocity

Referring to Figure 6.3 (a) and (b), the peak flight altitude and heave velocity attained is 16 m and 6 m/s respectively. The time to reach peak altitude is approximately 3.9 seconds and the time to reach peak heave velocity is appromately 1 second. Once the system reaches peak altitude, the direction of motion is downwards and the system reaches a negative peak heave velocity of -3 m/s. The settling time is 25 seconds, this is when the system reaches steady state conditions. The response in flight altitude is highly unfavorable with respect to the overshoot being high. This implies that for a set mass flow rate, the system would reach 16 m prior to reaching the desired altitude of 10 m, which requires a feed hose length of atleast 16 m to allow the water jetpack to remain linked to the AUV. A high overshoot in flight altitude also poses the risk of dynamic flight instability occurring which is not favorable.

6.2.2.3   Force, Mass and Acceleration Response

The thrust force, net force, mass of system, and acceleration response from the simulation is shown in Figure 6.3 (a), (b), (c) and (d) respectively. These responses are significant for designing a system and selecting material grades that can withstand these forces. The responses shown by Figure 6.4 illustrate Newton's Second Law. The net force is equal to the vector sum of thrust force and weight which is also equal to the product of mass and acceleration of the system.

(a)   (b)

(c)   (d)
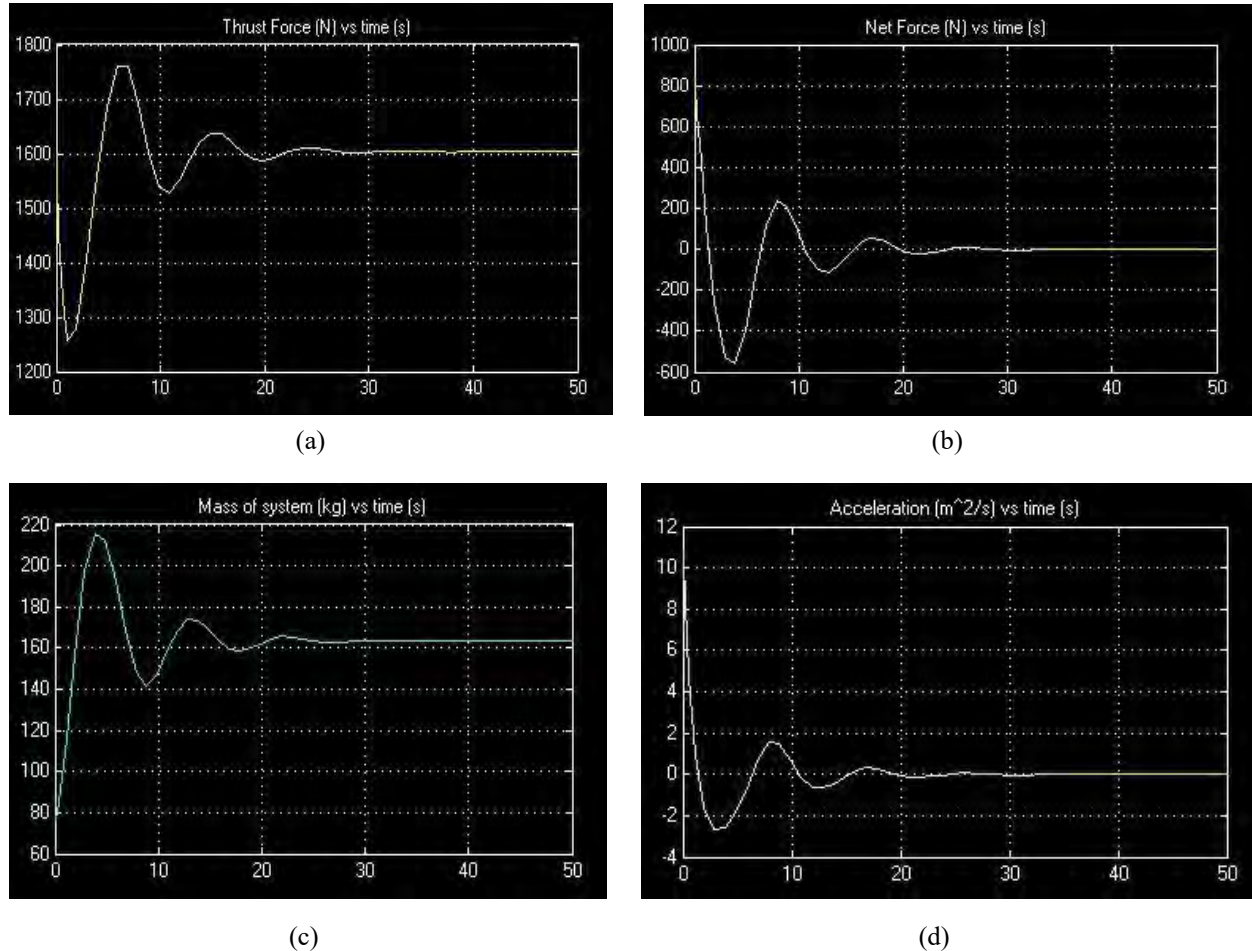
Figure 6.4: (a) Thrust force, (b) Net force, (c) Mass of system, and (d) Acceleration

Referring to Figure 6.4 (a) the initial thrust force generated is 1600 N and the minimum peak thrust force is 1250 N at 1 second. The peak thrust force is 1750 N at 7 seconds and the steady thrust force is 1600 N, therefore the peak negative overshoot is -21.88% and maximum positive overshoot is 9.4%. Referring to Figure 6.4 (b), The initial net force is 800 N and the peak negative net force is -580 N at 4 seconds. Referring to Figure 6.4 (c), the initial mass of the system is 77 kg, which represents the dry mass. The mass of the system is described by the accumulative mass model in Chapter 3 which describes the linear relationship between mass and flight altitude. As flight altitude increases, the mass of water in the system being lifted increases proportionally. The system reaches peak flight altitude

of 16 m and a peak mass of 216 kg at 4 seconds. At this instant of time it is noted that the weight of the system is greater than the thrust force generated, hence both the net force and acceleration at 4 seconds is less than zero (negative), which implies that the system experiences a net force downwards, however, the motion of the system is in the upward direction as illustrated in the flight altitude response in Figure 6.3 (a). The acceleration response in Figure 6.4 (d) is computed by dividing the net force in Figure 6.4 (b) by the mass of the system in Figure 6.4 (c), this comes directly from Newton's Second Law. The initial acceleration is 10.4 m/s^2 and the peak minimum acceleration is -2.7 m/s^2. The system reaches steady state conditions from 25 seconds into the simulation whereby the net force and acceleration reach zero. The steady state mass of the system and thrust force generated is 163.9 kg and 1600 N respectively.

6.2.3   Simulink Model 2: Motion in One-Dimension (Closed-Loop System)

6.2.3.1   Mathematical and Simulink Model

In this section, a closed-loop system is developed from the Simulink model in Figure 6.2. The aim of developing a closed-loop system for motion in the z-direction is to improve the response of flight altitude that was observed in Figure 6.3 (a) previously. The Simulink model developed in this section is based on Newton's Second Law for the water jetpack system in the z-direction and Equation 6.1 and 6.2 are fully applicable. However, the difference in this model is that the input mass flow rate is the controlled variable. The closed-loop Simulink model for motion of the water jetpack system in the z-direction is shown in Figure 6.5 below. A PID controller is introduced in the system to control the mass flow rate input.

The layout of the Simulink model shown in Figure 6.4 is the same as the Simulink model in Figure 6.3 (open-loop system) except that the mass flow rate input in Figure 6.3 is replaced by a PID controller in Figure 6.4 (closed-loop system). The functionality of a PID controller is detailed in Chapter 2. Essentially, the PID controller in Figure 6.4 compares the difference between the desired flight altitude and the actual flight altitude (referred to as the steady state error) of the water jetpack system and performs three functions: proportional gain multiplication, integration, and differentiation such that adjustment is made to the mass flow rate input until the steady state error reaches zero. However, the effectiveness of a PID controller is highly dependent on the selection of the three control parameters used in the controller achitecture as described in Chapter 2.
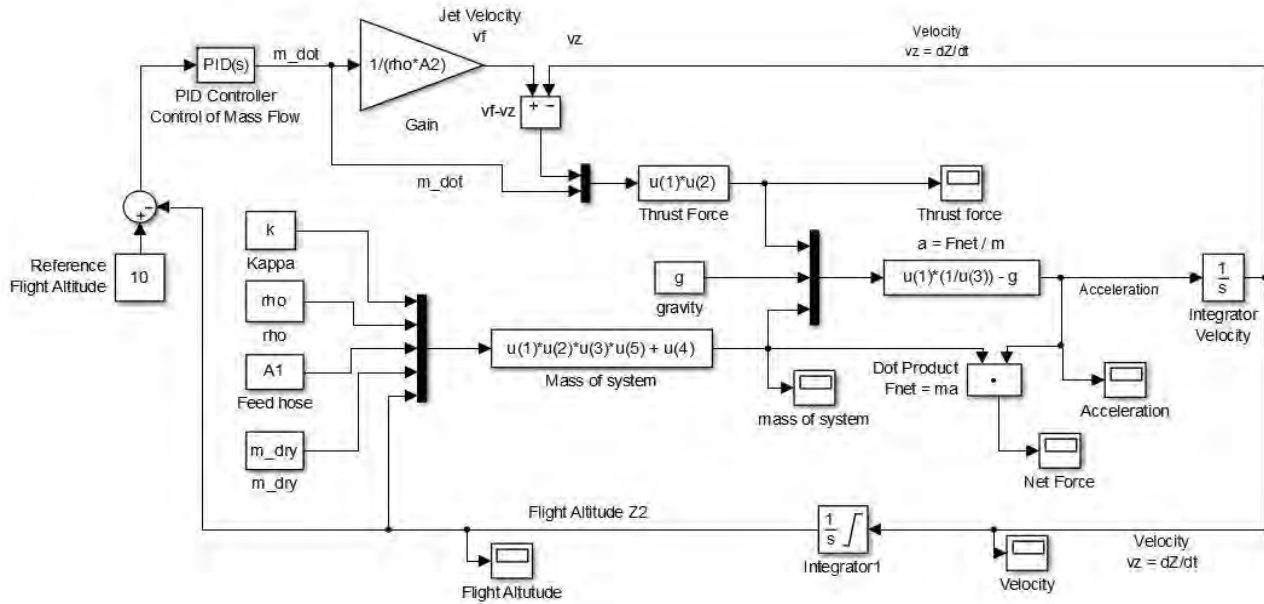
Figure 6.5: Water jetpack z-direction Simulink model (Closed-loop sysem)

The inputs and outputs of the Simulink model in Figure 6.5 is shown in Table 6.3.

Table 6.3: Input and output parameters for one-dimensional closed-loop Simulink modelling

Inputs		Outputs	
Dry mass	m_{dry}	Mass flow rate	$\dot{m}$
Gravitational acceleration	g	Thrust force	F_T
Jet-exit area	A_2	Net force	F_{net}
Kappa	κ	Heave velocity	v_z
Feed hose area	A_1	Acceleration	dv_z/dt
Density of water	ρ	Mass of system	$\sum m$
Reference flight altitude	Z_{20}	Steady state error	E_{ss}

The inputs for the closed-loop system are: dry mass, gravitational acceleration, jet-exit area, kappa, feed hose area, density of water, and reference flight altitude. The values of the input parameters are given in Table 6.1. The outputs are: mass flow rate, thrust force, heave velocity, net force, acceleration, mass of system, and the steady state error. The most significant output parameters that are observed in this simulation are: mass flow rate, thrust force, flight altitude, and the steady state error. The response of net force, heave velocity, acceleration, and mass of system is shown in Appendix C.

6.2.3.2   PID Controller Architecture

MATLAB Simulink allows for automatic PID controller parameter tuning to attain a desired response of flight altitude. This is accomplished by double clicking on the PID block shown in Figure 6.5 and a PID automated tuning window opens. Thereafter, MATLAB displays the open- and closed-loop response of the system along with reference tracking bode and step plot, response time and transient behavior, performanance and robustness data (see Appendix A). The tuned and default controller parameters for the PID controller are shown in Figure 6.6.

Controller parameters		
	Tuned	Block
P	49.7701	1
I	8.0088	1
D	42.3359	3
N	80.236	1

Figure 6.6: Tuned and block PID controller parameters

Referring to Figure 6.6, the tuned parameters are the parameters that result when peforming automated PID tuning on MATLAB Simulink. The block parameters are the parameters that are preset in the PID controller prior to automated tuning. The proportional gain, integral, derivative and filter coefficient parameters are represented by P, I, D and N respectively.The values for the tuned P, I, D and N are shown as 49.7701, 8.0088, 42.3359 and 80.236 respectively. MATLAB linearizes the system and converts the system from the time-domain to the Laplace-domain (Ogata, 2013). The Laplace-domain (also referred to as the frequency domain) is denoted by s. The equation of the PID controller used by automated PID tuning is given by:

$$G(s) = P + \frac{I}{s} + \frac{DN}{\left(1 + \frac{N}{s}\right)} \tag{6.3}$$

where $G(s)$ is the controller function in the s-domain, P is the proportional gain parameter, I is the integrator parameter, D is the derivative parameter, N is the filter coeffiecient and s represents frequency. By substituting the tuned parameters shown in Figure 6.5, the PID controller function for the system is given by:

$$G(s) = 49.77 + \frac{8.01}{s} + \frac{3396.86}{\left(1 + \frac{80.24}{s}\right)} \tag{6.4}$$

6.2.3.3   Mass Flow Rate and Thrust Force Control

A PID controller with the parameters displayed in Figure 6.6 is for the Simulink model in Figure 6.5. The aim of this controller is to improve the response in flight altitude of the water jetpack system. The controller is able to improve the response in flight altitude by controlling the mass flow rate input and thrust force generated. The controlled mass flow rate is shown in Figure 6.7 (a) and the thrust force is shown in Figure 6.7 (b).

(a)   (b)
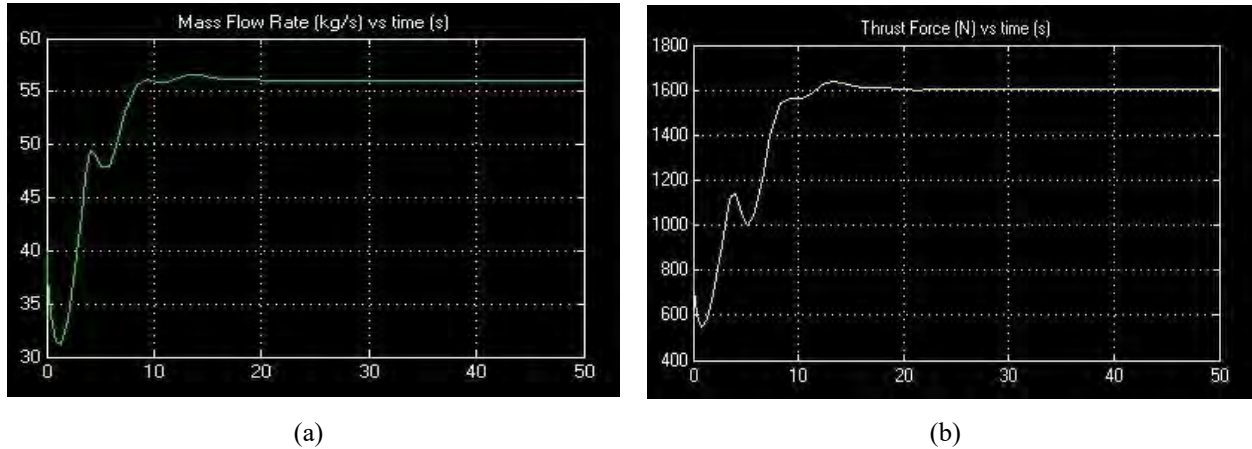
Figure 6.7: (a) Mass flow rate (b) Thrust force

Referring to Figure 6.7 (a) and (b), the initial mass flow rate is 40 kg/s and the minimum mass flow rate is 32 kg/s at 1 second. Since thrust force is proportional to the sqaure of mass flow rate (as detailed in Chapter 3), thrust force increases when mass flow rate increases and vice versa. This is observed by referring to Figure 6.7 (b) at 1 second where the thrust force reaches a minimum of 520 N. Thereafter, both mass flow rate and thrust force increase with no oscillatory response until the mass flow rate and thrust force reach steady state values of 56.1 kg/s and 1600 N respectively after 15 seconds. The response in mass flow rate and thrust force indicates that the controller experiences a high steady state error in the first second of the simulation, thereafter the controller controls the mass flow rate fairly steadily until the steady state mass flow rate is attained. However, the control of mass flow rate is less important than the actual response in flight altitude.

6.2.3.4   Flight Altitude and Steady State Error

The response in flight altitude and steady state error in flight altitude after implementing the PID controller in the system is shown in Figure 6.8 (a) and (b) respectively. The flight altitude response is significant since it provides a visual result of how the water jetpack system responds in real-time when with the implementation of a PID. The steady state error in flight altitude represents the margin by which the actual flight altitude of the system deviates from the desired flight altitude.
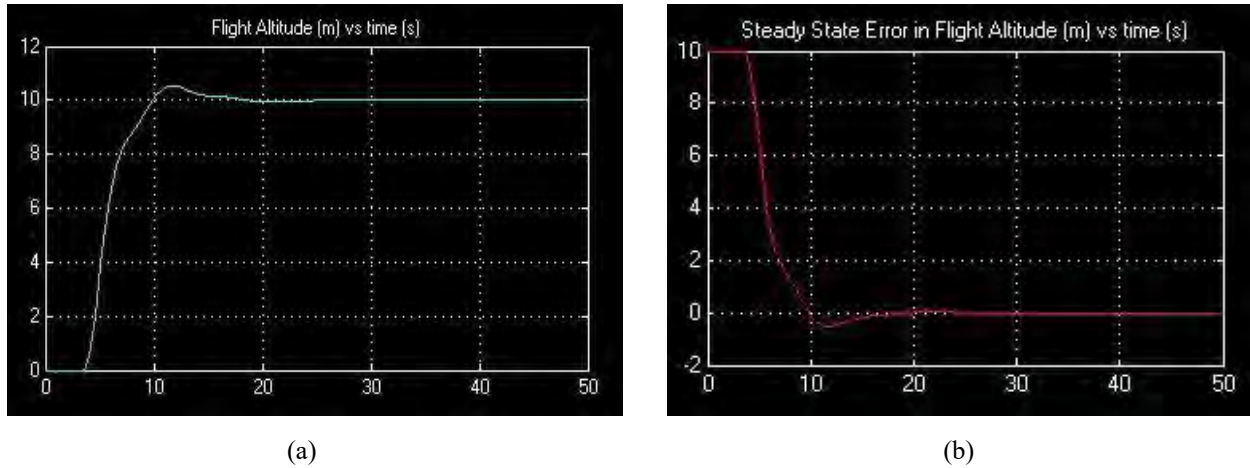
Figure 6.8: (a) Flight altitude, (b) Steady state error in flight altitude

Referring to flight altitude response in Figure 6.8 (a), it can be observed that the flight altitude of the system is zero for the first 4 seconds of the simulation and thereafter the system takes-off. Referring to the steady state error in flight altitude in Figure 6.8 (b), the steady state error is 10 m for the first 4 seconds, which is equal to the difference between the reference or desired flight altitude (10 m) and the actual flight altitude response in Figure 6.8 (b). The system then reaches a peak flight altitude of approximately 10.3 m at 11 seconds (time to peak). The system experiences a peak overshoot in flight altitude by 3%. This result is 57% less than the peak overshoot in flight altitude experienced without the use of a PID controller. It is observed that the steady state error gradually decays to zero, this is desired from a PID controller (Ogata, 2013). The system reaches steady state conditions after 15 seconds, which implies that there is a 40% improvement in the settling time of the system.

In this section, the use of a PID controller was introduced. It is conclusive that PID controller implementation is highly effective for the control of mass flow rate to attain a desired flight altitude with zero oscillatory motion and a low value for the peak overshoot in flight altitude response. By tuning the PID and altering the response time and robustness of the controller on MATLAB Simulink, the response in flight altitude may be varied. The parameters observed are: 1) controlled mass flow rate, 2) thust force, 3) flight altitude, and 4) steady state error in flight altitude. The response of heave velocity, acceleration and net force are shown in Appendix C.

6.2.4 Simulink Model 3: Motion in Two Dimensions (Open-Loop)

6.2.4.1 Mathematical and Simulink Model

The Simulink model developed in this section is based on Newton's Second Law for the water jetpack system in the x- and z-direction respectively. This is given by Equation 6.5 and 6.6:

$$\sum F_x = (m_{dry} + \kappa \rho A_1 Z_2)\frac{dv_x}{dt} = \dot{m}(v_f - v_{xz})\sin\alpha - C_{Dh}\frac{1}{2}\rho_{air}A_h v_x^2 \qquad (6.5)$$

$$\sum F_z = (m_{dry} + \kappa \rho A_1 Z_2)\frac{dv_z}{dt} = \dot{m}(v_f - v_{xz})\cos\alpha - (m_{dry} + \kappa \rho A_1 Z_2)g \qquad (6.6)$$

The utility of Equation 6.5 and 6.6 is to develop a Simulink model for the water jetpack system to simulate the transient response of the system. There are two main controlled input variables for the open-loop response: 1) mass flow rate and 2) thrust vector angle. Increasing the mass flow rate increases the water jet thrust force generated and increasing the thrust vector angle increases the surge velocity of the system.

The Simulink model developed to represent the open-loop response of the water jetpack system in the x-z direction is shown in Figure 6.9. This Simulink model represents Equation 6.5 and 6.6 as a system. The utility of such a model at this stage is to observe the transient behavior and dynamic response of the system for a defined thrust vector angle and a controlled mass flow rate as in Section 6.2.3.

Referring to Figure 6.9, the parameters defined in Table 6.1 are represented by constant blocks, which include: thrust vector angle, kappa, density of water, density of air, feed hose area, dry mass, gravitational acceleration constant, drag coefficient, average area of a human. There are nine function blocks, these represent the equations for total thrust force, thrust force in the x-direction, thust force in the z-direction, accumulative mass of the system, drag force, Newton's Second Law for the x- and z-direction, absolute /acceleration in the x-z direction, and absolute/velocity in the x-z direction. The type of physical quantity computed after each function is labelled and shown next to the signal lines.

There are two gain blocks, one of these computes the water jet-exit velocity from mass flow rate by the contuinuity equation, and the second converts the thrust vector angle input from degrees to radians to satisfy the condition of Equation 6.5. There are four integrators in the Simulink model; the first intgrator integrates the acceleration in the z-direction to compute heave velocity, the second integrator integrates heave velocity to compute flight altitude, the third integrator integrates the acceleration in the x-direction to compute the surge velocity, and the fourth integrator integrates the surge velocity to compute the position of the system in the x-direction.
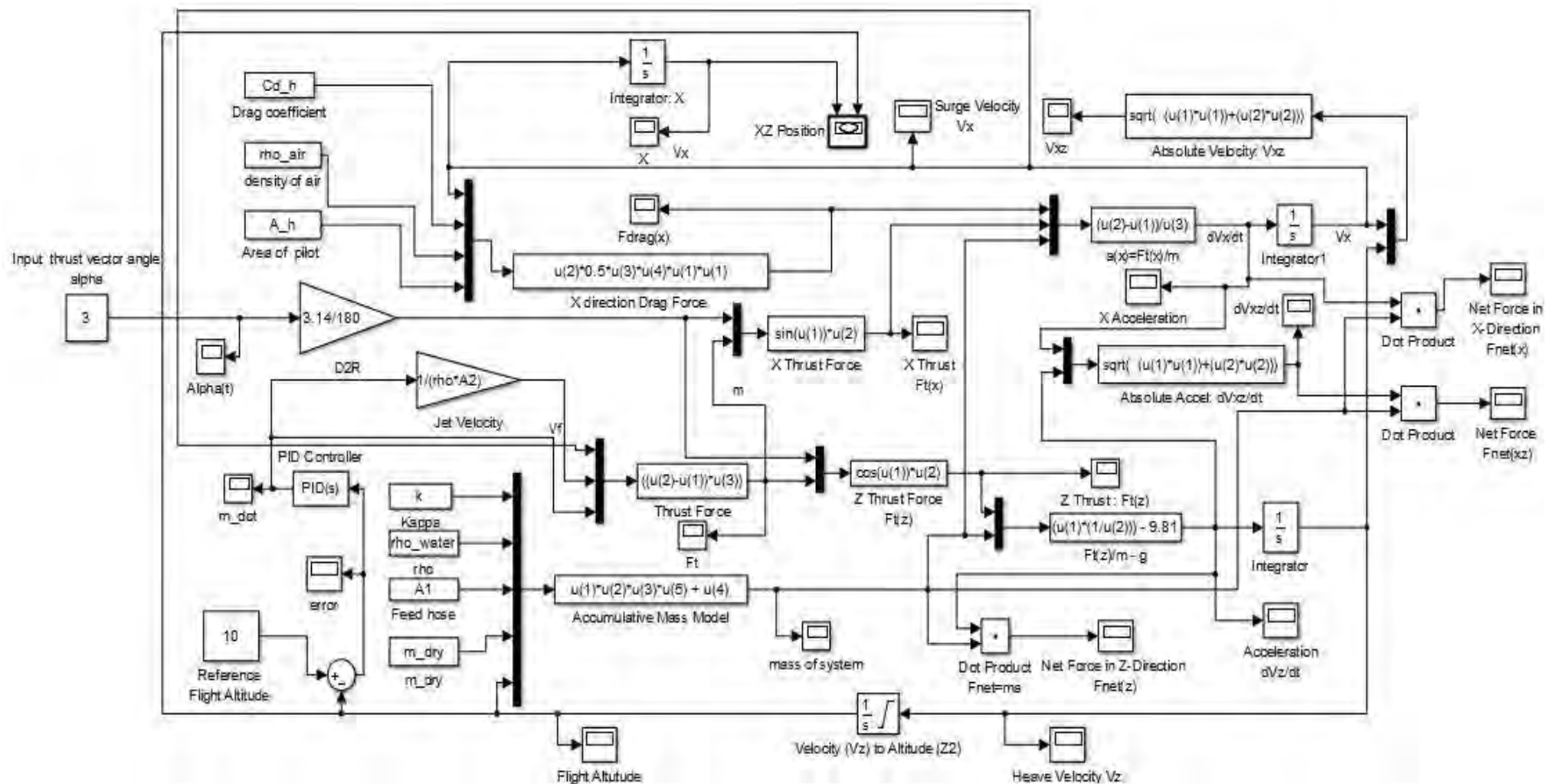
Figure 6.9: Water jetpack x-z direction Simulink model (open-loop sysem)

138

There are 18 scopes in the Simulink model, the function of these scopes is to display the response signals in the system. The scopes have no effect on the actual dynamics of the Simulink model. The inputs and outputs of the Simulink model in Figure 6.9 are summarized in Table 6.4.

Table 6.4: Input and output parameters for two-dimensional open-loop Simulink modelling

Inputs		Outputs	
Dry mass	m_{dry}	Mass flow rate	$\dot{m}$
Gravitational acceleration	g	Thrust force	F_T
Jet-exit area	A_2	Thrust force in x-direction	F_{Tx}
Kappa	κ	Thrust force in z-direction	F_{Tz}
Feed hose area	A_1	Absolute acceleration	dv_{xz}/dt
Density of water	ρ	Acceleration in x-direction	dv_z/dt
Reference flight altitude	Z_{20}	Acceleration in z-direction	dv_z/dt
Thrust vector angle	α	Mass of system	$\sum m$
Drag coefficient of human	C_{Dh}	Drag force	F_D
Density of air	ρ_{air}	Surge velocity	v_x
Average area of human	A_h	Heave velocity	v_z
		Absolute velocity	v_{xz}
		Net force in x-direction	F_{net_x}
		Net force in z-direction	F_{net_z}
		Net force	F_{net}
		Steady state error	E_{ss}
		Flight altitude	Z_2
		X-position	X

The new inputs required for simulating motion of the water jetpack system in the x-z direction as compared to the previous simulation of the system in the z-direction are: thrust vector angle, drag coefficient of a human, average area of a human, and the density of air. The values of all the input parameters are given previously in Table 6.1. The new outputs in this simulation as compared to the z-direction (one-dimensional) simulation are : thrust force in the x- and z-direction, surge velocity, net force in the x- and z-direction, acceleration in the x- and z-direction, x-position, drag force, absolute acceleration, and the absolute velocity. The most significant output in this simulation is flight altitude, mass flow rate control, and surge velocity.

6.2.4.2   Thrust Vector Angle Input and Mass Flow Rate Control

The thrust vector angle input and controlled mass flow rate for this simulation is shown in Figure 6.10 (a) and (b). In this simulation, the thrust vector angle is kept a constant value of 3 degrees relative to the body-fixed vertical axis. The reference flight altitude remains at 10 m, as in the previous simulations. According to Equation 6.6, increasing

the thrust vector angle while still attaining the same flight altitude would require an increase in mass flow rate to compensate for the loss of thrust force in the z-direction when a non-zero thrust vector angle is induced in the system. The mass flow rate in this simulation is controlled with the same PID controller that was developed in Section 6.2.3. This PID controller adjusts the mass flow rate in the system according to the desired flight altitude. The increase in mass flow rate due to an induced thrust vector angle is illustrated by Figure 6.10 (b).

(a)   (b)
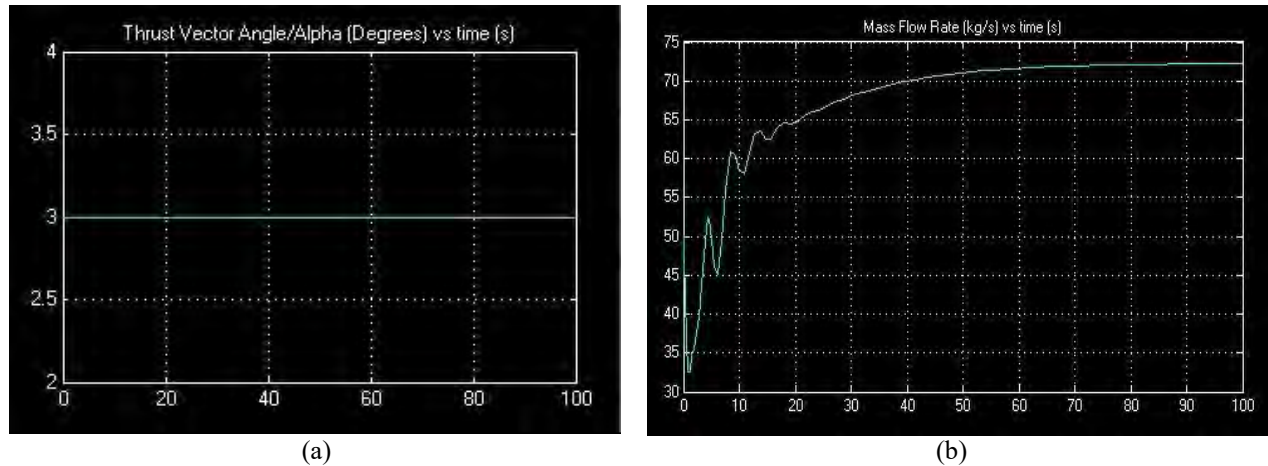
Figure 6.10: (a) Thrust vector angle, (b) Mass flow rate control

In Figure 6.10 (a), the thrust vector angle is shown as a constant value of 3 degrees. In Figure 6.10 (b), it is observed that the PID controller starts with an initial mass flow rate of 50 kg/s and thereafter there is a rapid increase in the gradient of the controlled mass flow rate with the presence of minor oscillations that decays in amplitude within 20 seconds into the simulation. Thereafter the mass flow rate increases from 65 kg/s to 72 kg/s over a period of 40 seconds before the system reaches steady state conditions and the mass flow rate is kept constant.

6.2.4.3   Flight Altitude and Surge Velocity

The Simulink model in Figure 6.9 was run with a simulation time of 100 seconds since it was expected that there would be an increase in time required to attain steady state conditions for a two-dimensional simulation as compared to the previous simulations. Figure 6.11 (a) shows the flight altitude response and Figure 6.3 (b) shows the surge velocity response.

140

(a)   (b)
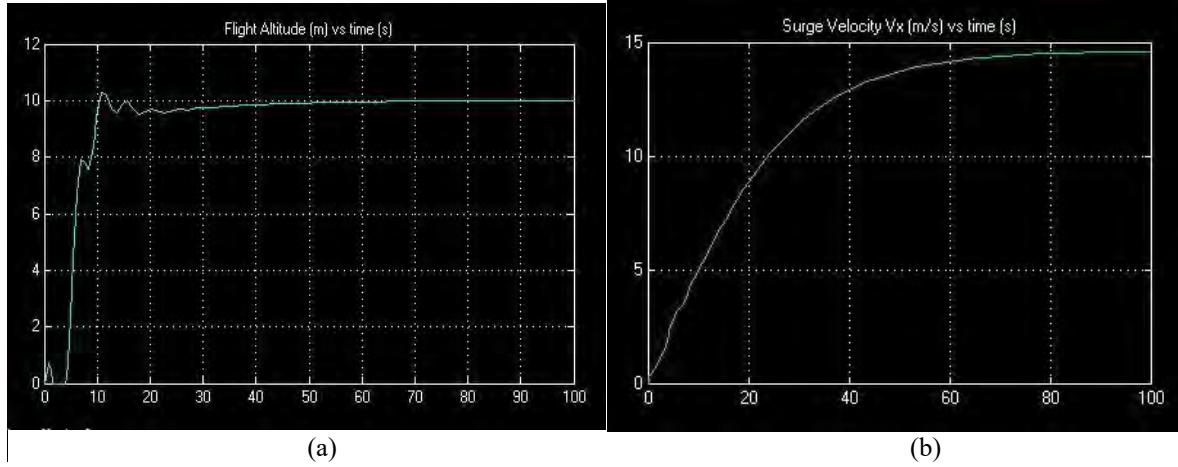
Figure 6.11: (a) Flight altitude, (b) Heave velocity

Referring to Figure 6.11 (a), the system takes-off at 4 seconds and reaches a peak flight altitude of 10.2 m (peak overshoot of 2%) at 11 seconds. The system then experiences slight oscillatory motion for a duration of 15 seconds and reaches steady state condions after 60 seconds. Referring to Figure 6.11 (b), it is observed that the surge velocity increases at a steady rate over a duration of 60 seconds until reaching a steady state surge velocity of 14.6 m/s. The response in flight altitude is favorable in terms of a low peak overshoot, however, the mild oscillations observed in Figure 6.11 (a) indicate that the PID controller may require slight optimization and robustness tuning to dampen the response of flight altitude (Ogata, 2013).

6.2.4.4   Thrust Force and Drag Force

Surge velocity is attained when the thust force in the x-direction is greater than or equal to the drag force acting on the water jetpack system. The thrust force and drag force acting on the water jetpack system in the x-direction with an induced thrust vector angle of 3 degrees is shown in Figure 6.12.

(a)   (b)
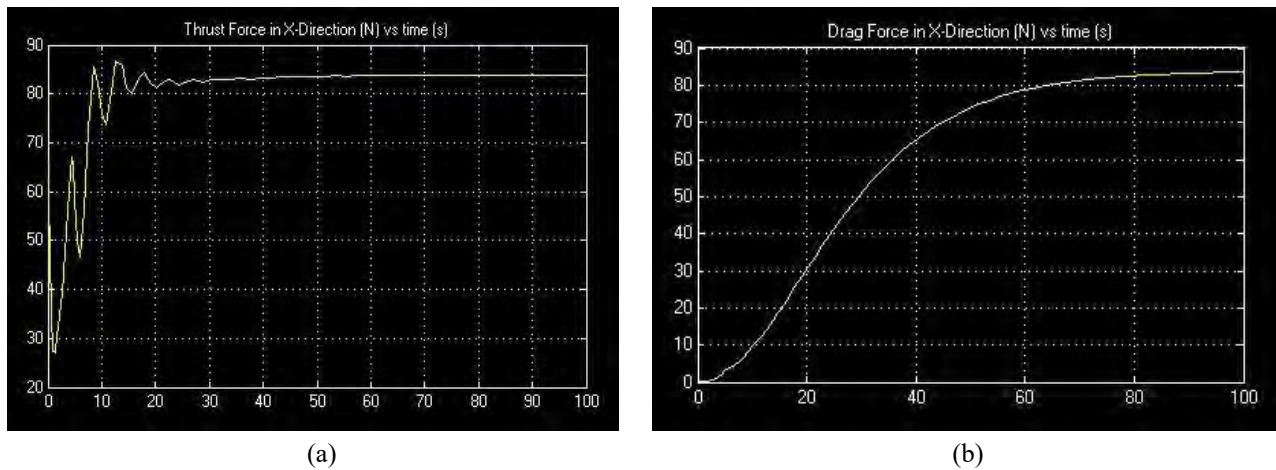
Figure 6.12: (a) Thrust force in x-direction, (b) Drag force in x-direction

141

According to the general thrust equation derived in Chapter 3, thrust force is proportional to the square of mass flow rate. This relationship is observed by referring to Figure 6.10 (b) and Figure 6.12 (a), the osillations occur at the same instants of time. Thrust force in the x-direction increases and reaches the steady state value of 84 N after 60 seconds. The drag force in Figure 6.12 (b) is proportional to the square of the surge velocity in Figure 6.11 (b). Drag force is observed to increases at a steady and rate over a duration of 80 seconds before reaching a steady state value of 84 N. When thrust force equals to the drag force, the net force acting on the system in the x-direction equals to zero.

6.2.5   Simulink Model 4: Water Jetpack Motion in Two Dimensions (Closed-Loop System)

6.2.5.1   Mathematical and Simulink Model

In this section, a closed-loop system is developed from the Simulink model in Figure 6.9. The aim of developing a closed-loop system for motion in the x-z direction is to enable flight altitude and surge velocity control for the system. The Simulink model developed in this section is based on Newton's Second Law for the water jetpack system in the x- and z-direction and Equation 6.5 and 6.6 are fully applicable. In this model the input thrust vector angle is the new controlled variable. The closed-loop Simulink model for motion of the water jetpack system in the z-direction is shown in Figure 6.13. A second PID controller is introduced in the system to control the thrust vector angle.
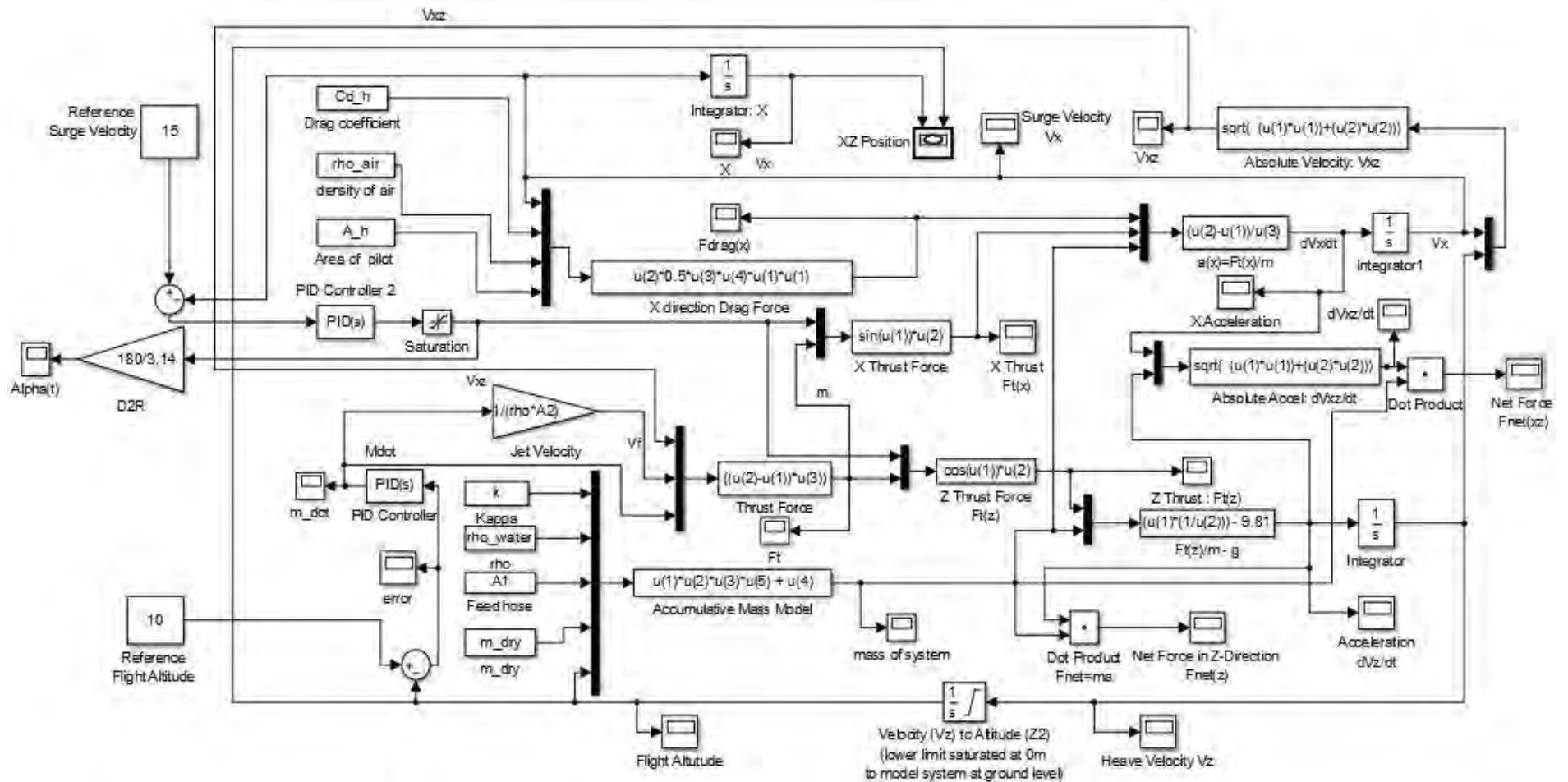
Figure 6.13: Water jetpack x-z direction Simulink model (Closed-loop sysem)

143

The layout of the Simulink model shown in Figure 6.13 is the same as the Simulink model in Figure 6.9 (open-loop system) except that the thrust vector angle input in Figure 6.8 is replaced by a PID controller in Figure 6.13 (closed-loop system). The reference surge velocity is 15 m/s and represented by a constant block. The second PID controller controls the thrust vector angle, this mechanical action can be achieved with the use of servo or stepper motors (Naidoo et al., 2015a). The servo or stepper motors can be set-up to control the nozzle thrust vector angle of the water jetpack, the design and implementation of this mechatronic system is left for future work. Ideally, the thrust vector component in the x-direction should not be greater than the thrust vector component in the z-direction, this ensures that the water jetpack system remains stable in flight and the pitch moment does not cause the system to rotate forward (Jetlev-Flyer, 2015). This condition implies that the maximum positive value of the thrust vector angle is 45 degrees. This condition is imposed by saturating the output of the PID controller between -45 degrees and 45 degrees, the function block that allows for this is shown in Figure 6.14.
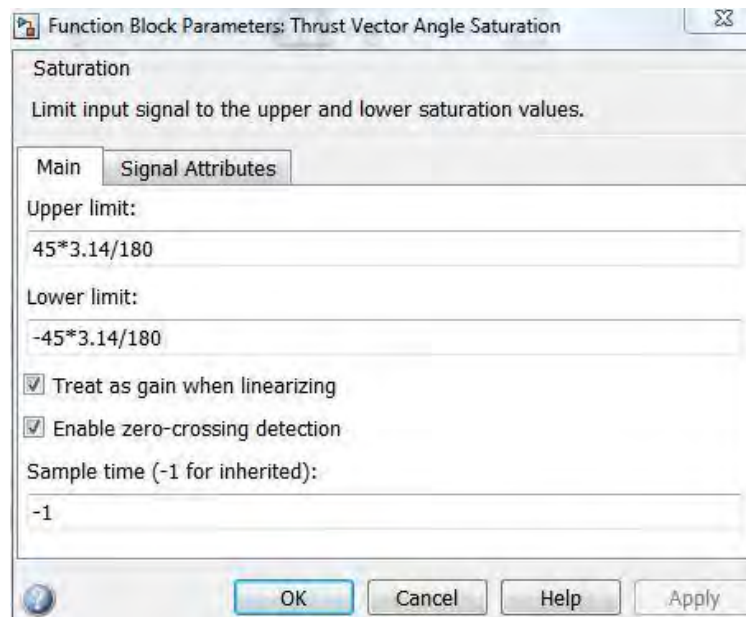
Figure 6.14: Thrust vector angle saturation

The output of the PID controller thrust vector angle is in radians, thus the saturation limits are also in radians. As shown in Figure 6.14, the upper limit is 45 degrees which is equivalent to 0.785 radians, and the lower limit is -45 degrees which is equivalent to -0.785 radians. The saturation can also be implemented in the PID controller. The inputs and outputs of the Simulink model in Figure 6.12 is shown in Table 6.5.

Table 6.5: Input and output parameters for two-dimensional closed-loop Simulink modelling

Inputs		Outputs	
Dry mass	m_{dry}	Thrust vector angle	α
Gravitational acceleration	g	Mass flow rate	$\dot{m}$
Jet-exit area	A_2	Thrust force	F_T
Kappa	κ	Thrust force in x-direction	F_{T_x}
Feed hose area	A_1	Thrust force in z-direction	F_{T_z}
Density of water	ρ	Absolute acceleration	dv_{xz}/dt
Reference flight altitude	Z_{20}	Acceleration in x-direction	dv_z/dt
Average area of human	A_h	Acceleration in z-direction	dv_z/dt
Drag coefficient of human	C_{D_h}	Mass of system	$\sum m$
Density of air	ρ_{air}	Drag force	F_D
Reference surge velocity	v_{x0}	Surge velocity	v_x
		Heave velocity	v_z
		Absolute velocity	v_{xz}
		Net force in x-direction	F_{net_x}
		Net force in z-direction	F_{net_z}
		Net force	F_{net}
		Steady state error	E_{ss}
		Flight altitude	Z_2
		X-position	X

The new input for the closed-loop system is the desired surge velocity. The outputs are the same as in the previous open-loop simulation with the addition of the controlled thrust vector angle. The most significant output parameters that are observed in this simulation are: thrust vector angle, mass flow rate, thrust force, flight altitude, and the steady state error. The response of net force, heave velocity, acceleration, and mass of system is shown in Appendix C.

6.2.5.2 PID Controller Architecture

There are two PID controllers used in this simulation. PID controller 1 controls mass flow rate and PID controller 2 controls the thrust vector angle. Selecting the parameter values for PID controller 1 involved an iterative process of using different combinations for the PID parameters until a favorable response in flight altitude was established. PID controller 2 was tuned using MATLAB's PID controller function block. The parameter setting for PID controller 1 and 2 are shown below in Figure 6.15.

(a)

(b)

Figure 6.15: PID controller parameters (a) PID controller 1 parameters, (b) PID controller 2 parameters

Referring to Figure 6.15, the values for P, I, D and N are shown as 1, 2, 5 and 1 respectively. The equation of the PID controller is given by:

$$G_1(s) = 1 + \frac{2}{s} + \frac{5}{\left(1 + \frac{1}{s}\right)} \tag{6.5}$$

$$G_2(s) = 0.451 + \frac{0.033}{s} + \frac{8.32}{\left(1 + \frac{8.32}{s}\right)} \tag{6.6}$$

where $G_1(s)$ is the transfer function equation for PID controller 1 and $G_2(s)$ is the transfer function equation for PID controller 2.

6.2.5.3   Mass Flow Rate and Thrust Vector Angle Control

The mass flow rate and thrust vector angle control responses for this simulation is shown in Figure 6.14 (a) and (b) below. The mass flow rate and thrust vector angle are controlled by two PID controllers as illustrated in the Simulink model of the system in Figure 6.16. The reference flight altitude remains at 10 m and the reference surge velocity is

15 m/s. The mass flow rate in this simulation is controlled with the same PID controller that was developed in Section 6.2.3.

<table>
<tr><td>(a)</td><td>(b)</td></tr>
</table>
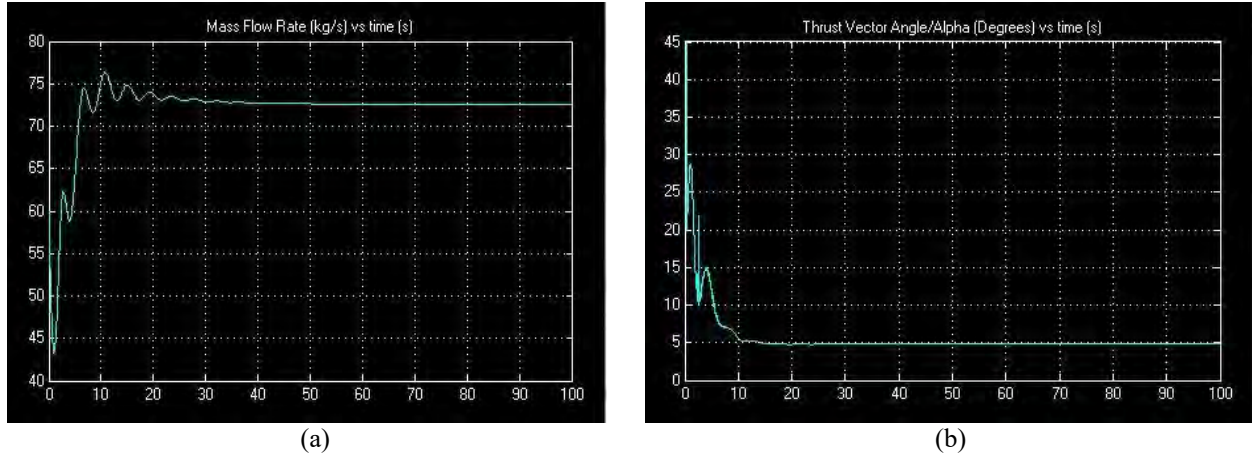
Figure 6.16: (a) Mass flow rate control, (b) Thrust vector angle control

In Figure 6.16 (a), it is observed that the PID controller starts with an initial mass flow rate of 60 kg/s and thereafter there is a rapid increase in the gradient of the controlled mass flow rate with the presence of low amplitude oscillations that decay after the mass flow rate reaches the peak value of 76 kg/s at 11 seconds into the simulation. Thereafter the mass flow rate decays to 73 kg/s and reaches steady state conditions after 38 seconds. In Figure 6.16 (b), the initial thrust vector angle is 45 degrees and there is a rapid decrease in the thrust vector angle from 45 degrees to 5 degrees within the first 10 seconds of the simulation, with the presence of sharp oscillations. The thrust vector angle then remains constant at 5 degrees. The response in thrust vector angle shown in Figure 6.14 (b) indicates that the controller adapts quickly to attain the steady state value. However, the controller action is less important than the actual output response of flight altitude and surge velocity that result from the controlled response of mass flow rate and thrust vector angle.

6.2.5.4   Flight Altitude and Surge Velocity Response

The reference flight altitude and surge velocity for this simulation is 10 m and 15 m/s respectively. The aim of using the PID controllers is to attain the reference flight altitude and surge velocity.The flight altitude and surge velocity response is shown below in Figure 6.17 (a) and (b) respectively.

(a)   (b)
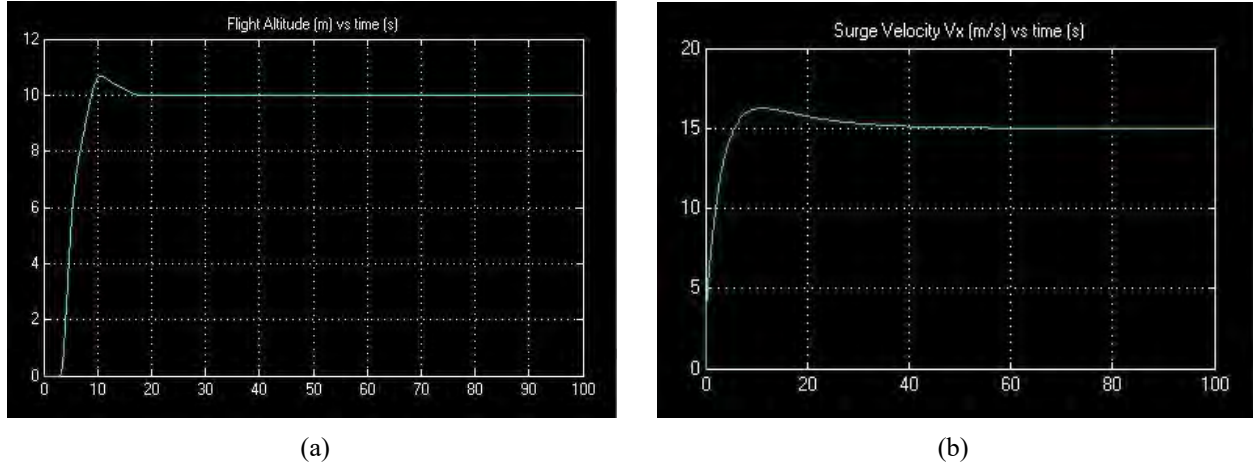
Figure 6.17: (a) Flight altitude, (b) Surge Velocity

Referring to flight altitude response in Figure 6.17 (a), it can be observed that the flight altitude of the system is zero for the first 3 seconds of the simulation and thereafter the system takes-off and reaches a peak flight altitude of 10.5 m at 10 seconds. The system experiences a peak overshoot in flight altitude by 5% which is 2% higher than the overshoot experienced by the open-loop response. Referring to Figure 6.17 (b), it is observed that the surge velocity increases from zero to a peak value of 16 m/s within 5 seconds. Thereafter the surge velocity drops gradually to 15 m/s (reference value) at 40 seconds. The response in flight altitude and surge velocity indicates that the PID controllers used provide the desired responses with no oscillations and peak overshoot of 5% and 6.7% respectively.

6.2.5.5 Speed Saturation and Sub-System Drag Coefficient Modelling

In this section, the system is analyzed under maximum mass flow rate and surge velocity conditions to verify the controllers' response to a high reference surge velocity. The thrust vector angle is saturated between positive and negative 45 degrees; in this analysis, the maximum output of the water jetpack system is established by setting the reference flight altitude to 10 m and the reference surge velocity to 50 m/s. However, the reference surge velocity may be set at infinity; although this this is not attainable, the system is expected to reach the saturation conditions whereby the maximum surge velocity, mass flow rate and thrust force generated is reached. In order to improve the reliability of the responses obtained when modelling and simulating the water jetpack system in two dimensions for maximum conditions, further investigation into the forces acting on the system in the x-direction is considered. In particular, the effects of aerodynamic drag is analyzed to yield an improved estimate of the drag coefficient and area term in the drag force equation. The general expression for drag force of the entire water jetpack system may be expressed as:

$$F_D = C_{D_{av}} \frac{1}{2} \rho_{air} A_{total} v_x^2 \qquad (6.7)$$

where $C_{D_{av}}$ is the average drag coefficient and A_{total} is the total area of the water jetpack system as seen from the x-direction. The average drag coefficient $C_{D_{av}}$ is expressed as the area-weighted average of the sub-systems that are significant contributors to the total drag on the system:

$$C_{D_{av}} = \frac{\sum_{i=1}^{N}(C_{D_i} A_i)}{\sum_{i=1}^{N} A_i} \qquad (6.8)$$

where C_{D_i} is the drag coefficient of sub-system i, A_i is the area of sub-system i, and N is the total number of sub-systems. In this analysis, N will be modelled for two sub-systems: the pilot and the feed hose. Therefore, the average drag coefficient may be expressed as:

$$C_{D_{av}} = \frac{C_{D_h} A_h + C_{D_{hose}} A_{hose}}{A_h + A_{hose}} \qquad (6.9)$$

where C_{D_h} is the drag coefficient of a human pilot, A_h is the frontal area of a human pilot, $C_{D_{hose}}$ is the drag coefficient of the feed hose, and A_{hose} is the frontal area of the feed hose. The drag coefficient and area of a human pilot is 0.55 and 1.16 [2] as given previously. The area of the feed hose A_{hose} is given by:

$$A_{hose} = Z_2 \, D_1 \qquad (6.10)$$

where Z_2 is the flight altitude and D_1 is the feed hose diameter. The feed hose area used in the drag force equation is dependent on flight altitude and not the actual length of the feed hose since the length of the feed hose as seen from the x-direction would be equal to the flight altitude, and thus the drag force contribution by the feed hose is dependent on the flight altitude. Since D_1 and Z_2 is 0.1 m and 10 m respectively, the feed hose area A_{hose} is equal to 1 m^2. The drag coefficient of the feed hose is 1, this is computed by treating the feed hose as a cylindrical tube and using a low Reynolds number for the air flow (Fox et al., 2010).

Substituting the values for drag coefficient and area of the feed hose and pilot into Equation 6.8 results in the average drag coefficient of the system as 1.06 and the total area as 1.55 m^2. These are the new values that will be used in computing the drag force in the preceeding Simulink models. The Simulink model for this analysis is shown in Figure 6.18.
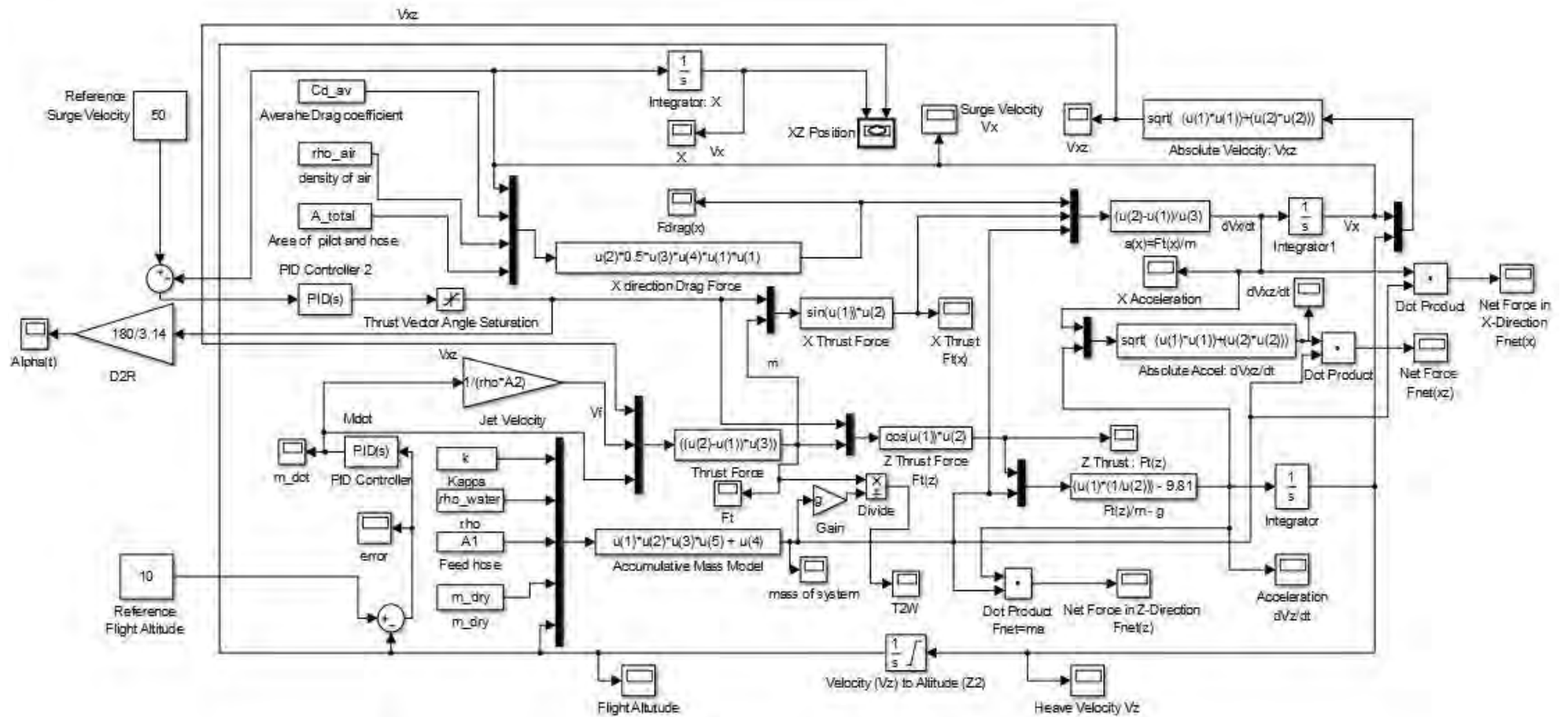
Figure 6.18: Water jetpack x-z direction Simulink model with speed saturation and average drag modelling

150

Referring to Figure 6.18, the reference surge velocity is 50 m/s which is represented by a constant block. The drag coefficient and area terms used for computing the drag force actin on the system is replaced by $C_{D_{av}}$ and A_{total} in the MATLAB workspace (see Appendix A).

6.2.5.6   System Response for Speed Saturation and Average Drag Coefficient Modelling

The system response of mass flow rate, thrust vector angle, flight altitude, surge velocity, drag force, and the thrust-to-weight ratio is shown in Figure 6.19.
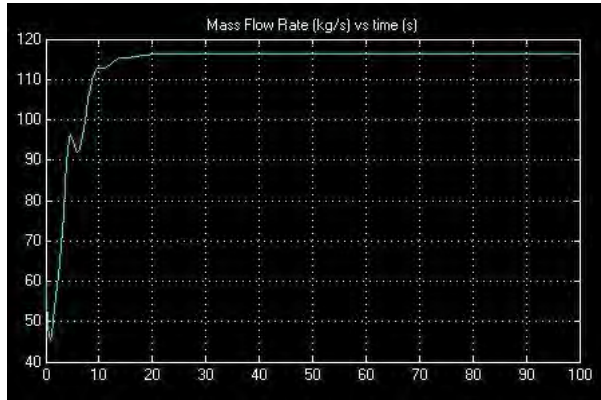
(a)
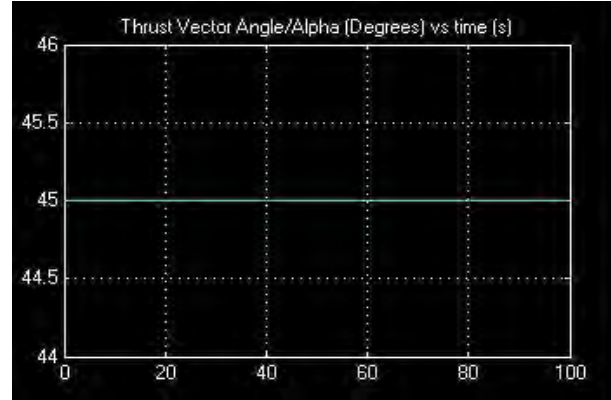
(b)
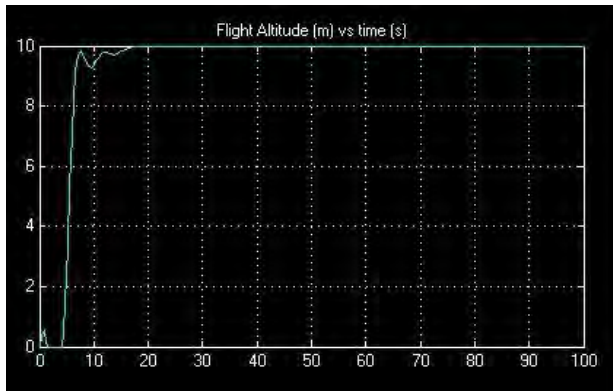
(c)
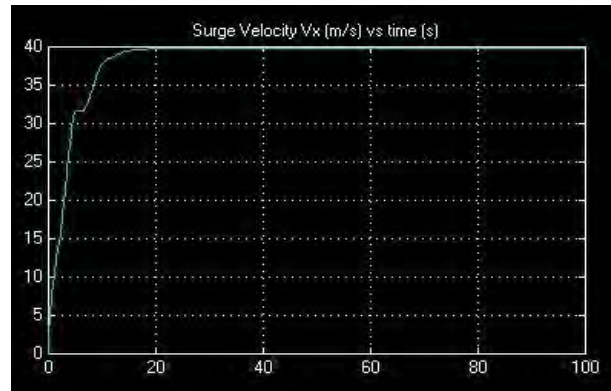
(d)
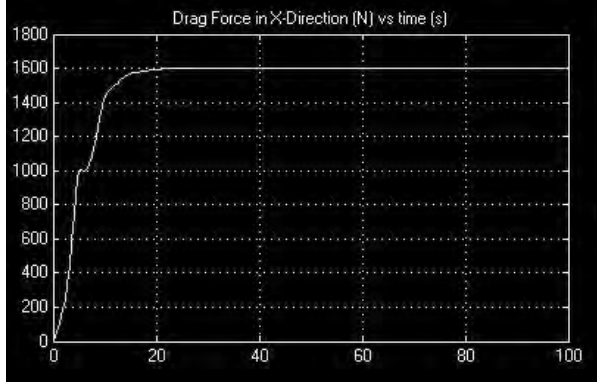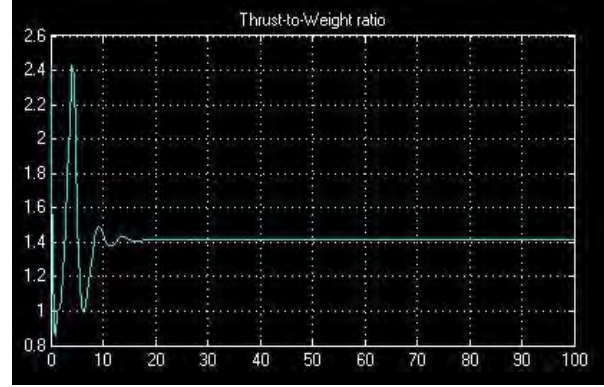
(e)	(f)

Figure 6.19: Speed saturation responses (a) Mass flow rate, (b) Thrust vector angle, (c) Flight altitude, (d) Surge velocity, (e) Drag force, and (f) Thrust-to-weight ratio

Referring to Figure 6.19 (a), the controlled mass flow rate reaches a peak steady state value of 116 kg/s within 20 seconds, which is more than double the mass flow rate required for steady state hovering as in Section 6.2.3. The controlled thrust vector angle in Figure 6.19 (b) remains constant at 45 degrees. The flight altitude response in Figure 6.19 (c) shows that the reference flight altitude is reached within 20 seconds with zero overshoot. However, there is slight oscillatory motion that occurs prior to the system reaching steady state. Figure 6.19 (d) shows that the maximum attainable surge velocity is 40 m/s under maximum conditions. The system reaches the maximum surge velocity within 20 seconds with zero overshoot. The drag force is shown by Figure 6.19 (e), it is observed that there is a steady rise in drag force until the system reaches steady state with a peak drag force of 1600 N. This implies that the thrust force generated in the x-direction is also 1600 N. The thrust-to-weight ratio of the system is shown in Figure 6.19 (e), this ratio starts at a maximum value of 2.4 and oscillates over a period of 18 seconds until reaching a steady state thrust-to-weight ratio of 1.4. The thrust-to-weight ratio is useful when specifying the nominal and peak performance of the water jetpack propulsion system.

6.2.6   Simulink Simulation 5: Water Jetpack Three-Dimensional Modelling

6.2.6.1   Mathematical and Simulink Model

The Simulink model developed in this section is based on Newton's Second Law for the water jetpack system in the x-, y-, x-y, and z-direction respectively. The equations given below are derived from the three-dimensional water jetpack modelling equations given in Chapter 3.

$$\sum F_x = \left(m_{dry} + \kappa \rho A_1 Z_2\right) \frac{dv_x}{dt} = \dot{m}\left(v_f - v_{xyz}\right) \sin\alpha \cos\psi - C_{D_{av}} \frac{1}{2} \rho_{air} A_{total} v_{xy}^2 \cos\psi \quad (6.11)$$

$$\sum F_y = \left(m_{dry} + \kappa \rho A_1 Z_2\right) \frac{dv_y}{dt} = \dot{m}\left(v_f - v_{xyz}\right) \sin\alpha \sin\psi - C_{D_{av}} \frac{1}{2} \rho_{air} A_{total} v_{xy}^2 \sin\psi \quad (6.12)$$

$$\sum F_{xy} = \left(m_{dry} + \kappa \rho A_1 Z_2\right) \frac{dv_{xy}}{dt} = \dot{m}\left(v_f - v_{xyz}\right) \sin\alpha - C_{D_{av}} \frac{1}{2} \rho_{air} A_{total} v_{xy}^2 \quad (6.13)$$

$$\sum F_z = \left(m_{dry} + \kappa\, \rho\, A_1\, Z_2\right) \frac{dv_x}{dt} = \dot{m}\left(v_f - v_{xyz}\right)\cos\alpha - \left(m_{dry} + \kappa\, \rho\, A_1\, Z_2\right)g \qquad (6.14)$$

It must be noted that the drag force term in Equation 6.11, 6.12, and 6.13 are derived expressions from the average drag coefficient model in Equation 6.6 as described in the previous section. The utility of the above equations is to develop a three-dimensional Simulink model for the water jetpack system to simulate the transient response of the system. The difference between the three-dimensional Simulink modelling done in this section and the two-dimensional closed-loop Simulink modelling done in the previous section is the inclusion of the yaw angle in the force balance equations given above. As discussed in Chapter 3, the yaw angle is controlled by shifting the CM of the pilot from side to side such that there is an induced thrust force in the y-direction. The controlled variables in the open-loop system are 1) mass flow rate and 2) thrust vector angle. The yaw angle is regarded as a pilot defined input, if the yaw angle is zero then the water jetpack system may be modelled in 2-dimensions as done previously.

The Simulink model developed to represent the open-loop response of the water jetpack system in the x-y-z direction is shown in Figure 6.20 below. The Simulink model represents Equations' 6.11, 6.12, 6.13 and 6.14 as a system. The utility of this Simulink model is to observe the transient responses of the system for a pilot defined yaw angle input along with a controlled mass flow rate and thrust vector angle. The inputs and outputs of the Simulink model above are shown in Table 6.6.

The inputs are identical to the inputs used for the two-dimensional closed-loop system previously, however in this case there is an additional input which is the yaw angle. The values of all inputs are defined in Table 6.1. The outputs are shown to the right half of Table 6.6, the new outputs in this section are the thrust force, drag force, net force, acceleration, and velocity in the y-direction. In this simulation, the most significant outputs are: flight altitude, mass flow rate, velocity in the x-y direction, sway velocity, thrust and drag force in the y-direction. The other results of the outputs shown in Table 6.6 are given Appendix C.
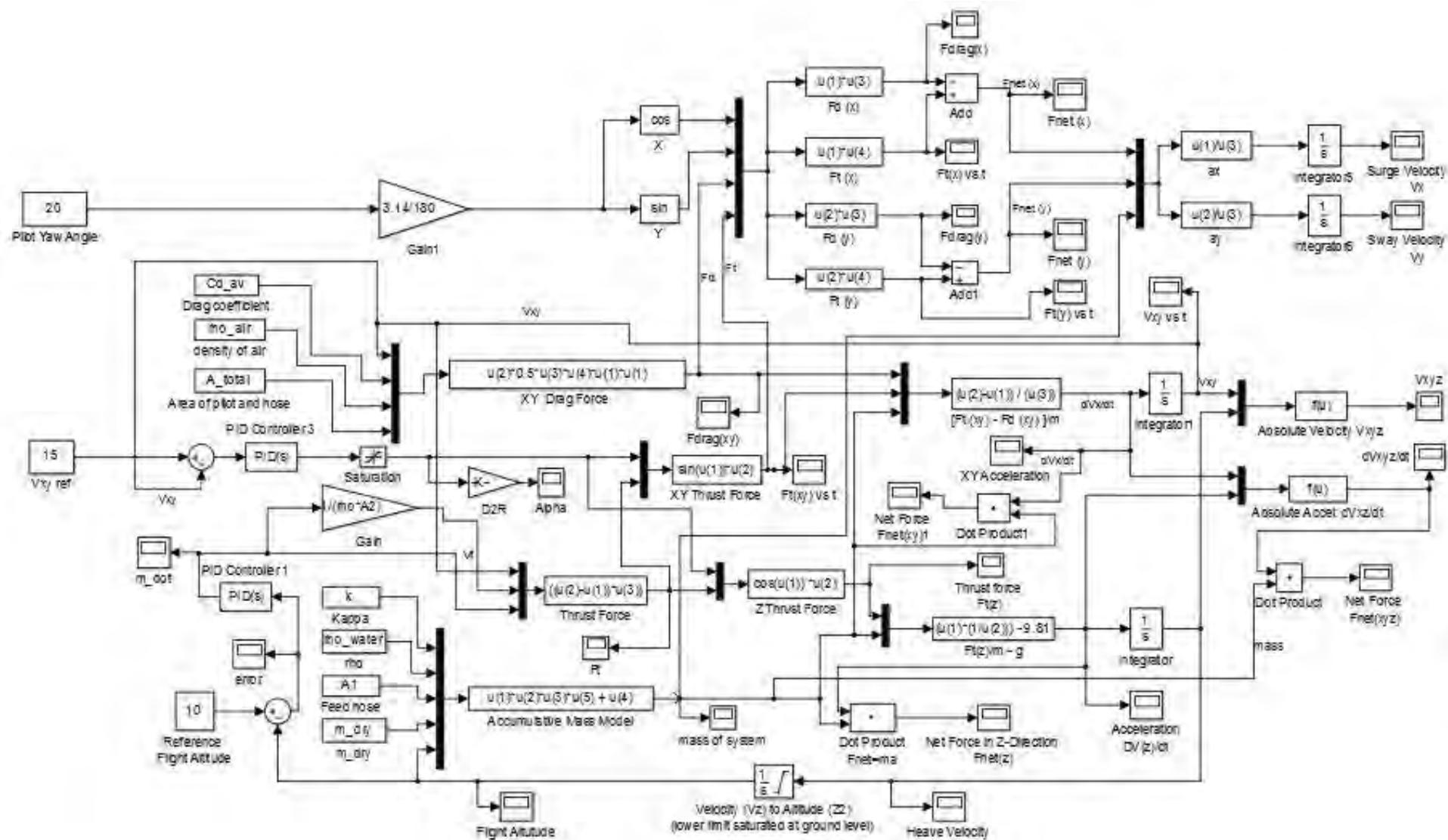
Figure 6.20: Water jetpack three-dimensional Simulink model

154

Table 6.6: Input and output parameters for three-dimensional Simulink modelling

Inputs		Outputs	
Dry mass	m_{dry}	Thrust vector angle	α
Gravitational acceleration	g	Mass flow rate	$\dot{m}$
Jet-exit area	A_2	Thrust force	F_T
Kappa	κ	Thrust force in x-direction	F_{T_x}
Feed hose area	A_1	Thrust force in y-direction	F_{T_x}
Density of water	ρ	Thrust force in x-y direction	$F_{T_{xy}}$
Reference flight altitude	Z_{20}	Thrust force in z-direction	F_{T_z}
Total area of jetpack system	A_h	Acceleration in x-direction	dv_x/dt
Average coefficient of jetpack system	$C_{D_{av}}$	Acceleration in y-direction	dv_y/dt
Density of air	ρ_{air}	Acceleration in x-y direction	dv_{xy}/dt
Reference surge velocity	v_{x0}	Acceleration in z-direction	dv_z/dt
Yaw angle	ψ	Absolute acceleration	dv_{xyz}/dt
		Mass of system	$\sum m$
		Net force in x-direction	F_{net_x}
		Net force in y-direction	F_{net_y}
		Net force in x-y direction	$F_{net_{xy}}$
		Net force in z-direction	F_{net_z}
		Net force	F_{net}
		Surge velocity	v_x
		Sway velocity	v_y
		Heave velocity	v_z
		Absolute velocity	v_{xyz}
		Drag force in x-direction	F_{D_x}
		Drag force in y-direction	F_{D_y}
		Drag force in x-y direction	$F_{D_{xy}}$
		Flight altitude	Z_2

6.2.6.2 Controller Architecture

There are two PID controllers used in the Simulink model shown in Figure 6.20. PID controller 1 controls mass flow rate and PID controller 2 controls the thrust vector angle. In this simulation, it was observed that the parameters used for PID controller 2 in the two-dimensional closed-loop simulation do not yield favorable responses of thrust vector angle control because sharp oscillations occur in short time intervals, the cause of which is the yaw angle. Therefore, PID controller 2 was tuned using MATLAB's PID controller function block. The parameter settings for PID controller 1 and 2 are shown in Figure 6.21.

(a)

(b)

Figure 6.21: PID controller parameters (a) PID controller 1 parameters, (b) PID controller 2 parameters

Referring to the previous Simulink model shown in Figure 6.13, PID controller 1 parameters remain the same as previous, however, in PID controller 2, the integral and derivative terms have changed during the tuning process. The transfer function equation for PID controller 1 and 2 is given by :

$$G_1(s) = 1 + \frac{2}{s} + \frac{5}{\left(1 + \frac{1}{s}\right)} \tag{6.15}$$

$$G_2(s) = 0.450543371284897 + \frac{0.04}{s} + \frac{0.5(8.31763771102671)}{\left(1 + \frac{8.31763771102671}{s}\right)} \tag{6.16}$$

where $G_1(s)$ is the transfer function equation for PID controller 1 and $G_2(s)$ is the transfer function equation for PID controller 2.

6.2.6.3   Thrust Vector Angle and Mass Flow Rate Control

The controlled thrust vector angle and mass flow rate responses are shown in Figure 6.22 (a) and (b). These variables are controlled by the two PID controllers in the system. The simulation run-time was selected as 50 seconds.

<div align="center">(a)   (b)</div>
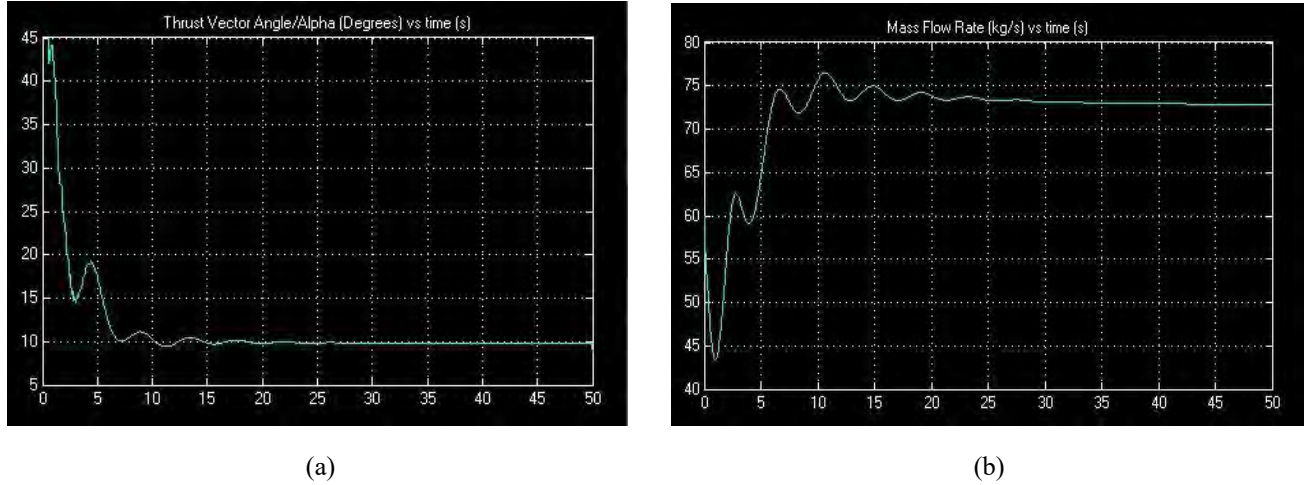
Figure 6.22: (a) Thrust vector angle control, (b) Mass flow rate control

Referring to Figure 6.22 (a), it is observed that the thrust vector angle starts at 45 degrees and decays to 10 degrees over a time interval of 15 seconds. There are minor oscillations present in this response. The thrust vector angle remains at 10 degrees as the system reaches steady state conditions. Referring to Figure 6.22 (b), it is observed that the mass flow rate starts initiates at 60 kg/s and drops to 43 kg/s in the first 2 seconds, thereafter there is a steady and oscillatory rise in mass flow rate. The mass flow rate stabilizes at 73 kg/s after 35 seconds.

6.2.6.4   Absolute, Surge, Sway and X-Y Velocity

The reference velocity in the x-y direction (forward velocity) is 15 m/s and the pilot input yaw angle is 20 degrees in this simulation. The aim of PID controller 2 is to control the thrust vector angle such that the net forward flight velocity is 15 m/s at a fixed flight altitude of 10 m. Figure 6.23 (a), (b), (c) and (d) show the response of surge, sway, x-y and absolute velocity.
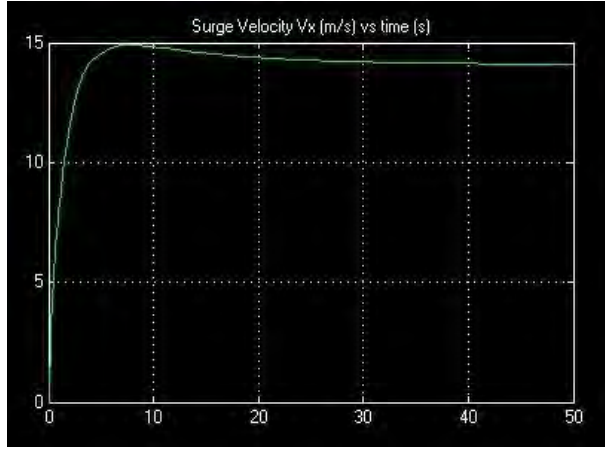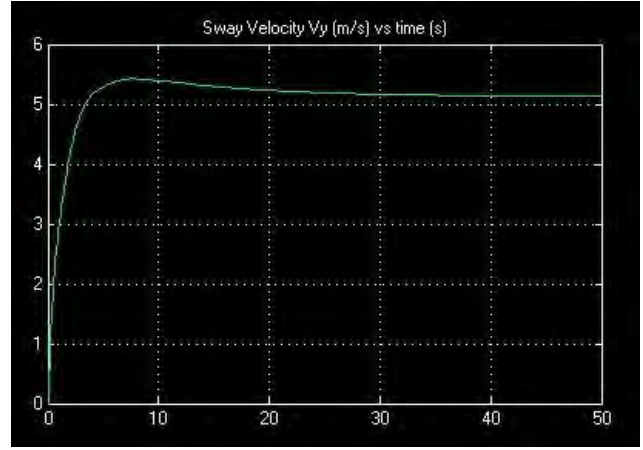
(a)   (b)
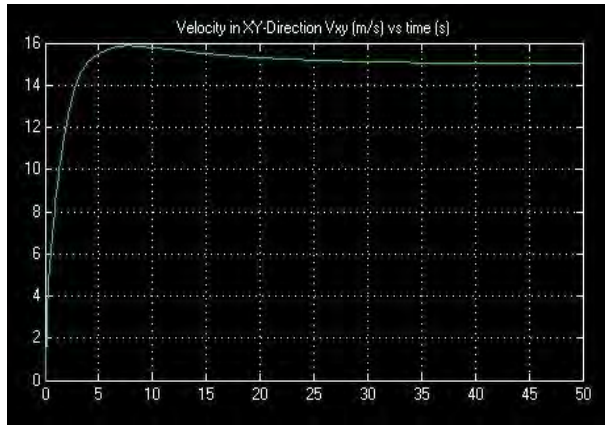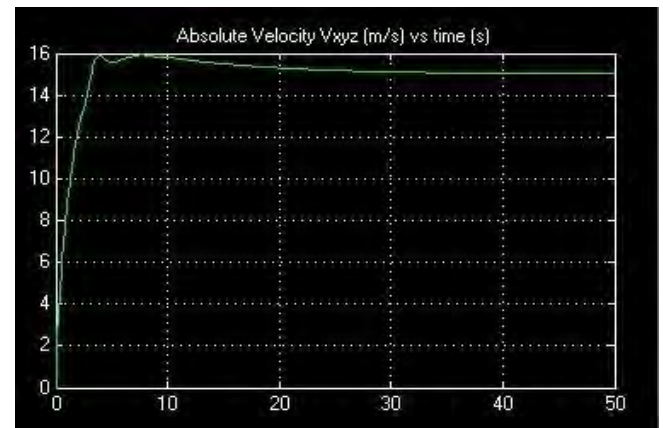
(c)   (d)

Figure 6.23: (a) Surge velocity, (b) Sway Velocity, (c) Velocity in x-y direction, (d) Absolute velocity

It can be observed from Figure 6.23 (c) that the reference x-y velocity of 15 m/s is attained within 30 seconds. A peak overshoot of 6.7% occurs at 7.5 seconds in Figure 6.23 (c). Since the pilot yaw angle is 20 degrees, Figure 6.23 (a) and (b) represent the x and y components of the absolute velocity in Figure 6.23 (d). The surge velocity reaches a peak value of 15 m/s (5.6% overshoot) in 8 seconds and attains a steady state value of 14.2 m/s after 30 seconds. The sway velocity reaches a peak value of 5.4 m/s (5.88% overshoot) in 8 seconds and attains a steady state value of 5.1 m/s after 30 seconds. The sway velocity is almost three times smaller than the surge velocity with the pilot yaw angle being 20 degrees. As the yaw angle increases, the sway velocity is expected to increase proportionally. Figure 6.21 (d) shows the absolute velocity of the system in the x-y-z direction. It is observed that a peak absolute velocity of 16 m/s is reached at 4 seconds and 8 seconds respectively. Thereafter the absolute velocity drops and reaches the steady state value of 15 m/s. At this stage, the water jetpack system is at constant flight altitude, and the velocity in the x and y-directions are 14.2 m/s and 5.1 m/s respectively as shown in Figure 6.23 (a) and (b).

6.2.7   Autonomous Underwater Vehicle Simulink Modelling

6.2.8   Input Parameters

The MATLAB Simulink model developed in this section is based on approximate parameters for the AUV based on statistical analysis and the survey of AUV's contained in Chapter 2. Table 6.7 shows the default values selected for the parameters used in the development of the Simulink model of the AUV for motion in all three dimensions (z, x-z and x-y-z direction).

Table 6.7: Input parameters for AUV Simulink modelling.

Parameter	Symbol	Units	Value
AUV mass	m_{AUV}	kg	120
Gravitational acceleration	g	m/s^2	9.81
Propeller area	A_{prop}	m^2	0.0094
AUV frontal area	A_A	m^2	0.0707
AUV cross-flow area	A_{AL}	m^2	0.6
Density of water	ρ	kg/m^3	1000
Drag coefficient – Frontal	C_{D_A}	Dimensionless	0.7
Drag coefficient – Cross flow	$C_{D_{AL}}$	Dimensionless	0.83
Desired sway velocity	v_y	m/s	2
Desired heave velocity	v_z	m/s	0
Desired velocity in X-Y*	v_{xy}	m/s	15
Volume of AUV	Vol_{AUV}	kg/m^3	1.23

The mass of the AUV system m_{AUV} is approximated as 120 kg. The gravitational acceleration constant is taken as 9.81 m/s^2. The propeller area is computed as 0.0094 m^2 using a propeller with diameter 150 mm and blade width 20 mm. The shape of the AUV is taken to be cylindrical with a mean body diameter of 300 mm and total length of 2 m, thus the frontal- and cross-flow area of the AUV is computed as 0.0707 m^2 and 0.6 m^2 respectively. The density of water is taken as 1000 kg/m^3. The frontal drag coefficient of the AUV is 0.7, this is based on treating the frontal section as a rectangular rod (Cengal and Cimbala, 2010). The cross-flow drag coefficient is 0.83, this is computed by considering the longitudinal section of the AUV as a finite cylinder, and since the length-to-diameter ratio of the AUV is 6.67 (see Appendix A) and interpolating between L/D of 5 and 10 yields 0.83 as the cross-flow drag coefficient. The desired sway, heave, and velocity in the x-y direction is chosen as 2 m/s, 0 m/s and 15 m/s respectively. The sway velocity is chosen as 2 m/s to observe the response of the horizontal deviation angle for the propeller to result in the desired sway velocity. The heave velocity is chosen as 0 m/s such that the AUV maintains a constant depth of between 0 m and 1 m below the surface of the water. The volume of the AUV is computed just as the volume of a cylinder with length 2 m and diameter 300 mm.

6.2.9   Mathematical and Simulink Model

The three-dimensional Simulink model developed in this section is based on an AUV with a three-dimensional thrust vectoring system as described in Chapter 4. The Newtonian force balance equations for the AUV in the x-, y- and z-directions are given as:

$$\sum F_x = m_{AUV}\frac{dv_x}{dt} = F_{prop}\cos(\delta_d)\cos(\delta_r) - C_{D_A}\frac{1}{2}\rho v_x{}^2 A_A \tag{6.17}$$

$$\sum F_y = m_{AUV}\frac{dv_y}{dt} = F_{prop}\cos(\delta_d)\sin(\delta_r) - C_{D_{AL}}\frac{1}{2}\rho v_y{}^2 A_{AL} \tag{6.18}$$

$$\sum F_z = m_{AUV}\frac{dv_z}{dt} = F_{prop}\sin(\delta_d) + \rho g V_B - m_{AUV}g \tag{6.19}$$

The Simulink model that is developed to represent the closed-loop response of the AUV is shown below in Figure 6.22. The utility of such a model is to observe the performance of the AUV in three dimensions.

Referring to Figure 6.22, the constant parameters defined in Table 6.7 include: AUV mass, gravitational acceleration, propeller area, AUV frontal area, AUV cross-flow area, density of water, frontal drag coefficient, cross-flow drag coefficient, desired sway velocity, desired heave velocity, desired velocity in x-y direction, and the volume of the AUV. There are 11 function blocks that compute thrust force, drag force, velocity, and acceleration for each direction as illustrated. There are three reference inputs: desired velocity in the x-y direction, desired sway velocity, and desired heave velocity. There are three PID controllers in Figure 6.22, these control the propeller mass flow rate, horizontal deviation angle, and vertical deviation angle respectively. There are 16 scopes in total that display the signals of the main transient response signals of interest in the system. The main inputs and outputs of the Simulink model in Figure 6.24 are summarized in Table 6.8.
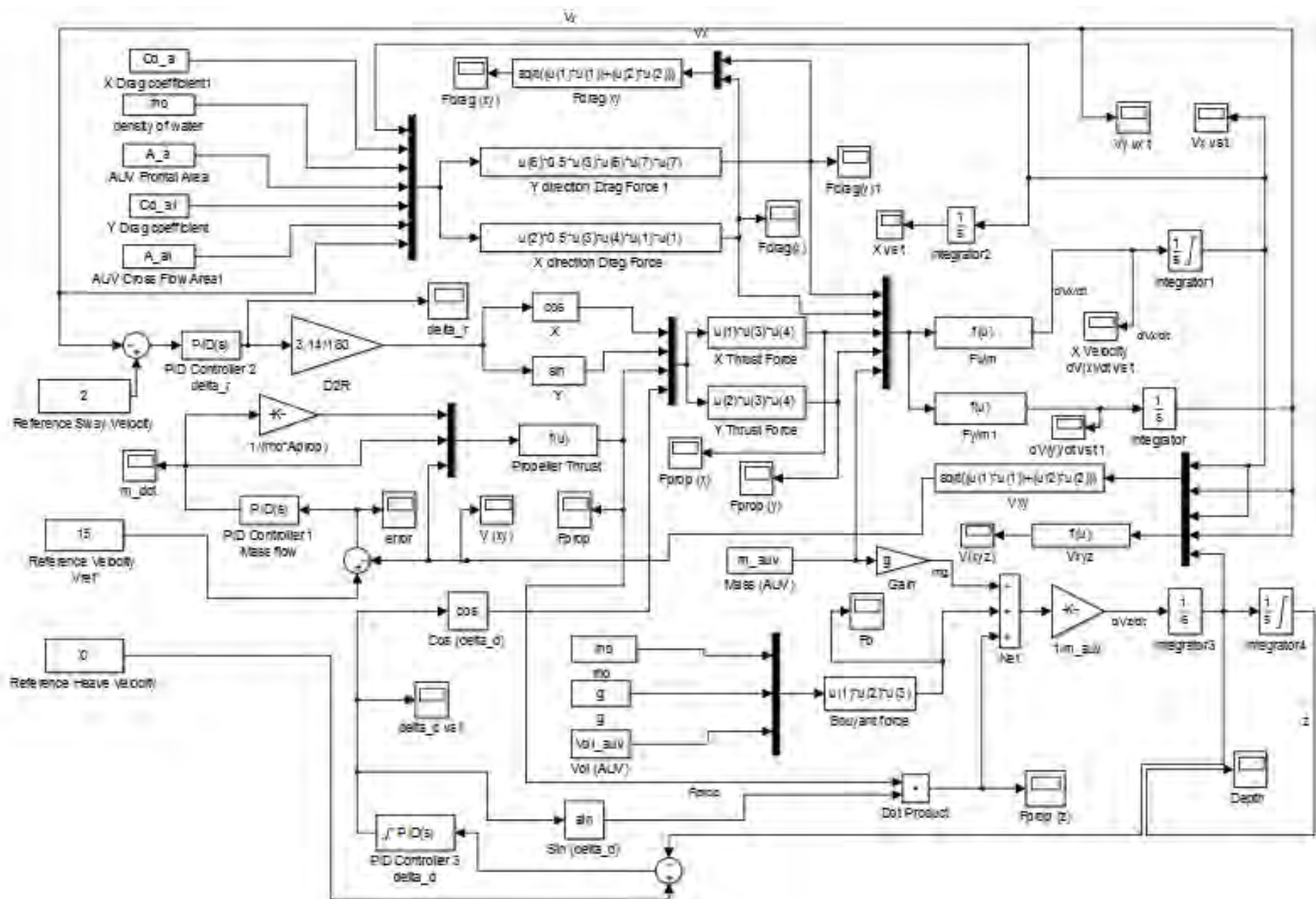
Figure 6.24: Three-dimensional AUV MATLAB Simulink model

Table 6.8: Input and output parameters for three-dimensional closed-loop AUV Simulink modelling

Inputs		Outputs	
AUV mass	m_{AUV}	Horizontal deviation angle	δ_r
Gravitational acceleration	g	Vertical deviation angle	δ_d
Propeller area	A_{prop}	Mass flow rate	$\dot{m}$
AUV frontal area	A_A	Buoyant force	F_B
AUV cross-flow area	A_{AL}	Propeller thrust force	F_{prop}
Density of water	ρ	Propeller thrust in x-direction	F_{prop_x}
Drag coefficient – Frontal	C_{D_A}	Propeller thrust in y-direction	F_{prop_y}
Drag coefficient – Cross flow	$C_{D_{AL}}$	Propeller thrust in z-direction	F_{prop_z}
Desired sway velocity	v_y	Acceleration in x-direction	dv_x/dt
Desired heave velocity	v_z	Acceleration in y-direction	dv_y/dt
Desired velocity in X-Y*	v_{xy}	Acceleration in x-y direction	dv_{xy}/dt
Volume of AUV	Vol_{AUV}	Acceleration in z-direction	dv_z/dt
		Absolute acceleration	dv_{xyz}/dt
		Net force in x-direction	F_{net_x}
		Net force in y-direction	F_{net_y}
		Net force in x-y direction	$F_{net_{xy}}$
		Net force in z-direction	F_{net_z}
		Net force	F_{net}
		Surge velocity	v_x
		Sway velocity	v_y
		Heave velocity	v_z
		Absolute velocity	v_{xyz}
		Drag force in x-direction	F_{D_x}
		Drag force in y-direction	F_{D_y}
		Drag force in x-y direction	$F_{D_{xy}}$
		Depth	Z

The inputs and outputs are summarized in Table 6.8, the main outputs are: mass flow rate control, vertical deviation angle control, horizontal deviation angle control, velocity in the x-y direction, depth control, sway velocity, and propeller thrust force. However, for the analysis of a tracking-type of system, the surge velocity, sway velocity, and depth are the essential quantities required to be observed and analyzed as transient response signals.

6.2.10   PID Controller Architecture

There are three PID controllers in the three-dimensional AUV Simulink model as illustrated in Figure 6.22. As stated previously, PID controller 1 controls the mass flow rate through the propeller, PID controller 2 controls the horizontal deviation angle, and PID controller 3 controls the vertical deviation angle. PID controller 1 measures the error of velocity in the x-y direction and adjusts the propeller speed, thus increasing the mass flow rate through the propeller. PID controller 2 measures the error of sway velocity and adjusts the horizontal deviation angle such that the AUV reaches its reference sway velocity. PID controller 3 measures the error in heave velocity and depth of the AUV, and thereafter adjusts the vertical deviation angle such that the AUV remains within 1 m from the surface of the water and the heave velocity remains zero. The parameters for PID controller 1, 2 and 3 are shown in Figure 6.25. The parameters of PID controller 1 and 2 were achieved by using the auto tuning controller function block on MATLAB, however, the parameters of PID controller 3 were set manually by an iterative process until the desired heave velocity and depth control was attained.

Controller parameters

Proportional (P):	48.37197339482
Integral (I):	98.8402313651596
Derivative (D):	0.303013779317044
Filter coefficient (N):	27.5703209092859

(a)

Controller parameters

Proportional (P):	11.1253161856707
Integral (I):	0.975904644133957
Derivative (D):	-0.312605091902132
Filter coefficient (N):	10

(b)

Controller parameters

Proportional (P):	1
Integral (I):	1
Derivative (D):	0
Filter coefficient (N):	1

(c)

Figure 6.25: AUV Simulink modelling- PID controller parameters: (a) PID controller 1, (b) PID controller 2, (c) PID controller 3

Referring to Figure 6.25, The transfer function equations for PID controller 1, 2 and 3 is given by the following equations:

$$G_1(s) = 48.37 + \frac{98.84}{s} + \frac{(0.303)(27.57)}{\left(1 + \frac{27.57}{s}\right)} \qquad (6.20)$$

$$G_2(s) = 11.125 + \frac{0.976}{s} + \frac{(-0.313)(10)}{\left(1 + \frac{10}{s}\right)} \qquad (6.21)$$

$$G_3(s) = 1 + \frac{1}{s} \qquad (6.22)$$

where $G_1(s)$ is the transfer function equation for PID controller 1, $G_2(s)$ is the transfer function equation for PID controller 2, and $G_3(s)$ is the transfer function equation for PID controller 3.

6.2.11   Deviation Angles, Depth and Velocity Responses

The horizontal deviation angle, vertical deviation angle, surge velocity, sway velocity, velocity in the x-y direction, and depth control responses for this simulation are shown below in Figure 6.26 (a), (b), (c), (d), (e) and (f) respectively. The responses are shown for the simulation run-time of 100 seconds. The desired responses in sway velocity, velocity in the x-y direction, and depth were 2 m/s, 15 m/s, and 0 to 1 m below the water surface.
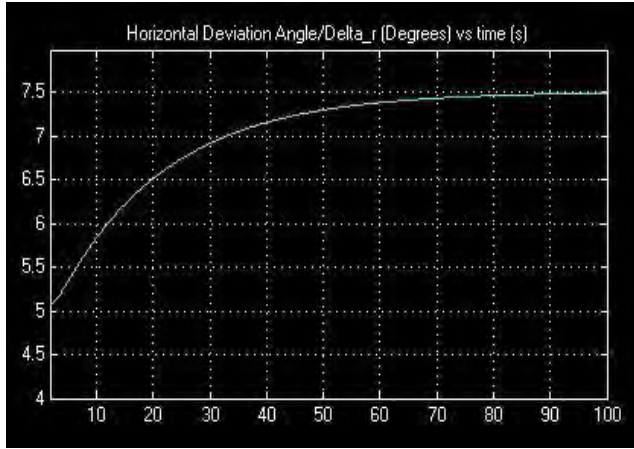
(a)
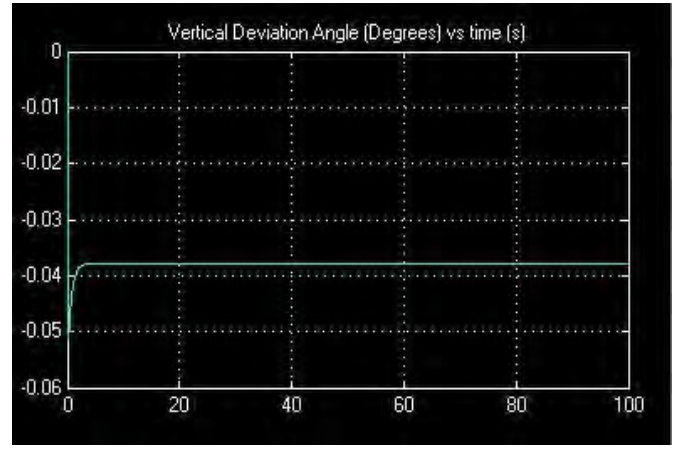
(b)
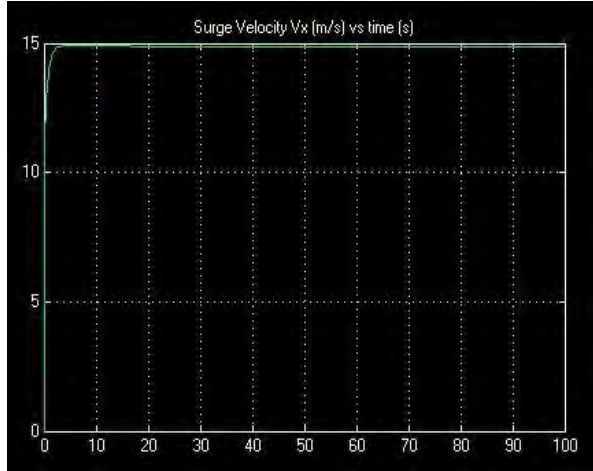
(c)
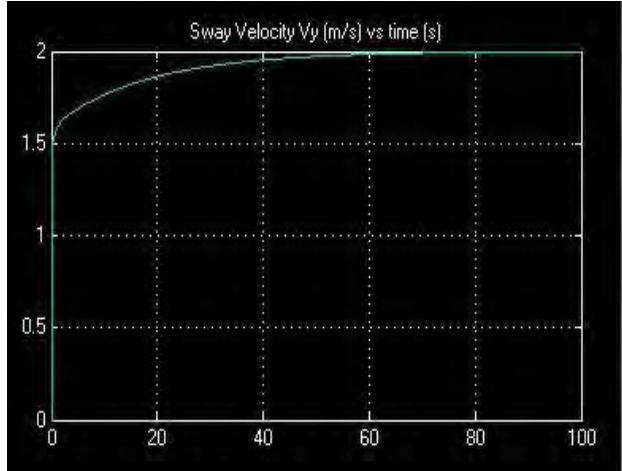
(d)
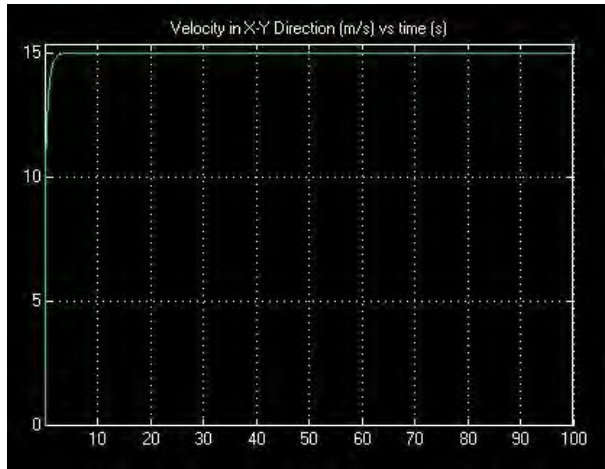
(e)
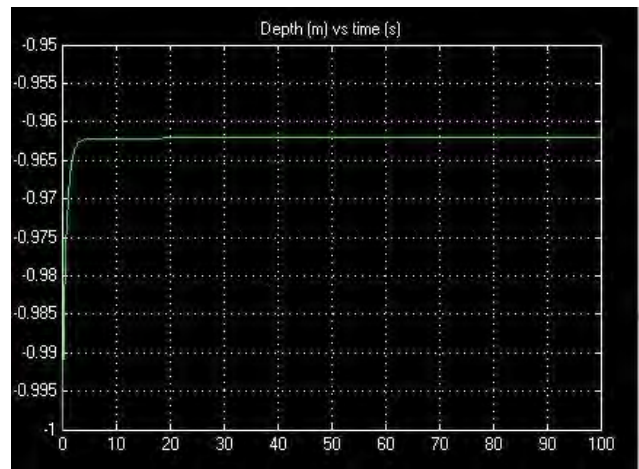
(f)

Figure 6.26: AUV Simulink modelling deviation angles, depth and velocity responses: (a) Horizontal deviation angle, (b) Vertical deviation angle, (c) Surge velocity, (d) Sway velocity, (e) Velocity in the x-y direction, (f) Depth

It is observed that the horizontal deviation angle response in Figure 6.26 (a) starts at 5 degrees and thereafter increases to 7.5 degrees in 90 seconds. The vertical deviation angle in Figure 6.26 (b) starts from 0 degrees, then at 0 seconds, moves to -0.05 degrees, thereafter increasing to -0.038 degrees within 2 seconds. The surge, sway and velocity in the x-y direction response in Figure 6.26 (c), (d) and (e) show that the reference velocities were attained without any oscillations occurring. The sway velocity reaches 2 m/s within 60 seconds, and the velocity in the x-y direction reaches 15 m/s in 2.5 seconds. The response in the horizontal deviation angle and sway velocity are directly related according to the force balance on the AUV in the y-direction, the results shown in Figure 6.26 (a) and (d) indicate that there is a slow response in the horizontal deviation angle. The desired sway velocity could be attained within a shorter time interval by tuning the PID to deliver quicker response. The depth response of the AUV is shown in Figure 6.26 (f), it is observed that the AUV reaches a steady state depth of -0.962 m, which implies that the AUV maintains a constant depth of 0.962 m below the surface of the water.

6.2.12   Mass Flow Rate, Propeller Thrust and Drag Force Responses

The mass flow rate, total propeller thrust, propeller thrust in the z-direction, and total drag force responses are shown in Figure 6.27 (a), (b), (c), and (d) below respectively. The mass flow rate is controlled by PID controller 1. The propeller thrust is the force required to overcome drag force and attain steady state motion. The propeller thrust in the z-direction is the thrust force required that allows the AUV to maintain a constant depth within 1 m from the surface of the water.

(a)

(b)

(c)

(d)
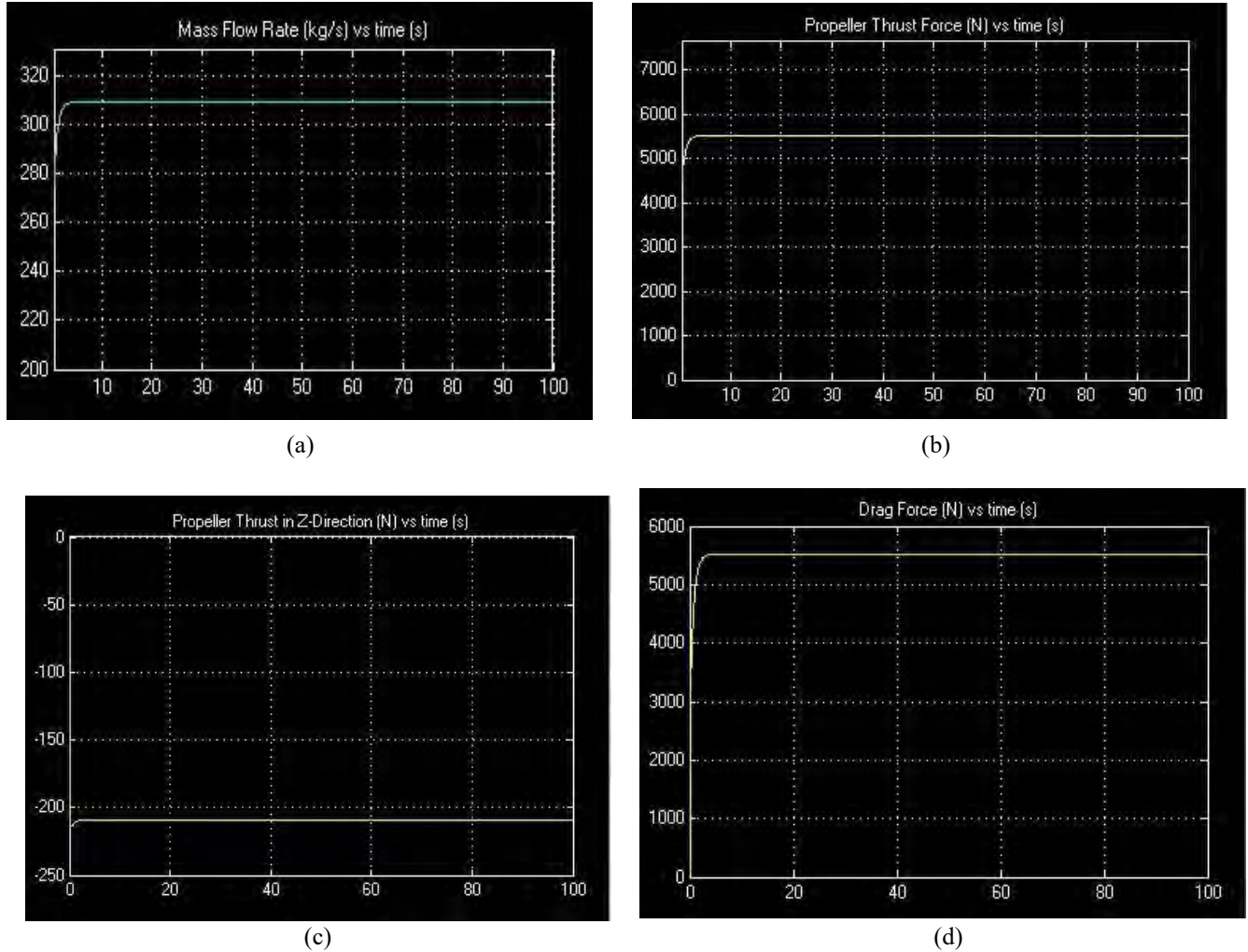
Figure 6.27: AUV Simulink modelling – mass flow rate, propeller thrust and drag force responses: (a) Mass flow rate, (b) Propeller thrust, (c) Propeller thrust in the z-direction, drag force

Referring to Figure 6.27 (a), the mass flow rate reaches a steady state value of 308 kg/s. This is the mass flow rate through the AUV propeller. The mass flow rate is dependent on the external forces acting on the AUV and the reference conditions specified. With the mass flow rate being 308 kg/s, the propeller with a diameter of 150 mm can generate a maximum thrust force of 5500 N as observed in Figure 6.27 (b). The propeller thrust is equal to the drag force of 5500 N as seen in Figure 6.27 (d), thus confirming that the system reaches steady state conditions in the x-y

direction. The propeller thrust in the z-direction is -205 N, the negative sign indicates that the propeller thrust in the z-direction acts downwards such that the AUV remains below the surface of the water.

6.2.13   Buoyancy and Weight Analysis

Buoyancy and weight analysis of an AUV is one of the most critical aspects to consider when modelling an AUV. The buoyant force and weight of the AUV model used in this simulation is shown in Figure 6.28. As described in the theory of Chapter 2, the buoyant force is dependent on the volume of the AUV and the weight is dependent on its mass. In a static situation, when the buoyant force is greater than the weight of an AUV, the AUV would float on the surface of the water. If the buoyant force is equal to the weight, then the AUV is neutrally buoyant, which implies that any external disturbance forces acting on the system would result in a change in the state of motion of the AUV which can be described by Newton's Second Law. In the case of the water jetpack powered by an AUV, it is desired that the AUV floats when the system is stationary, furthermore, it is desired that the AUV remains within 1 m below the surface of the water. These two conditions are met by modelling the AUV such that the buoyant force is slightly greater than its weight. The depth control of the AUV is achieved when the vertical deviation angle changes such that there is a component of the propeller thrust force acting on the AUV in the z-direction such that the AUV keeps a depth of under 1 m below the surface when the entire system is in motion, and the AUV floats when the system is stationary.

(a)   (b)
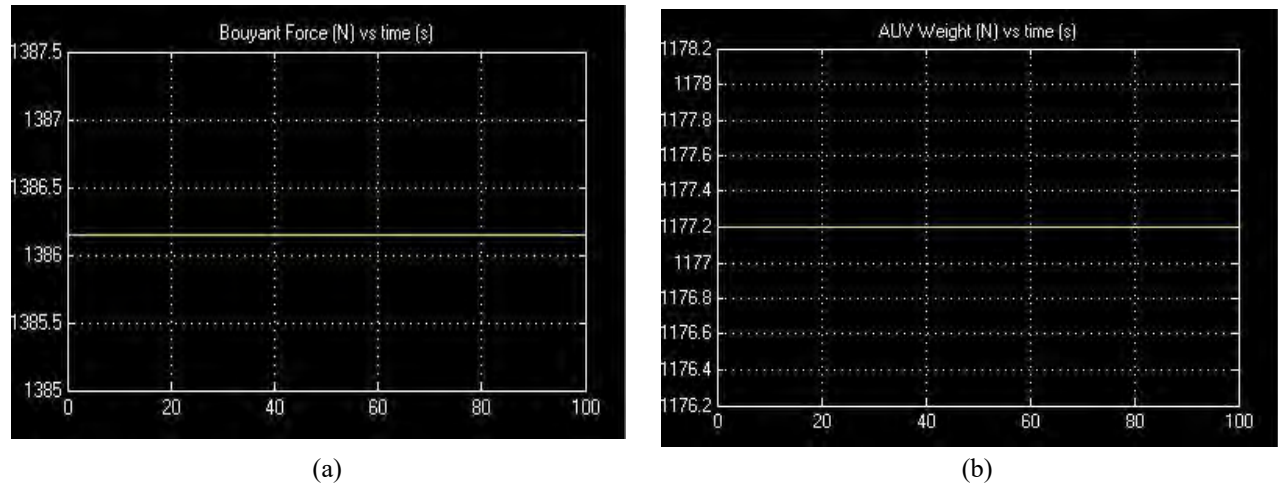
Figure 6.28: AUV buoyancy and weight analysis: (a) Buoyant force, (b) Weight

As illustrated in Figure 6.28 (a) and (b), the buoyant force is computed as 1382.15 N and the weight of the AUV is computed as 1177.2 N (see Appendix A). Therefore, the propeller thrust in the z-direction is 209 N in the downward direction, to keep the system in steady state motion. These results indicate that the geometric dimensions of the AUV and the selected mass yield a favorable combination of the buoyant force and weight of the AUV. The aim is to keep the difference between the buoyant force and weight to be small in relative comparison to the magnitude of the these forces such that the propeller thrust required is minimized, thus improving the efficiency of the propulsion system, but at the same time the difference between buoyant force and weight must be large enough such that the external

disturbance forces such as turbulence and drag force would not severely affect the state, stability and position of the AUV.

6.3   Combined System Simulink Modelling

This section details the development of a combined water jetpack and AUV system closed-loop Simulink model. The Simulink model of the combined system is based on merging the three-dimensional Simulink models that were developed for the water jetpack system and AUV in Section 6.2 and 6.3 respectively. The aim of the combined system is to allow the pilot to define three reference inputs: 1) flight altitude, 2) flight velocity (velocity in the x-y direction), and 3) induced yaw angle. The flight altitude and flight velocity are defined by the pilot or a flight controller as digital input signals, which is similar to an autopilot system in an aircraft as described in Chapter 2. As described previously, the yaw angle is induced when the pilot's CM shifts, this is created by a shift in body position.

6.3.1   Mathematical and Simulink Model

The mathematical equations that describe the combined system are given previously as Equations 6.11, 6.12, 6.13, and 6.14 for the water jetpack system, and Equation 6.17, 6.18, and 6.19 for the AUV. The fully developed closed-loop combined system Simulink model is shown in Figure 6.29. The input parameters for the combined system Simulink model used in this section are equivalent to the input parameters used for three-dimensional modelling of the water jetpack and AUV as given in Table 6.5 and 6.7 respectively. The inputs and outputs of the combined system are the same as the inputs and outputs for the three-dimensional modelling of the water jetpack and AUV as shown in Table 6.6 and 6.8. The three reference inputs are flight altitude, flight velocity, and yaw angle, these are shown as green, blue, and red blocks respectively in the Simulink model. There are five PID controllers in the system, these are shown as yellow blocks in the Simulink model. It must be noted that the two reference inputs for the AUV system segment of the combined Simulink model are: 1) water jetpack y-position, and 2) water jetpack flight velocity. In the combined system, Simulink model, the new outputs of the system are: x-position of water jetpack, y-position of water jetpack, x-position of AUV, y-position of AUV, water jetpack thrust-to-weight ratio, feed hose velocity, jet-exit velocity, head rise, pressure rise, power generated by the water jetpack propulsion system pump, power required from water jetpack propulsion system motor, power generated by the AUV propeller, and power required by the motor of the AUV propeller. The mechanical efficiency of the motors is assumed to be 80% in this analysis.
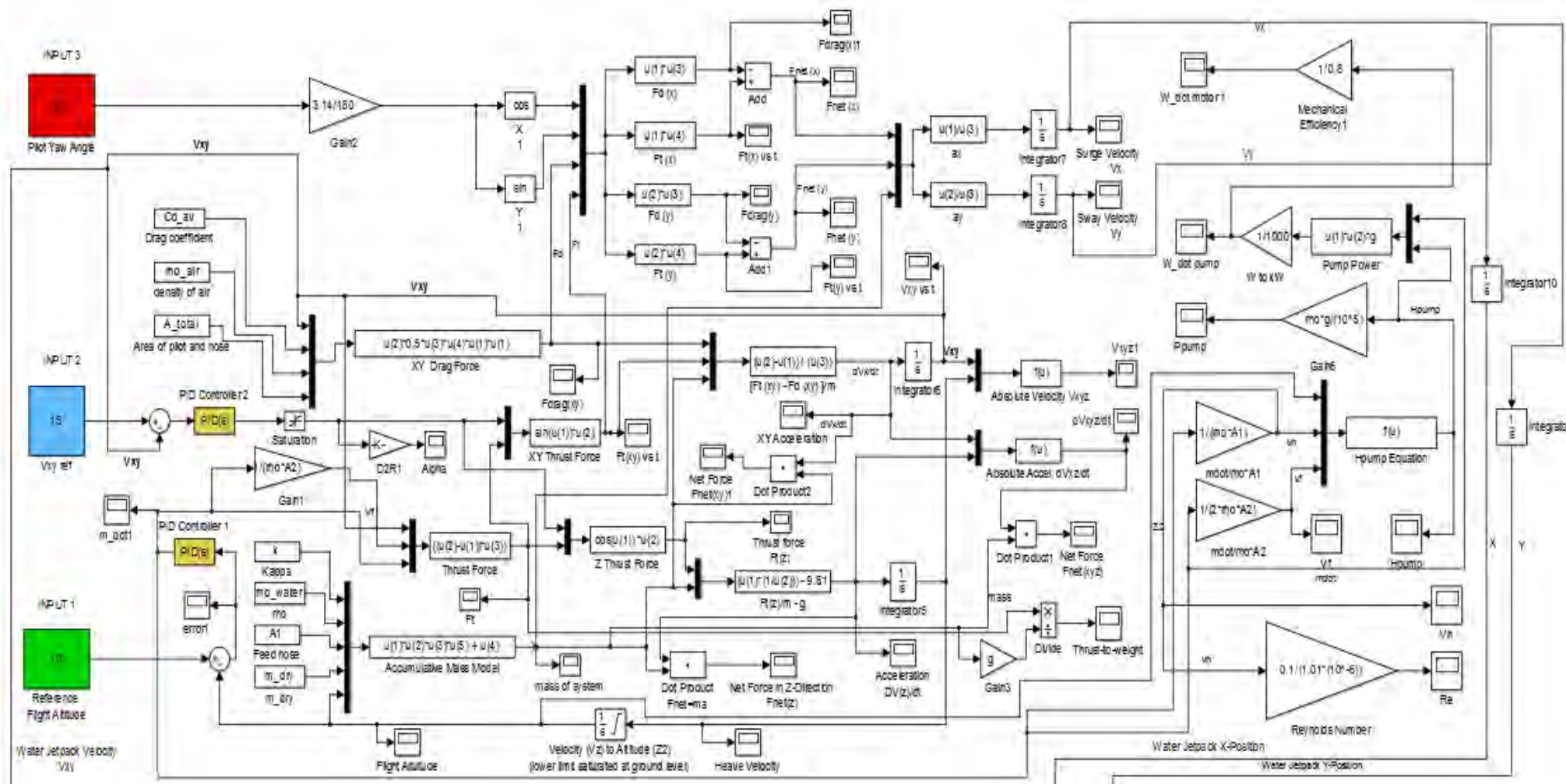
(continued on the following page)
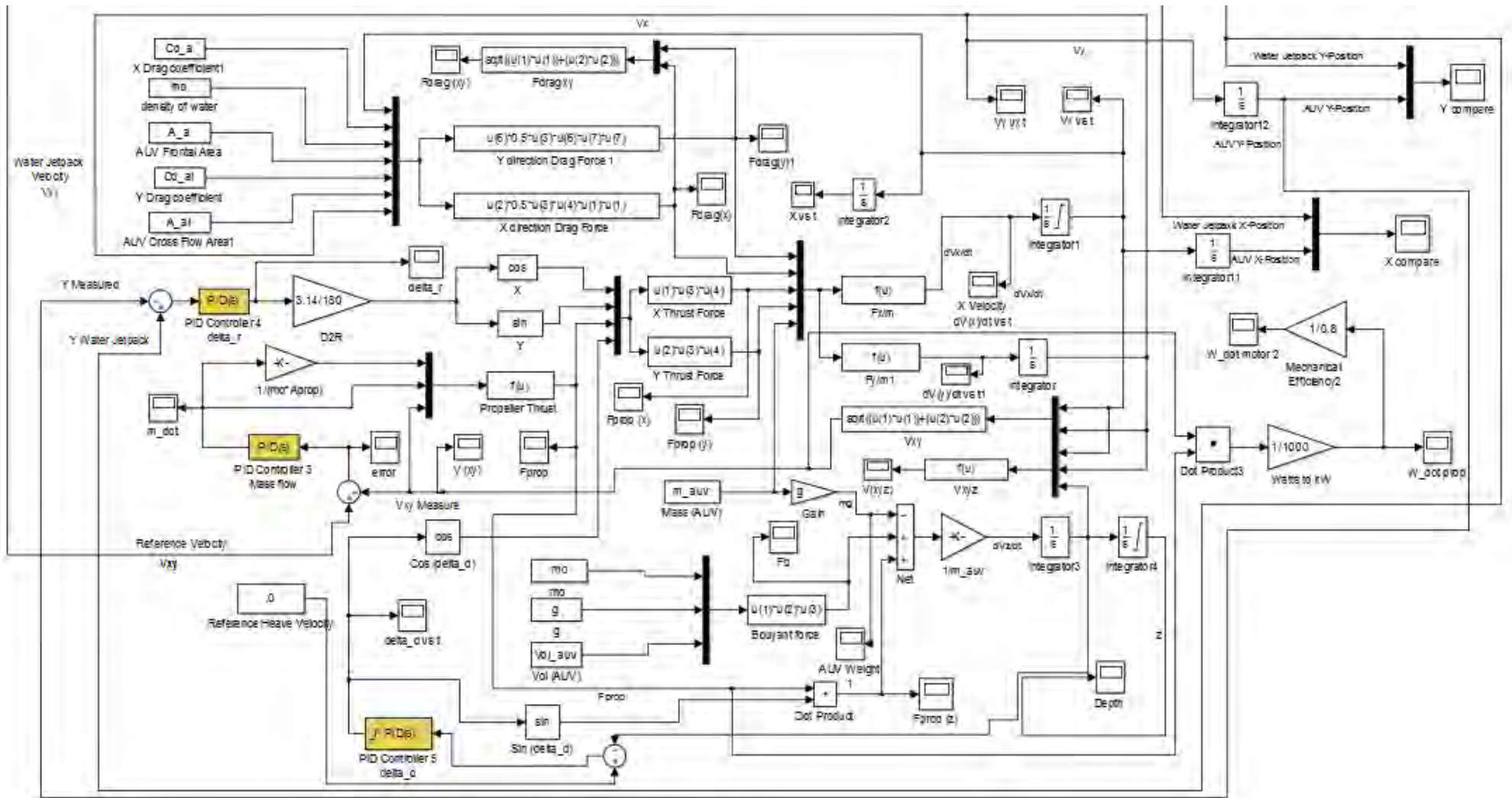
Figure 6.29: Combined system Simulink model

6.3.2 PID Controller Architecture

There are five PID controllers in the combined system Simulink model as shown in yellow in Figure 6.29. PID controller 1 controls the mass flow rate through the water jetpack system, PID controller 2 controls the thrust vector angle on the water jetpack, PID controller 3 controls the mass flow rate through the AUV propeller, PID controller 4 controls the horizontal deviation angle of the AUV thruster, and PID controller 5 controls the vertical deviation angle of the AUV thruster. The parameters for each PID controller are given previously in the three-dimensional modelling of the water jetpack and AUV system. The transfer function equations for PID controller 1, 2, 3, 4 and 5 are given by the following equations:

$$G_1(s) = 1 + \frac{2}{s} + \frac{5}{\left(1 + \frac{1}{s}\right)} \tag{6.23}$$

$$G_2(s) = 0.451 + \frac{0.04}{s} + \frac{0.5(8.32)}{\left(1 + \frac{8.32}{s}\right)} \tag{6.24}$$

$$G_1(s) = 48.372 + \frac{98.84}{s} + \frac{(0.303)(27.57)}{\left(1 + \frac{27.57}{s}\right)} \tag{6.25}$$

$$G_2(s) = 11.125 + \frac{0.976}{s} + \frac{(-0.313)(10)}{\left(1 + \frac{10}{s}\right)} \tag{6.26}$$

$$G_3(s) = 1 + \frac{1}{s} \tag{6.27}$$

where $G_1(s), G_2(s), G_3(s), G_4(s)$ and $G_5(s)$ is the transfer function equation for PID controller 1, 2, 3, 4 and 5 respectively.

6.3.3 Combined Subsystem Simulink Model Implementation

The full scale combined system Simulink model is given by Figure 6.29. MATLAB Simulink has a useful function for simplifying complex Simulink models, this function is called 'create subsystem from selection'. The subsystem Simulink model of the combined system is shown in Figure 6.30. The subsystem of the combined system is created by forming subsystems of the three-dimensional water jetpack Simulink model (shown to the left) and for the three-dimensional AUV Simulink model (shown to the right), and thereafter defining the inputs and outputs for the water jetpack subsystem and AUV subsystem.

There are three reference inputs in the water jetpack subsystem: 1) reference flight altitude, 2) reference flight velocity, and 3) yaw angle, these are shown by the green, blue, and red blocks respectively. These are the inputs that the pilot

would define. As shown in Figure 6.28, there are multiple outputs in the water jetpack and AUV section of the combined system. However, when creating the subsystem Simulink model, MATLAB allows for user defined input and output subsystem parameters. It is therefore possible to define the main outputs of interest for the analysis of the combined subsystem Simulink model as illustrated in Figure 2.30. The outputs selected for the water jetpack subsystem in numerical order shown from top to bottom are:1) y-position,2) x-position, 3) flight velocity, 4) surge velocity, 5) sway velocity, 6) flight altitude, 7) power generated by pump, 8) mass flow rate through system, 9) thrust vector angle, and 10) thrust-to-weight ratio.

Referring to the AUV subsystem block shown to the right, there are three reference inputs: 1) water jetpack y-position, 2) water jetpack x-position, and 3) water jetpack flight velocity. These inputs are required to enable the AUV to follow the path of the water jetpack system and allow for autonomous tracking of the system. The outputs of the AUV subsystem are: 1) y-position, 2) x-position, 3) surge velocity, 4) sway velocity, 5) depth control, 6) propeller power, 7) propeller mass flow rate, 8) horizontal deviation angle, and 9) vertical deviation angle.

There are scopes at each output for both the water jetpack subsystem and AUV subsystem. There are also four scopes that display the position and velocity of the water jetpack and AUV in the x- and y-direction on a single scope, this is used for comparison and path tracking observation. Although there is a total of 19 outputs as shown in the subsystem Simulink model of the combined system, the remaining outputs such as drag force, thrust force, net force, mass, acceleration in all three directions are still accessible in the subsystem model. The full scale combined system Simulink model can be opened by double clicking on the subsystem blocks. For reference purposes, the remaining results and observations as shown in the full scale combined system Simulink model for the simulations contained in this section are available in Appendix A.
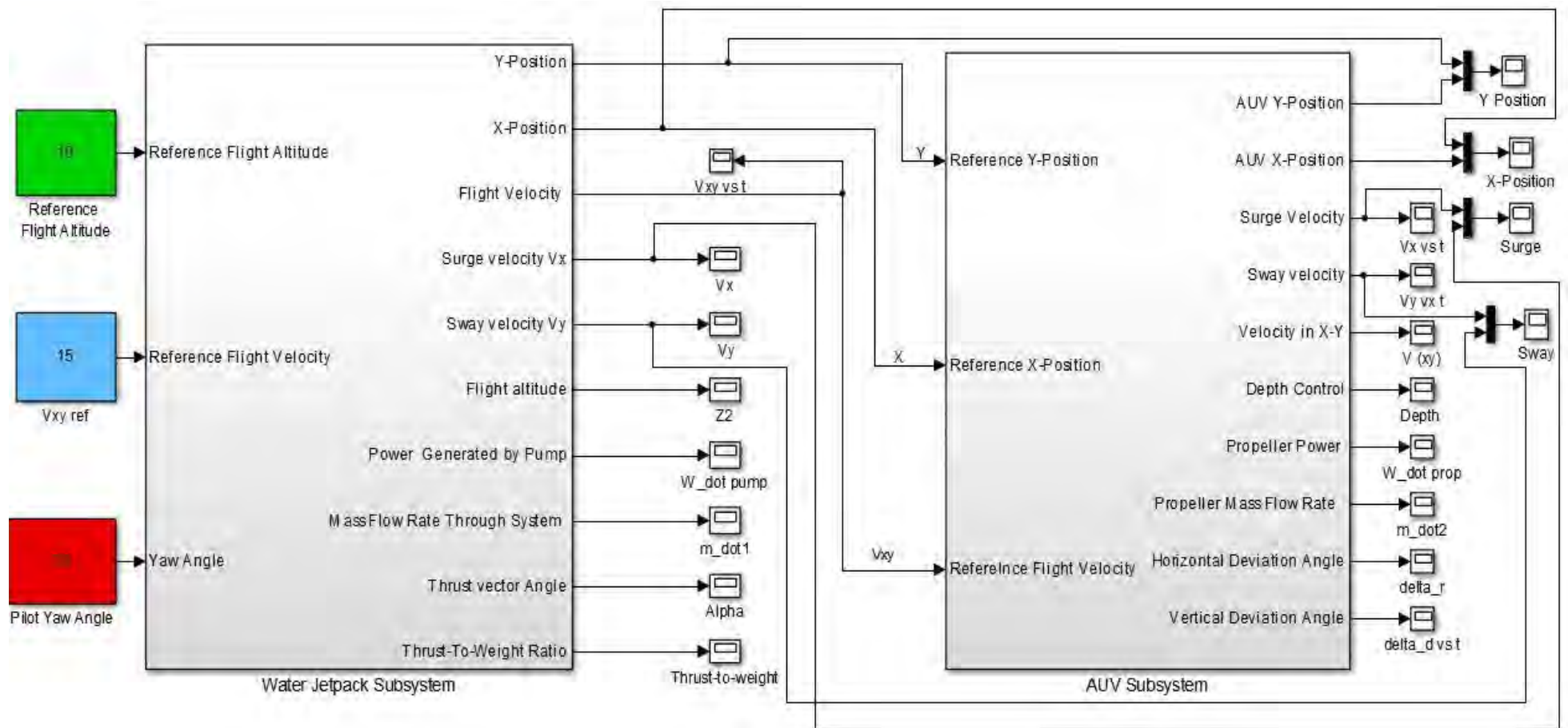
Figure 6.30: Combined subsystem Simulink Model

6.3.4   Steady State Static Hovering Simulation

In this section, the combined system is simulated to model static conditions at fixed flight altitude as conducted in the initial optimization process for the water jetpack system that was employed in Chapter 5. It is useful to determine and compare the performance of the water jetpack and AUV system under steady state static hovering conditions using Simulink since the transient analysis of the system can be observed.

6.3.4.1   Reference Inputs and Objectives

In this section, the system reference inputs for the combined subsystem Simulink model shown in Figure 6.30 are as follows:

- Reference flight altitude (green block): 10 m.
- Reference flight velocity (blue block): 0 m/s.
- Yaw angle (red block): 0 degrees.

The objectives of this simulation are as follows:

- Observe the steady state mass flow rate, pump power, thrust-to-weight ratio, and flight altitude response for the water jetpack system.
- Compare the transient output responses of the water jetpack system with the non-transient responses obtained in Chapter 5.
- Verify that the x-position, y-position, surge velocity, sway velocity, and thrust vector angle for the water jetpack system are zero.
- Verify that all outputs for the AUV system are zero.
- Observe the depth control response of the AUV and ensure that the AUV floats as discussed in Section 6.3.

6.3.4.2   Water Jetpack Mass Flow Rate, Flow Velocity and Reynolds Number Response

The response of mass flow rate, feed hose velocity, jet-exit velocity, and Reynolds number for the water jetpack propulsion system responses are shown in Figure 6.31. It is essential to compare these responses with the responses obtained in Chapter 5.
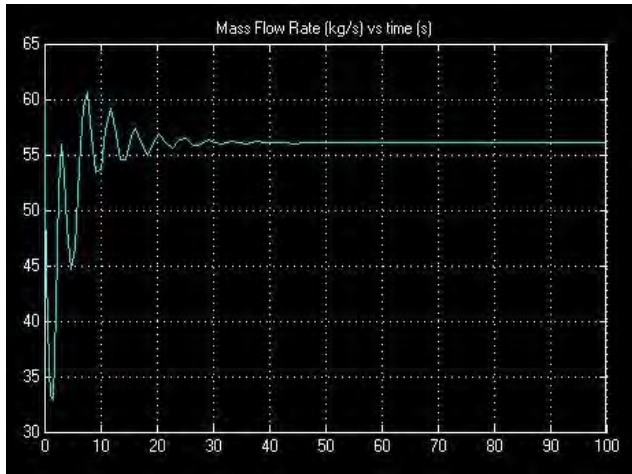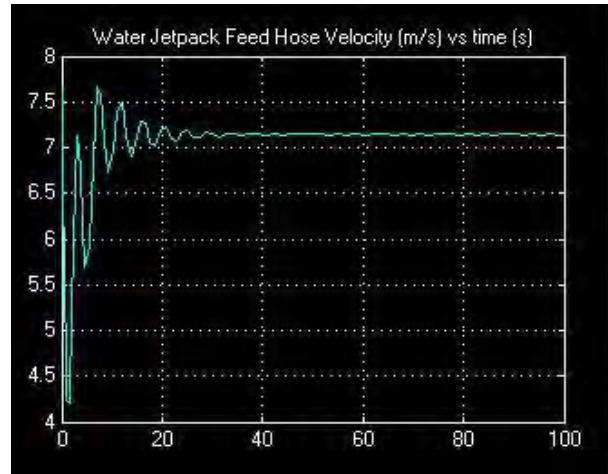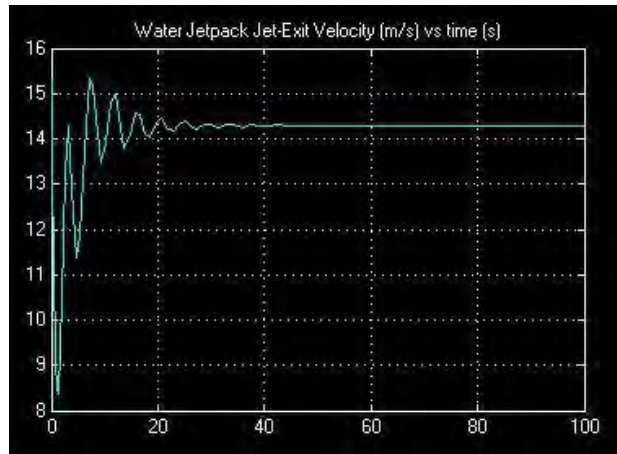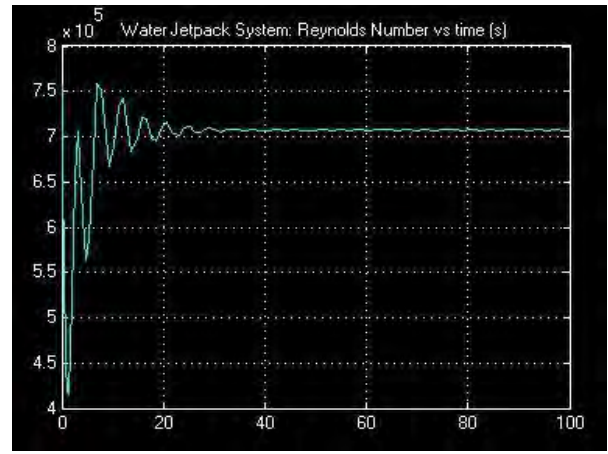
Figure 6.31: Water jetpack static simulation response: (a) Mass flow rate, (b) Feed hose velocity, (c) Jet-exit velocity, and (d) Reynolds number

Referring to Figure 6.31 (a), the mass flow rate response shows that the peak mass flow rate is 60.5 kg/s, the settling time is 30 seconds and the steady state mass flow rate is 56.1 kg/s. The feed hose velocity response in Figure 6.31 (b) is the velocity of water flowing in the feed hose; it is observed that the steady state feed hose velocity is 7.1 m/s with settling time 40 seconds. The jet-exit velocity response in Figure 6.31 (c) is the velocity of the water jet exiting the nozzles of the water jetpack; it is observed that the steady state jet-exit velocity is 14.2 m/s with settling of 40 seconds. The Reynolds number in Figure 6.31 (d) is computed using the feed hose velocity in Figure 6.31 (b); it is observed that the steady state Reynolds number is 7.1×10^5. The responses shown in Figure 6.31 are within proximity to the responses obtained in Chapter 5.

175

6.3.4.3 Water Jetpack Pump Power, Pressure and Head Rise Response

The water jetpack propulsion system responses of power, pressure and head are shown in Figure 6.32. These responses are computed using the Bernoulli equation across the water jetpack propulsion system. The friction factor and feed hose length are 0.02 m and 15 m respectively as used in Chapter 5. The remaining parameters are the same as those used in previous simulations.

(a)   (b)

(c)   (d)
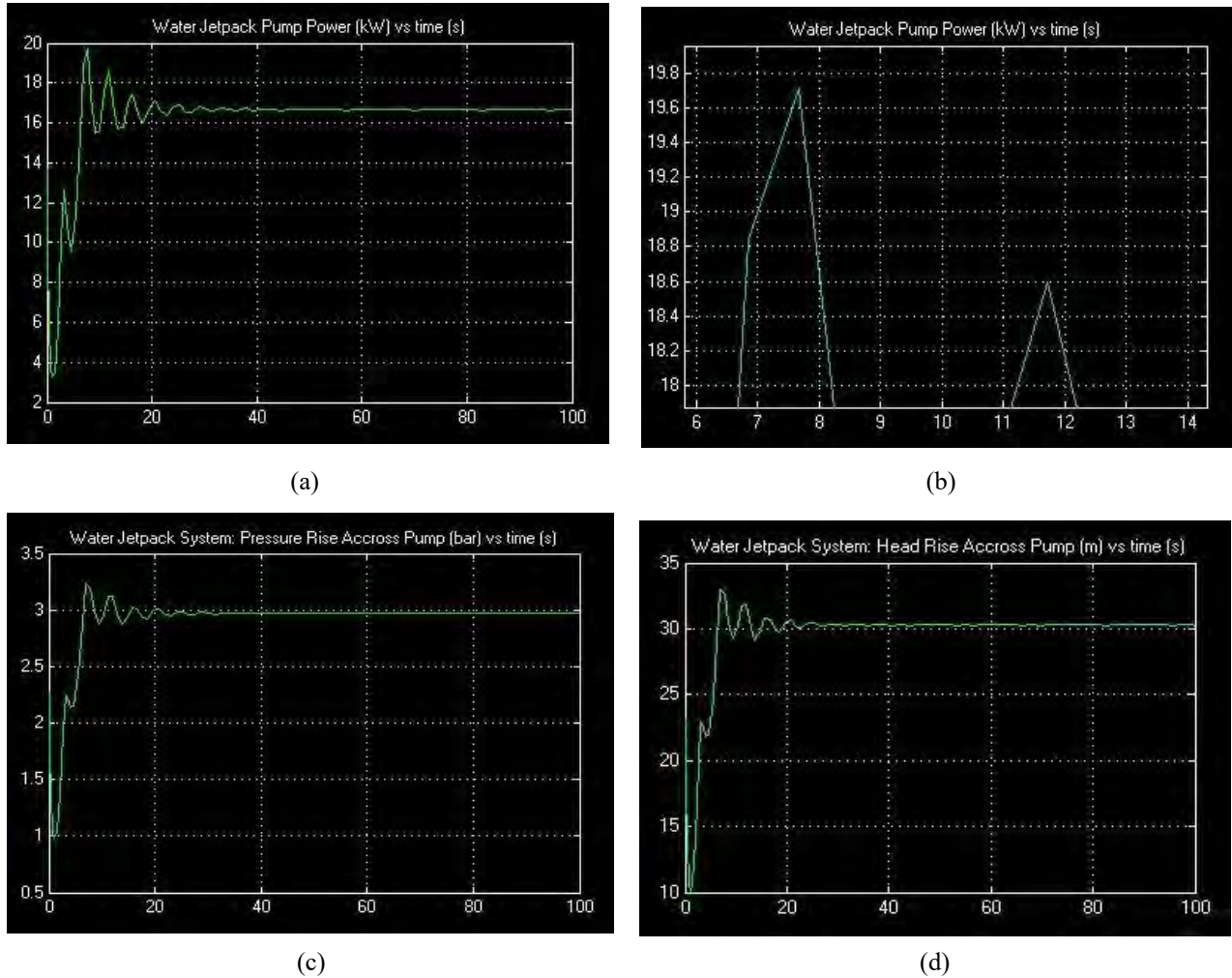
Figure 6.32: Water jetpack static simulation response: (a) Pump power, (b) Pump peak power, (c) Pressure rise across pump, and (d) Head rise across pump

Referring to Figure 6.32 (a), the pump power required at steady state conditions is 16.5 kW. The power response is oscillatory for the first 30 seconds and the settling time is 40 seconds. The peak pump power response is shown in Figure 6.32 (b); it is observed that the peak power is 19.7 kW which is reached at 7.7 seconds. The second peak pump power occurs at 11.8 seconds with a magnitude of 18.6 kW.

6.3.4.4   Water Jetpack Thrust-to-Weight Ratio

The thrust-to-weight ratio is defined as the ratio of instantaneous thrust by the instantaneous mass of the system. The thrust-to-weight response for the water jetpack system is shown below in Figure 6.33. At steady state conditions, the thrust-to-weight ratio is always equal to one. This implies that the net force acting on the system is zero and the system is in steady state.

| (a) | (b) |
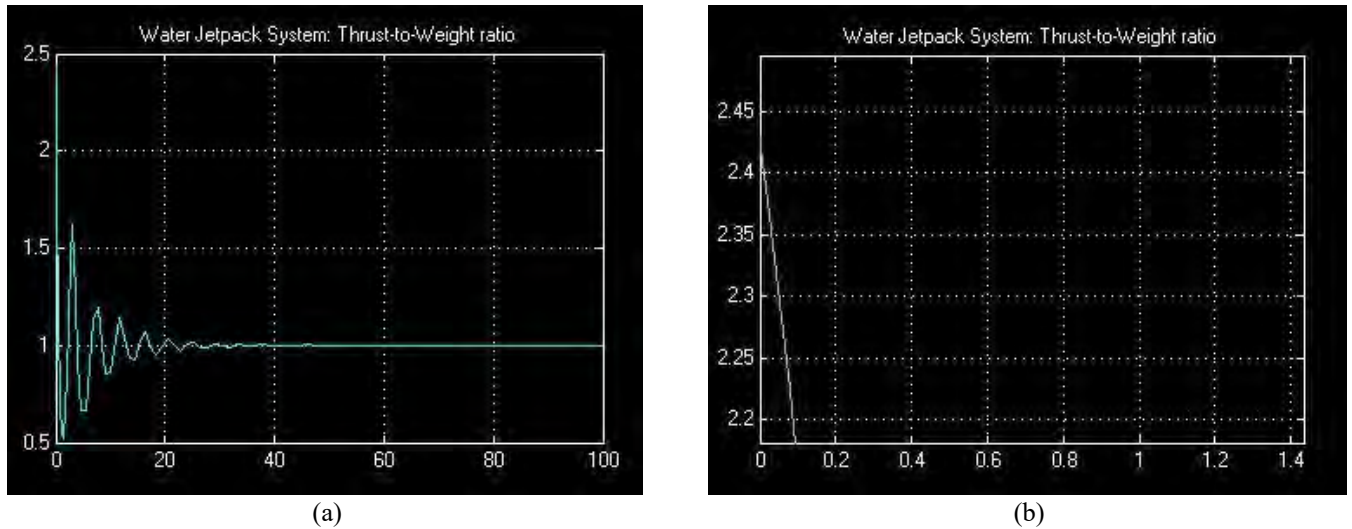
Figure 6.33: Water jetpack thrust-to-weight ratio: (a) Thrust-to-weight ratio, (b) Peak thrust-to-weight ratio

It is observed in Figure 6.33 (a) that the thrust-to-weight ratio is a maximum at take-off, this defines the performance specification for the water jetpack system. The exact value of the peak thrust-to-weight ratio can be seen in Figure 6.33 (b) as approximately 2.43. The thrust-to-weight ratio oscillates and decays over 30 seconds until the system reaches steady state.

6.3.4.5 Combined System Position and Velocity

The position and velocity response of the combined system is shown below in Figure 3.34 which shows the flight altitude of the water jetpack, depth of the AUV, surge and sway velocity of the combined system.

(a)   (b)

(c)   (d)
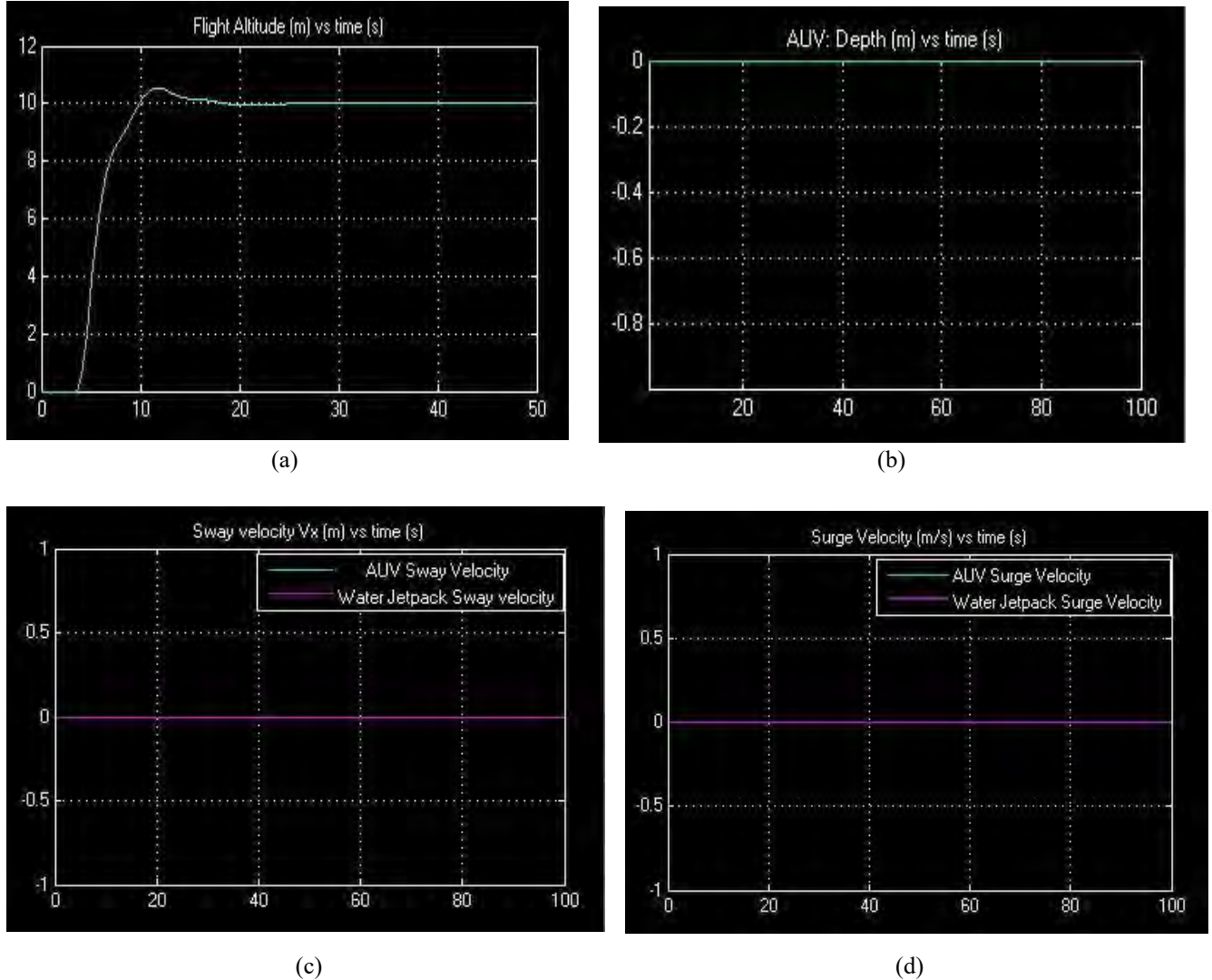
Figure 6.34: Combined system position and velocity response: (a) Flight altitude, (b) AUV depth, (c) Sway velocity, and (d) surge velocity

The flight altitude response in Figure 6.34 (a) is identical to the closed-loop two-dimensional response obtained previously which has a peak overshoot of 5% and settling time of 20 seconds. Figure 6.34 (b) shows the depth of the AUV, it is observed that the AUV depth is zero throughout the simulation run-time, this confirms that the depth control condition for the AUV is met for the case of static hovering. Figure 6.34 (c) and (d) show the sway and surge velocity response of the water jetpack and AUV, it is observed that the surge and sway velocity of both the water jetpack and AUV are zero which confirms that the system functions according to the specified reference inputs defined by the pilot.

6.3.5 Combined System Tracking and Speed Control

In this section, a simulation of the combined system is conducted to observe and verify the position and velocity of the water jetpack and AUV. The outcome of this simulation verifies the ultimate objective of all the MATLAB Simulink modelling and simulation contained in this chapter. As previously stated, the ultimate objective is to allow the pilot to define three reference inputs: 1) flight altitude, 2) flight velocity, and 3) yaw angle, such that the combined system achieves the desired flight conditions with the use of the PID controller which was detailed previously.

6.3.5.1 Reference Inputs and Objectives

In this section, the system reference inputs for the combined subsystem Simulink model shown in Figure 6.29 are as follows:

- Reference flight altitude (green block): 10 m.
- Reference flight velocity (blue block): 15 m/s.
- Yaw angle (red block): 20 degrees.

The flight altitude is 10 m which is the standard maximum flight altitude for all water jetpacks that are commercially available. The maximum safe reference flight velocity that the system is modelled for is 15 m/s (or 54 km/h). This is the forward flight velocity that the pilot would move at, the commercially available water jetpacks such as Jetlev-Flyer (2016) specify that the maximum cruise speed is 47 km/h (13.06 m/s), this is to ensure safety of the pilot and control of the system. However, in this simulation and the development of the combined system model, a maximum cruise speed of 15 m/s will be used as the specification speed and for the development of the water jetpack system. This can be implemented by saturating the upper limit of the PID controller that controls mass flow rate in the water jetpack system such that the net flight velocity does not exceed 15 m/s. The extra 2 m/s in flight speed specification accounts for added effects of drag force on the system or any external disturbances that may affect the net flight speed of the system. The yaw angle is 20 degrees in this simulation, which allows for a component of the water jet thrust force to act in the y-direction, as detailed earlier.

The objectives of this simulation are follows:

- Observe the response of position and velocity of the water jetpack and AUV to verify that tracking and speed control is achieved.
- Observe position and velocity response lag between the water jetpack and AUV such that an optimal feed hose length is suggested.
- Determine the peak thrust-to-weight ratio, mass flow rate, and pump power output of the water jetpack system.
- Determine the peak mass flow rate and power output of the AUV propeller.
- Verify the depth control specification of the AUV as being within a meter below the surface of the water.

6.3.5.2 Position and Velocity

The x- and y-position and velocity responses for water jetpack and AUV are shown below in Figure 6.35. As shown in the combined subsystem Simulink model in Figure 6.29, the output x-position, y-position, and flight velocity of the water jetpack subsystem are the inputs to the AUV subsystem. Therefore, the AUV is modelled and designed to follow the exact GPS coordinates of the water jetpack.
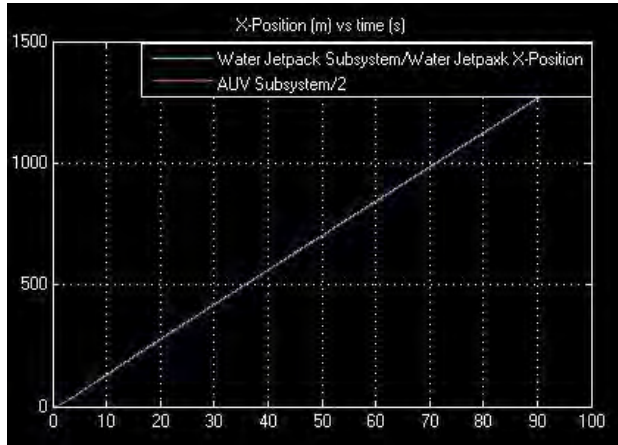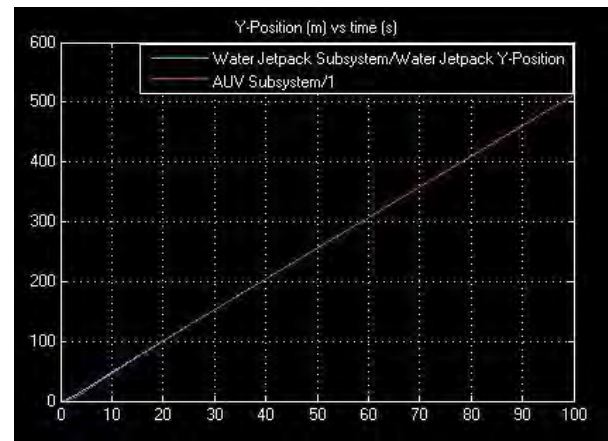
(a)   (b)
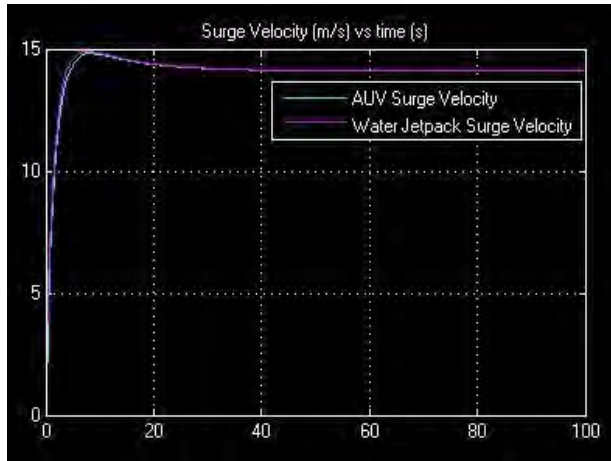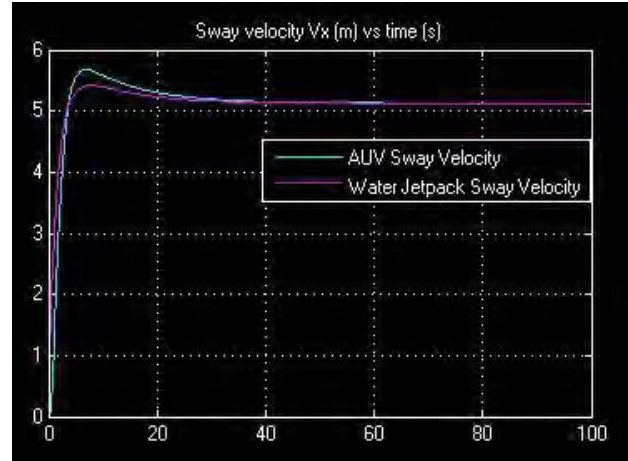
(c)   (d)

Figure 6.35: Combined system position and velocity response: (a) X-position, (b) Y-position, (c) Surge velocity, and (d) Sway Velocity

Referring to Figure 6.35 (a) and (b), it is observed that the x- and y-position for the AUV (shown in purple) is closely equal to the x- and y-position of the water jetpack (shown in blue). This shows that the AUV tracks the water jetpack. The surge and sway velocity response in Figure 6.35 (c) and (d) also confirm that the AUV tracks the water jetpack, it is observed in (c) that both the water jetpack and AUV reach peak surge velocity of 15 m/s at 4 seconds and reach steady state surge velocity of 14 m/s with settling time of 30 seconds. It is observed in Figure 6.35 (d) that the peak

sway velocity of the AUV is slightly higher than the peak sway velocity of the water jetpack, the steady state sway velocity of 5.1 m/s is reached with settling time of 40 seconds.

6.3.5.3   Position and Velocity Lag

The responses shown in Figure 6.34 confirm that the combined system functions according to specification, however, due to the physical nature of the two subsystems, there exists slight lag in the x- and y-position and velocity responses for the AUV as it follows the water jetpack, this is shown in Figure 6.36.

(a)

(b)

(c)

(d)
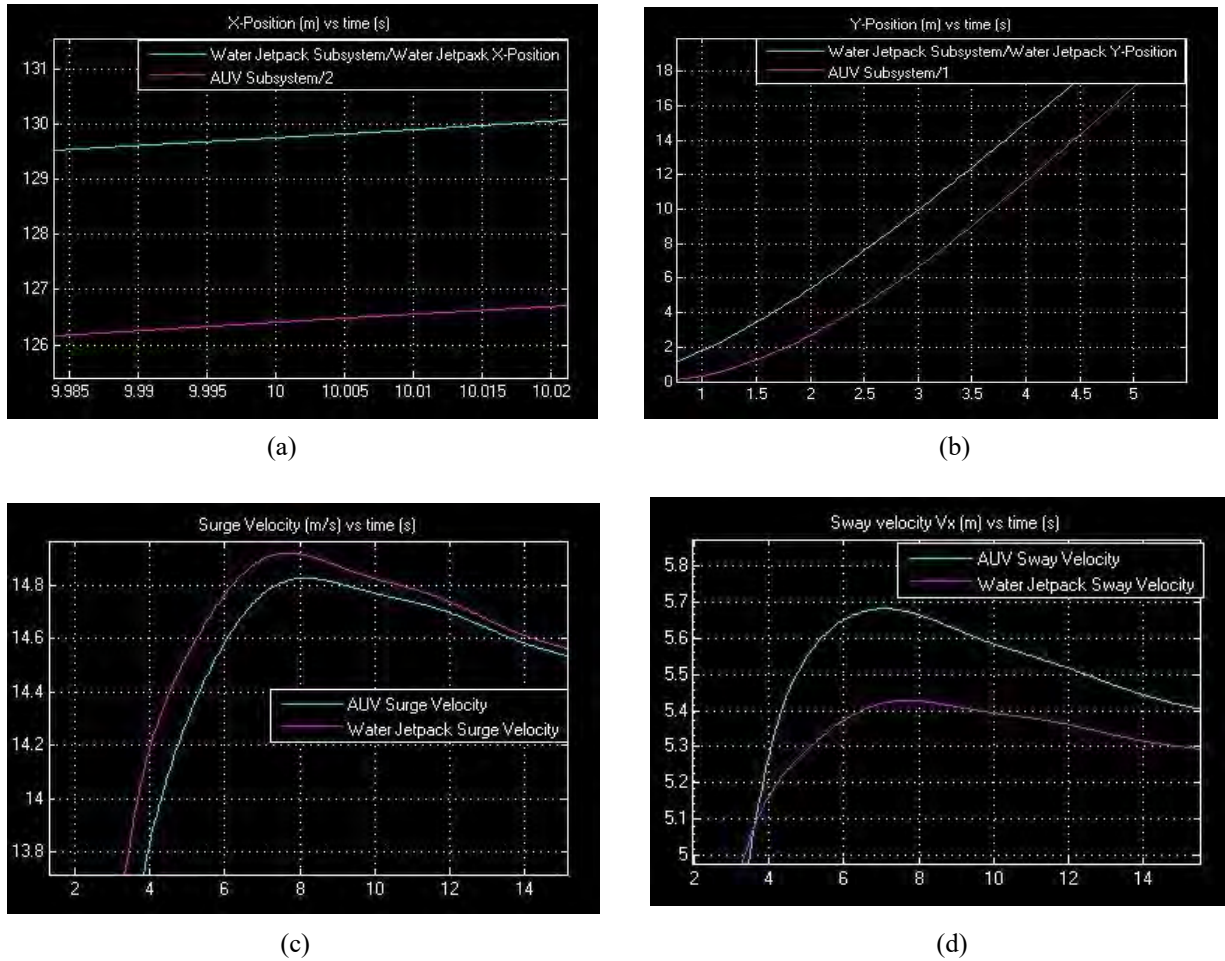
Figure 6.36: Combined system position and velocity lag: (a) X-position lag, (b) Y-position lag, (c) Surge velocity lag, and (d) Sway velocity lag

It can be observed in Figure 6.36 (a) that there is a mean lag of 3.2 m at 10 seconds in the x-position. The y-position lag in Figure 6.36 (b) shows that there is a mean lag of 3.5 m at 3 seconds between the water jetpack and AUV. However, both the lag in the x- and y-position of the water jetpack and AUV converges as the system approaches steady state as illustrated in Figure 6.35. Figure 6.36 (c) and (d) show the lag in surge and sway velocity that occur at the peak velocity of each system. Referring to the surge velocity lag in Figure 6.36 (c), the maximum lag in surge

velocity is 0.2 m/s which occurs at 6 seconds. The sway velocity lag in Figure 6.36 (d) shows that the maximum lag in sway velocity is 0.28 m/s at 7 seconds. The cause of lag is due to the response time of the PID controllers in the system, and the difference in external conditions of the water jetpack and AUV. The water jetpack moves in air, which has a lower density than water. The AUV moves in water, which has a much greater density than air, and therefore there is greater drag force acting on the AUV than the water jetpack. The position and velocity lag between the AUV and water jetpack depicted in Figure 6.35 show that there is a maximum lag of 3.5 m between these two subsystems, peak lag in the x-position occurs at a different time instant than the peak lag in the y-position which is favorable since the total x-y distance between the water jetpack and AUV would be limited to 3.5 m. The feed hose length selected and used in the analysis of optimization of the system in Chapter 5 is justified by the lag responses shown in Figure 6.35. A total length of 15 m ensures that the water jetpack can reach the peak flight altitude of 10 m and the extra 5 m of length in the feed hose compensates for position lag between the water jetpack and AUV. This ensures that the system can operate according to the theoretical Simulink modelling developed in this chapter.

6.3.5.4　Water Jetpack Thrust-to-Weight Ratio, Mass Flow Rate and Pump Power

It is useful to determine the peak thrust-to-weight ratio, mass flow rate, and pump power of the water jetpack system when simulating the system under maximum flight conditions. These responses are illustrated in Figure 6.37.
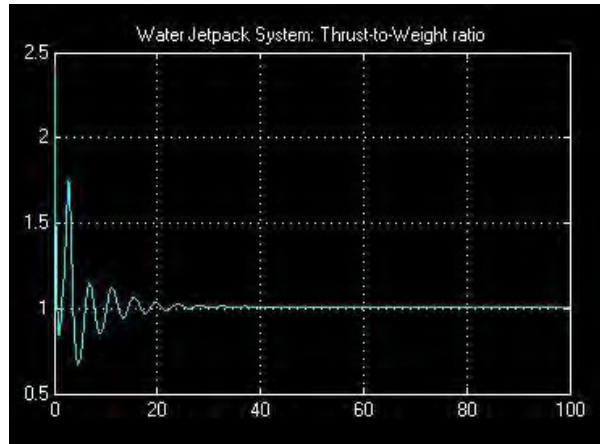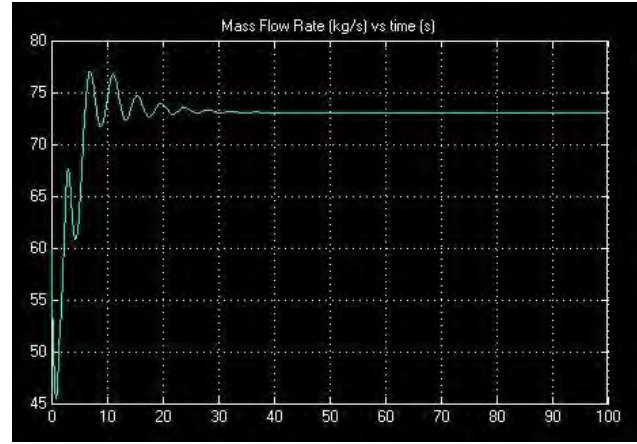
(a)   (b)
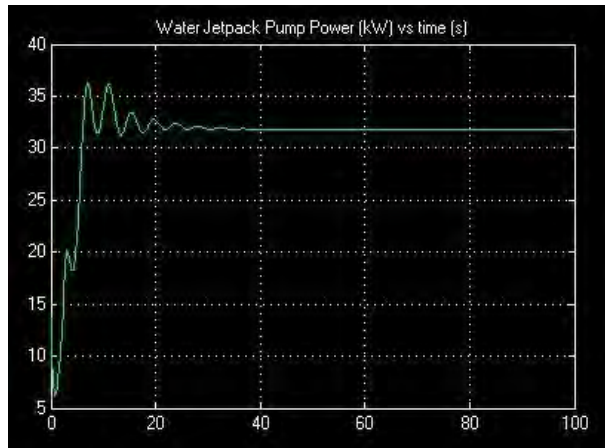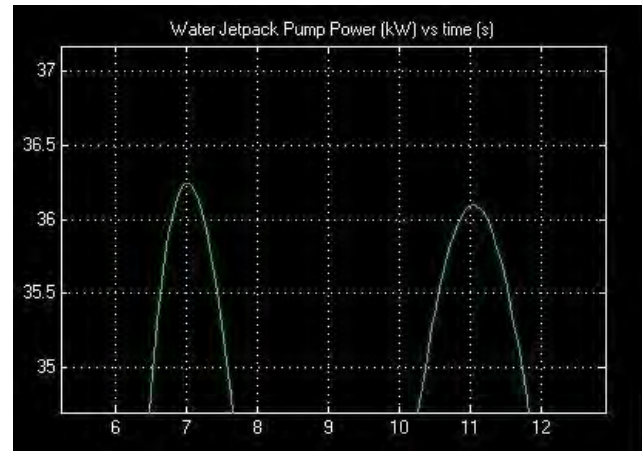
(c)   (d)

Figure 6.37: Water jetpack responses: (a) Thrust-to-weight ratio, (b) Mass flow rate, (c) Pump power, and (d) Peak pump power

It can be observed in Figure 6.37 (a) that the peak thrust-to-weight ratio of the water jetpack system is 2.43 as observed in the previous simulation. The mass flow rate response in Figure 6.37 (b) oscillates up to 30 seconds before reaching steady state mass flow rate of 73 kg/s. The peak mass flow rate is observed as 77 kg/s at 7 seconds and 11 seconds. Figure 6.37 (c) shows the pump power for the water jetpack system which reaches a steady state value of 32 kW with settling time of 38 seconds. The peak power is seen in Figure 6.37 (d) as 36.2 kW which occurs at 7 seconds. These results are necessary for sizing and selecting the actual supply system for the water jetpack system.

To achieve tracking control of the AUV, it is necessary to determine the power and mass flow rate specification of the propeller system. Figure 6.38 shows the mass flow rate and propeller power developed by the AUV.
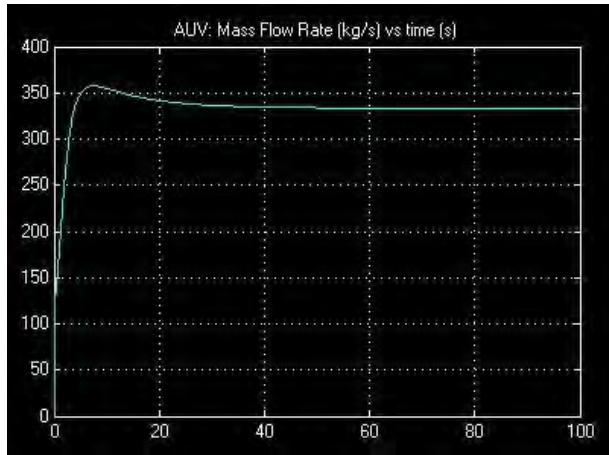
(a)
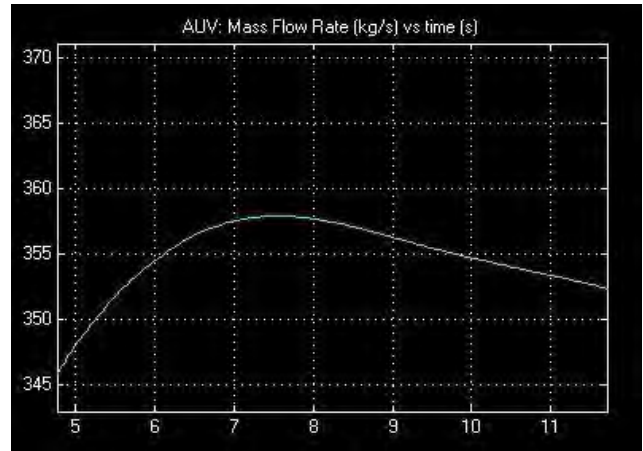
(b)
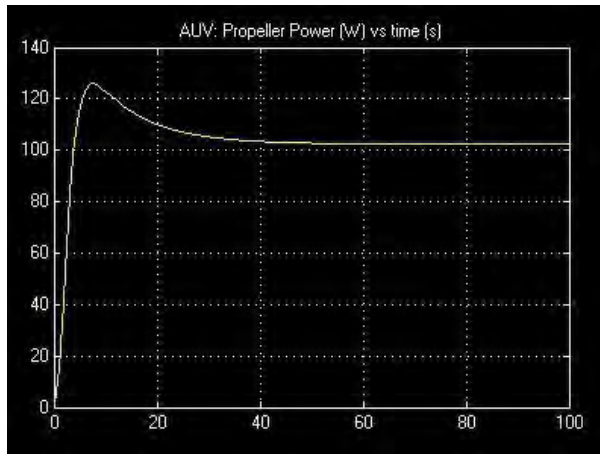
(c)
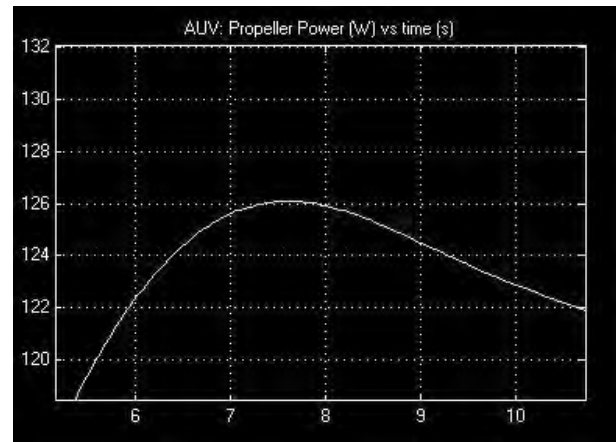
(d)

Figure 6.38: AUV responses: (a) Mass flow rate through propeller, (b) Peak mass flow rate through propeller, (c) Propeller power, and (d) Peak propeller power

Referring to Figure 6.38 (a), the mass flow rate through the propeller rises and reaches a peak value of 357.5 kg/s as illustrated in Figure 6.38 (b), the steady state mass flow rate through the propeller is 335 kg/s which is reached in 45 seconds. The propeller power in Figure 6.38 (c) reaches a peak of 126 kW at 7.5 seconds and thereafter descends to a steady state value of 102 kW in 45 seconds. These results are necessary to size and select the actual power supply system that meets these specifications.

6.3.5.5   AUV Depth Control

The objective for the three-dimensional AUV thruster is to allow the AUV to float when the water jetpack is stationary in air, and to travel within a meter from the surface of the water when the water jetpack has a non-zero flight velocity. In the static hovering simulation presented earlier, it was established that the AUV floats when the system is stationary. Figure 6.39 below shows the resulting depth control and vertical deviation angle of the AUV for this simulation.

(a)   (b)
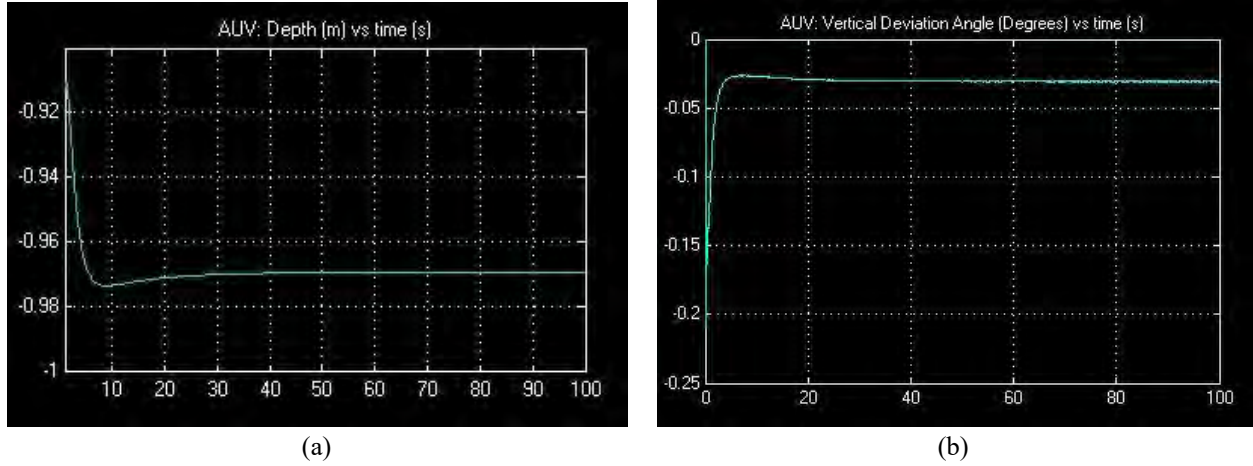
Figure 6.39: AUV depth control response: (a) Depth, (b) Vertical deviation angle

It is observed from Figure 6.39 (a) that the AUV reaches a steady state depth of -0.97 m in 30 seconds. This implies that the AUV tracks the water jetpack while maintaining a steady state depth of 0.97 m below the surface of the water. The vertical deviation angle response by the thruster of the AUV is shown in Figure 6.39 (b); it is observed that the vertical deviation starts from 0 degrees, then reaches -0.2 degrees, and thereafter reaches a steady state position of -0.035 degrees. This implies that the thruster's vertical deviation angle is 0.035 degrees in a direction such that there is a net downward thrust force acting on the AUV in the z-direction such that the depth response in Figure 6.39 (a) is attained. This confirms that the AUV functions as specified.

CHAPTER 7 : SYSTEM DESIGN PROPOSAL AND COMPUTATIONAL SIMULATION

7.1 Overview

This chapter details the development of a computational model for the water jetpack and AUV system together with conducting analysis from CFD simulation and FEA of the water jetpack wye propulsion system and AUV hull structure in the combined system. The main objective of this chapter is to obtain an initial virtual model of the system which can form the baseline model for future analysis and design optimization. In this chapter, the wye propulsion system and AUV hull computational model is developed using SolidWorks. The CFD simulation of the wye propulsion system was conducted using the computational package Star CCM. The FEA simulations for the wye propulsion system and AUV hull was conducted using SolidWorks Simulation. The outcome of this chapter forms the first phase for the full scale combined system development, the development of the complete system is beyond the scope of this current study, however, an insight into this development is provided.

7.2 Water Jetpack System Model

7.2.1 Propulsion System Performance

A full performance analysis of the water jetpack propulsion system is required prior to the development of a computational model of the system. An initial development of the propulsion system optimization process is described in Chapter 5. Steady state and transient analysis of the system is detailed in Chapter 6. Table 7.1 summarizes the key performance parameters and the magnitude observed from Simulink simulations in Chapter 6 for steady state, peak conditions, along with the nominal/specification value.

Table 7.1: Water jetpack propulsion system performance specifications

Parameter	Units	Static and Steady State	Peak Value	Specification
Jet-exit diameter	m	0.05	0.05	0.05
Feed hose diameter	m	0.1	0.1	0.1
Flight velocity	m/s	0	16	15
Mass flow rate	kg/s	56.1	77	73
Flight altitude	m	10	11	10
Pump power	kW	19.7	36.3	32
Flow rate	m/s	56.1	77	73
Thrust-to-weight ratio	-	1	2.43	2.43

Referring to Table 7.1, the main performance parameters of the water jetpack propulsion system is shown in the left column, the magnitude of each performance parameter along with its respective units are shown. The static and steady state condition values are computed for the case of static hovering, the peak conditions are computed as the absolute maximum values in the transient response of each parameter, and the specification values describe the performance of the water jetpack system under peak steady state conditions, whereby the water jetpack and AUV travel at maximum flight altitude at the maximum allowable flight velocity.

7.2.2   Wye System Model

The wye system is the component in which flow enters through the feed hose, splits into two identical flow paths, and exits the system through a set of convergent nozzles. This component serves as the critical structure in the water jetpack propulsion system.

The factors to consider when implementing a wye system are described as follows:
- Fluid flow performance
- Ease of manufacture
- Accuracy of achieving a symmetrical structure
- Convergence and divergence of flow
- Structural rigidity and robustness

To achieve an ideal model of a wye system, the first condition would be to model the dimensions of the propulsion tubing such that in this location the fluid flow performance is optimized. There is always a loss of energy in flow when fluid flow enters a path of expansion or contraction. In Chapter 5, it was established that the feed hose diameter used throughout the analysis in this study is 100 mm and the jet-exit diameter is 50 mm. Furthermore, the optimization process was based on the relative performance of the propulsion system and the effects of pressure loss within the wye system were unknown.

In this section, a model of the wye system as shown in Figure 7.1 is suggested for future development with consideration of the pressure losses in the system. However, an alternate model, as shown in Figure 7.2, is introduced and used for comparison with the suggested model. The comparison involves two CFD simulations of the flow through the wye system under static steady state and transient steady state conditions using the flow parameters shown in Table 7.1.
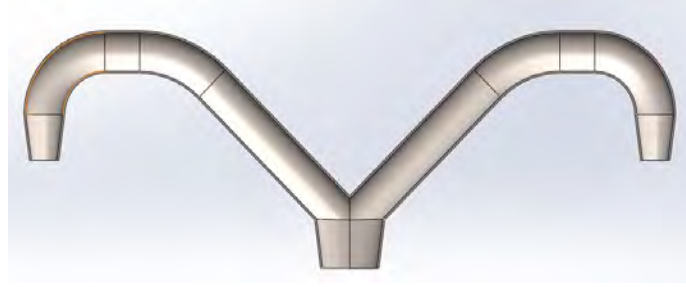
(a)
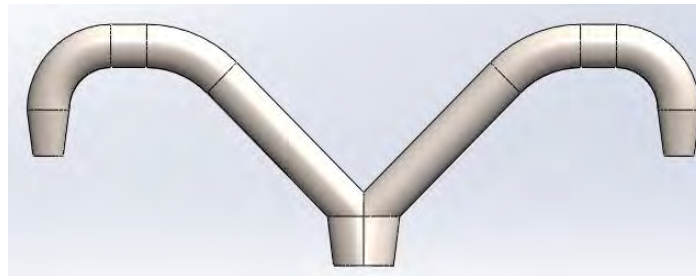
(b)

Figure 7.1: Wye system CAD model (a) Front-view, (b) Sectional Front-view

Figure 7.2: Wye system alternate model

Referring to Figure 7.1 (a), the inlet section of the wye system consists of a circular-to-ellipsoid shaped duct. The diameter of the circle at the inlet is 100 mm and the ellipsoid has minimum and maximum dimensions of 70 mm and 120 mm respectively. The inlet section is followed by a symmetrical set of 70 mm diameter tubes that are initially angled at 45 degrees followed by zero-degree path and thereafter a 90-degree bend before entering the converging nozzles. The straight path section prior to the 90-degree bend would consist of a frictional swivel coupling that allows the 90-degree bend together with the nozzle to rotate freely, this coupling is commercially available from local suppliers and a model of this component is not incorporated in the wye system illustrated in this study. However, it will be assumed that the nozzles can free rotate such that thrust vectoring is achieved within specified limits as modelled and described in Chapter 6. The converging nozzles used in this model consist of a diameter reduction of 70 mm at inlet to 50 mm at outlet (refer to Appendix D for a detailed drawing on the wye model in Figure 7.1). Figure 7.2 shows a computer-aided design (CAD) model of the alternate wye system. The inlet section consists of a circular-to-circular converging nozzle with a diameter of 100 m to 80 mm. The inlet converging nozzle is followed by a

symmetrical set of 80 mm diameter tubing rolled to a radius of 300 mm which is followed by a straight path (which would include a swivel coupling) which is then followed by a 90-degree bend and a converging nozzle (refer to Appendix D for detailed drawings for the alternate wye system).

7.2.3 Computational Fluid Dynamics Simulation

The velocity and pressure distribution in the wye system in Figures 7.1 and 7.2 was shown and analyzed using the computational fluid package, Star CCM+. This is an essential step as part of the optimization of the CAD model for the wye system. CAD models of the wye system were developed using SolidWorks and imported as a solid body into Star CCM+ in 'iges' file format.

7.2.3.1 Meshed Models

The first step performed on Star CCM+ was the development of a volume mesh model of the wye systems. The meshed models, as shown in Figure 7.3 were developed using polyhedral cells which capture the fluid flow characteristics with the minimum number of cells, thus reducing the computational cost and processing requirements.

Figure 7.3: Mesh model of main wye system

The base size of 0.007 m was used with five prism layers to capture the highest accuracy of the flow with minimum computational cost. The surface remesher tool was selected, this further refines the meshed model.

7.2.3.2 Boundary Conditions and Physics Model

The boundary conditions used in the CFD simulation for both wye systems are listed below:
- Inlet: Mass flow, with a specified value of 56.1 kg/s and 73 kg/s for conditions 1 and 2 as specified previously.
- Outlet: Pressure outlet, with atmospheric pressure.
- Walls: No slip wall.

The physics models that were specified for the CFD analysis are listed below:

- Steady state flow with constant mass flow rate throughout the wye system.
- Turbulent flow with the selected of k-epsilon turbulence model to accurately capture flow vorticity and recirculation.
- Constant density of water.
- Three-dimensional analysis.
- Segregated flow solver, which enables Star CCM+ to solve the specified fluid flow problem by modelling time and space independently.

7.2.3.3   CFD Simulation 1: Velocity and Pressure Analysis

The velocity distribution of fluid flow was observed on Star CCM+ by setting up a scalar scene and selecting velocity as the scalar function. The velocity distribution of fluid flow in the main and alternate wye system for the first CFD simulation is shown in Figure 7.4 (a) and (b) respectively. The inlet mass flow rate for this simulation set was 56.1 kg/s.
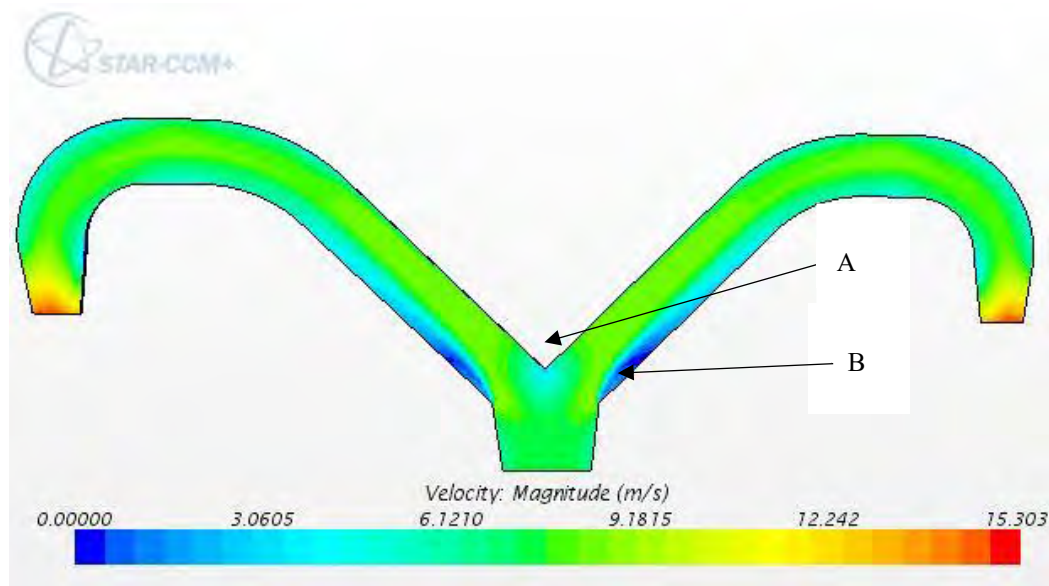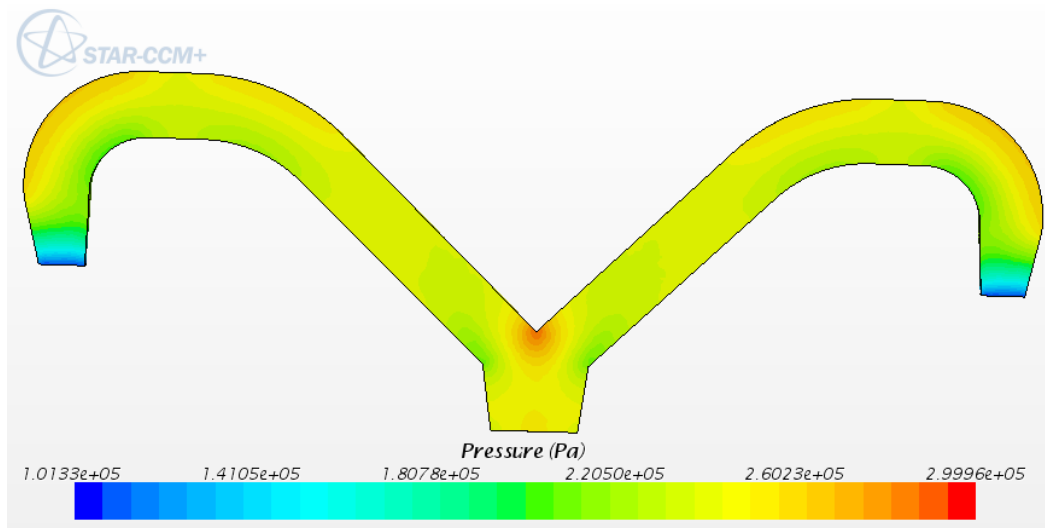

(a)
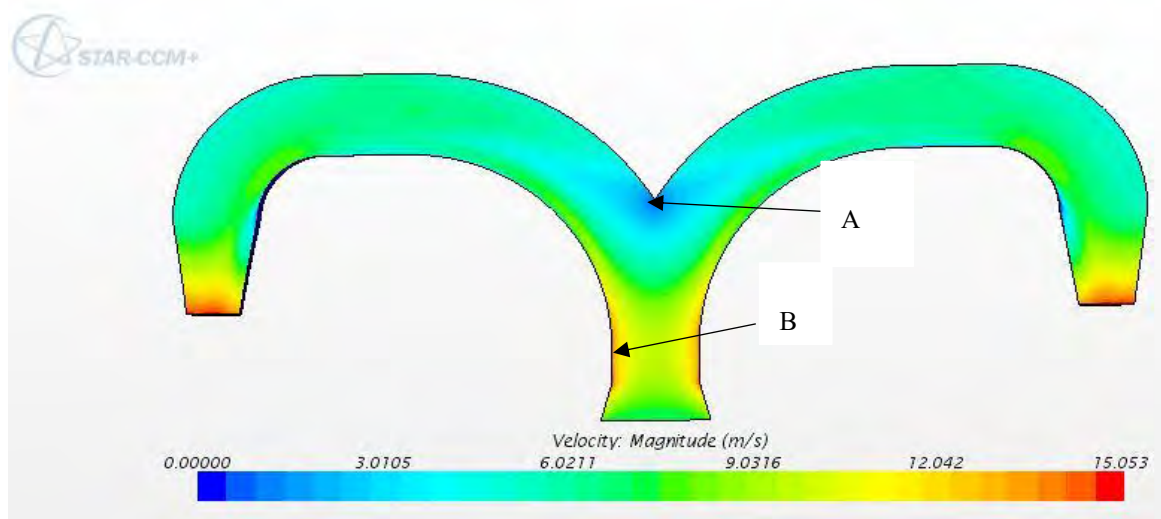
(b)

Figure 7.4: CFD simulation 1- velocity distribution: (a) Main model, (b) Alternate model

Referring to Figure 7.4 (a), it is observed that the average velocity in the main wye system is between 6.1210 m/s and 9.1815 m/s. The maximum velocity in (a) is 15.3032 m/s which is the velocity of the flow at the nozzle exit points. The mean color shown in the distribution remains nearly constant along the centerline of the wye system which indicates that the velocity is near constant. However, it is noted that there three zones shown in blue and denoted by A and B, these indicate zones where there is stagnation of fluid flow and recirculation is present.

In Figure 7.4 (a), there is a region of high pressure, labelled as A, which is discussed below. Stagnation zone labelled B is larger than the stagnation zone located at A. Recirculation occurs at B due to a change in flow direction along the 45-degree bend.

In Figure 7.4 (b), it is observed that there is an acceleration of flow along the inlet converging nozzle section. This is caused by the net decrease in flow area. Thereafter there is a decrease in fluid flow velocity as the flow splits in the main 90-degree bend. The region of high fluid flow velocity at the inlet section is labelled by B, the sudden acceleration and deceleration within the entrance section of the wye system is an undesirable result as there is a greater loss of pressure and energy of fluid flow. There is a large region of stagnation labelled by A, this indicates that there is significant pressure of the fluid flow at this region, which results in significant stress on the wye system at the point where the flow splits.

The pressure distribution for the main and alternate wye system is illustrated in Figure 7.5 (a) and (b) respectively:
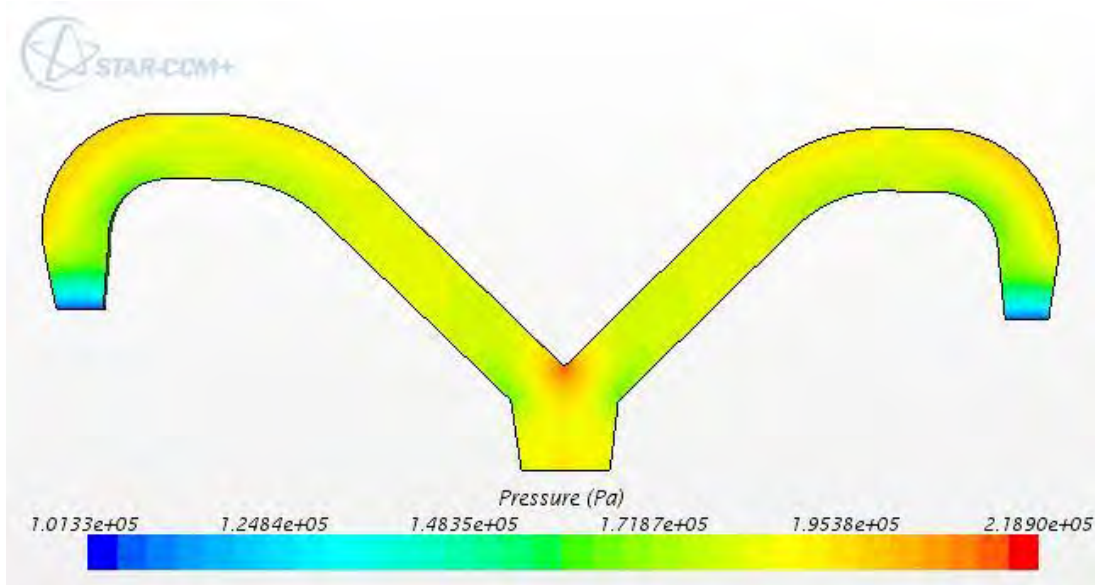
(a)
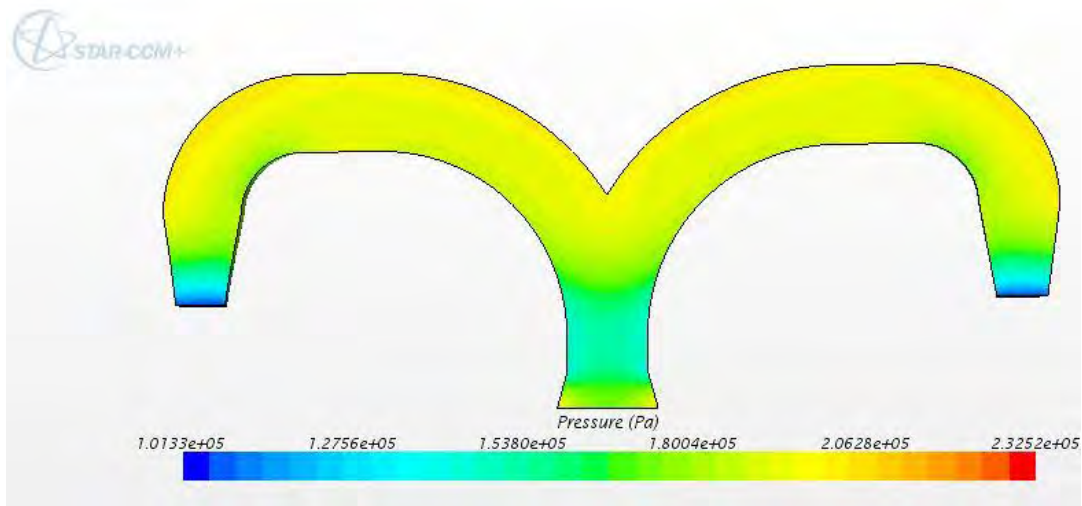
(b)

Figure 7.5: CFD simulation 1- pressure distribution: (a) Main model, (b) Alternate model

Referring to Figure 7.5 (a), the mean pressure in the wye system is between 1.7181 bar and 1.9538 bar. The maximum pressure occurs at the region where the flow splits, the magnitude of the maximum pressure is 2.1890 bar. In Figure 7.5 (b), there is a region of low pressure at the inlet section. The magnitude of the pressure along the inlet section is approximately 1.5380 bar. The maximum pressure in the wye system in Figure 7.5 (b) is 2.3252 bar, which is greater than the maximum pressure observed in Figure 7.5 (a). The pressure difference along the inlet section of the alternate wye system in Figure 7.5 (b) is an undesirable effect as this results in loss of energy and pressure of the flow. It is noted that the pressure fluctuation in Figure 7.5 (b) is greater than the pressure fluctuation in Figure 7.5 (a), indicating that Figure 7.5 (a) is favorable in terms of energy efficiency.

7.2.3.4   CFD Simulation 2: Velocity and Pressure Analysis

In second simulation, the inlet mass flow rate was set to 73 kg/s, this is the magnitude of the mass flow rate required to maintain maximum flight conditions as detailed in Chapter 6. The velocity distribution for the main and alternate wye system is shown in Figure 7.6 (a) and (b) respectively.
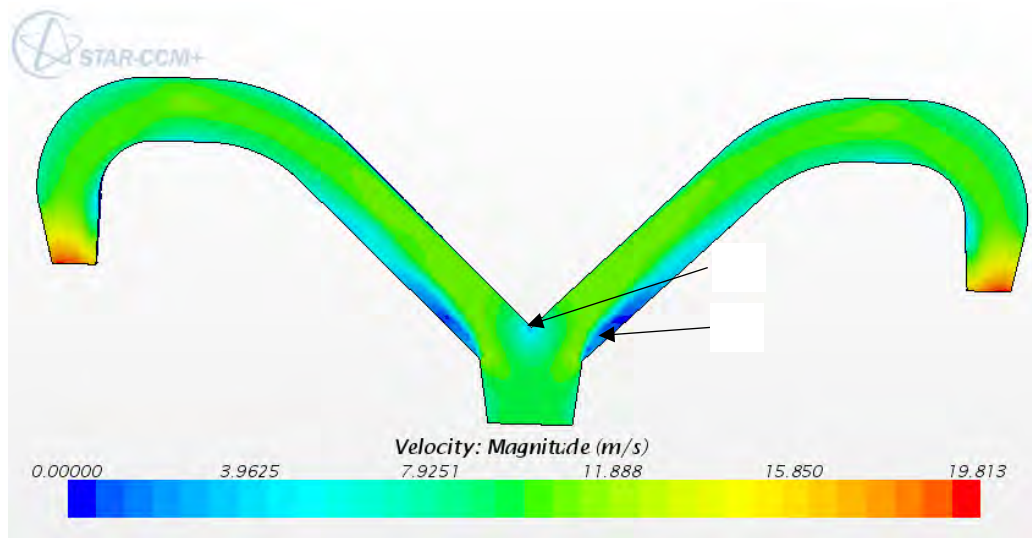
(a)
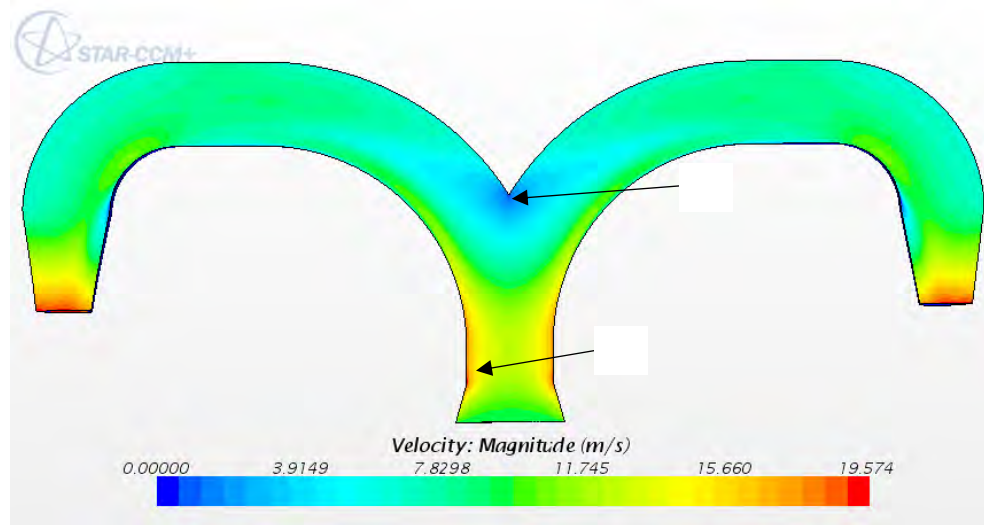
(b)

Figure 7.6: CFD simulation 2- velocity distribution: (a) Main model, (b) Alternate model

Referring to Figure 7.6 (a), it is observed that the average velocity in the main wye system is between 7.9251 m/s and 11.888 m/s. The average velocity in Figure 7.6 (b) is approximately 7.8298 m/s. The maximum velocity is 19.813 m/s, which is the velocity of the flow at the nozzle exit points. As previously observed in CFD simulation 1, the stagnation zones are indicated by A and B. These are zones of high pressure and flow recirculation. Stagnation zone labelled B

is larger than the stagnation zone located at A. Recirculation occurs at B due to a change in flow direction along the 45-degree bend.

In Figure 7.4 (b), the velocity distribution is similar to the velocity distribution in CFD simulation 1. The mean velocity in the system is between 7.8298 m/s and 11.745 m/s. The maximum velocity is 19.574 m/s, which is the fluid flow velocity at the nozzle exit points.

The pressure distribution for the main and alternate wye system is illustrated in Figure 7.5 (a) and (b) respectively:

(a)
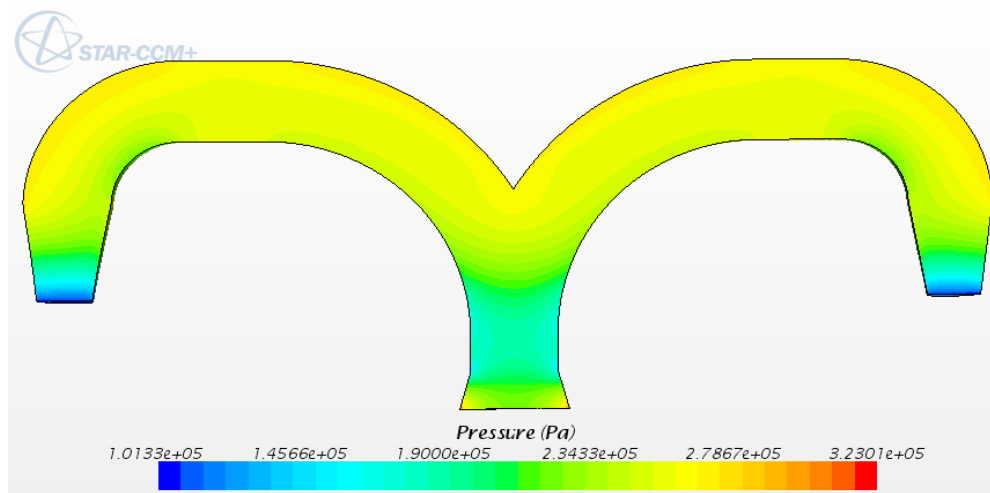
(b)

Figure 7.7: CFD simulation 2- pressure distribution (a) Main model, (b) Alternate model

Referring to Figure 7.7 (a), the mean pressure in the main wye system is between 2.205 bar and 2.6023 bar. The maximum pressure occurs at the region where the flow splits, the magnitude of the maximum pressure is 2.9996 bar.

Referring to Figure 7.7 (b), the low pressure region is located near the inlet section where there is a decrease in flow area. The magnitude of the pressure in this region is between 1.4566 bar and 1.9 bar. The maximum pressure is 3.2301 bar. As previously observed in CFD simulation 1, the pressure fluctuation in Figure 7.7 (b) is greater than the pressure fluctuation in Figure 7.7 (a). Hence, this indicates that Figure 7.7 (a) is favorable in terms of optimizing the energy efficiency of the flow. However, a more useful quantity to aid in comparing the efficiency of the main and alternate wye system is the pressure drop across the entire control volume. The pressure drop can be numerically expressed in Star CCM+ by generating a pressure drop report after the fluid flow solution has been solved and the residuals have reached steady state. The pressure drop for the main and alternate wye system for this simulation as observed from Star CCM+ is 0.1738875 bar and 1.000878 bar. This implies that there is a greater loss of pressure in the alternate wye system. This is caused by the sudden convergence and divergence of flow along the inlet section of the alternate wye system, which consequently causes a significant pressure loss in the system.

7.2.4   Finite Element Analysis Simulation

Finite Element Analysis simulation of the main wye system was conducted using SolidWorks. The objective of performing FEA simulation on the wye system is to observe and determine the structural integrity of the wye system when assigned with the material property of stainless steel 316L. Stainless steel 316L is chosen as an appropriate material for the wye system since it has suitable properties for the application of a water jetpack that functions in both fresh and salt water. Stainless steel 316L has a yield strength of 170 MPa and a tensile strength of 485 MPa.

7.2.4.1   Loading and Fixtures

The loading and fixtures of the wye system is displayed Figure 7.8 which shows the wye system in cross-section. The wye system was fixed at three regions, which are shown in green. These are the mounting points for the wye system onto the backrest of the water jetpack. The loading applied to the wye system was a pressure loading with a magnitude of 3 bar. This is the value of the maximum pressure experienced in the main wye system which was observed in CFD simulation 2 previously. The pressure loading condition was applied throughout the wye system and this is shown in red.
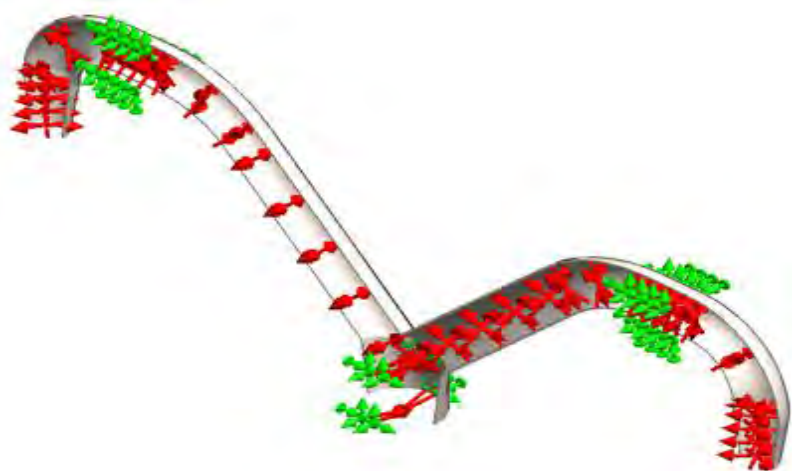
Figure 7.8: Wye system FEA simulation – loading and fixtures

7.2.4.2   Displacement

The FEA simulation was run and the displacement scene was observed as shown in Figure 7.9. The maximum displacement observed is 0.02293 mm which occurs at node 7802, located at the nozzle exit points.
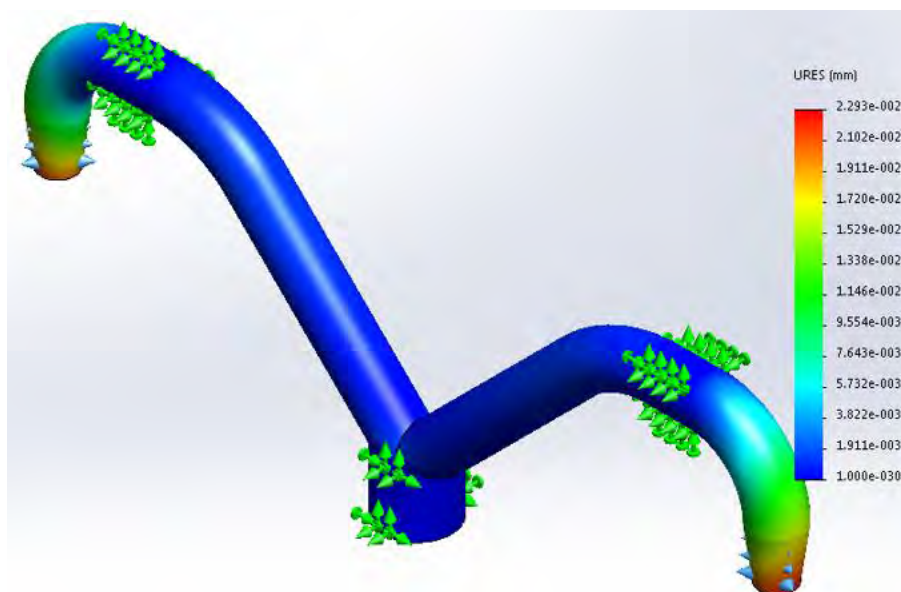

Figure 7.9: Wye system FEA simulation – displacement

7.2.4.3   von Mises Stress Analysis

The von Mises stress was observed as illustrated in Figure 7.10 below. The maximum stress is 11.59 MPa which occurs at node 1999. Since the yield strength of stainless steel 316L is 170 MPa, the von Mises stress results shown in Figure 7.10 indicate that the structure can withstand the applied pressure loading of 3 bar without yielding. This

result also validates that the material selection for the wye system is appropriate for maximum conditions experienced within the wye system of the water jetpack propulsion system.
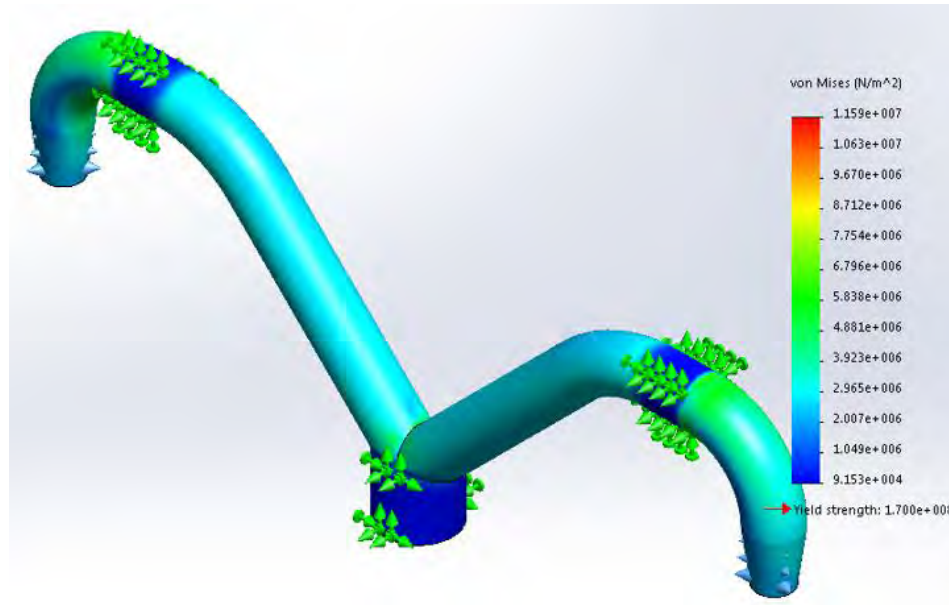
Figure 7.10: Wye system FEA simulation – von Mises stress

7.3   AUV Model

In this section, a proposed model of the AUV is developed using SolidWorks. The parameters for the development of the AUV were optimized and used in Chapter 6. Table 7.2 summarizes the key performance parameters of the water jetpack propulsion system and its magnitude under steady state and peak conditions along with a specification value for each parameter

Table 7.2: Water jetpack propulsion system performance specifications

Parameters	Units	Peak Value	Specification
Length	m	2	2
Diameter	m	0.3	0.3
Propeller Power	kW	102	126
Velocity	m/s	15	15
Thrust	N	5500	5500
Mass flow	kg/s	310	358
Depth	m/s	-1	-1
Average mass	kg/s	120	120
Buoyant force	N	1383	1383

Referring to Table 7.2, the main performance parameters of the AUV system is shown in the left column, and the magnitude of each performance parameter along with its respective units are shown. The peak values represent the peak performance of the AUV when the combined system travels at a velocity of 15 m/s in a forward direction. The specification values represent the performance of the AUV system when the combined system travels at a constant velocity of 15 m/s.

7.3.1 Hull Development

The structural shape and dimensions of the AUV hull is shown in Figure 7.11. The hull of the AUV is composed of three segments: 1) nose cone, 2) mid-body, and 3) tail end. Aluminium 5052 is suggested as an appropriate material for the AUV hull due to high strength-to-weight ratio and resistance to corrosion. Aluminium 5052 has a yield strength of 90 MPa, tensile strength of 195 MPa, and mass density of 2680 kg/m^3 (Thivey et al., 1998).
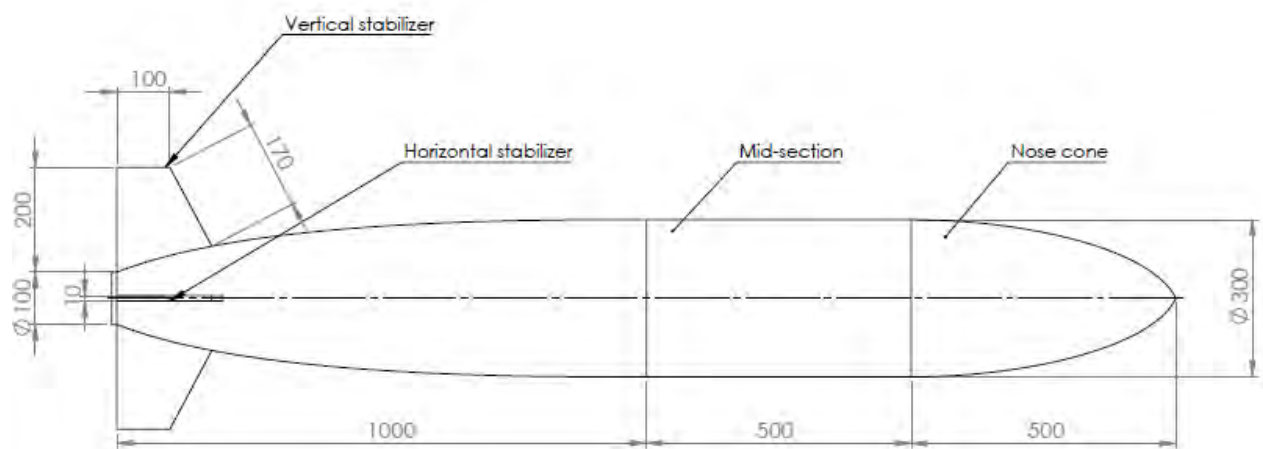
Figure 7.11: AUV hull shape and dimensions schematic

Referring to Figure 7.11, the total length of the AUV is 2 m, which includes the three segments as previously stated. The nose cone is 500 mm in lateral length, and consists of a streamlined shape profile as seen from the left view. The diameter of the nose cone section ranges from zero to 300 mm. In this AUV model, the streamlined shape profile of the nose cone was arbitrarily modelled using an equation driven spline-type of line when generating the CAD model on SolidWorks. A streamlined shape nose cone optimizes the performance of the AUV in the direction of travel by reducing the effect of drag on the frontal section of the AUV. The mid-section is 500 mm in length with a constant diameter of 300 mm. The tail end section is 1000 mm in length with a diameter ranging from 300 mm to 100 mm at the extreme rear end.

7.3.2   Propulsion and Steering

A full assembly view of the AUV is shown in Figure 7.12. The propeller and flow deflector is located at the extreme rear end of the AUV and is attached to the AUV hull by a shaft and set of actuators. There are four fixed stabilizers attached to the hull of the AUV: two vertical and two horizontal stabilizers. The purpose of the vertical and horizontal stabilizers is to ensure that the AUV maintains constant orientation during motion, with zero roll.

(a)   (b)
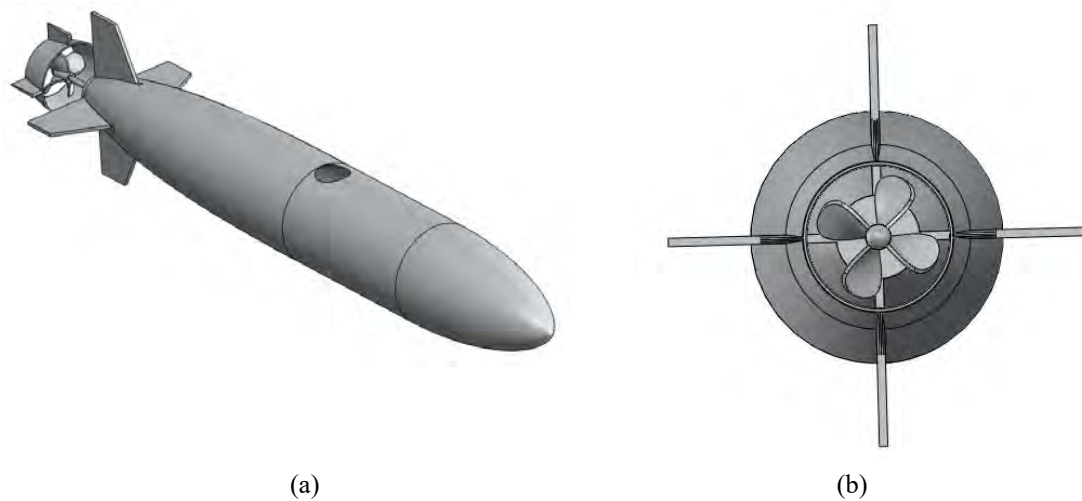
Figure 7.12: AUV Model: (a) Isometric view, (b) Rear view

Referring to Figure 7.12 (a), the propeller flow deflector has a slight converging shape with four fixed flow stabilizers positioned parallel to the vertical and horizontal stabilizers on the hull of the AUV. The flow deflector is positioned around the propeller such that it may be mechanically rotated about the vertical and horizontal axis and thus allow for three-dimensional thrust vectoring. Figure 7.12 (b) shows the rear view of the AUV, the relative size of the propeller and flow deflector to the hull size is illustrated. At the mid-section of the hull, there is feed hose inlet which has a diameter of 100 mm. This is the point where the feed hose is linked to the AUV as illustrated in Figure 7.13.

(a)   (b)
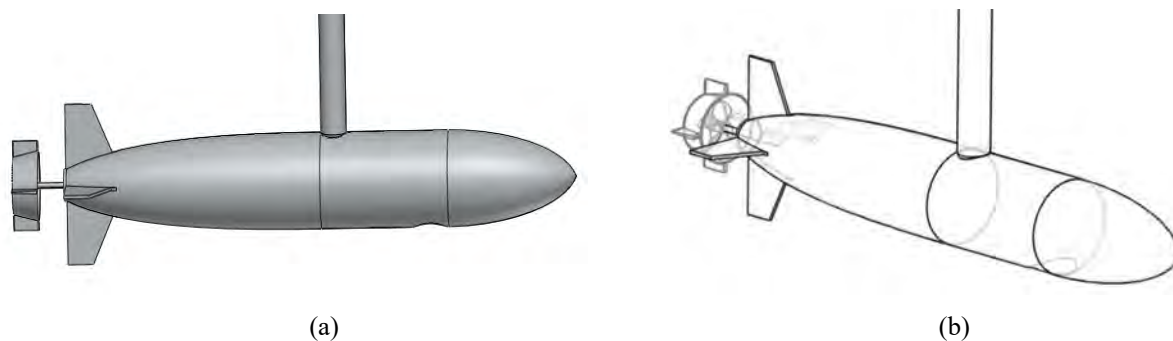
Figure 7.13: AUV with feed hose: (a) Left view, (b) Isometric sketch view

The feed hose is attached to the AUV at the upper-rear part of the mid-section of the hull. The attachment of the feed hose to the hull can be achieved using a swivel coupling as prescribed for the wye system. The purpose of this type of coupling is to allow the AUV to change its orientation without affecting the state of the feed hose such that the flow of water in the water jetpack propulsion system is independent of yaw motion experienced by the AUV.

7.3.3   Computational Fluid Dynamics Simulation

The velocity, pressure, and shear stress distribution of the AUV hull was analyzed using a built in CFD analysis package on SolidWorks. This simulation involves external fluid flow modelling and simulation of the AUV in water when the system travels at the maximum allowable velocity of 15 m/s. The objective of this simulation was to observe the fluid flow characteristics around the AUV hull along with the magnitude and location of the maximum shear stress on the AUV hull to determine if the aerodynamic shape of the AUV hull shown in Figure 7.11 is viable for future development.

7.3.3.1   Velocity

The velocity profile of fluid flow around the hull of the AUV is shown in Figure 7.14 (a) and (b). The velocity profile illustrates the velocity of the fluid flow along the entire surface of the hull of the AUV. The velocity profile also illustrates stagnation zones whereby the velocity of the fluid flow is zero.
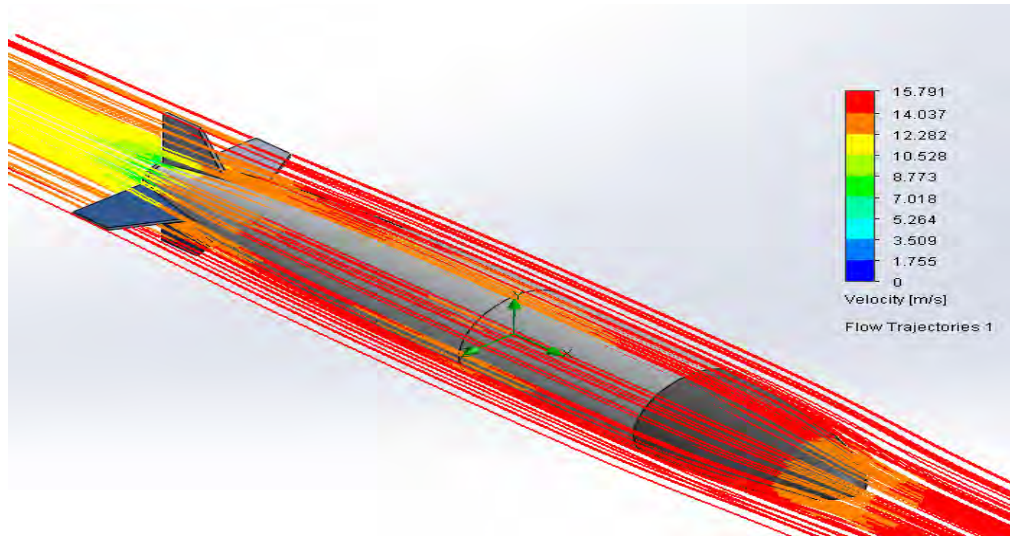
(a)
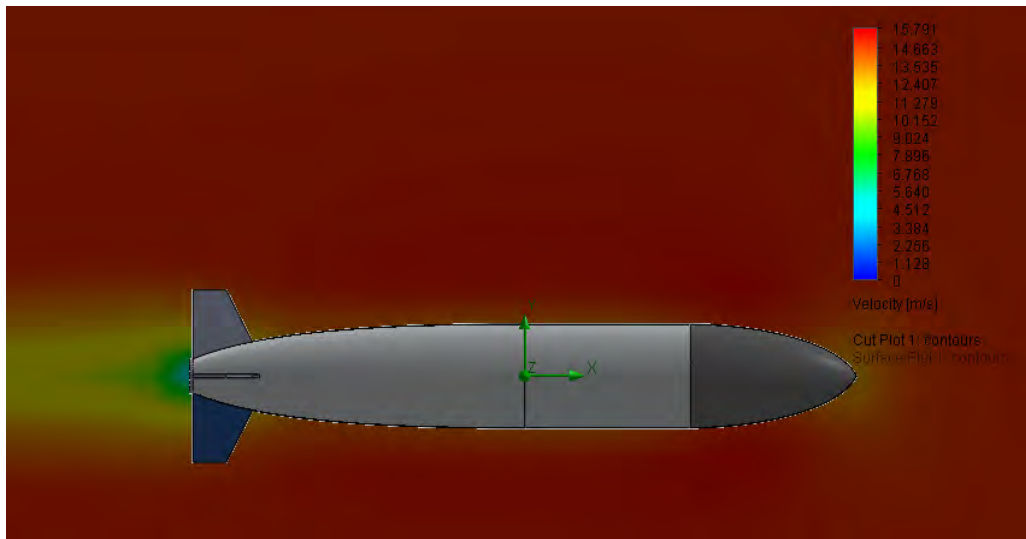
(b)

Figure 7.14: AUV hull CFD simulation: (a) Velocity flow trajectory, (b) Velocity cut plot

Referring to Figure 7.14 (a), maximum velocity of fluid flow on the surface of the hull is 15.791 m/s which is indicated by the red flow trajectory lines. The velocity of the fluid flow at the frontal section of the AUV nose cone is between 12.282 m/s and 14.037 m/s which is indicated by the orange flow trajectory lines. The exact velocity at this region can be read-off by referring to Figure 7.14 (b) which shows a cut plot of the fluid flow velocity around the hull. The velocity at the frontal section of the nose cone is approximately 13.535 m/s and the fluid flow velocity along the mid and rear end section of the hull is between 13.353 m/s and 14.663 m/s. At the rear end of the AUV, the velocity of the fluid flow varies from 0 m/s to 11.279 m/s. This is the region where the fluid flow velocity reaches the stagnation condition and the fluid flow velocity is relatively low. The aim of modelling an aerodynamic hull profile is to minimize

the size of the stagnation zone at the rear end of the AUV hull since this leads to the formation of a wake. In a wake, there is vorticity and flow reversal present.

7.3.3.2   Pressure

The pressure distribution of fluid flow around the hull of the AUV is shown in Figure 7.15. The pressure distribution illustrates the pressure experienced by the hull of the AUV which is caused by the interaction of the hull and flow of water.
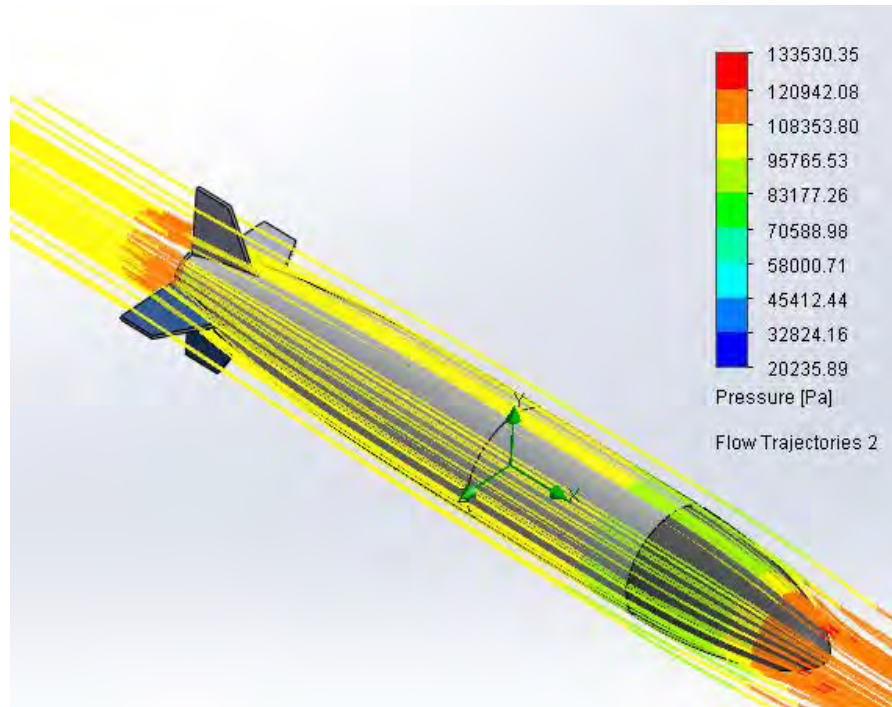
Figure 7.15: AUV hull CFD simulation: Pressure distribution flow trajectory

Referring to Figure 7.15, the maximum and minimum pressure is 133530.35 Pa and 20235.89 Pa respectively. The maximum pressure is experienced at the frontal section of the nose cone which is indicated by the red flow trajectory lines. The pressure along the nose cone decreases from 133530 Pa at the frontal section to 95765.53 Pa at the end of the nose cone. The pressure along the mid-section and tail section is between 108353.8 and 95765.53 Pa.

7.3.3.3   Shear Stress

The shear stress distribution of AUV hull is illustrated in Figure 7.16. The shear stress distribution is useful in determining the regions of the hull that experience the greatest shear stress and therefore validates material selection and the thickness of the hull.
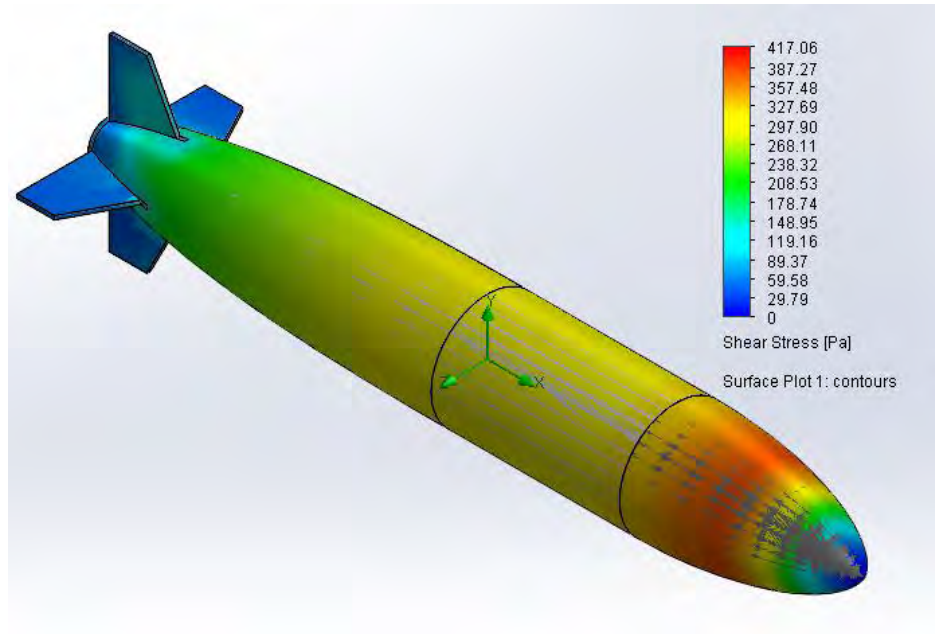
Figure 7.16: AUV hull CFD simulation: Shear stress distribution

It can be observed that the shear stress ranges from zero Pa to 417.06 Pa. The maximum shear stress is 417.06 Pa which is experienced at the mid-section of the nose cone. Since the yield strength of aluminum 5052 is 90 MPa, the maximum shear stress is well below this and therefore it can be deduced that the hull would not yield due to the shear stress experienced during transient motion. It is observed that the shear stress along the nose cone increases from zero Pa to the maximum shear stress value, and thereafter decreases to 297.9 Pa. The shear stress variation along the nose of is due to its streamlined shape. The shear stress decreases from 297.9 Pa at the mid-section to zero Pa at the rear of the AUV hull.

CHAPTER 8 : DISCUSSION AND TECHNICAL ANALYSIS

A survey of water jet propulsion, water jetpack development, and AUVs was conducted in Chapter 2 to develop the theoretical background required for the development of a combined water jetpack and AUV system. The water jetpack and AUV system functionality was briefly described which forms part of the system model layout presented in Chapters 3 and 4. The fundamental theory of jet propulsion and fluid dynamics presented in the literature review consists of Newton's Second Law and the thrust equation, water jet thrust, control volume analysis, conservation laws, and fluid flow fundamentals. The two main conservation laws presented are the law of conservation of mass and the law of conservation of energy. This formed the theory required to model the water jetpack and AUV system externally. The fluid dynamic fundamentals section introduced the essential aspects of fluid mechanics required to model the internal and external performance of the water jetpack and AUV, including pressure, Reynolds number, the Bernoulli equation, pressure loss, drag force, along with buoyancy and stability. The literature review also comprised theory related to dynamic control system modelling, which introduced fundamental aspects of modelling both open- and closed-loop dynamic systems, PID controllers, and second-order transient response characteristics. This formed part of the essential theoretical background used for the development of MATLAB Simulink modelling and simulation as presented in Chapter 6. The last section presented in the literature review was the basic theory and functionality of hydrogen fuel cells and AIP systems. In this section, the principle of a fuel cell, advantages and disadvantages, efficiency and lifetime, and hydrogen AIP propulsion for an underwater vehicle was introduced.

A series of static and dynamic models of the water jetpack and its propulsion system was developed in Chapter 3. The aim was to develop a system of equations that would be used to model the steady state and transient motion of the water jetpack and AUV system. The development of the water jetpack propulsion system model consisted of three essential state points: AUV inlet, feed hose, and the jet-exit located at the exit of the nozzles of the water jetpack. The models developed in this chapter were derived by applying Newton's Second Law of motion for each set of flight conditions. An accumulative mass model was developed such that the net mass of the system being lifted is dependent on the fixed masses plus the mass of water contained in the feed hose. The mass of water contained in the feed hose was shown to be a linear function with respect to flight altitude and area of the feed hose.

The water jetpack was modelled in the z, x-z, and x-y-z direction for both steady state and transient flight conditions. These models were derived by applying the fundamental theory of fluid dynamics as presented in Chapter 2. In each case, it was demonstrated that the motion of the water jetpack system is dependent on the mass flow rate of water through the propulsion system. Increases in the mass flow rate increases the flight altitude, velocity and acceleration in the respective direction of flight. In the case of motion in the x-z direction, varying the thrust vector angle (alpha) with constant mass flow rate of water through the propulsion system results in the total thrust force generated constant, results in a change in the thrust force in either the x- or z-direction. This would cause an increase in either the surge or heave velocity and a corresponding change in flight altitude. However, if the pitch angle of the system reaches a

maximum critical value such that the jetpack system reaches the point of critical stability, then changing the thrust vector angle (alpha) in either the positive or negative direction at that instant or time results in a corresponding increase or decrease in pitch angle. However, an increase in the pitch angle past the maximum critical value results in instantaneous instability of the entire jetpack system. This explanation regarding critical stability of the water jetpack system was observed by Naidoo et al. (2015b) during tests of the UKZN Water Jetpack in the coastal area located in the northern part of Durban in South Africa. Stability of the water jetpack system depends on the design of the jetpack system and the position. Motion in y-direction is attained when the pilot changes the yaw angle of flight, such that there is a non-zero component of the water jet thrust force acting in the y-direction, consequently inducing a positive sway velocity.

Modelling of the AUV system involved applying the theory of jet propulsion and fluid dynamics as given in Chapter 2. The AUV was modelled by producing a series of static and dynamic differential equations for motion in the x, x-y, and x-y-z directions. This involved generating the system of equations for force, acceleration, and velocity along with various other physical quantities for the case of steady state and transient motion. For each case, the position, velocity and acceleration of the AUV is dependent on the mass flow rate of water through the propeller of the AUV. The propeller thrust was shown to be dependent on the propeller area, AUV velocity, and the jet velocity of water exiting the propeller. The rudders of an AUV control the steering direction of the AUV; it was shown that the propeller thrust components in the x- and y-direction are dependent on the cosine and sine components of the rudder angel respectively. Lastly, the AUV was modelled in three dimensions, whereby the weight and buoyant force acting on the AUV was considered in the Newtonian force balance equations. The force balance in the z-direction is controlled using fins which generate lift forces when the fin angle is changed, however it was deduced that the use of fins for controlling the depth of an AUV is limited. A proposed three-dimensional thrust vectoring system developed by Cavalla et al. (2004) was suggested as an alternate steering and depth control mechanism. This mechanism works by directing the propeller thrust generated by the rotating propeller such that the desired sway velocity and depth of the AUV is attained by controlling two angles: horizontal deviation angle and vertical deviation angle. A set of equations was produced for the AUV motion in three dimensions using the three-dimensional thrust vectoring mechanism.

Chapter 5 of this dissertation detailed the water jetpack propulsion system optimization process modelling. In this chapter, the steady state model of the water jetpack in the z-direction was generated as a code on MATLAB. The utility of the code was to optimize the selection of the feed hose and jet-exit area for the system such that several conditions were met. The first primary condition was that the jet-exit velocity of water be less than 15 m/s such that the water jet cannot cause injury to the pilot during steady state flight conditions. The selected values of the feed hose and jet-exit diameter were 100 mm and 50 mm respectively. The second primary condition was that the feed hose water velocity be less than half the jet-exit velocity. This condition was imposed such that the head loss due to friction in the feed hose is minimized. The feed hose and jet-exit water velocity conditions formed the primary conditions of the optimization process. The secondary conditions were: thrust-to-weight ratio at least 1.5, absolute pressure rise across the AUV pump remains under 4 bar, and the Reynolds number be greater than 6000 such that the Darcy friction factor was less than 0.02, which minimizes the loss of pressure in the feed hose. It was observed that all conditions

were met with the chosen size for the feed hose and jet-exit diameter. The ideal power consumption for this analysis was found to be 18.0978 kW. It was observed that power consumption increases significantly when the feed hose diameter decreases and the jet-exit diameter increases.

Following the development of the second-order non-linear and transient mathematical models described in Chapter 3 and Chapter 4 of this dissertation, a closed-loop feedback control system model of the water jetpack and AUV system was developed on MATLAB Simulink in Chapter 6. The aim of developing the MATLAB Simulink model was to determine the closed-loop response of the combined system such that a fully automated system could be developed in future work. The development of the combined system model involved developing an initial model for the water jetpack and AUV for one-dimensional motion, and thereafter expanding these Simulink models to form two- and three-dimensional open- and closed-loop Simulink models.

A PID controller for thrust vector angle control was introduced in two-dimensional modelling. It is evident that the PID controller implementation for thrust vector angle control is highly effective to attain a desired surge velocity with zero oscillatory motion and a low value for the peak overshoot. The implementation of thrust vector angle control enables surge velocity control of the water jetpack system. It is also noted that the sensitivity of the system's response to changing the thrust vector angle is high; minor increases in the thrust vector angle result in a high increase of surge velocity. The system was also simulated for maximum conditions whereby the thrust vector angle and mass flow rate reached peak and the responses of the system was observed. It is clear that the PID controller saturates the mass flow rate at 116 kg/s and the surge velocity at 40 m/s. It was also observed that the maximum and nominal thrust-to-weight ratio of the water jetpack system is 2.4 and 1.4 respectively.

A three-dimensional water jetpack Simulink model was developed. The three-dimensional model developed in this section allows a pilot to define a forward flight velocity and flight altitude and these reference values can be attained with the use of two PID controllers. The PID controller for controlling the thrust vector angle was further tuned for optimization of the thrust vector angle response. The yaw angle was defined as a pilot input; this angle is controlled by a shift in the CM of a pilot such that there is a component of thrust force acting in the y-direction. By varying the yaw angle, a pilot may move from left to right. It was observed that for the case of a fixed reference forward flight velocity, the mass flow rate is independent of the yaw angle, however, the thrust vector angle increases slightly.

The function of the combined system Simulink model was to enable speed control and tracking between the water jetpack and AUV. This system has a set of pilot defined system inputs which are: 1) desired flight altitude, 2) desired steady state velocity, and 3) yaw angle. The combined system registers the inputs of the pilot and controls several variables of the water jetpack and AUV propulsion system which are: 1) mass flow rate, 2) thrust vectoring, 3) speed saturation, 4) AUV propeller mass flow rate, 5) AUV propeller thrust vectoring, and 6) AUV depth control. The outcome of this chapter was the development of the control parameters required to achieve the desired reference inputs defined by the pilot along with the ideal transient responses obtained for the combined system.

A computational model of the water jetpack and AUV system along with CFD analysis and FEA of the essential components of the system is detailed in Chapter 7. The objective of this was to develop an initial virtual model of the system that could be developed in future work. The first step prior to developing a computational model of the system involved full performance analysis of the water jetpack propulsion system for steady state and peak transient conditions. From the full performance analysis, the size of the propulsion system along with the mass flow rate expected during peak conditions were used as the inputs in the CFD simulations conducted. The wye system suggested in this work was detailed and CFD simulations were conducted on Star CCM+ using the steady state mass flow rate of 56.1 kg/s and peak mass flow rate of 73 kg/s. The velocity and pressure distributions were analyzed. Finite element analysis was conducted on the wye system to verify the structural integrity of the wye system when subjected to maximum pressure loading of 3 bar. The von Misses stress and displacement was illustrated and it was deduced that stainless steel 316L with wall thickness of 2 mm would suffice for the design of the wye system. The second part of the computational model development consisted of the development of the AUV hull. The performance specifications for the AUV for steady state and peak conditions was analyzed to obtain the essential parameter values to develop and simulate the AUV hull. The hull development was detailed using a specified diameter and length. Aluminium 5052 was suggested as a suitable material for the hull. The shape of the hull is streamlined, and consists of three main sections together with vertical and horizontal stabilizers to control the orientation of the AUV. The AUV has an inlet connection for the water jetpack propulsion system, which feeds flow of water to the water jetpack via the feed hose. Computational fluid dynamics analysis was conducted on Solidworks to simulate the flow of water around the hull when the AUV travels at a specified maximum velocity of 15 m/s. The velocity, pressure, and shear stress distribution was analyzed and the results show that the shape and size of the AUV is suitable for future development.

CHAPTER 9 : CONCLUSION, FUTURE WORK AND RECOMMENDATIONS

The aim of this study was to research, model, simulate and develop an initial proposed computational model of the water jetpack powered by an AUV system. The AUV model developed provides duel functionality by providing power to the water jetpack propulsion system as well as providing power for its propeller which provides the necessary thrust required. The water jetpack and AUV system model developed in this work can achieve the pilot defined reference inputs: flight altitude, flight velocity, and yaw angle. To meet the objectives described in Chapter 1 in this dissertation, the theoretical development of the system was described in each chapter. Chapter 2 provides detailed insight into water jetpacks, AUVs, fluid dynamic fundamentals, control system modelling, as well as a brief description on hydrogen fuel cells and AIP. Chapter 3 details the development of a series of steady state and transient equations for the water jetpack. Chapter 4 details the development of a series of steady state and transient equations for the AUV. In both Chapter 3 and 4, modelling of the system was conducted for motion in one, two and three dimensions. The water jetpack and AUV modelling was based on the basic equations and laws of fluid dynamics described in Chapter 2. The fluid dynamic theory, together with simple mathematical operations and basic rules calculus, formed the basis for the equations used in Chapters 3, 4, 5, and 6 of this work. Chapter 5 describes the methodological approach and analysis of a MATLAB optimization code for the water jetpack propulsion system. The code was based on the peak steady state condition model for the water jetpack which was developed in Chapter 3. The optimization code provided a set of distribution graphs that describe the performance of the water jetpack system under peak steady state conditions for different linear combinations of feed hose and jet-exit diameter. In Chapter 6, the water jetpack and AUV system was modelled and simulated using MATLAB Simulink. This was done in a step-wise approach by developing one-, two- and three-dimensional Simulink models for the water jetpack and AUV as open-loop and closed-loop systems, thereafter combining the three-dimensional closed-loop models to form a combined system Simulink model. The combined system controls the main variables in the system such as mass flow rate, thrust vectoring, depth and saturation limits. This allows the pilot to define and attain a desired flight velocity, flight altitude, and flight path. Chapter 7 details the development of an initial proposed model of the water jetpack and AUV. The initial model developed in this chapter consisted of developing the water jetpack wye propulsion system along with the AUV hull system assembly. The objective was to develop a model that would provide optimal flow performance for the water jetpack propulsion system and have the structural rigidity to withstand the forces that the system would experience under peak transient conditions in flight. This was done and validated by performing CFD analysis and FEA on the wye propulsion system and AUV hull. The model developed and simulated under peak conditions is ideal for implementation into the complete system.

Future work on the development of the complete water jetpack and AUV computational model is required. This would involve development of the water jetpack backrest and seat structure, feed hose selection, coupling, hull internal

components, AUV hull optimization, three-dimensional thrust vectoring system of the AUV, and propulsion system pump selection. The aim of this development should be to minimize the mass of the total system while ensuring optimal functionality. Future work would also include development and implantation of a control system to control the mechanical systems that are responsible for controlling the dynamic performance of the combined system. Future work into the in-depth study of hydrogen fuel cells and AIP systems for the AUV is required. This would include selection of a hydrogen powered system that provides the electrical power required to run the pump of the water jetpack propulsion system and run the propeller of the AUV. This system could be split into two separate sub-systems with different performance characteristics for the AUV and water jetpack propulsion system.

REFERENCES

Anderson, J. (2001). *Fundamentals of aerodynamics* (3rd ed.). New York, NY: McGraw-Hill.

Ballard, R. (1987). *The discovery of the Titanic*. New York, NY: Warner/Madison Press Books.

Barr, R. A. and Etter, R. J. (1975). Selection of propulsion systems for high-speed advanced marine vehicles. *Marine Technology*, 12(1), 33-49.

Bennett, S. (1993). *A history of control engineering.* London: Peter Peregrinus Ltd.

Beushausen, D. M. (1993) *Airwalker: A date with destiny: Rocket-belt history and construction plans: Exhaustive study manual*. Bridgeview, IL: Airwalker Society.

Blevins, R. (1984). *Applied fluid dynamics handbook*. New Yorkny: Van Nostrand Reinhold.

Blidberg, D. (2001). *The development of autonomous underwater vehicles (AUV): A brief summary*, Proceedings of the IEEE International Conference on Robotics and Automation (ICRA2001), Seoul, Korea, May 2001.

Brutzman, P. (1994). *A virtual world for an autonomous underwater vehicle*. PhD thesis, Naval Postgraduate School.

Cavallo, E. and Michelini, R. (2004). *A robotic equipment for the guidance of a vectored thrustor AUV*. 35th International Symposium on Robotics, ISR 2004, Paris, pp. 88, Volume 5, March 2004.

Cavallo, E., Michelini, R., Filaretov, V. and Ukhimets, D. (2005). *Control features of a vectored-thruster underwater vehicle*. Institute for Automation and Control Process FEB RAS, Russia.

Cengal, and Cimbala, J. (2010). *Fluid mechanics: Fundamentals and applications* (3rd ed.). New York, NY: McGraw-Hill.

Colebrook, C. (1938). Turbulent flow in pipes, with particular reference to the transition region between the smooth and rough pipe laws. *Journal of the Institution of Civil Engineers*, 11, 133-156.

Charkrit, S. (2013). *On the solutions of first and second order nonlinear initial value problems*. Proceedings of the World Congress on Engineering Vol I, WCE, July 3-5, London, U.K.

Chowdbury, B and Singh, M. (2011). *Control of autonomous underwater vehicles, Undergraduate dissertation*, Department of electrical engineering, national Institute of Technology, Rourkela, May 2011.

Dorf, R and Bishop, R. (2001). *Modern control systems*, Prentice Hall.

Dynamics, N. (2012) *Absolute roughness of pipe material – Neutrium*. Available at: https://neutrium.net/fluid_flow/absolute-roughness/. Accessed on 30 October 2016.

Emanuelsson, S and Persson, J. (2007). *Design of a fuel cell system: Design of a specification of requirements for a fuel cell system for the electric power generation in a 77-foot sailing ship.* MSc dissertation, Chalmers University of Technology, Göteborg, Sweden.

Etter, R., Krishnamoorthy, V. and Sherer, J. (1980). *Model testing of waterjet propelled craft*. Proceedings of 19th ATTC, Ann Abor, MI, pp. 783-806.

Fox, R, Pritchard, P. and McDonald, A. (2010). *Fox and McDonald's introduction to fluid mechanics* (8th ed.). Chichester, United Kingdom: John Wiley & Sons.

Geridonmes, F. (2007*). Simulation of motion of an underwater vehicle. Master of Science dissertation*. Middle East Technical University, September 2007.

Gonzalez, L. (2004). *Design, modelling and control of an autonomous underwater vehicle*. Mobile Robotics Laboratory, Centre for Intelligent Information Processing Systems, School of Electrical, Electronic and Computer Engineering, The University of Western Australia.

Gosselin, C. and Angeles, J. (1989). The optimum cinematic design of a spherical three-degrees of freedom parallel manipulator. ASME Mechanisms, *Transmissions and Automation in Design*, 111.

Greatrix, D. (2012). *Powered flight: The engineering of aerospace propulsion*. London: Springer.

Griffiths, G. and Edwards, I. (2003). AUVs: designing and operating next generation vehicles. *Elsevier Oceanography Series,* 69, 229-236.

Haaland, S. (1983). Simple and explicit formulas for the friction factor in turbulent flow. *Journal of Fluids Engineering*, 103(5), 89-90.

Hall, N. (2016). *General thrust equation*. NASA-Glen Research Center. Available at: https://www.grc.nasa.gov/www/k-12/airplane/thrsteq.html. Accessed on 12 May 2016.

Hoerner, S. (1966). Fluid-dynamic drag. [Published by the author.] Library of Congress No. 64.

Howe, S. (2006). *Electrical energy equipment: Pumps and pumping systems*. Energy Efficiency Guide for Industry in Asia.

Humble, R., Henry, G. and Larson, J. (1995). *Space propulsion analysis and design*. New York, NY: McGraw-Hill.

Hirsch, M., Smale, S. and Devaney, R. (2012). *Differential equations, dynamical systems, and an introduction to chaos* (3rd ed.). Waltham, MA: Academic Press.

Jetlev-Flyer. (2016*). Jetlev-Flyer Jetpacks*. Available at: http://www.jetlev-flyer.com/. Accessed on 10 March 2016.

Jetpack America. (2016). *Jetpack America History*. Available at: http://www.jetpackamerica.com/jetpack-america-history.html. Accessed on 15 May 2016.

Karlström, M. (2007). *Hydrogen fuel cell basics, PhD thesis*, Sweden. (September-November,2007)

Kiam, H., Gregory, C. and Yun, L. (2005). PID control system analysis, design, and technology. *IEEE Transactions on Control Systems Technology*, 13(4), 559-576.

Kiijarvi, J. (2011). *Darcy friction factor formulae in turbulent pipe flow*. Lunowa Fluid Mechanics, Paper 110727, July 29.

Kupperman, S., Ryan, C. and Turi, A. (1999). Personal watercraft: Safety and environmental impact. Vermont Legislative Research Shop, University of Vermont. Available: http://www.uvm.edu/~vlrs/doc/personal_watercraft.htm. Accessed on 10 July 2016.

Le Page, Y. and Holappa, K. (2000). *Simulation and control of an autonomous underwater vehicle equipped with a vectored thruster*. The AUV 2000 conference, Pennsylvania State College, USA.

Leveille, E. (2007). *Analysis, redesign and verification of the Iver2 autonomous underwater vehicle motion controller*. Masters dissertation, Discipline of Electrical Engineering, University of Massachusetts, Dartmouth.

Leonard, J., Bennett, A., Smith, C. and Feder, H. (1998). *Autonomous underwater vehicle navigation*. Proceedings IEEE ICRA Workshop Navigation Outdoor Autonomous Vehicle, May 1998.

Lee, P., Jun, B., Kim, K., Lee, J, Aoki, T. and Hyakudome, T. (2007). Simulation of an inertial acoustic navigation system with range aiding for an autonomous underwater vehicle. *IEEE Journal of Oceanic Engineering*, 32(2), 327-345.

Little, B., McKenzie, C. and McKay, C. (2015). *Pelico Water Jetpacks*. Final group project dissertation in MECH 3492, Team 7, Department of Mechanical Engineering, University of Manitoba, Canada.

Lygouras, J., Lalakos, K. and Tsalides, P. (1998). THETIS: an underwater remotely operated vehicle for water pollution measurements. *Microprocessors and Microsystems*, 22(5), 227-237.

Mart, P and Margeridis, J. (1995*). Fuel cell air independent propulsion of submarines*, Aeronautical and maritime research laboratory, Defense science and technology organization, Australia, May 1995.

Miller, R. (1996). *Flow measurement engineering handbook* (3rd ed.). New York, NY: McGraw-Hill.

Mishra, S. and Dinesh, K. (2010). *Heading control of an underwater vehicle*, Department of electrical engineering, Nation Institute of Technology, Rourkela.

Morell, K. (2013). *Raymond Li of Jetlev: How James Bond inspired him to invent a jet pack*. Available at: https://www.americanexpress.com/us/small-business/openforum/articles/raymond-li-of-jetlev-how-james-bond-inspired-him-to-invent-a-jet-pack/. Accessed on 30 October 2016.

Moody, L. (1944). Friction factors for pipe flow. *Transactions of the ASME*, 66(8), 671-684.

Naidoo, J., Ramrup, K., Gerken, H. and Govender, Y. (2015a). *Flying water jetpack design. Design and Research Project 1, Dissertation*. School of Agriculture, Science and Engineering, University of KwaZulu-Natal, Durban, South Africa, Vol. 1, June 2015.

Naidoo, J., Ramrup, K., Gerken, H. and Govender, Y. (2015b). *Flying water jetpack design. Design and Research Project 2, Dissertation*. School of Agriculture, Science and Engineering, University of KwaZulu-Natal, Durban, South Africa, Vol. 2, November 2015.

Ogata, K. (2013) *Modern control engineering* (5th ed.). Boston, MA: Pearson Education.

Pacella, R. (2009). A water powered jetpack. *Popular Science*. Available at: http://www.popsci.com/diy/article/2009-07/water-powered-jetpack. Accessed on 12 March 2016.

Packard, A. (2005). *Dynamic systems and feedback*, ME 132 class notes, Department of mechanical engineering, University of California, Berkeley, United States of America.

Sabersky, R., Acosta, A., Hauptmann, E. and Gates, E. (1999). *Fluid flow: A first course in fluid mechanics* (4th ed.). Upper Saddle River, NJ: Prentice Hall.

Strotospheric Industries. (2014) *Jetpack history Timeline*. Available at: http://www.x-jetpacks.com/jetpack-history-timeline/. Accessed on 1 November 2016.

Strotospheric Industries. (2015) *X Jetpacks – Jet blades, Hydro sport equipment*. Available at: http://www.x-jetpacks.com/. Accessed on 30 October 2016.

Stewart, J. (2011) *Calculus: Early transcendentals* (7th ed.). Boston, MA: Cengage Learning.

Swamee, P. and Jain, A. (1976). Explicit equations for pipe-flow problems. *Journal of the Hydraulics Division (ASCE),* 102(5), 657-664.

Tivey, M., Johnson, H., Bradley, A. and Yoerger, D. (1998). Thickness of a submarine lava flow determined from near-bottom magnetic field mapping by autonomous underwater vehicle. *Geophysical Research Letters*, 25(6), 805-808.

Valavanis, K., Gracanin, D., Matijasevic, M., Kolluru, R. and Demetriou, G. (1997). Control architectures for autonomous underwater vehicles. *Control Systems Magazine*, 17(6), 48-64.

Von Alt, C. (2003). *Autonomous underwater vehicles: Autonomous underwater Langrangian platforms and sensors workshop*, LaJolla, CA, March-April 2003.

Vonk, M. and Bohacek, P. (2013). Carried by impulse: The physics of water jetpacks. *Physics Today*, 66(1), 54-55.

Wernli, R. (2001). *Low cost AUV's for military applications: Is the technology ready*? In Pacific Congress on Marine Science and Technology 2001, San Francisco, CA, July 2001.

Williams, C. (2004). *AUV systems research at the NRC-IOT: An update* In International Symposium on Underwater Technology, 2004, 59-73.

White, F. M. (2007). *Fluid mechanics* (6th ed.). New York, NY: McGraw-Hill.

Willcox, S., Vaganay, J., Grieve, R. and Rish, J. (2001). *The Bluefin BPAUV: An organic wide area bottom mapping and mine-hunting vehicle*, in Proceedings UUST '01.

Woods Hole Oceanographic Institution. (2016). *REMUS 600*. Available at: http://www.whoi.edu/main/remus600. Accessed on 8 July 2016.

Young, H., Freedman, R. and Ford, L. (2010) *University physics with modern physics* (13th ed.). Boston, MA: Addison-Wesley Educational Publishers.

Zapata Racing. (2015). Available at: http://zapata-racing.com/flyboard-en/. Accessed on 17 April 2016.

Zraiqat, A. and Al-Hwawcha, L. (2015). On exact solutions of second order nonlinear ordinary differential equations. *Applied Mathematics*, 06(06), 953-957. DOI: 10.4236/am.2015.66087.

APPENDIXES

APPENDIX A: Fluid Dynamics Data

A1. Reynolds Number Analysis

Figure A1 below shows a visual representation of laminar, transitional and turbulent fluid flow over a flat plate. Laminar flow is characterized by well-ordered and smooth layers of fluid. Laminar flow occurs typically when high-viscosity fluids flow at low velocity. Turbulent flow is characterized by highly disordered fluid motion at higher velocities than that of laminar fluid flow. Flow that falls between the region of laminar and turbulent is called transitional flow.
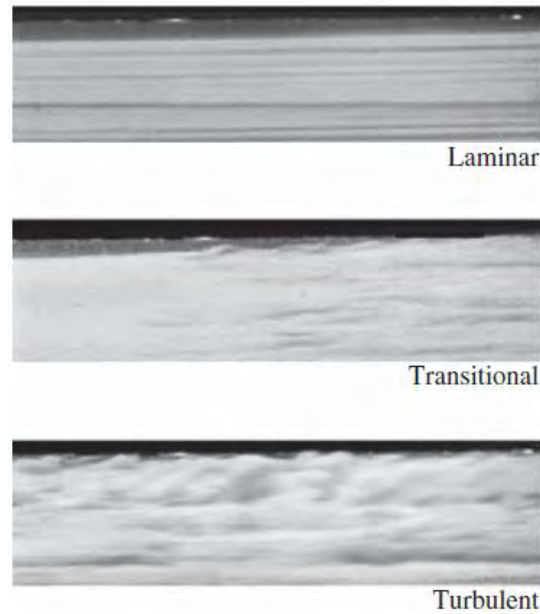
Figure A1: Laminar, transitional, and turbulent flows over a flat plate
Source: Cengal and Cimbala, 2010

In the case of fluid flow in a duct that is circular in cross-sectional area, a Reynolds number less than 2300 indicates laminar flow, a Reynolds number in the region of 2300 to 10000 indicates transitional flow and a Reynolds number above 10000 indicates turbulent flow (Fox et al., 2010).

A2. Darcy Friction Factor

A2.1 Darcy Friction Factor - Laminar Flow (Hagen Poiseuille Equation)

For laminar flow, the Darcy friction factor can be calculated using the *Hagen Poiseuille* equation:

$$f = 64/Re \qquad (A1)$$

A2.2 Darcy Friction Factor – Turbulent Flow

For turbulent flow, there is no existing exact solution for determining the Darcy friction factor. However, there are many empirical methods or close approximations for determining the Darcy friction factor for turbulent flow. The commonly used method is by graphically obtaining the Darcy friction factor from the Moody diagram shown (Moody, 1944). in Figure A2. The Moody diagram below is used to determine the Darcy friction factor for internal flow in a circular pipe of internal roughness.
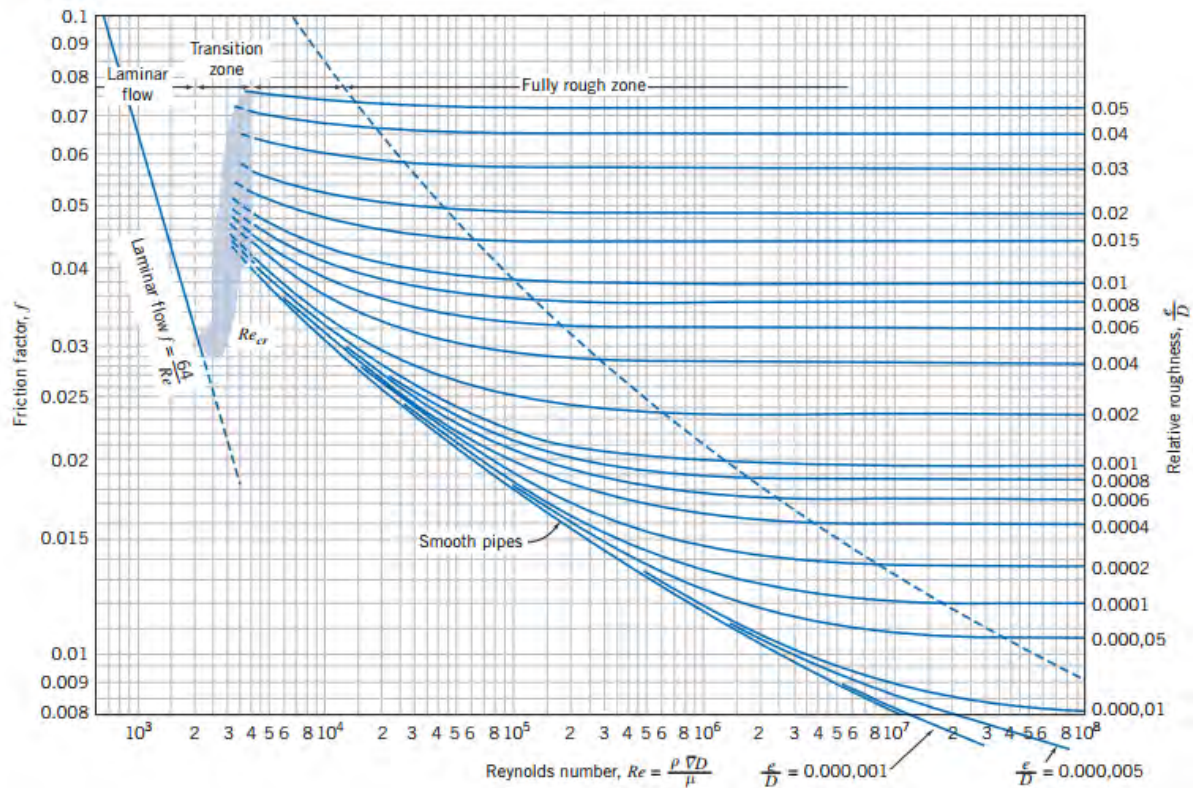
Figure A2. Friction factor for fully developed flow in circular pipes
Source: Fox et al., 2010

Colebrook Equation

An alternate way of obtaining the Darcy friction factor is by use of the Colebrook equation in which a solution is obtained by iteration. The Colebrook equation is given by:

$$\frac{1}{\sqrt{f}} = -2.0 \log \left[\frac{2.51}{Re\sqrt{f}} + \frac{\frac{\epsilon}{d}}{3.7} \right] \qquad (A2)$$

In which: f is the Darcy-Weisbach friction factor, Re is the Reynolds number, ϵ is the inner surface roughness of the pipe, and d is the pipe inner diameter. Both graphical and iterative methods of finding the Darcy friction factor depend on the roughness of the inner surface of the pipe as well as the value of the Reynolds number for the flow. Three alternate equations for calculation of the Darcy friction factor have been developed which are derived from the Colebrook equation: Blasius, Swamee-Jain and Haaland. These are valid only for steady turbulent circular pipe flow (Colebrook, 1939).

Blasius

Blasius, in 1913 derived an equation for finding the Darcy friction factor, for flow in smooth pipes (negligible roughness) in which the Reynolds number is less than 10^5. The Blasius equation is a simplified form of the Colebrook equation as the roughness term is negligible. In some fluid flow problems involving rough pipes, the Blasius equation is used due to its simplicity, this depends on accuracy of the solution needed as well a tolerance for the pressure loss in the system (Fox et al., 2010). The maximum error using the Blasius equation is 5% for Reynolds number up to 10^5. The Blasius equation is given by:

$$f = 0.316/Re^{0.25} \qquad (A3)$$

Swamee-Jain

Swamee and Jain (1976) developed the following equation which avoids iteration to calculate the Darcy friction factor, this equation is given by:

$$f = 0.25 \left[\log \left(\frac{5.74}{Re^{0.9}} + \frac{\frac{\epsilon}{d}}{3.7} \right) \right]^{-2} \qquad (A4)$$

Haaland

Haaland (1983) developed an equation used to calculate the Darcy friction factor without the need for iteration. The maximum error of the solution obtained using the Haaland equation is 2% for flow in which the Reynolds number exceeds 3000.

$$\frac{1}{f} = -1.8 \log \left[\frac{6.9}{Re} + \left(\frac{\frac{\epsilon}{d}}{3.7} \right)^{1.11} \right] \qquad (A5)$$

A3. Turbulent Effects and the Bernoulli Equation

Gaspard Coriolis (1792-1843) showed that the calculation of the kinetic energy term, $v^2/2$, in the Bernoulli equation is not equal to the actual kinetic energy in the flow stream for turbulent flow. Mathematically, this is due to the square of a sum is not equal to the sum of the squares for an arbitrary turbulent flow profile. This results in an error when using the Bernoulli equation for turbulent flow type problems. The dynamic head term in Equation 2.51 is valid for fully developed laminar pipe flow. Gaspard showed that this could be resolved by simply adding a kinetic energy correction factor, α, to the kinetic energy term (Cengal and Cimbala, 2010). The Bernoulli equation can therefore be expressed as:

$$P_1/\rho g + \propto_1 v_1^2/2g + Z_1 + h_{pump} = P_2/\rho g + \propto_2 v_2^2/2g + Z_2 + h_{loss} \qquad (A6)$$

where $\propto_1$ and $\propto_2$ represent the kinetic energy correction factor at state point 1 and 2 respectively. Note that $\propto$ equals to 2 for fully developed laminar pipe flow. For fully developed turbulent flow in a round pipe, a kinetic energy factor value between 1.04 and 1.11. A recommended value used when turbulence exists at the inlet and outlet of a pipe is 1.05 which results in a conservative estimate for the head loss in the system due to the effects of turbulent flow (Cengal and Cimbala, 2010).

A4. Absolute Roughness of Pipe Material

The roughness value for pipes of common engineering materials is shown below in Table A1:

Table A1. Typical values of absolute roughness for common construction materials
Source: Dynamics, 2012

Material	Roughness (mm)
Drawn Tubing, Glass, Plastic	0.0015-0.01
Drawn Brass, Copper, Stainless Steel (New)	>0.0015-0.01
Flexible Rubber Tubing - Smooth	0.006-0.07
Flexible Rubber Tubing - Wire Reinforced	0.3-4
Stainless Steel	0.03

A5. Drag Coefficient
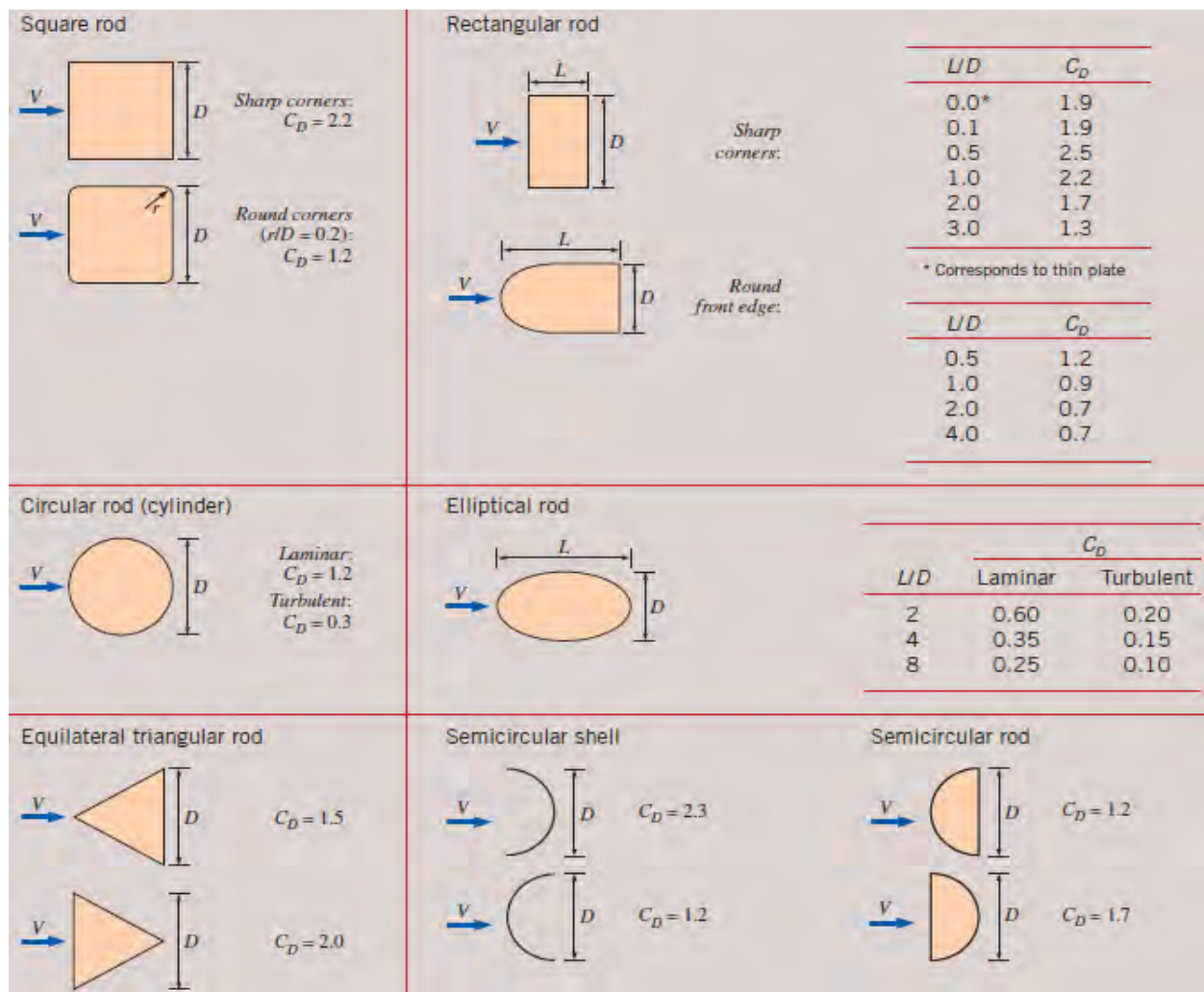
Figure A3. Drag coefficients of various two-dimensional bodies
Cengal and Cimbala, 2010

219

Cube, $A = D^2$

$C_D = 1.05$

Thin circular disk, $A = \pi D^2/4$

V D $C_D = 1.1$

Cone (for $\theta = 30°$), $A = \pi D^2/4$

V D $C_D = 0.5$

Sphere, $A = \pi D^2/4$

Laminar:
Re $\leq 2 \times 10^5$
$C_D = 0.5$
Turbulent:
Re $\geq 2 \times 10^6$
$C_D = 0.2$

See Fig. 11–36 for C_D vs. Re for smooth and rough spheres.

Ellipsoid, $A = \pi D^2/4$

	C_D	
L/D	Laminar Re $\leq 2 \times 10^5$	Turbulent Re $\geq 2 \times 10^6$
0.75	0.5	0.2
1	0.5	0.2
2	0.3	0.1
4	0.3	0.1
8	0.2	0.1

Hemisphere, $A = \pi D^2/4$

$C_D = 0.4$

$C_D = 1.2$

Finite cylinder, vertical, $A = LD$

L/D	C_D
1	0.6
2	0.7
5	0.8
10	0.9
40	1.0
∞	1.2

Values are for laminar flow (Re $\leq 2 \times 10^5$)

Finite cylinder, horizontal, $A = \pi D^2/4$

L/D	C_D
0.5	1.1
1	0.9
2	0.9
4	0.9
8	1.0

Streamlined body, $A = \pi D^2/4$

$C_D = 0.04$

Rectangular plate, $A = LD$

$C_D = 1.10 + 0.02 (L/D + D/L)$ for $1/30 < (L/D) < 30$

Parachute, $A = \pi D^2/4$

$C_D = 1.3$

Tree, $A = $ frontal area

$A = $ frontal area

V, m/s	C_D
10	0.4–1.2
20	0.3–1.0
30	0.2–0.7

Figure A4. Representative drag coefficients C_D for various three-dimensional bodies based on the frontal area
Source: Cengal and Cimbala, 2010

APPENDIX B: Propulsion System Optimization MATLAB Code

```matlab
clear all %Clears Editor
close all %Closes all current processes


%------------------------------------------------------------------------
% Water Jetpack Optimization Process Modelling
% Steady State Flight Analysis
%------------------------------------------------------------------------

%Input parameters:

g = 9.81;
m_jetpack=15;%Mass of jetpack (kg)
m_pilot=62; %Average mass of pilot (kg)
kappa=1.1;%factor to take into account minor losses in system
rho=1000;%density of water (kg/m^3)
Z2=10;%Steady state flight height (m)
L=15; %Length of feed hose (m)
vi=0;%velocity of AUV (m/s)

%Optimization range for feed hose diameter (80mm to 150mm)
D1 = 0.08:0.01:0.15;

%optimization range for jet exit diameter (30mm to 80mm)
D2 = 0.03: 0.01: 0.08;

% cycle through the diameter of the hose pipe (state point 1)
for(i = 1:length(D1))

  % Area of the hose pipe for each incremental diameter D1 (m^2):
  A1 = 0.25*pi*D1(i)^2;

  %cycle through the diameter of the jet exit diameter (state point 2)
  for (j = 1: length(D2))

      % Area of the jet exit for each incremental area D2 (m^2):
      A2 = 0.25*pi*D2(j)^2;

      %Dry mass of the system (kg):
      m_dry=m_jetpack+m_pilot;

      %Net mass of the system (kg):
      m_net = m_dry+kappa*rho*A1*Z2;

      %Mass flow rate through the system (kg/s):
      m_dot = sqrt(m_net*g*rho*A2);

      % Water jet exit velocity (m/s):
      vf = m_dot/(rho*2*A2);

      %Water feed hose velocity (m/s):
      vh = m_dot/(rho*A1);
```

```matlab
        %Reynolds Number
        %kinematic viscosity of water = 1.01 * 10^-6
        Re = (vh*D1(i))/(1.01*(10^-6));


        %volumetric flowrate (m^3/s)
        Q=vh*A1;


        %Thrust force required for steady state hovering at height Z2 (N):
        Ft=m_dot*vf;


        %head loss due to friction (m):
        %Friction factor selected to model maximum allowable friction
        %loss
        h_loss=(0.02*L*vh*vh)/(2*D1(i)*9.81);


        % Head required by pump for steady state flight
        h_pump = 1.2*(vf*vf)/(2*g) + Z2 + h_loss;


        % Pressure required by pump for steady state flight
        p_pump=rho*g*h_pump;


        % Power required for steady state flight
        P_pump = p_pump*Q;



        % The next few lines are to store the results as an array
        Ar1(i,j) = sqrt(A1*4/3.14); %Diameter of hose
        Ar2(i,j) = sqrt(4*A2/3.14);%Diameter of jet
        POW(i,j) = (p_pump)*Q/1000;%Pump power required
        Qr(i,j)= Q;%Volumetric flowrate
        T(i,j) = Ft;%Thrust force required
        V1(i,j) = vh;%Hose velocity
        V2(i,j) = vf;%Jet velocity
        MDOT(i,j) = m_dot;%mass flow rate
        HL(i,j)=h_loss;%Head loss due to friction
        T2W(i,j)=Ft/(m_dry*g); %thrust to weight ratio
        RE (i,j)= Re; %Reynolds number


    end
end


%-----------------------------------------------------------------------
% Plotting the results:
%-----------------------------------------------------------------------

figure
contourf(Ar1, Ar2, HL)
title('Head loss due to friction [N]')
xlabel('D1 [m]')
ylabel('D2 [m]')
colorbar

figure
```

```matlab
contourf(Ar1, Ar2, T)
title('Thrust force generated [N]')
xlabel('D1 [m]')
ylabel('D2 [m]')
colorbar
%------------------------------------------------------------------------
figure
contourf(Ar1, Ar2, T2W)
title('Thrust to Weight ratio [N/N]')
xlabel('D1 [m]')
ylabel('D2 [m]')
colorbar
%------------------------------------------------------------------------
figure
contourf(Ar1, Ar2, Qr)
title('Flow rate [m^3/s]')
xlabel('D1 [m]')
ylabel('D2 [m]')
colorbar
%------------------------------------------------------------------------
figure
contourf(Ar1, Ar2, HL)
title('Head Loss due to Friction [m]')
xlabel('D1 [m]')
ylabel('D2 [m]')
colorbar
%------------------------------------------------------------------------
figure
contourf(Ar1, Ar2, RE)
title('Reynolds Number')
xlabel('D1 [m]')
ylabel('D2 [m]')
colorbar
%------------------------------------------------------------------------
figure
contourf(Ar1, Ar2, V2)
title('Jet Exit Velocity [m/s]')
xlabel('D1 [m]')
ylabel('D2 [m]')
colorbar
%------------------------------------------------------------------------
figure
contourf(Ar1, Ar2, POW)
title('Ideal Power Required by Pump [kW]')
xlabel('D1 [m]')
ylabel('D2 [m]')
colorbar
%------------------------------------------------------------------------
```

APPENDIX C: MATLAB Simulink Simulation: Additional Responses

C1. Simulink Model 1: Motion in the Z-Direction (Closed-Loop)

C1.1 Automated PID Controller Tuning
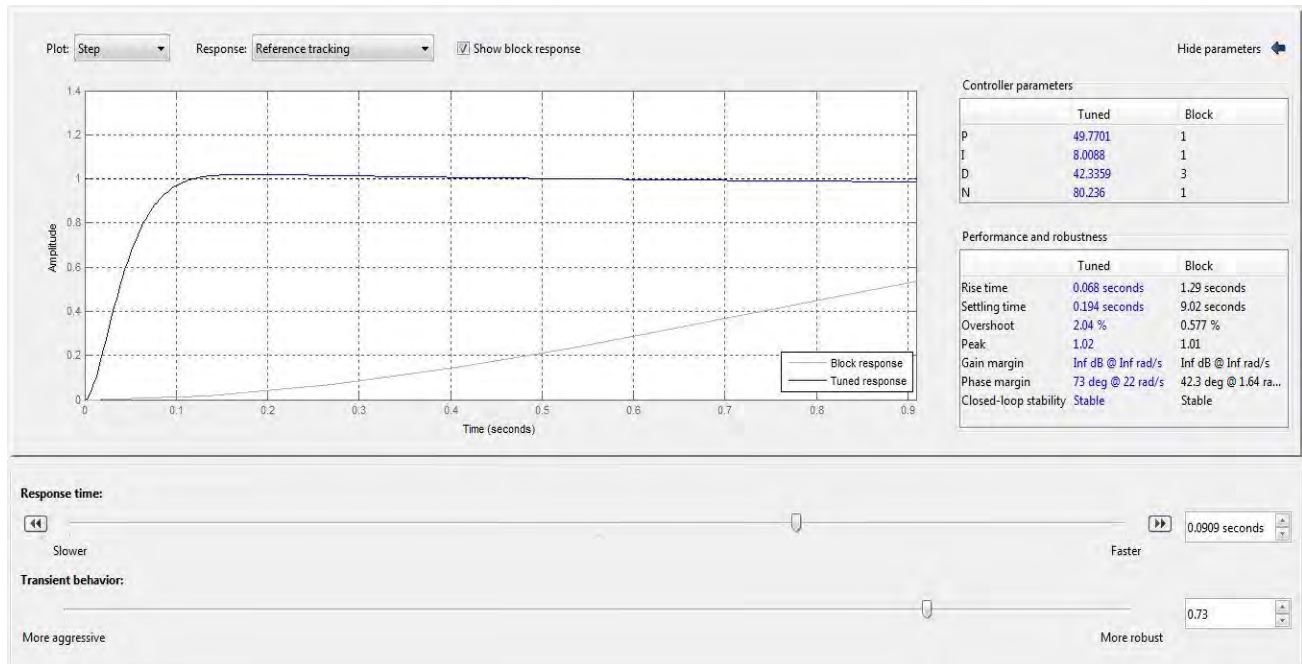
(a)
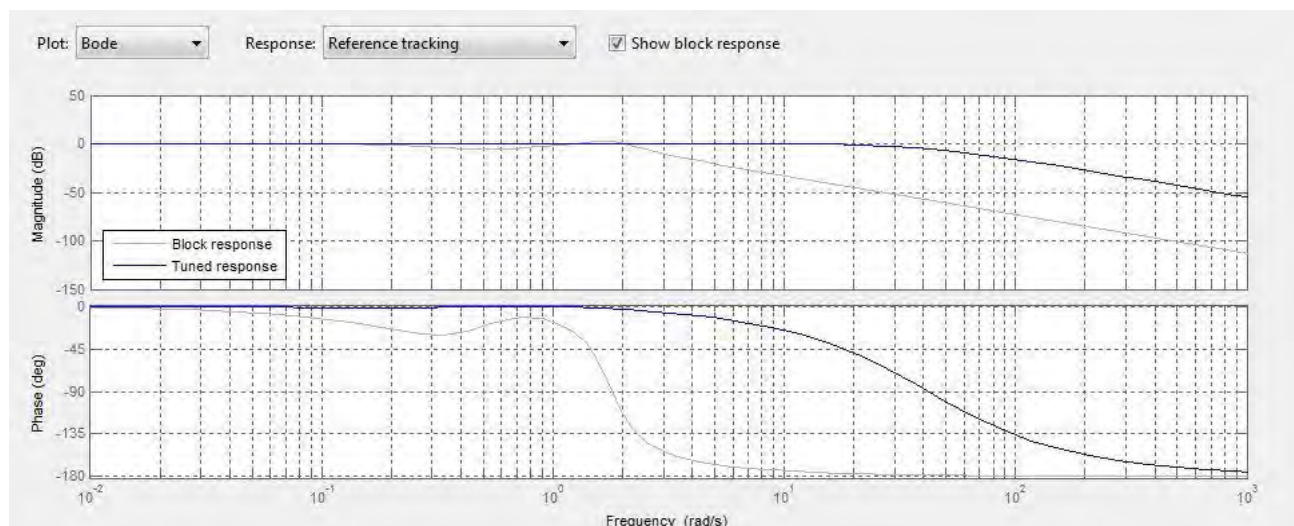
(b)

Figure C1. Controller design (a) Controller parameter setting, performance and robustness and reference tracking response, (b) Reference tracking bode plot

C1.2 Simulation Results
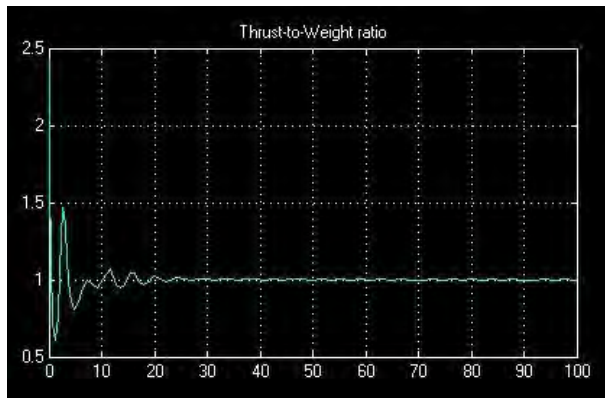
(a)
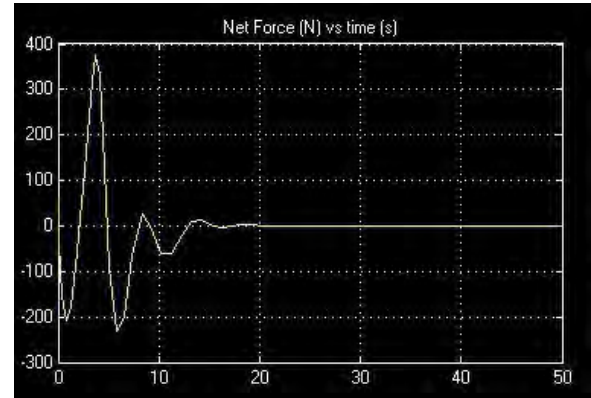
(b)
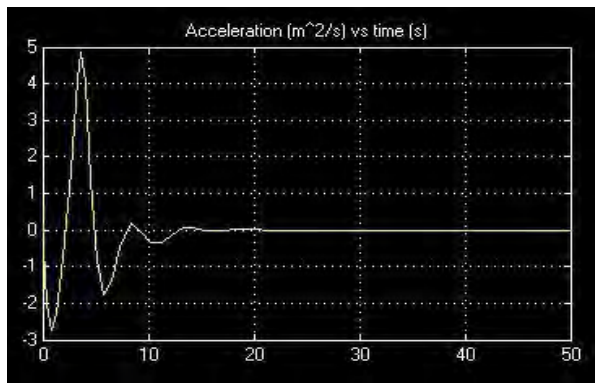
(c)
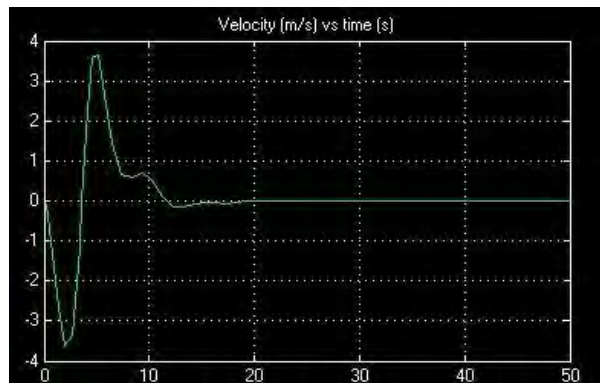
(d)

Figure C2. Simulation 2 results: (a) Thrust-to-weight ratio, (b) Net force, (c) Acceleration, and (d) Velocity

D2. Simulink Model 3: Motion in 2-Dimensions (Open-Loop)
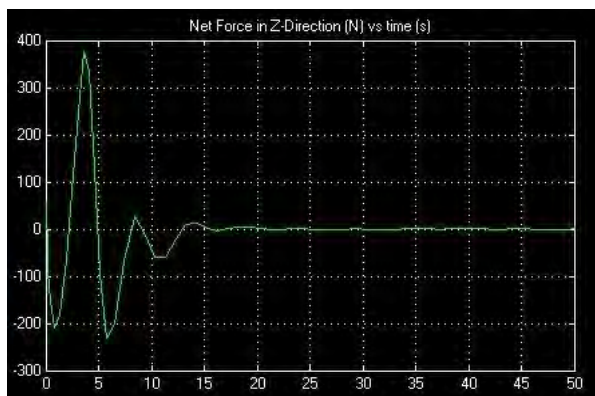
(a)
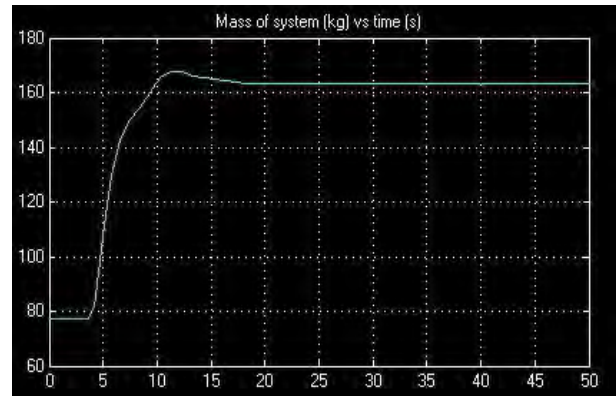
(b)

Figure C3. Simulink simulation 3 results: (a) Net force in z-direction, (b) Mass of system

C3. Simulink Model 4: Water Jetpack Motion in Two Dimensions (Closed-Loop System)

C3.1. Controller Response and Function Blocks

(a)

(b)

(c)

(d)

(e)

Figure C4. (a) Reference tracking, (b) Performance and robustness, (c) Open-loop bode plot, (d) Plant bode plot, (e) Reference tracking bode plot

C3.2 Simulation Results Set 1

(a)

(b)

(c)

(d)

228
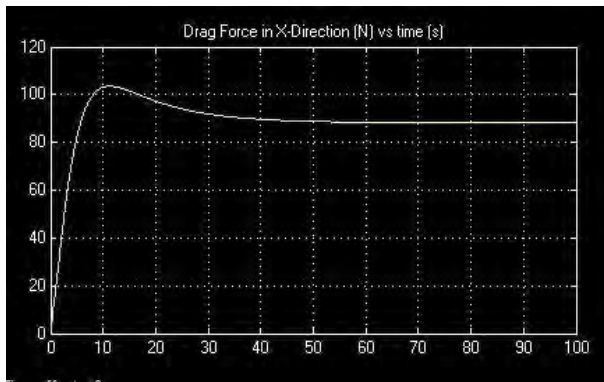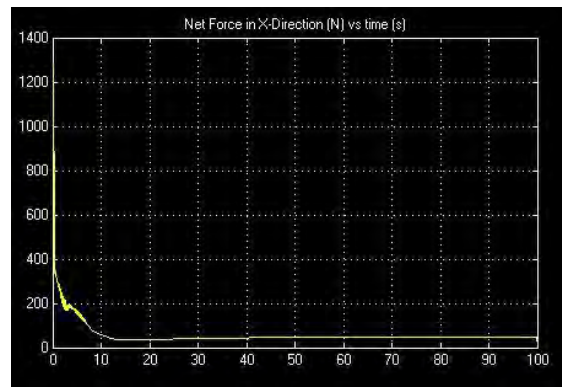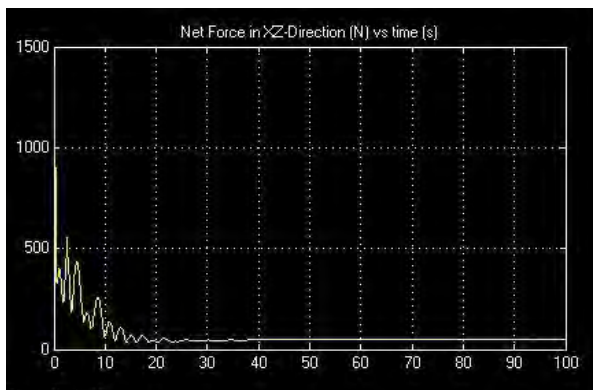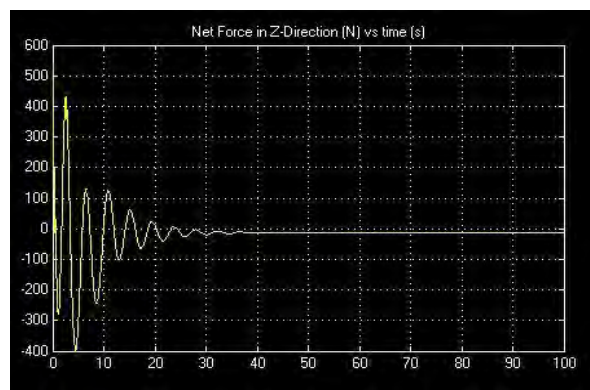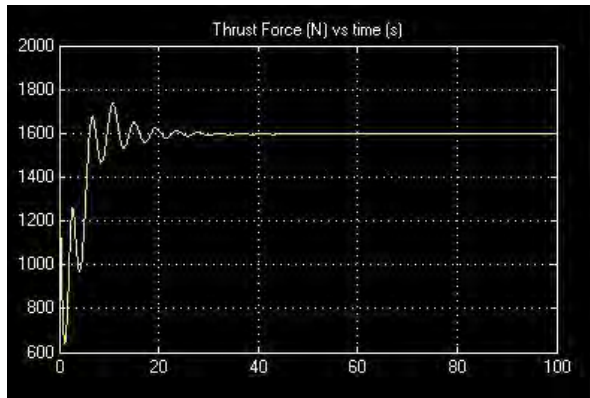
(e)
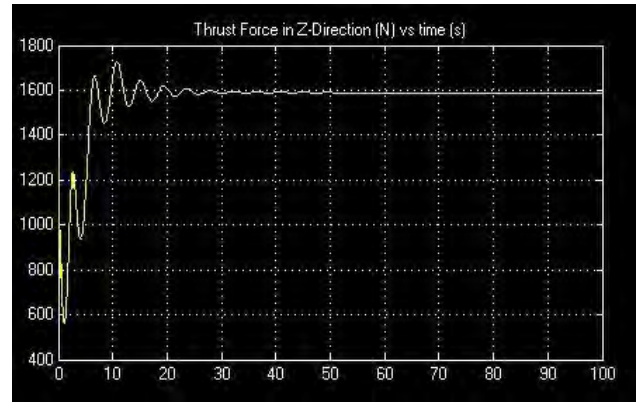
(f)
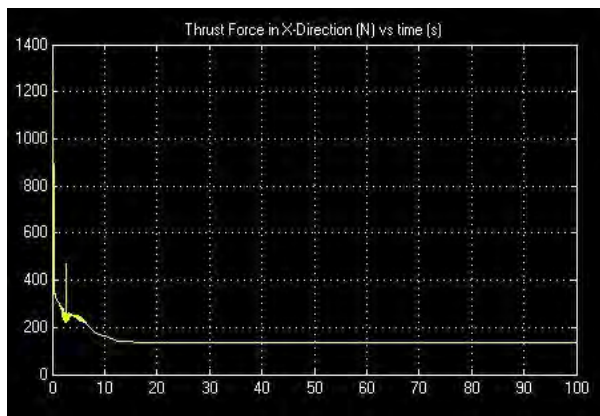
(g)
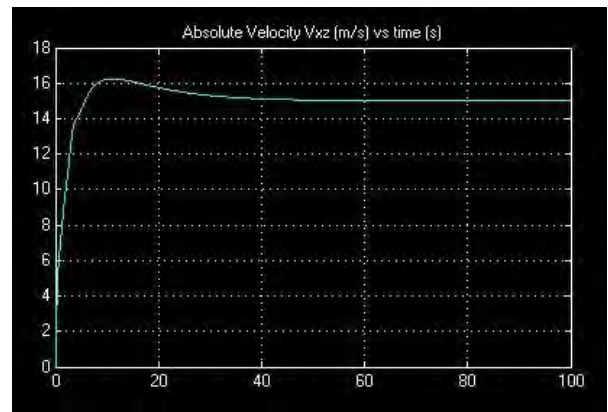
(h)
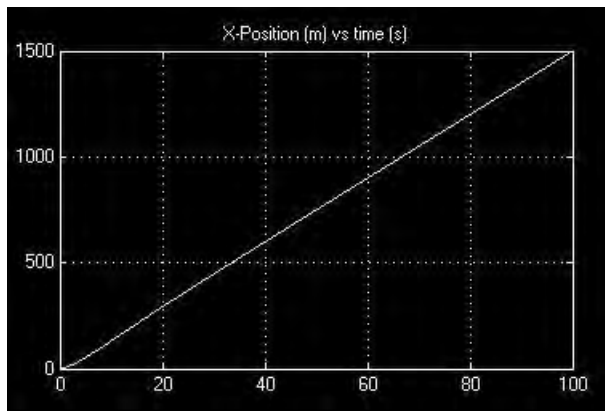
(i)
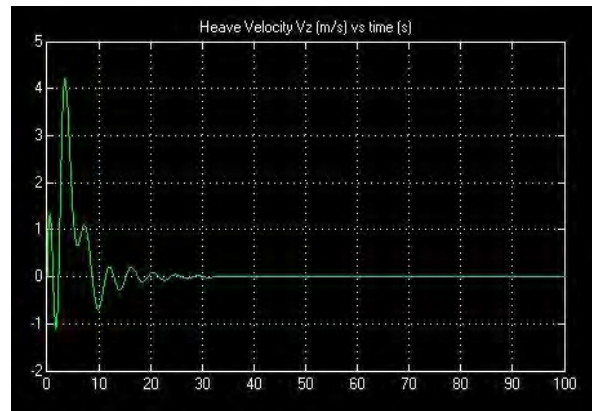
(j)
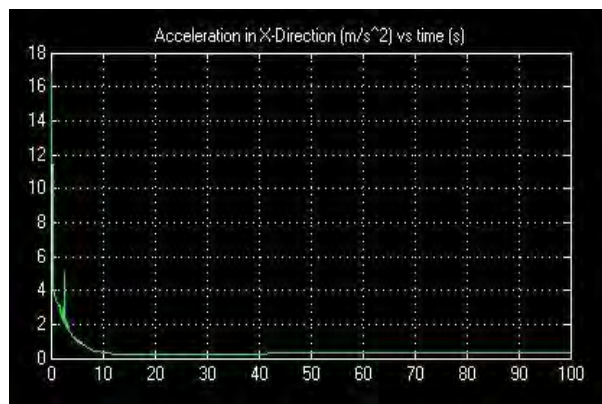
(k)
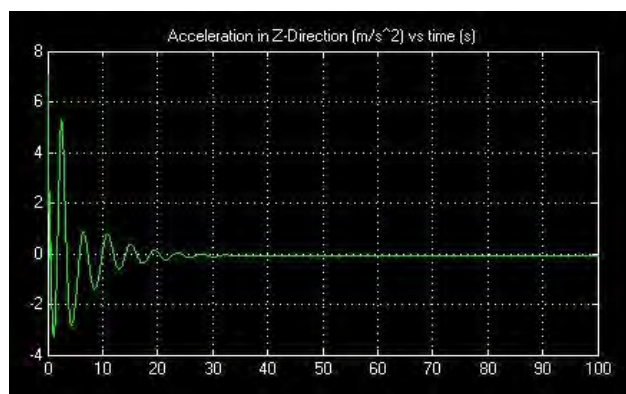
(l)
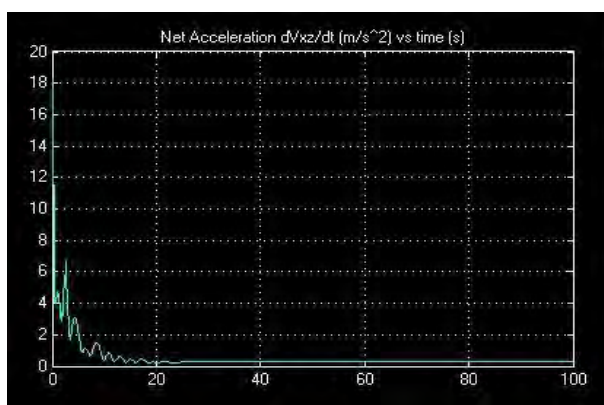
(m)
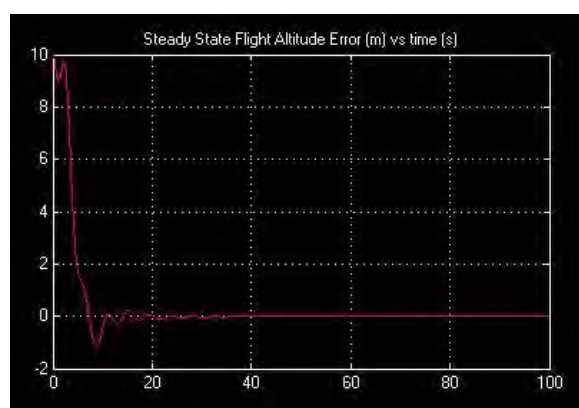
(n)

Figure C5. Simulation 4 results: (a) Drag force in x-direction, (b) Net force in x-direction, (c) Net force in x-z direction, (d) Net force in z-direction, (e) Thrust force, (f) Thrust force in z-direction, (g) Thrust force in x-direction, (h) Absolute velocity, (i) X-position, (j) Heave velocity, (k) Acceleration in the x-direction, (l) Acceleration in the z-direction, (m) Net acceleration, (n) Steady state error in flight altitude

230

C3.3. Simulation Results Set 2: Speed Saturation and Average Drag Modelling
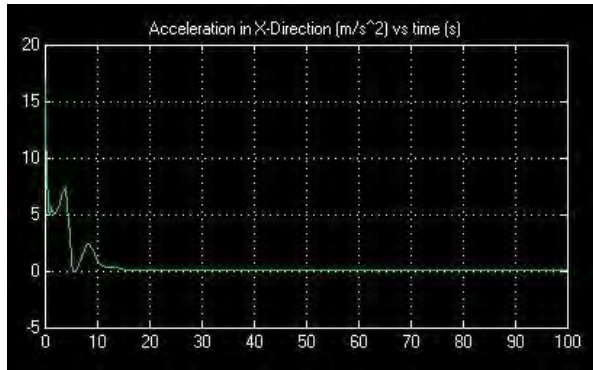
(a)
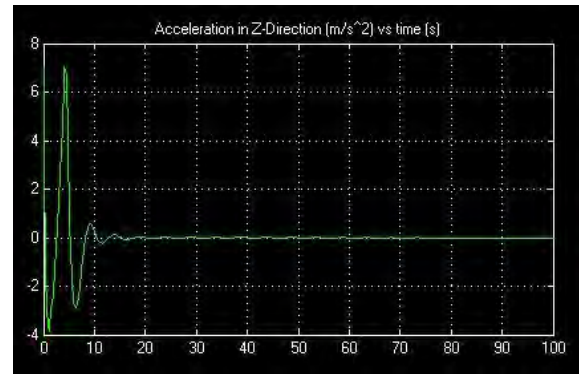
(b)
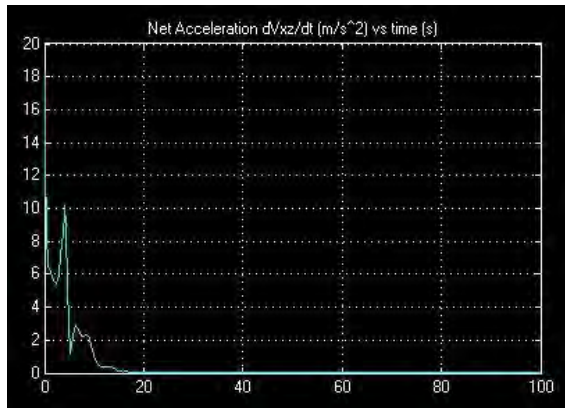
(c)
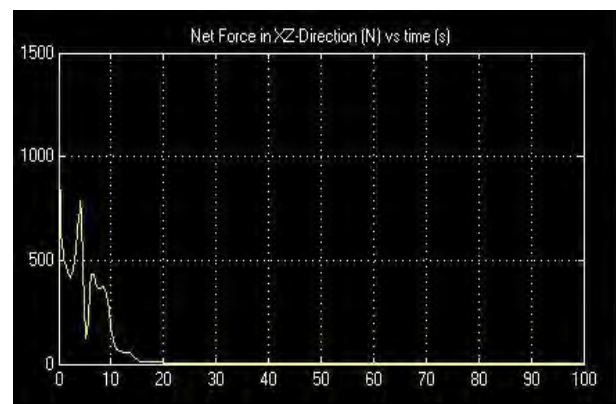
(d)
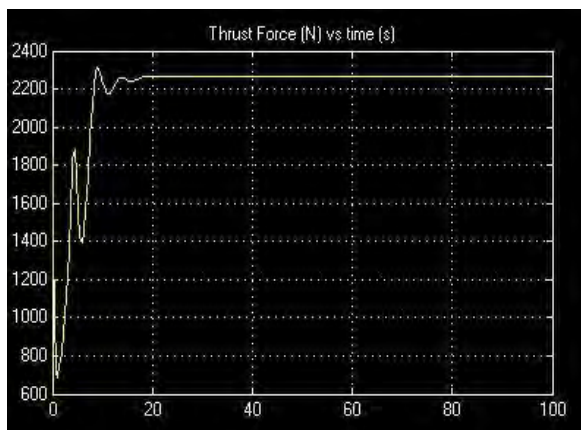
(e)
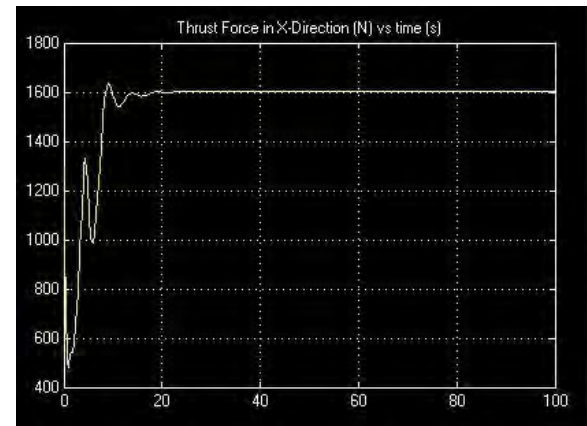
(f)
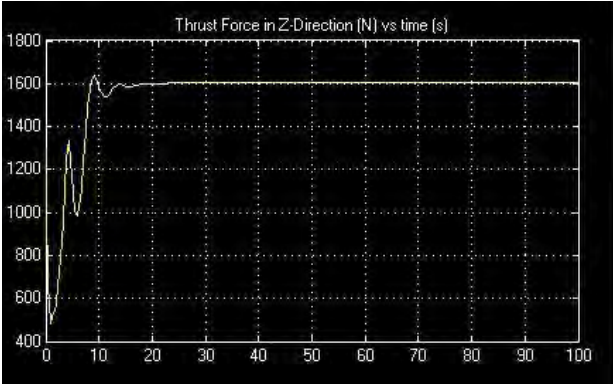
(g)
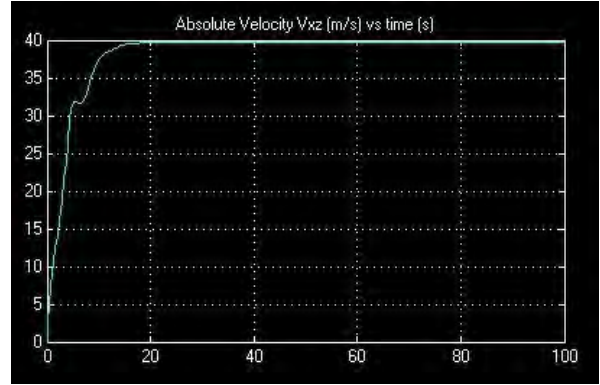
(h)

Figure C6. Simulation set 2 results-speed saturation and average drag modelling: (a) Acceleration in the x-direction, (b) Acceleration in the z-direction, (c) Net acceleration, (d) Net force in x-z direction, (e) Thrust force, (f) Thrust force in x-direction, (g) Thrust force in z-direction, (h) Absolute velocity

C4. Simulink Simulation 5: Water Jetpack Three-Dimensional Modelling
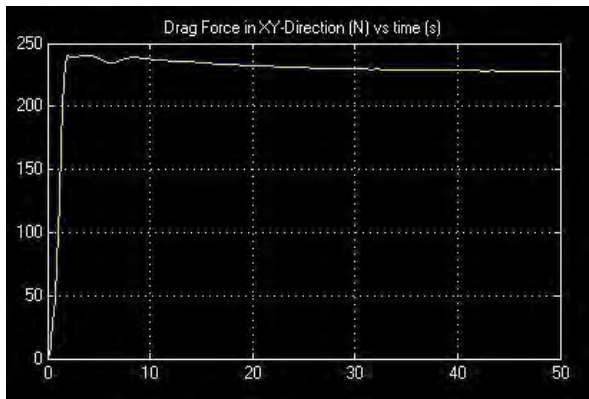
(a)
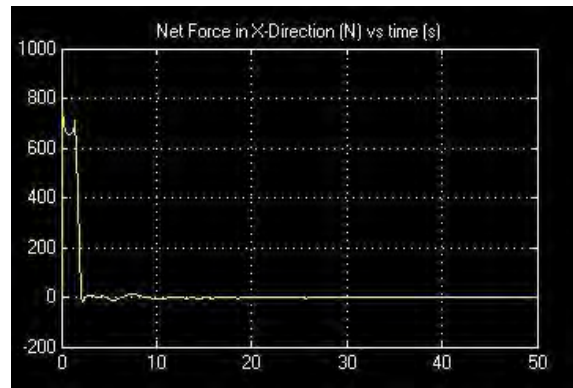
(b)
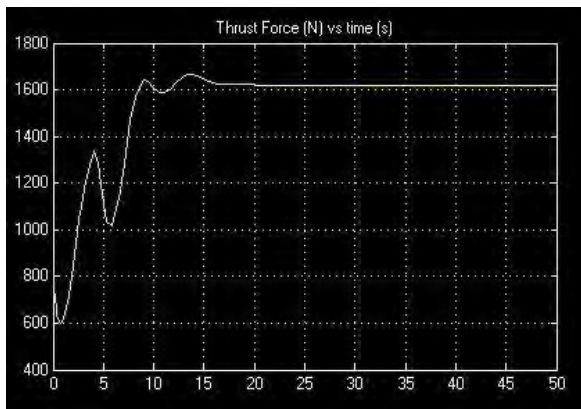
(c)
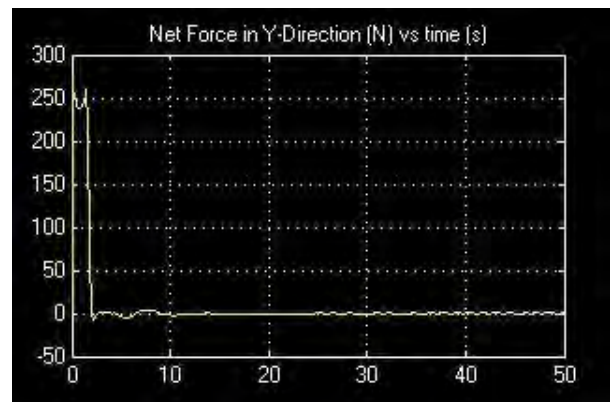
(d)

Figure C7. Simulation 5 results: (a) Drag force in the x-y direction, (b) Net force in the x-direction, (c) Thrust force, (d) Net force in the y-direction

232

C6. Autonomous Underwater Vehicle Simulink Modelling
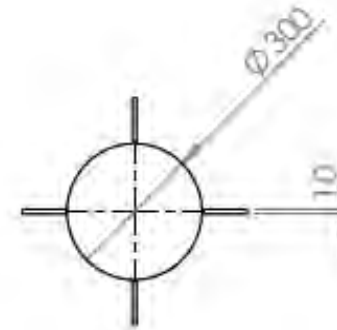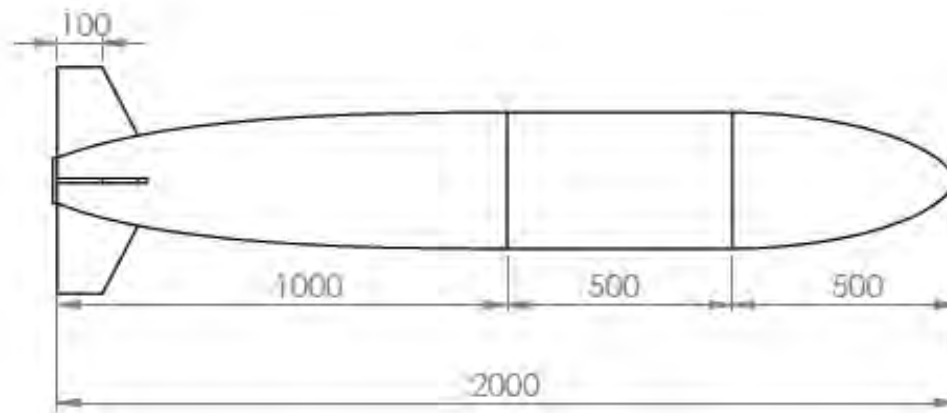

(a)
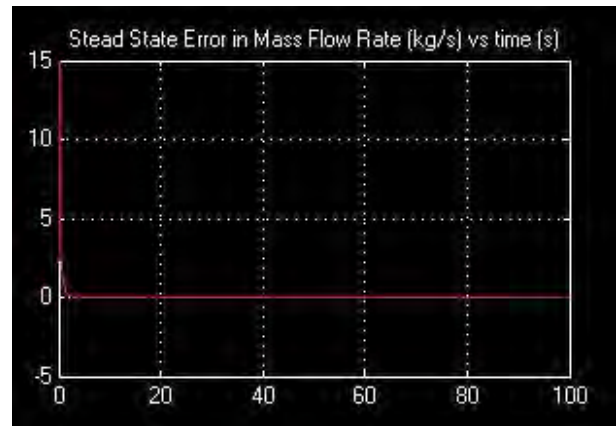
(b)

(c)
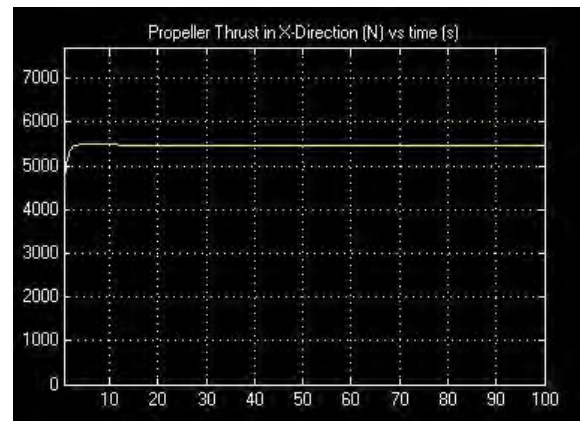
(d)

Figure C8. AUV Simulation results: (a) Drag force in the y-direction, (b) Steady state error in mass flow rate, (c) Propeller thrust in y-direction, (d) Propeller thrust in x-direction
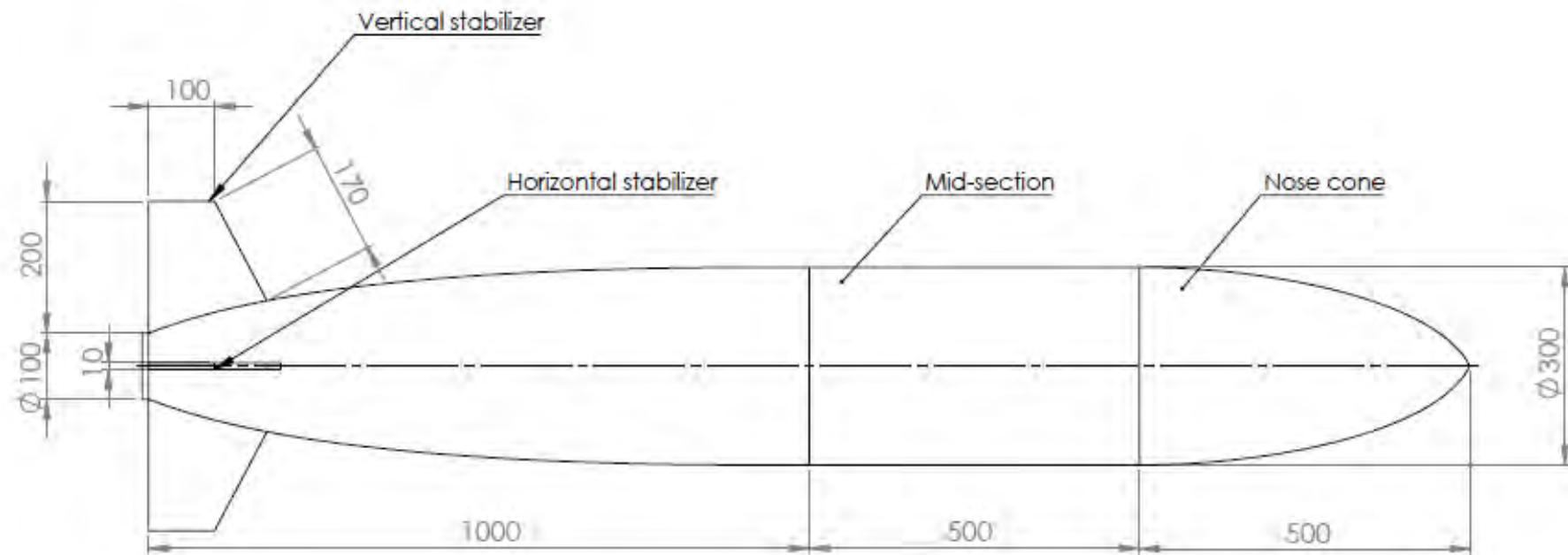
APPENDIX D: Mechanical Drawings

R210

60

R139

Ø64

R72

Ø50

Ø70

40

80

120

60

100

UNIVERSITY OF KWAZULU-NATAL	MAT: Stainless steel 316		No. REQ.: 1		SCALE 1:5	UNITS: mm	PROJECT: Propulsion system		No.:
		DATE	CHECKED		STUDENT NAME: Justin edwin naidoo				1
SCHOOL OF ENGINEERING	PROJECT SUPERVISOR				STUDENT No.: 211510893				
	WORKSHOP TECHNICIAN				E-MAIL:		TITLE: Wye system		
MECHANICAL ENGINEERING	TECHNICAL OFFICER				TEL No.:				

UNLESS OTHERWISE STATED GENERAL TOLERANCES : ± mm
ANGLES : ± °

100

1000   500   500

2000

Ø300

10

UNIVERSITY OF KWAZULU-NATAL	MAT.: Aluminium		No. REQ.: 1		SCALE 1:15	UNITS: mm	PROJECT: AUV	No.:
SCHOOL OF ENGINEERING		DATE	CHECKED		STUDENT NAME: Justin Edwin naidoo			
	PROJECT SUPERVISOR				STUDENT No.: 211510893			
MECHANICAL ENGINEERING	WORKSHOP TECHNICIAN				E-MAIL:		TITLE: Hull	
	TECHNICAL OFFICER				TEL. No.:			

UNLESS OTHERWISE STATED GENERAL TOLERANCES : ± , mm ANGLES : ± °

236

Vertical stabilizer

Horizontal stabilizer

Mid-section

Nose cone

100

170

200

Ø100

10

1000

500

500

Ø300

UNLESS OTHERWISE
STATED GENERAL
TOLERANCES : ± ° mm
ANGLES : ± °

UNIVERSITY OF KWAZULU-NATAL

SCHOOL OF ENGINEERING

MECHANICAL ENGINEERING

MAT.: Aluminium

No. REQ.: 1

DATE

PROJECT SUPERVISOR

WORKSHOP TECHNICIAN

TECHNICAL OFFICER

CHECKED

SCALE: 1:9

UNITS: mm

STUDENT NAME: Justin Edwin Naidoo

STUDENT No.: 211510893

E-MAIL:

TEL. No.:

PROJECT: AUV

TITLE: Hull

No.:

R8

R15

16 mm Shaft with 2x2 mm Keyway

⌀30

60 Deg. Curvature Angle

5 mm

150

UNLESS OTHERWISE
STATED GENERAL
TOLERANCES : ±   mm
ANGLES : ±   °

UNIVERSITY OF KWAZULU-NATAL	MAT: Stainless steel		No. REQ.: 1		SCALE: 1:2		UNITS: mm	PROJECT: AUV		No.:
SCHOOL OF ENGINEERING		DATE	CHECKED		STUDENT NAME: Justin Edwin Naidoo					
	PROJECT SUPERVISOR				STUDENT No.: 211510893					
MECHANICAL ENGINEERING	WORKSHOP TECHNICIAN				E-MAIL: 211510893@stu.ukzn.			TITLE: Propeller		
	TECHNICAL OFFICER				TEL No.: ac.za					

238

APPENDIX E: Editing Certificate

DR RICHARD STEELE
BA, HDE, MTech(Hom)
HOMEOPATH
Registration No. A07309 HM
Practice No. 0807524
Freelance academic editor
Associate member, Professional
Editors' Guild of South Africa

110 Cato Road
Glenwood, Durban 4001
031-201-6508/082-928-6208
Fax 031-201-4989
Postal: P.O. Box 30043, Mayville 4058
Email: rsteele@telkomsa.net

EDITING CERTIFICATE

Re: Justin Edwin Naidoo
Master's dissertation: **Modelling, Design and Analysis of a Water Jetpack Powered by an Autonomous Underwater Vehicle (AUV) System**

I confirm that I have edited this dissertation and the references for clarity, language and layout. I am a freelance editor specialising in proofreading and editing academic documents. My original tertiary degree which I obtained at UCT was a B.A. with English as a major and I went on to complete an H.D.E. (P.G.) Sec. with English as my teaching subject. I obtained a distinction for my M.Tech. dissertation in the Department of Homeopathy at Technikon Natal in 1999 (now the Durban University of Technology). During my 13 years as a part-time lecturer in the Department of Homoeopathy I supervised numerous Master's degree dissertations.

Dr Richard Steele
05 February 2017
electronic